1991

Observations of Estuarine Turbulence and Floc Size Variations

McCabe, Jeremy Charles

Observations of Estuarine Turbulence and Floc Size Variations.

Jeremy Charles McCabe MA.

A thesis submitted to the CNAA
in partial fulfilment of the requirements for the degree of
Doctor of Philosophy.

Polytechnic South West Institute of Marine Studies, Plymouth
in collaboration with
Plymouth Marine Laboratory, Plymouth.

October 1991.

Observations of Estuarine Turbulence and Floc Size Variations

Jeremy Charles McCabe

Abstract

Laboratory studies show that turbulence controls the size of flocs by disrupting those flocs which exceed a critical diameter. Estuarine floc sizes have been shown to vary with the spring/neap cycle and turbulence has been suggested as the mechanism.

A survey of the tidal variations of cohesive sediment floc size distributions and turbulence parameters has been undertaken in the Tamar estuary in south-west Britain. *In-situ* particle size distributions have been obtained using a 'marinised' version of the 'Malvern' laser diffraction sizing system. Turbulent current speeds were obtained using 10 cm diameter annular electromagnetic current meters. Velocity data is analysed using the inertial dissipation method to provide turbulent dissipation rates.

Turbulence and size data, along with profiles of current, salinity, temperature and suspended solids concentration, record the passage of turbidity maximum and salt intrusion over four complete tidal cycles.

Time series of observed particle size distributions vary smoothly over timescales of about one hour and these variations are linked to the flow conditions. Eight subsections of the tidal cycle were selected over which size distributions and flow conditions were slowly varying and the size distributions were time averaged over these subsections, and the resulting distributions compared.

Size distributions in the turbidity maximum are strongly influenced by the mean current speed and this is found to be due to the different resuspension characteristics of newly formed aggregates and consolidated primary particles. Distributions are less dependent on tidal range at other stages during the tidal cycle.

The size dependence of settling velocities strongly influences the size distribution of particles reaching the bed during the final stages of erosion of the salt intrusion, when the salt/fresh interface descends at a rate less than the settling velocity of large flocs but greater than that of small particles. This tends to sharpen the downstream edge of the turbidity maximum and preferentially retain floc aggregates in the upper reaches of the estuary.

Acknowledgements

I wish to thank my supervisors, Prof. KR Dyer, Prof. DA Huntley, Dr. AJ Bale and Dr. SH Alani, for their assistance and encouragement. The technical staffs of the Institute of Marine Studies and Plymouth Marine Laboratories provided filtering electronics and modified the bed frame, Cas well as providing support for many other parts of the project. The crew of the *Tamaris* made the fieldwork both effective and enjoyable.

I am grateful to Dr. Saad Alani for his guidance and for many hours of discussion of flocs - and many other matters. Members of the 'Coffee Club' have provided various forms of assistance over the years as well as good company.

CONTENTS

Abstract page i

Acknowledgements ii

Contents iii
List of Tables vi
List of Figures vii
List of Plots viii

Glossary of Symbols xii - viii

Chapter 1 Introduction
1.1 Importance of Sediment Transport 1
1.2 Problems of Modelling Cohesive Sediment Transport 1
1.3 Approaches to Prediction of Cohesive Sediment Transport 3
1.4 Organisation of Thesis 5

Chapter 2 Theory and Literature Review
Introduction 6
A Turbulence
1 Fluid Dynamics
1.1 Physics 8
1.2 Navier Stokes Equations 9
1.3 Energy Equations 9
2 Turbulence
2.1 Correlation Tensor 11
2.2 Autocorrelations 11
2.3 Dissipation Rate 12
2.4 Inertial Cascade 12
2.5 Subranges 13
2.6 Inertial Dissipation Method 13
3 Estuarine Aspects
3.1 Boundary Layer 14
3.2 Decelerating Flow 16
3.3 Richardson Number 16
B Flocs
1 Primary Particles
1.1 Primary Particles and Bonds 18
1.2 Factors Affecting Bond Strength 19
1.3 Relative Scales of Turbulence and Particles 20
2 Flocs
2.1 Floc Structure 20
2.2 Fractal Description of Flocs 21
2.3 Limiting Effect of Turbulence 23
3 Floc Behaviour
3.1 Settling Velocity 24
3.2 Effect of Concentration on Settling 25
3.3 Effect of Turbulence on Settling 26

C Floc Aggregation and Disruption
1 Aggregation
1.1 Aggregation Kernels 27
1.2 Brownian Motion 28
1.3 Shear 28
1.4 Turbulent Inertia 29
1.5 Differential Settling 29
1.6 Summary 30
2 Breakup
2.1 Disruption Kernels 31
2.2 Floc Model 31
2.3 'Bulgy Fracture' 32
2.4 Surface Stripping 33
2.5 Summary 33
D Flocs and Turbulence
1 Floc-size Distributions in Turbulence
1.1 Equilibrium Distribution 34
1.2 Timescales 35
2 Floc Strength
2.1 Vibrating Column Experiment 36
2.2 Tamar Mud Strengths 36
3 Estuarine Flocs and Turbulence
3.1 Particles and Size Distibutions 37
3.2 Turbidity Maximum 38
3.3 The Tamar Estuary 40
Objectives of Experimental Work 41

Chapter 3 Experimental Work
Introduction 43
A Instrumentation
1 EM Flowmeters
1.1 EM Flowmeters 43
1.2 Calibration 44
1.3 Noise 45
2 Optical Back-Scatter Sensors
2.1 OBS Sensors 47
2.2 Calibration 48
3 Laser Particle Sizer 48
4 Thermistor 49
5 Siltmeter 50
6 Current Meter 50
7 T-S Bridge 50
8 Pitch and Roll Sensor 50
9 Rig Layout 51
B Data Processing
General 52
1 Analogue to Digital Conversion 52
2 Data Storage 53
3 Processing
3.1 Reliability of Spectra 55
3.2 Tests of System 57
4 Sizer Data 58
C Deployment of Gear
1 Theoretical Constraints on Instrument Location 59
2 Practical Constraints 60
3 Siting of Experiment 62
D Sampling Strategy 64

Chapter 4 Results and Discussion

A Measurements

1 Auxiliary Data

1.1 Overview of Fieldwork 67
1.2 Tides 69
1.3 Weather 69
1.4 Pitch and Roll 69

2 Boundary Layer

2.1 Velocity 70
2.2 Concentration 70
2.3 Temperature 71
2.4 Turbulent Intensities 71
2.5 Turbulent Dissipation Rates 73

3 Sizer

3.1 Histograms 74
3.2 Quality 75

4 Profiles

4.1 Profiles 76
4.2 Contour Plots 76
4.3 Features 76

B Results

1 'Average Tide' Model

1.1 Flood 77
1.2 Ebb 79
1.3 Comparisons 80
1.4 Fluxes 81

2 Size Distributions

2.1 Two Floc Populations Z_P, Z_A 83
2.2 Behaviour of Z_P and Z_A 83
2.3 Time Variation of Z% 84

3 Averaged Size Distributions 85

C Interpretation

1 Flood - Formation of Turbidity Maximum

1.1 Resuspension 88
1.2 Settling 89

2 Ebb - Salt Wedge

2.1 Salt Wedge 89
2.2 Lowering of Interface 90
2.3 Entrainment Rate 91
2.4 Mixing and Turbulence 93
2.5 Sizer Data in Salt Wedge 95
2.6 Model of Settling 95
2.7 Possible Spring/Neap Variation 96
2.8 Overall Effect of Salt Wedge 97

3 Turbulence and Particle Sizes. 97
4 Processes during Tidal Cycle 99
5 Comparison With Other Observers Results 101

Chapter 5 Conclusions

1 Flocculation Processes 105
2 Evaluation of Experiment 107
3 Future Work 109

References 111 - 118

Appendix X X1 - X21
Appendix Y Y1 - Y17

List of Tables

Chapter Two

2.1 Relative scales of floc and turbulence parameters 20
2.2 Settling velocities and effective densities of flocs 24

Chapter Three

3.1 EM current meter calibrations 44
3.2 EM current meter noise tests 47
3.3 Laser sizer band diameters 49
3.4 Data processing program 55
3.5 Sinusoid test of logging system 57
3.6 Sampling strategy 65

Chapter Four

4.1 Fieldwork log 67
4.2 Tides 69
4.3 Weather 69
4.4 Pitch and Roll readings 69
4.5 Variability of turbidity maximum 81
4.6 Sizer averaging periods 85
4.7 Time of passing of salt/fresh interface 90
4.8 Linear Regression for d_{max} 98
4.9 Biological aspects 103

Appendix Y

*.FLO files - flow parameters, Y1-4
*.LAS files - sizer data, Z% Y5-8
*.PFL files - near bed profiled data Y9-10
*.VAR files - variances of rig data Y11-14
*.FLU files - fluxes and Richardson numbers Y15-16
*.AXL files - axial profiles Y17

List of Figures

Chapter One

1.1 Approaches to sediment transport 4

Chapter Two

2.1 Inter-relation of sections discussed in chapter two 7
2.2 Energy flow through estuary 10
2.3 Arrangement of flocculated clay platelets (microflocs) 18
2.4 Aggregate of aggregates structure 21
2.5 Fractal dimension related to structure 22
2.6 Aggregation kernels *plot* X1
2.7 Energy dissipation mechanisms in sheared floc 32
2.8 Principle of laboratory floc-strength experiments 36
2.9 Strength/size relationship for Tamar mud flocs 37

Chapter Three

3.1 EM calibrations *plot* X2
3.2 EM current meter noise spectra 46
3.3 OBS sensors 47
3.4 OBS calibrations *plot* X3
3.5 Thermistors 49
3.6 Layout of rig 51
3.7 Filter response 53
3.8 Data collection and storage schematic 53
3.9 Examples of data time series *plot* X21
3.10 Sinusoid test spectra 58
3.11 Positions of instruments on rig 59
3.12 Valid inertial ranges as function of mean flow 60
3.13 Deployment of rig 61
3.14 Location of experiment site 63

Chapter Four

4.1 Speed of advance of tidal wave 78
4.2 Relation of averaged size data to model tide 85
4.3 Formation of turbidity maximum 88
4.4 Definition sketch for 4B2.3 91
4.5 Variation of stratification parameters near bed 94
4.6 Overall effect of turbidity maximum and salt wedge 104

List of Plots

X1 (Fig. 2.6) Log aggregation kernels.

Each plot shows contours of log_{10}*(aggregation kernel)* for turbulent shear, T_{ij}, and for turbulent inertia, I_{ij}, for particles of diameter d_i and d_j. Blue contours are for $\log_{10}(T)$ and green contours are for $\log_{10}(I)$, black contours are for $\log_{10}(T+I)$. The upper plot evaluates kernels for a dissipation rate $\varepsilon = 1000$ cm^2/s^3, and the lower plot uses $\varepsilon = 1$ cm^2/s^3. Units of T and I are *collisions per second per* cm^3.

X2 (Fig. 3.1) EM current meter calibrations.

Each plot shows the two calibrations performed for one EM channel. Pre-fieldwork calibrations (June 1988) are shown with solid markers in blue, and post-fieldwork calibrations use open markers in green. The equations of the fitted lines are shown in Table 3.1.

X3 (Fig. 3.4) OBS calibrations.

The plot shows the calibrations for both OBS sensors obtained as described in section 3A2.2. OBS I calibration is shown by solid markers in blue, OBS II calibration uses open markers in green.

X4 (a)-(d) Boundary layer measurements.

Each page (labelled in top right corner) relates to one day's measurements of conditions on the bed Each point is the mean value of the parameter over one record (approx. 5½ mins.). Each plot shows data of two related parameters which are labelled in the upper left corner: the first label refers to the coloured points and the second label to the black points. The colour used for plotting the first parameter is irrelevant. The horizontal axis is time (BST) with tick marks at twenty minute intervals. The vertical axes are in c.g.s. units with the logarithm to the base ten of dissipations being plotted. Data is read from "*.FLO" files.

label	parameter	units
U,	mean current	cm/s
a	angle of attack	degrees
-m1, m2	vertical speeds (+ve. up)	cm/s
e0, e3	$\log_{10}$(hztl. dissipation)	$\log_{10}$ cm^2/s^3
e1, e2	$\log_{10}$(vert. dissipation)	$\log_{10}$ cm^2/s^3
c4, c5	OBS concentrations	mg/l
temp.	from thermistor	°C

X5 Comparison of OBS and 'Partech' concentrations.

Each plot refers to one day (labelled in upper left). OBS concentrations *c4* (red) and *c5* (black) are run averages. 'Partech' concentrations (line) are values from the lowest profile depth. Horizontal axis is time (BST). Vertical axis is marked as one tenth of SPM concentration (mg/l). Note that in order to roughly calibrate the OBS sensors with the 'Partech' instrument the OBS concentrations are reduced by a factor of four from the calibration of section 3A2.2. Data is read from "*.PFL" and "*.FLO" files.

X6 (a)-(d) Turbulent Intensities.

Each page (labelled in top right corner) relates to one day. Each plot relates to one parameter (labelled in upper left). Horizontal axis is time (BST), vertical axis is the intensity ratio. Intensity is obtained as the square root of the variance in the relevant channel, divided by the mean current, *i.e.* $\sqrt{\langle u^2 \rangle}/U$. Note that *c4* and *c5* are also divided by U. Variances are taken from "*.VAR" files.

X7 ℤ% Relative sizer data.

Each plot relates to one day (labelled in upper left). Horizontal axis is time (BST), vertical axis is percentage of total weight (volume). Relative weights (strictly volume) of particles in each of sixteen size bands are plotted cummulatively, with the smallest band at the bottom and the largest band at the top. The percentage weight of particles in the i-th band is represented by the vertical distance between the i-th and $i-1$th plotted lines. Bands ℤ1..10=$\mathbb{Z}_P$ are plotted in green and bands ℤ11..16=$\mathbb{Z}_A$ are plotted in red. Data is read from "*.LAS" files.

X8 ℤ Absolute sizer data.

Each plot relates to one day (labelled in upper left). Horizontal axis is time (BST), vertical axis is SPM in mg/l. Total SPM ('Partech') is plotted in black, $\mathbb{Z}_A$ in red, $\mathbb{Z}_P$ in green. Data is read from "*.LAS" and "*.PFL" files.

X9 ℤ(D) Sizer data 'corrected' for floc density.

Plot X8 is redrawn allowing for a size dependent floc density function using the model of McCave 1984 (Table 2.2). Note that no correction has been applied to the 'Partech' concentration (black).

X10 $\mathbb{Z}_P$, $\mathbb{Z}_A$

This plot is the same as X8 except that $\mathbb{Z}_P$ and $\mathbb{Z}_A$ are plotted independently. $\mathbb{Z}_P$ is shown in green, $\mathbb{Z}_A$ is shown in red. Total concentration, C, is shown in black.

X11 Time series of d_{max} and ε.

Values of d_{max} were obtained as in section 4B2.2 and are plotted here for the 90, 95, 99 percentiles. Also plotted are time series of turbulent dissipation rates, ε, from the EM current meters. Note that 950 μm particle diameter is an arbitrarily imposed upper limit on d_{max}.

X12 (a)-(d) Contour plots.

Profiled current, salinity, concentration and temperature data is presented as a time series and contoured. The vertical axis is marked in metres such that the surface is at a height of 6 m for each profile. The bed (marked by a black line) was obtained as the depth at which the current meter touched the bed. Positive velocities indicate flood currents.

X13 Fluxes.

Longitudinal fluxes (positive up-river) are obtained from each profile by integrating over height. Time series of fluxes are plotted. Units are indicated on the plot.

X14 Richardson numbers.

A layer Richardson number is obtained from each profile and the time series plotted. Also plotted are time series of terms relevant to the Richardson number: water depth, surface/bed salinity difference, and depth averaged flow. Units are indicated on the plot.

X15 C, $\mathbb{Z}_P$, $\mathbb{Z}_A$ against mean current.

Time series of total SPM concentration, C, and $\mathbb{Z}_P$ and $\mathbb{Z}_A$ are plotted against current speed, *U* (flood positive). Note that the time series for the 28th and 29th June begin with negative speeds, and those for 4th, 5th July begin with positive speeds.

X16 (a)-(d) Environment of rig.

Various parameters (*U, C, S, ϑ*) of the flow near the bed are plotted against each other to indicate typical variations over the tidal cycle. Values were obtained from '*.PFL' files.

X17 Dissipation rates *e0, e3* against mean current, and $\mathbb{Z}\%_A$.

In Fig. X17(a) log dissipation rates, *e0* and *e3*, are shown aginst the mean current, *U*, obtained from the same EM current meter record. Both *e0* (red), and *e3* (black) are plotted together. The upper plot uses data obtained on the ebb, and the lower plot uses flood data. Data from all four days is used.

Fig. X17(b) shows , in red, the percentage weight in bands 11 to 16, $\mathbb{Z}\%_A$, against turbulent dissipation rate, ε. Also plotted, in green, are percentage weights $\mathbb{Z}\%_P$, in the bands 1 to 10. NB $\mathbb{Z}\%_P = 100\% - \mathbb{Z}\%_A$. Upper plot uses ebb data, lower plot uses flood data. Data from all four days is used.

X18 (a)-(c) Axial Profiles of R. Tamar.

Fig. X18(a) shows the results of surface observations of the upper Tamar at HW on the 5th July 1989. Sample stations are approximately evenly spaced along the estuary above Calstock.

Figs. X!8 (b) and (c) were obtained during the fieldwork of 1988 and result from use of the sizer at the surface. Observations on both days began at about half tide and continued over about three hours to arrive at Morwellham at HW. Only the weights in bands 1 (*≤5.8μm*) and 16 (*261.6-564.0μm*) are indicated. Total SPM concentration is shown by the black line.

X19 (a)-(e) Averaged Sizer Data.

For each of the periods described in Table 4.6 the time-averaged size distributions are shown. (Note that 'Max.Ebb' should precede 'TM.Ebb'.) Figure X19(e) compares the averaged size distributions for both flood and ebb turbidity maxima. Neap distibutions are plotted in blue, and spring distributions in red.

X20 Salt Wedge Settling Model.

Output from the computer model described in 4C2.6 is shown. Different sized particles are tracked as they settle through a two layer flow. The vertical grid axis is height above the bed in metres, the horizontal axis is distance upstream of the sampling station that the particles were released. The subsequent motion of the particles is plotted at one tenth of the vertical and horizontal scales respectively (to avoid clutter).

X21 (Fig. 3.9) Examples of Data Time Series.

Output from program *Tamar* is shown. The mean value, over the total record length of just under six minutes, is given beneath each component label. data is plotted as deviations from the mean value. The horizontal scale for velocities, concentrations and temperatures is marked with ticks at 10 cm/s, 10 mg/l, 0.05 °C respectively. The time axis (downwards) is marked at one minute intervals. *U-bar* indicates the mean current.

Wavenumber spectra for each of the time series are plotted on logarithmic axes such that a '-5/3' slope is parallel to the diagonal. For each velocity plot the lower left corner is k=0.01 [cm^{-1}], $E(k)$=10^{-4} [cm^2/s^2] and the upper right corner is k=10, E=10.

Run G18 began at 1900 on 29th June during the ebb turbidity maximum. Run D04 began at 1700 on 5th July just before the flood turbidity maximum.

Glossary of Symbols

Abbreviations

A	denotes *aggregate*
A/D	analogue to digital (converter)
DFT	discrete Fourier transform
EM	electromagnetic (current meter)
FFT	fast Fourier transform (algorithm)
HW	high water
LW	low water
p	denotes *primary particle*
OBS	optical back-scatter (sensor)
SPM	suspended particulate matter
TM	turbidity maximum

Notation

bold type is used for vector and tensor quantities

$\approx$ and $\sim$	approximate equality, varies with
$\langle f \rangle$	time average of variable f
δf and Δf	small and discrete increments in f respectively
$\partial f/\partial x \quad \partial_x f \quad f_{,x}$	partial derivatives of function f with respect to x
$\nabla f = (\partial_x f, \partial_y f, \partial_z f)$	vector gradient operator (acting on f)
$D_t f = \partial_t f + (\mathbf{u}.\nabla)f$	total time derivative of f

$\mathbf{a}^T = (a^{ji})$ where $\mathbf{a} = (a^{ij})$ the transpose of $\mathbf{a}$

Y|X is used on figures to indicate that Y is plotted against X

DD/hhmm denotes the (24hr clock) time *hhmm* on the date *DD* (of June or July 1989)

Variables

Units are c.g.s except where otherwise indicated

$\mathbf{B} = (B^{ij})$	collision kernel for Brownian motion
C	suspended solids concentration
$\mathbb{C}$	speed of advance of tidal wave along estuary
c4, c5	SPM concentrations from OBS sensors (c4 is lower sensor)
$\mathbf{C} = \mathbf{C}(\mathbf{x}, r)$	two point velocity correlation
D	fractal dimension
d, d_{max}	floc or particle diameter, diameter of largest flocs in a distribution
$E = E(k)$	one dimensional, wavenumber, turbulent energy spectrum
e	porosity of floc
e0..e3	estimates of log(dissipation) for *u0..u3*
f4, f5	statistics corresponding to *e0..e3* but for *c4* and *c5*
f_q	Nyquist frequency
$\mathbf{G} = (G^{ij})$	collision kernel for differential settling
G	shear rate (laminar flow)
g	acceleration due to gravity
H	height above bed of incoming tide
h	height above bed of (outgoing) tide
$\mathbf{I} = (I^{ij})$	collision kernel for turbulent inertia
$i, j, k \in \mathbb{N}$	integers
k	wavenumber; Boltzmann constant
K	floc density/diameter exponent
$\mathbf{L} = (L^{ij})$	collision kernel for laminar shear
m	settling velocity/concentration exponent; mass

MKE	kinetic energy of mean flow
N	number of points used in DFT routines
P, p	mean and fluctuating parts of pressure
R	floc size ratio
$r \in \mathbb{R}^3$	displacement vector
$S = S(k)$	k^{th} power estimate obtained by DFT
S	salinity
$T = (T^{ij})$	collision kernel for turbulent shear
T	temperature
t	time
TKE	turbulent kinetic energy
U	mean current speed
$u = (u,v,w)$	current velocity vector
u^j	fluctuating part of velocity component
$u0..u3$	velocity components obtained from EMs
w_s, w_{so}	particle settling velocity, median settling velocity
$x = (x,y,z)$	cartesian coordinate vector
$\mathbb{Z} = \mathbb{Z}1..\mathbb{Z}16$	particle size distribution (in 16 bands)
$\mathbb{Z}\% = \mathbb{Z}\%1..16$	relative (percentage) particle size distribution
$\mathbb{Z}p$, $\mathbb{Z}A$	distribution of primary and aggregated particles respectively
α	Kolmogorov constant
β	rate of energy loss to floc break-up
γ	floc break-up exponent
δ^{ij}	Kronecker delta
ε	turbulent dissipation
η	Kolmogorov microscale
$\eta(x,t)$	density interface elevation
ϑ	temperature obtained from thermistor
ι	$\sqrt{-1}$
$\varkappa$	wavenumber
λ	wavelength
λ_f, λ_g	Taylor longitudinal and transverse microscales
μ	dynamic viscosity; arithmetic mean
ν	kinematic viscosity
$\xi(x,t)$	surface elevation
ρ, ρ_{eff}	density, floc effective density
σ	stress, standard deviation
(τ^{ij})	shear stress tensor
ψ^k	working dissipation parameter
ω	angular frequency

Values

gravitational acceleration: $g \approx 981\ cm/s^2$
density of fresh water: $\rho_w = 1.000\ g/cm^3$
density of primary particle (quartz): $\rho_0 \approx 2.65\ g/cm^3$
density of saltwater (35‰): $\rho_s \approx 1.025\ g/cm^3$
viscosity of water: $\mu \approx 0.014\ g/cm/s$, $\nu \approx 0.014\ cm^2/s$
Kolmogorov constant: $\alpha \sim 0.5$
Boltzmann constant [SI]: $k \approx 1.381 \times 10^{-23}\ J/K$

1.1 Importance of Estuarine Sediment Transport.

Estuaries are widely used by shipping as waterways to many important ports, as commercial and recreational fisheries, as drains for cities and industrial areas, and increasingly as yachting, boating and windsurfing centres. Some of the more inaccessible mudflats and marshes are vital to the survival of wildfowl and are very productive biologically.

All of these uses are affected by the movement of sediments within the estuary. Navigation may be impeded as mudbanks and bars change their position and configuration, and wharves and docks may be made unusable due to rapid silting-up; areas of tidal marsh may be eroded or expand when dredging or other changes alter the sediment fluxes. The health of people and wildlife may be affected when pollutants attach themselves to sediments and become trapped in the estuary. Neighbouring coastal regions may be affected by these industrial effluents if they do leave the estuary.

These effects are complicated by the cohesive nature of some estuarine silt particles and their ability to adsorb pollutants on their surfaces. In many estuaries particle properties combine with the water circulation to form a turbidity maximum where high suspended solids concentrations accumulate and settle out to form mudflats. Associated with the silt particles are dissolved metals, and bacteria and plankton which can have their own effect on the food chain.

1.2 Problems of Modelling Sediment Transport.

The prediction of the movement of cohesive sediments is hampered by the wide range of sediment properties. These are reviewed by Partheniades [1986] and van Leussen and Winterwerp [1990] with the following major features. A mud bed has a critical shear stress below which no erosion takes place but above which particles may be resuspended into the water. The value of the critical erosion stress depends on particle properties as well as on the history of the bed. Once in suspension particles may aggregate to form larger flocs which have varying degrees of porosity and a large range of settling velocities, moreover the

degree of flocculation may change while the particles are in suspension. Deposition and consolidation in the bed occurs only below a critical deposition stress which in general is lower than the critical erosion stress.

The complexity of flow in estuaries adds to the difficulty of modelling transport of sediment. Many estuaries are stratified over some of their length with a net circulation over several tidal cycles that is seaward at the surface and landward near the bed [Dyer 1986]. Vertical mixing is affected by the stratification [West and Shiono 1988] and the dispersal or formation of a turbidity maximum is related to the geometry of the particular estuary.

Owen [1976] considers the factors contributing to sedimentation processes and highlights the critical shear stresses for erosion and deposition, the erosion rate coefficient, and the particle settling velocity, as crucial to any modelling. Much work has been carried out on these estuarine processes, ranging from long timescale sediment flux studies [*eg* Bale et al. 1985], detailed surveys of tidal resuspension events [*eg* Schroder and Siedler 1989], and measurement of particle settling characteristics [*eg* Owen 1971]. Laboratory work has involved study of erosion and bed properties using a variety of flumes [*eg* van Leussen and Winterwerp 1990, Scarlatos and Mehta 1990]. The results of these, and many other, studies have been incorporated into simplified mathematical models of sedimentation in estuaries [*eg* Uncles and Stephens 1989], but the variable settling rates of flocculating particles have as yet been included only indirectly (as a function of concentration) [Dyer 1989].

Our work is concerned with the characterization of particle settling characteristics and the nature of their variability over the tidal cycle. The starting point for this is Owen's [1971] observation in the Thames estuary of the higher particle settling flux during neap tides than during spring tides. It was proposed that this effect was due to the greater disruption of flocs in the increased turbulence at spring tides. Since then much work has been carried out on characterizing floc properties such as structure [*eg* Krone 1978], strength [*eg* Alani 1987], settling velocity [*eg* Gibbs 1985], and coagulation rates [*eg* Burban et al. 1989].

1.3 Approaches to Prediction of Sediment Transport.

Erosion is usually modelled using a critical shear stress τ_e with the rate of erosion m_e proportional to the excess of the bed shear stress τ over the critical shear stress - $m_e \sim \tau - \tau_e$. The bed shear stress can be obtained from the mean flow profile and usually is based on the form $\tau \sim U|U|$. The depositional flux, m_d, of a suspension of particles with settling velocity, w_s, and concentration, C, near the bed is $m_d \sim Cw_s$; the transport of these particles can also be predicted if the flow structure is known as the particle is advected with the flow velocity while continuing to settle [Partheniades 1986]. However for a suspension of estuarine particles of differing sizes, shapes, densities and porosities the correct form of w_s is difficult to find.

Settling velocities can be predicted using modifications of Stokes' formula relating w_s to particle diameter and weight, and this is very successful in laboratory studies. However the inclusion of buoyant material in estuarine flocs is a complicating factor. Adequate models of settling require knowledge of particle size distributions found in the estuary and also of the relation of size to density. Theoretical and laboratory studies can provide the size/settling data but *in-situ* particle size distributions present serious problems because of the fragility of the flocs.

The fragility of estuarine flocs precludes standard particle-sizing procedures such as seiving or Coulter counting [Bale and Morris 1987], although such measurements can provide information on floc structure [Kranck and Milligan 1988]. Settling column measurements yield size/density relations but the transfer of a suspension from the water to the column is impossible to accomplish without floc breakage; the Owen tube [Owen 1971] is an attempt to reduce breakage but provides no information on sizes. The laser sizing technique used in this experimental work is the least destructive of available methods for obtaining size distributions [Bale and Morris 1987], but has the disadvantage of not providing any settling information.

Two possible influences on settling velocities are the concentration of the suspension and the extent to which flocs are disrupted, or aggregated, by their environment. Studies with the Owen tube relate settling velocity to

concentration, which in turn may be derived from flow parameters (via erosion). Laboratory studies (and water treatment industry experience) relate the size distribution of particles in a turbulent environment to the turbulent dissipation rate which again may be derived from flow measurements.

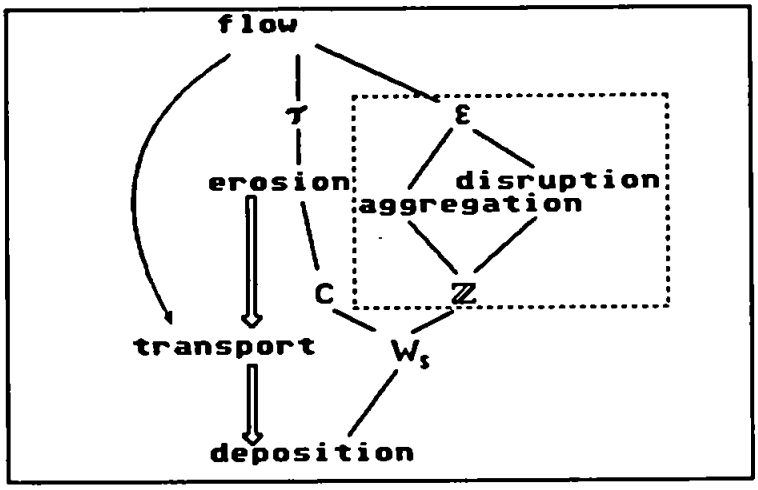

Fig. 1.1 Approaches to Sediment Transport. The flow controls erosion through the bed shear stress, and controls transport by advection. Particle size distributions, ℤ, are controlled by the turbulence, ε. Settling velocities may be estimated either from the suspended solids concentration or from the size distribution.

There are thus two routes linking the flow to deposition rates: (1) by assuming the floc size distribution to be determined wholly by the concentration and using empirical settling velocity/concentration relations, or (2) by measuring particle size distributions and deriving settling velocities from size/density relations (Fig. 1.1). Our experimental work aims to quantify the turbulence/size relation which controls particle size distributions, to give more accurate deposition data than can be estimated using the Owen tube.

Very little survey work on the *in-situ* size of estuarine flocs has been carried out however (but see Gibbs et al. [1989] for an axial survey of particle sizes in the Gironde, and Bale et al. [1989] and West et al. [1990] for work in the Tamar with laser particle sizing) and the present work combines such a survey with an appraisal of which floc processes are occuring during the various flow conditions during the tidal cycle. The experimental work is based on Owen's [1971] (indirect) observation of a floc-size/turbulence relation and Alani's [1987] laboratory work on the quantification of this relation.

This work has been carried out in the upper Tamar estuary for which a large body of information is already available on flow conditions (*eg* Uncles et al. 1983, West and Oduyemi 1989, West and Sangodoyin 1991), sediment movement [*eg* Bale et al. 1985], and the relation of suspended solids to biological and chemical processes [*eg* Morris et al. 1982, Ackroyd et al. 1986, Owens 1986, Plummer et al. 1987, Reeves and Preston 1991].

1.4 Organisation of Thesis.

Chapter One introduces the work.

Chapter Two reviews the previous work on the effects of turbulence on floc sizes. There are two threads leading to a predicted floc-size/turbulence relation; one looking at the composition and structure of flocs, and the other surveying turbulence and methods available for deriving the required statistics. Some aspects of estuarine flows are also reviewed.

In Chapter Three details of the experimental work are presented. The instrumentation and its characteristics are described in the first section and followed in section two by details of the data processing hardware and software. Section three discusses the theoretical and practical constraints on the details of the experiment and the resulting sampling strategy is presented in the fourth section.

Chapter Four discusses the data obtained in three parts. In part A the measurements from each instrument are presented and the main features of each data set picked out. Part B draws together related features from each instrument and characterises different stages of the tidal cycle in terms of flow parameters and size distributions. The third part (C) describes and discusses the processes believed to be contributing to the observed size distributions and the evidence for these processes.

In Chapter Five the main conclusions of this work are presented followed by an appraisal of the experimental work and recommendations for future work.

Data plots and computer output are collected in Appendix X and referred to by figure numbers. Printouts of the files used to produce the figures are collected in Appendix Y.

General.

The study of sedimentation in estuaries is complicated by the variable nature of cohesive sediment flocs. The most important effect of flocculation is that larger, heavier, flocs settle more quickly than smaller, lighter, ones and this is a controlling factor in sedimentation rates. However the structure of flocs is important in determining both floc density: which affects settling velocity, and floc strength: which influences the floc size distribution, again with effects on sedimentation rates. Also, the turbulence of the environment acts on flocs in two opposite directions, with turbulence being necessary for production of flocs and also being responsible for limiting their growth.

This chapter reviews the literature on the relevant aspects of flocculation and turbulence. The chapter is in four parts with the intention (except in part A) of moving from small scale processes to larger. The inter-relation of the sections is depicted in Fig. 2.1 where it should be observed that the object of this work is to establish an experimentally measurable link from turbulence parameters (part A) to deposition rates (section B3).

Part A deals with the measurement of flow and turbulence parameters, and in particular the inertial dissipation method used in the experimental work.

Part B describes the composition and structure of individual flocs as revealed by microscopy and settling data together with factors which affect floc structure.

Part C discusses the dynamic behaviour of numbers of flocs: this falls into two parts dealing with aggregation and with disruption.

Part D links parts A and C by discussing the influence of turbulence on floc size distributions. The formation of estuarine turbidity maxima is reviewed and the Tamar estuary described. Also reviewed are some results of previous workers in measuring relevant parameters, with particular reference to the Tamar estuary.

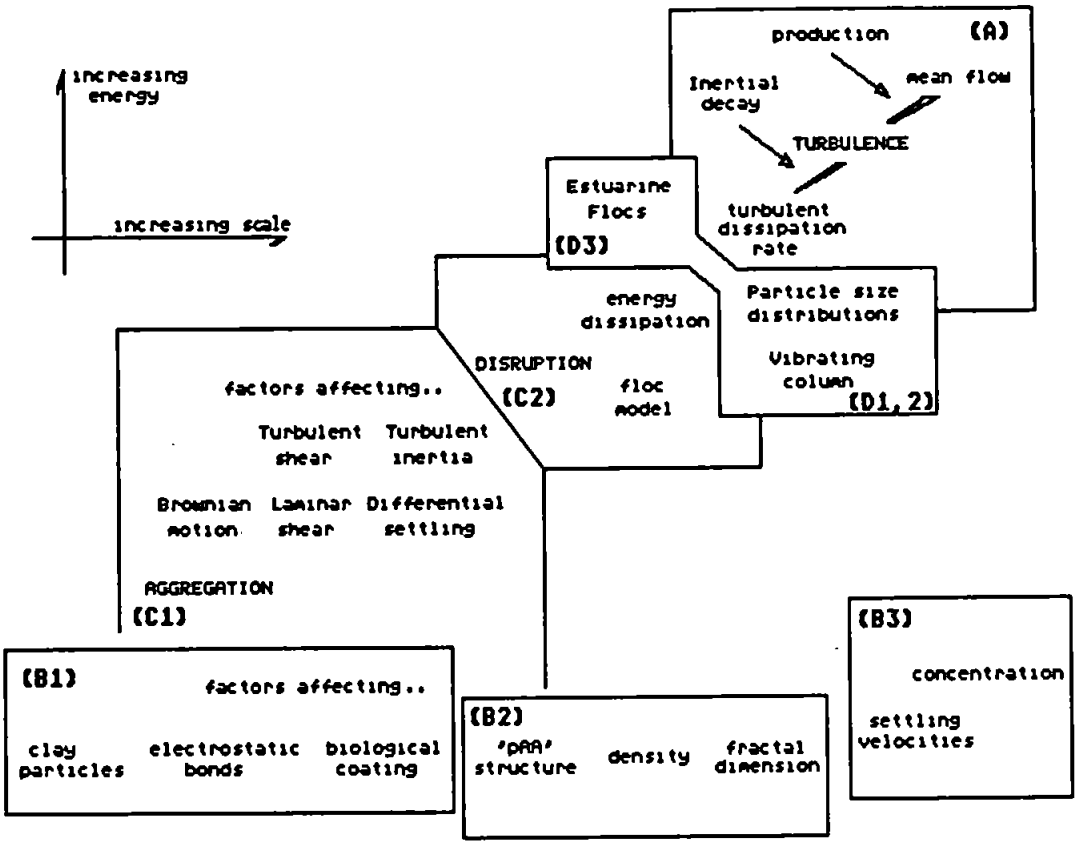

Fig. 2.1 Inter-relation of Parts of Chapter 2. (Section labels are shown bracketted) Showing the chain of reasoning linking settling velocities (section B3) to flow (section A).

Published work on floc size distributions comes from a variety of sources with much of the study on floc strength coming from the water treatment industry where floc quality has economic ramifications. Work in estuaries has until recently tended to bypass flocculation processes, mainly because of the difficulties in observing undisturbed flocs in highly turbid waters. Marine snow has attracted attention and some of the theoretical work may be adapted to estuaries although estuarine turbulence is far more energetic than in the sea. There is, however, a large body of work on the hydrodynamics of estuaries, including the modelling of suspended solids concentrations from mean flow parameters. The gap in knowledge with regard to estuarine flocculation is in knowing which of the turbulent processes involved in aggregation and breakup are most important to the particle size distribution.

Part (A) Turbulence

2A1 Fluid Dynamics

2A1.1 Physics.

The motion of a parcel of fluid is determined by (i) the forces acting upon each particle: here gravity, and (ii) those acting on each part of the surface: the pressure and viscous shear stress. The effects of these forces are summed up in the Navier-Stokes equations (Eqns. 2.1) below). The accelerations produced depend on the inertia of the parcel: the ratio of inertia to viscous forces can be indicated by the dimensionless number (Reynolds number) $Re=U\lambda/\nu$, where ν is the kinematic viscosity $\nu=\mu/\rho$ and U and λ are, respectively, a velocity and length characteristic of the region of flow being considered.

A high Reynolds number indicates that inertia dominates over the frictional terms and such flows have instability: perturbations of the flow increase chaotically and turbulence sets in. At small scales in the flow however, the Reynolds number is small and viscosity dominates: kinetic energy is dissipated as heat at molecular scales.

There are a number of Reynolds numbers associated with estuarine processes. The flow as a whole has a value for Re of the order 10^5 at LW (1 m depth, 20 cm/s mean flow), and up to 5×10^6 on spring floods (at the experimental site on the Tamar), while the boundary layer (see section 2A3) is defined as the region near the bed for which the local Reynolds number is of order one and less. For suspended particles settling under gravity, grain Reynolds numbers range from 1 for millimetre sized flocs down to 10^{-4} for 10 μm particles: suspended matter 'sees' the water as being dominated by viscosity.

The main property of turbulence is its chaotic redistribution of fluid at all scales. The importance of turbulence is this redistribution, or diffusion, of fluid properties such as momentum, salinity, heat, and suspended solids concentration. In many flows, turbulent diffusivities are far higher than the corresponding molecular diffusivity values; this applies particularly in estuaries.

2A1.2 Navier–Stokes Equations.

$$\partial_t u + (u.\nabla)u = -\nabla p + \nu\nabla^2 u \qquad (2.1)$$

The inertial term $(u.\nabla)u$ is the non-linear term responsible for the chaotic nature of turbulence. The fluid density is included in the pressure term; $p := press./\rho$.

A turbulent velocity field $u(r)$ may be split into a mean flow $U(r)$ and a fluctuating part $u'(r)$, where $u = U + u'$ and $\langle u' \rangle = 0$. This may be substituted into the Navier-Stokes equations which are then time averaged to obtain, (dropping the prime on u, and using cartesian coordinates: i, j, k=1, 2, 3).

$$\partial_t U^I + U^J U^I_{,j} = -\partial_j (P\delta^{Ij} + U^I \langle u^I u^j \rangle - \nu U^I_{,j}) \qquad (2.2)$$

The second term on the RHS involves the Reynolds stress, $-\langle uu^T \rangle$, which is responsible for the transfer of energy between the mean flow and the turbulence. Note that the term $\langle uu^T \rangle$ is found to be negative in wall flows thus acting to slow the flow.

2A1.3 Energy Equations.

The mean kinetic energy (MKE) carried by the flow is $U.U/2$ per unit mass, and the turbulent kinetic energy (TKE) is $\langle u.u/2 \rangle$ per unit mass. The time averaged energy equations may be obtained by taking the product of the equations (2.1) with U and u [Hinze 1975]:

$$D_t(MKE) = \partial_j (-U^j P - U^I \langle u^I u^j \rangle + \nu U^I U^I_{,j}) + U^I_{,j} \langle u^j u^j \rangle - \nu U^I_{,j} U^I_{,j} \qquad (2.3)$$

$$D_t(TKE) = \partial_j \langle -u^j p + u^I u^I u^j/2 + \nu u^I u^I_{,j} \rangle - U^I_{,j} \langle u^I u^j \rangle - \nu \langle u^I_{,j} u^I_{,j} \rangle \qquad (2.4)$$

In a steady homogeneous channel flow the gradient terms make no net contribution to the equation, and only the last two terms in each equation are important.

The Reynolds stress term occurs with opposite sign in each equation and corresponds to the transfer of energy from the mean flow to the turbulence by means of the work done by the (vertical) Reynolds stress $-\langle uv \rangle$ against the mean shear (dU/dz). This term is the 'production' term.

The last term of each equation represents the dissipation of MKE and TKE to heat by the action of the mean/turbulent viscous shear stress against the mean/turbulent shear.

The transfer of energy through a section of the estuary is represented in Fig. 2.2. The supply of gravitational potential energy is maintained by the surface slope and modified by the mean velocity profile. In a steady flow the rate of supply of gravitational energy to the mean flow is balanced by the rate at which energy is removed from the mean flow by viscosity and turbulence. The transfer rates of these two processes are shown in Fig. 2.2 as *'D'* and *'P'* respectively and correspond to the terms $\nu U'_j U'_j$ and $U'_j \langle u'u' \rangle$ in the energy equations (2.3) and (2.4). Hou and Kuo [1987] obtain laminar and turbulent flow profiles by assuming that the required profile minimises the overall rate of dissipation of energy; the method is further illustrated by Yang and Song [1986].

The introduction of flocs into the system provides an alternative route by which energy may be dissipated, that is by the removal of turbulent energy to disrupt flocs. Application of the theory of Yang and Song [1986] suggests that energy will be dissipated in this way with a corresponding decrease in the energy dissipated by turbulent viscosity and 'mean flow viscosity'. The model of van de Ven and Hunter [1977], discussed in section 2B2, provides a theoretical discussion of the details of energy dissipation processes within flocs, while the observations of Gust and Walger [1976], (section 2A3), in a turbid boundary layer suggest that the modifiction of velocity profiles due to floc related energy dissipation may be measurable. The work of Alani et al. [1990], (section 2D2) in defining the range of floc sizes which interact with turbulence might be used to parametrize the interaction of mean flow profile and 'floc dissipation' via turbulent dissipation rate. This approach might merit some further theoretical work but has not yet been pursued.

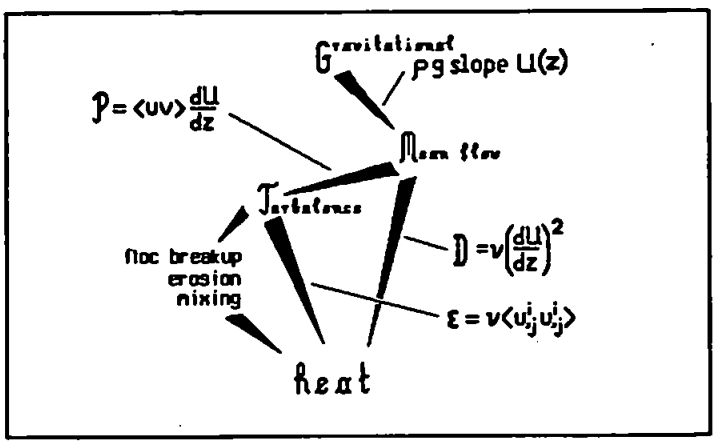

Fig. 2.2 Flow of energy through estuary.

2A2 Turbulence

2A2.1 Correlation Tensor.

A turbulent flow consists of many variously sized parcels of fluid moving with varying velocities. In order to study the properties and evaluate the effects of turbulence at different scales, we wish to partition the turbulent energy according to the size of parcel.

The size of a parcel of coherent fluid motion can be estimated by considering the two point velocity correlation tensor $C(r)=\langle u(x)u(x+r)^T\rangle = (\langle u^i(x).u^j(x+r)\rangle)$. If the velocities at the two points x and $x+r$ (separated by distance $r=|r|$) are correlated then the two points are likely to be within the same eddy; if this correlation persists when the correlation is time-averaged an estimate of the energy contained in motions with a length scale r can be made. In order to obtain statistically reliable results the average of uv^T, where $v=u(x+r)$ over a large volume (or more usually a long time) is taken and denoted by $\langle uv^T\rangle$. The energy contained in motions with characteristic length λ, or wavenumber $k=2\pi/\lambda$, is given by $|\hat{u}|^2$ where $\hat{u}(k)$ is the Fourier transform of $u(r)$:

$$\hat{u}(k) = \frac{1}{2\pi}\int_{r=0}^{\infty} u(r)\, exp(-\iota kr)\, dr \qquad (2.5)$$

2A2.2 Autocorrelations.

The two point velocity covariance $C(r)$ can be used to derive parameters describing the small scales of turbulence. The Taylor microscales λ_f, λ_g describe the sizes of the smallest eddies, and are derived from the curvature of the longitudinal and transverse correlations [Hinze 1975]:

$$C_{11}(r) = U^2(1 - r^2/\lambda_f^2) \qquad (2.6)$$

$$C_{22}(r) = U^2(1 - r^2/\lambda_g^2) \qquad \text{where } U=(U,0,0) \text{ and } r=(r,0,0) \qquad (2.7)$$

The longitudinal and transverse autocorrelations, C_{11} and C_{22} respectively, are obtained from velocity time series using the 'frozen turbulence' substitution $r=Ut$, which assumes that the time scales of turbulent eddies are large compared with the time taken for them to advect past the origin. Thus

$$C_{ij}(t) = \frac{1}{T-t}\int_{\tau=0}^{T-t} u^i(\tau)\, u^j(\tau+t)\, d\tau \qquad (2.8)$$

The scale of the largest eddies present may be estimated as $r=\Lambda_f, \Lambda_g$, known as the integral scales of the turbulence, and are found as the smallest values which satisfy $C_{11}(\Lambda_f)=0$ and $C_{22}(\Lambda_g)=0$.

2A2.3 Dissipation Rate.

The turbulent dissipation rate, ε, measures the rate at which turbulent energy is dissipated as heat through the action of viscosity. Viscosity is most important at the smallest scales (for which the Reynolds number is small) and it is here that most energy is dissipated. From the equations (2.4) for homogeneous turbulence the dissipation rate is

$$\varepsilon = \left\langle \nu \frac{\partial u^i}{\partial x^j} \frac{\partial u^i}{\partial x^j} \right\rangle \qquad (2.9)$$

The velocity gradients may be obtained from the velocity covariances [Hinze 1975] and under under the assumption of isotropy the dissipation rate can be estimated from $\varepsilon = 15\nu u^2/\lambda_g^2$. This is the derivation of ε used by many workers in floc disruption [Parker et al. 1972, Tambo and Hozumi 1979].

In order to compare experiments using turbulent flows with those made under laminar flow conditions the laminar shear rate $G=dU(z)/dz$, is equated with the root mean square turbulent shear derived from the dissipation rate as $G \approx \sqrt{(\varepsilon/\nu)}$. Cleasby [1984] discusses the merits of using turbulent mean shear as a flocculation parameter and concludes that the dissipation rate ε, is the most relevant to the floc size distribution.

2A2.4 Inertial Cascade.

Turbulence consists of vortices of random strength, orientation and size, the action of larger vortices on smaller is to stretch them, decreasing their size and increasing their vorticity, as well as altering their orientation. This results in the passing of energy from large scales to smaller with the eventual dissipation at the smallest scales. Where the production of turbulent motions occurs at scales far removed from the dissipation scales, that is where $\Lambda \gg \lambda$, the turbulence at intermediate scales is governed mainly by the inertial terms in the energy equations. Kolmogorov made the suggestion [Hinze 1975] that there might be a universal turbulent energy spectrum determined by the mechanics of this transfer process and independent of the details of how the turbulence is produced.

Assuming the energy spectrum to have a universal form where the energy is transfered from larger to smaller scales at rate P and dissipated at small scales at rate ε, with $P=\varepsilon$, dimensional analysis gives a characteristic length, $\eta=\sqrt[4]{(\nu^3/\varepsilon)}$ - the Kolmogorov microscale, and a wavenumber energy spectrum:

$$E(k) = \alpha \varepsilon^{2/3} k^{-5/3} \qquad k \ll 1/\eta \qquad (2.10)$$

This spectrum has been observed in many flows [Williams and Paulson 1977, Champagne 1978, Huntley and Hazen 1988] and the value of the constant α found to be approximately 0.5.

The Kolmogorov spectrum assumes isotropic turbulence and although eddies are generally produced highly anisotropically, the straining action of larger eddies on smaller tends to smooth out the anisotropy at smaller scales, so that an assumption of isotropy is justified in many situations. However Anwar [1981] observes that the '-5/3' decay can occur in non-isotropic flows.

2A2.5 Subranges.

The molecular diffusivities of heat and particles become important in the transport of heat and suspended solids as scales become smaller. Microscales, $\chi = \sqrt[4]{(\nu \varkappa^2/\varepsilon)}$ where $\varkappa$ is diffusivity, similar to the Kolmogorov microscale may be defined to compare the importance of turbulent and molecular processes (for example as ratios of the diffusivities of heat, salinity, suspended solids to that of momentum). The relative sizes of the different microscales have effects on the forms of the temperature and suspended solids concentrations fluctuations. In particular a viscous convective subrange may exist beyond the inertial range, where molecular diffusion acts to smooth out fluctuations; beyond this subrange lies the viscous dissipative range of wave numbers, where viscosity rapidly reduces velocity gradients. In a viscous convective range ($\eta > 2\pi/k > \chi$) the spectrum is expected to vary as k^{-1} [Hinze 1975, Garrett 1989].

2A2.6 Inertial Dissipation Method.

The inertial dissipation method of obtaining turbulence statistics uses the tendency towards isotropy of turbulence at scales removed from the production range to simplify the derivation of turbulence parameters from current

measurements [Grant et al. 1984, Huntley and Hazen 1988]. Since isotropy may be assumed in the inertial range (under non-stratified conditions), the alignment of velocity sensors is not critical; misalignment by 90° results in an error in the one dimensional turbulent energy spectrum of only 33%, or 50% in the dissipation rate (since the ratio of transverse to longitudinal spectra, $E_{22}:E_{11}$ is 4:3) [Huntley 1988]. If a valid inertial range of dissipation is present then the theoretical spectrum $E(k)=\alpha\varepsilon^{2/3}k^{-5/3}$ may be fitted and the dissipation rate, ε, obtained.

It should be noted that the dissipation rate, ε, does not account for the dissipation of all the turbulent energy produced but only that reaching to scales smaller than the production range; mixing against salinity or suspended solids gradients and erosion may be removing energy at larger scales.

Use of the inertial dissipation method is essentially a filtering system for removing the influence of variable large scale energy from the turbulence statistics applicable to the smallest scales.

2A3 Estuarine Aspects

2A3.1 Boundary Layer.

In open channel flow friction is applied at the bed and this bed shear stress is transmitted through the bulk of the flow resulting in a mean velocity profile, $U(z)$, that reduces to zero flow at the bed and has zero stress at the surface. In laminar flow the velocity profile is parabolic while in turbulent flows the parabolic form is modified because the turbulence transports momentum vertically. Theoretical turbulent profiles can be derived [*eg* Dyer 1986 or, somewhat differently, Hou and Kuo 1987] and the main feature is a boundary layer near the bed in which vertical turbulent fluctuations are suppressed and mean flow is reduced.

A turbulent boundary layer can be considered as having three layers: (1) the viscous sublayer in which mean flow increases linearly with height and which transmits the fluid stress to the bed; (2) the 'logarithmic' layer in which turbulence becomes important for momentum transport; and (3) the outer region in which the effect of the bed is less apparent [Dyer 1986]. For estuarine flows the viscous sublayer is of the order millimetres in thickness (and does not exist in

a rough turbulent boundary layer) and the logarithmic layer includes most of the flow. The friction velocity, u^*, parametrizes the near bed flow

$$U(z) = \begin{cases} (u^*)^2 z/\nu & \text{viscous sublayer} \\ u^* [2.5 \log_e (u^* z/\nu) + 5.5] & \text{log. layer} \end{cases} \quad (2.11)$$

so that the bed shear stress is $\rho(u^*)^2$.

Anwar [1981] compares laboratory and estuarine turbulence measurements and documents the main observable features of turbulent tidal flows. In particular the logarithmic profile is observed in estuaries and the variation of turbulent intensity with height above bed is presented. The intensity, $\langle u^2 \rangle^{1/2}/U(z)$, decreases by a factor of two between the bed (where the value is 0.05 to 0.1) and the surface. Turbulent intensities and drag coefficients, $C_D = (u^*/U_{surface})^2$, also vary depending on whether the tidal flow is accelerating or decelerating. Typical values for the drag coefficient are around 2×10^{-3} over mud beds (and taking $U_{surface}$ to be the mean speed at 1m above the bed) [Dyer 1986]; thus $u^* \approx 0.05U$ approximately.

Gust and Walger [1976] find that the thickness of the viscous sublayer is increased in the presence of high concentrations of cohesive sediments with consequent reduction in shear transmitted by the layer. This effect may be important in the turbidity maximum region of the estuary where it would tend to augment the accumulation of fluid mud by inhibiting erosion and aiding deposition. Adler and Mills [1979] also predict this shear thinning behaviour in their mathematical model of flow through flocs.

Mixing length models of turbulence scale the size of turbulent eddies with distance from the wall (and surface), resulting in the logarithmic mean velocity profile. In order for an inertial dissipation range to exist the turbulence must be isotropic and this in turn requires that the eddies observed are not flattened by proximity with the bed (or surface). Thus isotropy requires $k \gg 1/(\text{height of sensor})$. Huntley [1988] discusses the use of the inertial dissipation method in boundary layer flows; however in the present work bed stresses are not required and it was not necessary to measure in the non-isotropic range of eddies.

2A3.2 Decelerating Flow.

In the equations for the rate of change of mean kinetic energy (Eqn. 2.3) a positive pressure gradient makes a negative contribution to $D_t(MKE)$ and increases the turbulent kinetic energy. This effect has been observed in estuaries and shows up as a tidal hysteresis in turbulence parameters as the surface slope varies during the tidal cycle [Gordon 1975]. Gordon [1974] and others [Heathershaw 1974, Jackson 1976] draw attention to the increased 'bursting' phenomenon in decelerating flows which increases the bed shear stress and results in increased resuspension. Bursts are coherent vortex structures in the flow which carry fluid from fast moving outer layers into the viscous sublayer, or cause ejection of slower (sediment laden) fluid outwards. The structure of bursts and statistics of their duration and frequency are studied by quadrant analysis of the vertical and horizontal velocity perturbations. The four types of event are: sweeps - for which faster moving fluid moves downward; ejections - where slower moving fluid moves outward; and outward and inward interactions where the product *uw* is positive [Offen and Kline 1975; Jackson 1976]. Anwar [1981] finds that ejections and sweeps make the largest contribution to the Reynolds stress and that the increased Reynolds stress in decelerating flows is due to increased duration of bursting events rather than increased frequency.

The effect of bursting is to increase resuspension of sediment [Jackson 1976] and this is borne out by the quadrant analysis of suspended solids fluxes in the Tamar [West and Oduyemi 1989] and the theoretical study of Wei and Willmarth [1991].

2A3.3 Richardson Number.

When less dense water overlies more dense, or there is a vertical density gradient, any mixing of the two requires the raising of the centre of gravity of the fluid. The extra energy needed for mixing comes from the mean flow via turbulence. The (dimensionless) *Richardson number* ($Ri = -g\rho_{,z}/\rho U_{,z}^2$) of a flow compares the potential energy needed to overcome buoyancy with the kinetic energy available from the flow. Theory [Turner 1973] predicts that a stratified flow becomes unstable when the Richardson number at some level within the flow falls below a critical value of $Ri = 1/4$. Conversely, when the

Richardson number is large, vertical turbulent mixing is suppressed and internal waves may form [West and Shiono 1988].

The data obtained during this experimental work is not sufficiently accurate for the evaluation of usable Richardson number estimates at each depth in the flow but, following New et al. [1986], a bulk Richardson number for the flow is obtained as

$$Ri = -g\Delta\rho h/\rho U^2 \qquad (2.12)$$

where $\Delta\rho = \rho_{surface} - \rho_{bed}$, U is the depth mean current and h is the water depth. Based on the form of observed salinity spectra $\hat{s}(k)$ in the Tees, New et al. [1986] suggest that the Richardson number may be used to distinguish between flows where internal waves dominate ($\hat{s} \sim k^{-3}$) and those where turbulent mixing is occurring ($\hat{s} \sim k^{-5/3}$); a value of $Ri \approx 30$ separated turbulent flows ($Ri > 30$), from internal wave flows ($Ri < 30$).

Part (B) Flocs

2B1 Primary Particles

2B1.1 Primary Particles and Bonds.

The cohesivity of cohesive sediments is due to the presence of clay particles. These clay particles are in the form of platelets of minerals such as illites, montmorillonites and kaolinites which, because of their chemical structure, tend to carry negative electrical charges on their faces and positive charges along their edges [van Olphen 1976, Dyer 1986]. The platelets have sizes up to about 2 μm.

In water containing few ions electrostatic attraction causes aggregation of platelets in an open 'edge to face' structure. (see Fig. 2.3, also Partheniades [1986]).

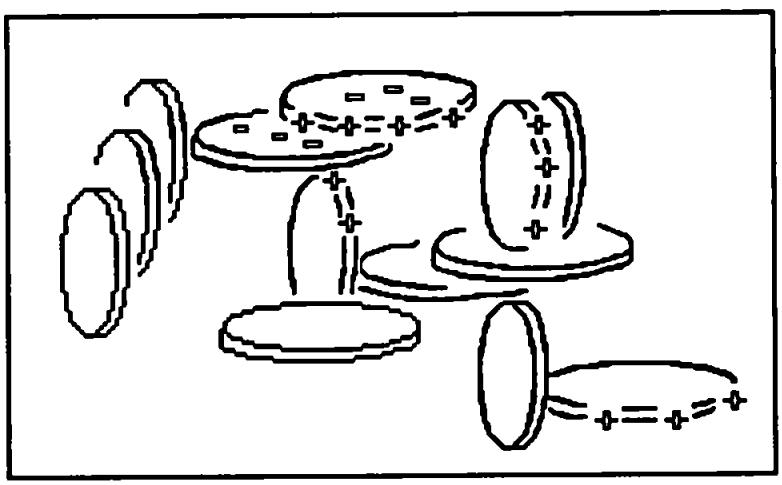

Fig. 2.3 Arrangement of flocculated clay platelets (Microflocs).

When immersed in an electrolyte positively charged ions gather around the negatively charged faces of the platelets forming a 'screen' around them. In a weak electrolyte the assemblage of platelets and ions is positively charged with respect to the bulk of the solution; that is the ions swarm most densely near the clay particles, with the result that the assemblages become mutually repulsive. In this state the suspension is colloidal [van Olphen 1976].

If the concentration of dissolved salts is increased the excess of charge near the clay particles over that of the bulk of the solution is reduced and so the repulsive forces are reduced. Particles can now approach each other

closely enough to bond electrostatically or by van der Waal's forces. Relatively dense structures can form in this destabilised suspension and these constitute 'microflocs' [Krone 1978]. Microflocs have diameters in the region of 5 to 20 microns and are effectively indestructible with regard to physical estuarine processes. Microflocs, then become the basic building blocks for estuarine flocculation processes. In laboratory experiments on microfloc formation with various clay minerals, Krone [1978] concludes that flocculation occurs when the salinity exceeds 0.6‰ to 2.4‰ and and is not greatly enhanced when salinity increases beyond about 4‰. Salt flocculation is thus important mainly in the head waters of the estuary where suspended material first enters the marine system.

In the estuary microflocs acquire a coating of organic molecules from various sources, including mucopolysaccharides [Eisma et al. 1983, 1986; Hicks 1988] secreted from mud-dwelling organisms, such as diatoms and bacteria. The mucus is used to bind the microbe to sediment particles on the mud surface which may later be eroded and form part of the suspended load. Mucus is also produced by diatoms during locomotion. Paterson [1989] relates the erodibility of mud beds to the diatom activity at the surface and gives evidence for the bonding of sediment particles by mucillages. When the mud beds dry out, mucillages may degrade and become easier to erode [Paterson 1989], and rafts of bound microbes and sediment may be lifted off the mud surface by surface tension [Hicks 1988]. Tsai and Lick [1988] find that biological bonding of bed sediments significantly alters their resuspension characteristics and, in particular, introduces a time dependence in the critical erosion stress.

The flocs taking part in estuarine processes are microflocs and aggregates of microflocs which are held together by biological polymers.

2B1.2 Factors Affecting Bond Strength.

Salinity may affect both biological and electrostatic flocculation mechanisms. Seawater contains dissolved salts and the nature of these determines the thickness of the electrostatic double layer around clay platelets and hence the probability that colliding flocs can come close enough to bond. However, Eisma [1986] finds that estuarine flocs are not as sensitive to salinity as might be expected from consideration of the electrostatics involved; observing the organic

content of flocs in the Ems he suggests that seawater at larger salinities has a deflocculating effect on aggregates of microflocs because of the action of dissolved borates on the carbohydrates in the organic coating.

The *p*H of the water is of great importance in the aggregation of clay platelets to form microflocs [Krone 1978]. The mineral composition of the primary particles is also important (clay minerals involved are illites, montmorillonites and kaolinites in varying proportions [Dyer 1986]). These factors influence the strength of the microflocs which are produced in the low salinity head waters of the estuary, however at larger scales microfloc-microfloc bonding by organic molecules occurs. The electrostatic properties of the organic coatings of estuarine particles are found to vary relatively little within and between estuaries and, moreover, their organic coatings are the controlling factor for flocculation [Hunter and Liss 1982].

2B1.3 (Table 2.1) Relative Scales of Turbulence and Particles.

1 µm			
5	clay particles		
10	microflocs	↑	
50	small flocs	laser sizer range	
100	(pA-pA^n)		*Kolmogorov microscale η(ε) (smallest eddies)*
500	large flocs	↓	*η(1000)= 60µm (v.turbulent)*
1 mm	largest flocs		*η(100) = 100 µm*
5			*η(1) = 320 µm (quiet)*
1 cm			
5			
10	inertial range turbulence		
50			
1 m	production of turbulence		
5			

2B2 Flocs

2B2.1 'pAA' Structure.

It has been observed in a variety of experiments, including microscopy [Krone 1978], settling columns [Tambo and Watanabe 1979] and laser diffraction [Sonntag and Russel 1986], that flocs become more diffuse in structure with increasing size. This has been observed in estuarine and laboratory flocculation

processes involving various particles and coagulants [*eg* Sonntag and Russel 1986 - latex beads; Bache and Alani 1989 - alum flocs; Rarity 1989 - colloidal gold] and can be explained on the supposition that flocs of a similar size tend to aggregate.

Van de Ven and Hunter [1977] proposed the structure of Fig. 2.4. A floc consists of a hierarchy of aggregates of larger and larger flocculi: primary particles (p) aggregate to form flocculi (pA) which in turn aggregate to form flocs (pAA) and so on. (The notation p, pA, pAA,.. follows Krone 1963 [Krone 1978])

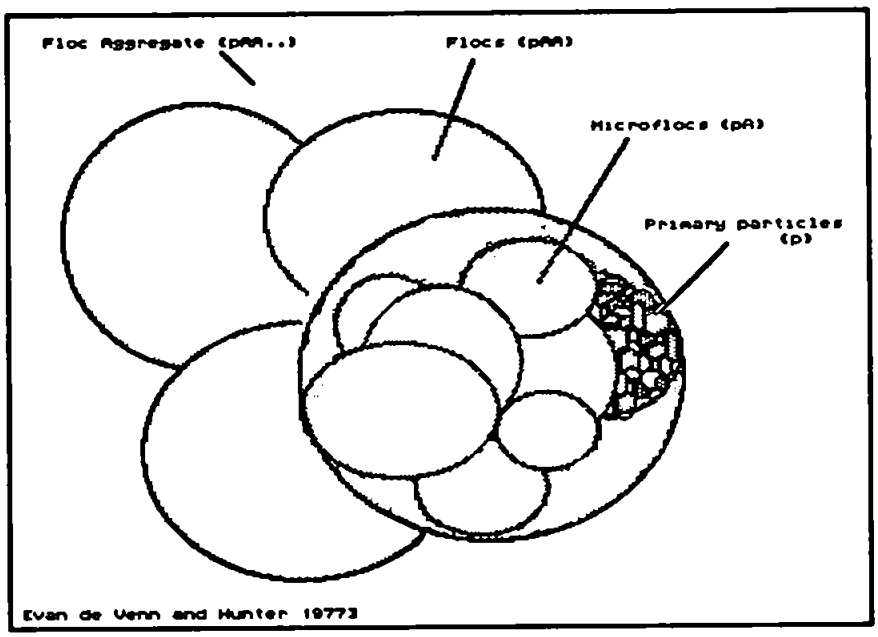

Fig. 2.4 Floc as aggregate of aggregates.

2B2.2 Fractal Description of Flocs.

The 'aggregate of aggregates' model of van de Ven and Hunter [1977] describes the decrease in density with floc size and suggests that floc structures have a fractal dimension [Mandelbrot 1983]; that is, the structure of flocs is similar at widely different scales. An often quoted example (due to Richardson [Mandelbrot 1983]) of a fractal curve is the coastline of Britain which seems to be similarly indented whatever the scale of map used.

Although not explicitly using fractal dimension Tambo and Hozumi [1979] use the approach to estimate the number of bonds holding flocs together and derive strength relationships. By noting that the intersection of a plane with an object of fractal dimension *D* has dimension *D-1* the cross-sectional area of flocs can be estimated and the number of bonds crossing this cross-section

obtained [Tambo and Hozumi 1979]. (Sreenivasan and Meneveau [1986] use this result in their analysis of the fractal dimension of turbulence). Tambo and Hozumi [1979] obtain the fractal dimension of flocs from settling column data [Tambo and Watanabe 1979].

Mandelbrot [1983] defines a 'self-similar' object as being similar geometrically to an enlarged portion of itself. If the scaling factor required is R then the fractal dimension D, is defined in terms of the number of repetitions, N, of itself that are used in producing a larger version of itself: $N=R^D$ or $D=\log N/\log R$. Fig. 2.5 illustrates flocs of various dimension, with floc volume expressed as number of primary particles used, n, and floc diameter as multiples of primary particle diameter, d. For any two stages i, j, the scale factor and volume factor are given by $R=d_i/d_j$ and $N=n_i/n_j$ respectively.

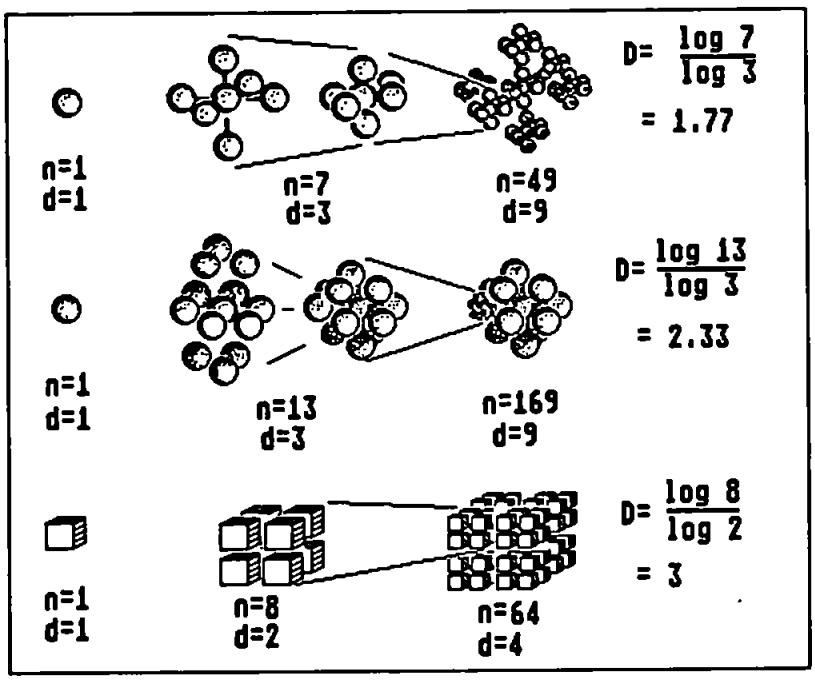

Fig. 2.5 Examples of Fractal Flocs. The solid floc (D=3) gives the usual mass /diameter relationship $m=\rho_0 d^3$, while a more 'stringy' floc which grows by attaching similar flocs to its arms, and has dimension D=1.77, becomes more and more tenuous as its diameter increases and gives $m\sim\rho_0 d^D$ so that $\rho_{eff}\sim\rho_0 d^D/d^3$. The floc which grows by surrounding itself at each stage with similar sized flocs has intermediate dimension, D=2.33.

The effective density of a floc is defined by its weight in water. In the notation of Fig. 2.5 effective volume is $\pi d^3/6$ while weight is given by $n\rho_0\pi d_0^3/6$ where ρ_0 is the primary particle effective density and d_0 is primary particle diameter. Thus floc effective density is given by $n\rho_0 d_0^3/d^3$ or $\rho_0 N R^{-3}$, and a

power law dependence of effective floc density on floc diameter is expected:

$$\rho_{eff} = a d^{D-3} \qquad (2.13)$$

The data of Tambo and Watanabe [1979] shows this behaviour with a fractal dimension of 2.1 down to 1.5. Work done by Alani et al. [1990, unpublished] on estuarine mud gives *D=1.8* to *2.0*. Sonntag and Russel [1986] find *D= 1.6, 2.2, 2.5* depending on the shear history of the flocs.

2B2.3 Limiting Effect of Turbulence.

The processes that bring flocs into contact with one another are discussed in part 2C; however it is important to note here that aggregation by collision proceeds fastest in a turbulent environment.

An opposite effect of turbulence is to apply stresses to the surfaces of flocs which result in deformation of the floc. Normal forces, due to turbulent pressure fluctuations, and tangential viscous shears can each cause breakup of a floc if the internal bonds are stressed enough.

A large straggly floc has fewer internal bonds than a more compact floc of the same diameter and would not be expected to withstand as high fluid shears across its body. The number of bonds can be estimated as proportional to cross-sectional area, which in turn varies as diameter to the power *D-1*. It can be seen that small flocs will be more likely to survive in a turbulent environment, while the same turbulence will also be tending to re-aggregate the fragments of larger flocs that have been disrupted.

Adler and Mills [1979] derived theoretical conditions for the rupture of a porous sphere of uniform density in a linear shear field, and Sonntag and Russel [1986] obtain the radius at which this rupture occurs. Due to the limited penetration of the flow into the sphere the rupture occurs at the centre of small diameter flocs, but moves rapidly to the surface as the diameter increases above a critical value. In the Adler and Mills theory, uniform density (*D=3*) flocs may grow indefinitely when the shear is less than a critical value. The critical shear is given by the asymptote of rupturing shear as diameter increases: for the fractal floc it seems unlikely that this asymptote exists (since the strength of floc decreases more rapidly than in the model considered): that is - floc growth is limited in even low energy environments. (This difference in radius of floc rupture

corresponds to the difference between the 'bulgy' fracture and surface stripping of flocs which are further discussed in section 2C2).

2B3 Floc Behaviour

2B3.1 Settling Velocities.

Particles settling under the action of gravity through a fluid reach a terminal velocity, or settling velocity, w_s, where their (immersed) weight is balanced by the frictional drag. Tambo and Watanabe [1979] document the equation for flocs of diameter, d_f as:

$$w_s \approx \frac{g}{34\mu} \rho_{eff} d_f^2 \qquad (2.14)$$

They then go on to obtain floc effective densities from observations of settling velocities of flocs formed under varying conditions. Their results have been used by McCave [1984] to model floc properties in the sea and typical values are presented in Table 2.2.

Table 2.2 Settling Velocities and Effective Densities of Flocs

dia [μm]	w_s [mm/s]	ρ_{eff} [g/cm^3]	porosity	K	D	
0.1	4×10^{-6}	1	0.375	0	3	
1	4×10^{-4}	1	0.375	0	3	
5	5×10^{-3}	0.506	0.68	0.42	2.58	
10	0.01	0.378	0.76	0.42	2.58	
50	0.17	0.191	0.88	-	-	
100	0.28	0.078	0.95	1.3	1.7	McCave 1984
200	0.46	0.032	0.98	1.3	1.7	
500	0.87	0.010	0.994	1.3	1.7	
1mm	1.41	0.004	0.998	1.3	1.7	
100μm to 1mm	0.4 to 2.0	0.06 to 0.02	0.988 to 0.992	1.0 to 1.18	2.0 to 1.82	Alani 1990

K is exponent in the density/diameter relation - $\rho_{eff} = ad^{-K}$
D is the fractal dimension $D = 3-K$

Approaching from the opposite direction many studies have been made of settling velocity of particles taken from flows. Typical estuarine flocs have median settling velocities (w_{so}) of 0.1 to 3 mm/s [Bale et al. 1988]. Because of the difficulties in measuring floc sizes most of these studies present median settling velocity as a function of concentration [Owen 1971, Bale et al. 1988, West et al. 1990] A power law dependence of settling velocity on concentration is generally fitted:

$$w_{so} = aC^m \qquad m \sim 1.0\text{-}2.0 \qquad (2.15)$$

Results from the Thames indicated that m varies over the spring-neap cycle of tides with greater settling velocities being obtained at neap tides ($m \approx 2.2$) than at springs ($m \approx 1.08$) [Owen 1971], with the implication that the higher turbulent energy at springs was responsible for breaking up flocs into more slowly settling parts. The reduction of particle sizes during strong ebb and flood conditions has also been observed using *in-situ* sizing in the Tamar [Bale et al. 1989].

It should be noted that although Burt [1984] found comparable settling velocity/concentration relations and m values in other muddy estuaries, he found no spring/neap variation in m.

2B3.2 Effect of Concentration.

There are a number of ways in which the suspended solids concentration may be expected to influence settling velocity and it is not obvious which, if any, is dominant. Field observation of settling velocities of estuarine particles consistently provide positive m values for equation 2.15, that is median settling velocity increases with increasing concentration. In laboratory experiments on the settling of estuarine particles Lick and Lick [1988] found that the median size of particles is reduced when the concentration in a stirred vessel is increased. This suggests that the observed increase in estuarine settling velocity is due to increased floc density. Burban et al. [1990] find floc density increases when the flocs are produced at high concentration or under conditions of strong shear. A complicating factor in the understanding of these phenomena is that significant disaggregation must be attributed to three body collisions [Burban et al. 1989] (see also section (2C2.1).

If concentrations are very high and the volume fraction of solids large, settling is slowed hydrodynamically, since the space between particles is considerably restricted. The influence of this hindered settling may be strong in fluid mud layers but for floc samples obtained at practical heights above the bed is not important. Note that a typical estuarine suspended solids concentration is 1000 mg/l (*eg* in the turbidity maximum); if this suspended matter were in the form of flocs of porosity 0.98, with primary particle density 2.65 g/cm^3, the volume fraction would be just under 1% - concentrations in fluid mud layers near the bed are of course much higher.

The concentration is also important in determining the rate of interparticle collisions and hence the degree of flocculation - this aspect of the effect of concentration is dealt with in part 2C.

2B3.3 Effect of Turbulence on Settling.

The settling velocities obtained from settling columns relate to particles settling vertically through still water. The rate of settling for a particle in a turbulent fluid has been observed to be reduced, due to the action of non-linear drag forces. Ludwick and Domurat [1982] review previous work and model turbulent settling. They find the magnitude of retardation to be negligible for quartz particles of diameter 100 μm but suggest that the effect increases with decreasing diameter. It seems likely that the uncertainty in the density of particles settling in the estuary is more important in influencing deposition rates.

Turbulent diffusion of particles will affect settling velocities when a gradient in dissipation rates is present since the fluid velocities, and hence particle displacements, will not be isotropic. Turbulent intensities are known to vary with height above the bed [Hinze 1975, Anwar 1981] with the intensity slowly increasing towards the bed: this will have the effect of increasing settling velocity due to the increased length of turbulent random walk as particles settle downwards. The magnitude of this effect will be masked by the turbulent diffusion of any concentration gradient which is likely to exist under such circumstances.

The effect of suspended particles on turbulence has been investigated by Gore and Crowe [1988] who find that a suspension of particles with small diameters compared to eddy size removes energy from the turbulence, while particles with large diameters relative to eddy size introduce turbulence by causing a turbulent wake. The work used in their review was mostly with jet and pipe flows so that it is difficult to relate it directly to estuaries, although the cut off at the Kolmogorov microscale seems reasonable. However floc breakup and aggregation processes are likely to be complicating the problem at these scales.

Part (C) Floc Aggregation and Disruption

2C1 Aggregation

2C1.1 Aggregation Kernels.

Aggregation occurs when two particles are brought close together and stick. There are several processes that bring particles together in a turbulent flow and these can be modelled by their effect on particle size distributions. There is less known about the 'collision efficiency' - the fraction of collisions which lead to new aggregates. McCave [1984] uses a nominal efficiency of 10% but observes that the organic coating of particles may play a large part in determining their 'stickiness'; here it is the processes which are of interest and the collision efficiency is taken to be unity in order that the different processes may be compared.

McCave [1984] also points out that the biota may also be responsible for producing aggregates on scales from that of faecal pellets to that of agglomerations of bacteria [Muschenheim et al. 1989]. The interactions of suspended matter with microbes are discussed further in relation to the turbidity maximum in section 2D3.

In modelling the aggregation, by two body collisions, of a distribution of particles in suspension, there are two contributions to the overall change in number of aggregates in any size band; (i) there are additions when two smaller particles collide and stick, entering the band; and (ii) there are collisions involving particles in the band which are then removed to larger bands.

This can be represented by 'collision kernels' which characterise the various coagulation mechanisms [Jeffrey 1982]. A survey of the main collision kernels is presented in McCave [1984]. The number distribution, $n(v)$, of particles of volume v, and diameter d, in each size band $d_i < d < d_{i+1}$ satisfies -

$$dn_i/dt = \tfrac{1}{2}\sum_{j<i} K_{ij}\, n_{i-j} n_j \;-\; \sum_{all\ j} K_{ij} n_i\, n_j \qquad (2.16)$$

(K includes the 'sticking' efficiency)

The collision kernel has the dimensions of 'collisions per unit time per unit volume' so that dn_i/dt is the rate of increase in number of particles in the i-th band. The first term counts all collisions between particles that combine to

form a particle of diameter d_i (counted twice - hence the factor of ½). The second term counts all collisions involving particles of diameter d_i since these increase the size of the aggregate.

The collision kernels K_{ij} [from Glasgow and Kim 1989] are

$$B_{ij} = \frac{2kT}{3\mu}\frac{(d_i+d_j)^2}{d_i d_j} \qquad L_{ij} = \frac{4}{3}\frac{dU}{dz}(d_i+d_j)^3 \qquad I_{ij} = \frac{1.27\rho_e}{\mu}\sqrt{\frac{\varepsilon^3}{\nu}}(d_i+d_j)^3|d_i-d_j|$$

$$T_{ij} = 2.3\sqrt{\frac{\varepsilon}{\nu}}(d_i+d_j)^3 \qquad G_{ij} = 0.7\frac{g\rho_e}{\mu}(d_i+d_j)^3|d_i-d_j| \qquad (2.17)$$

and describe the rates at which two particles come close to each other under the mechanisms of Brownian motion B, laminar shear L, turbulent shear T, turbulent inertia I and differential settling G, but do not take into account the liklihood of particles not sticking after collision. Inspection of the theoretically derived kernels highlights the more important mechanisms. (Note that the kernels given above assume no density change with floc diameter.)

2C1.2 Brownian Motion.

Small particles in suspension are buffetted by the thermal motion of fluid molecules. The random nature of this buffetting results in particles performing random walks through the fluid. Particles which approach each other closely enough stick. This process is most efficient where the suspended particles are small. McCave [1984] considers a monodisperse suspension typical of oceans and obtains the time (t_c) over which half the particles coagulate,

$$t_c = 3\mu/4kTN \qquad (2.18)$$

(where μ is dynamic viscosity, k is Boltzmann's constant, T is absolute temperature and N is the initial number density of particles). Substituting typical estuarine values (C= 100 mg/l, d= 10 μm) gives t_c= 1 hour suggesting that Brownian motion may not be the most important mechanism in high energy environments.

2C1.3 Shear.

In a shear flow particles are brought into contact with each other when carried along when an overtaking particle hits or approaches closely a slower particle. This mechanism is obviously affected by the rate of shear and size of particles. The shear may be laminar, when the kernel is given by L, or due to turbulent motions in which case the kernel is T.

Comparing kernels for Brownian motion and turbulent shear under typical estuarine conditions (C= 100 mg/l , ε=100 cm^2/s^3) shows turbulent shear to be the more important mechanism in the size range of flocs. Note that the ratio T_{ij}/L_{ij} depends only on the ratio of turbulent mean shear $\sqrt{(\varepsilon/\nu)}$ to shear dU/dz. In estuarine flow the mean shear is generally smaller than the turbulent mean shear except in the regions closest to the bed. Typical values observed during this fieldwork were $dU/dz \leq 1$ s^{-1} over the lower 50 cm and $\sqrt{(\varepsilon/\nu)} \geq 10$ s^{-1}.

2C1.4 Turbulent Inertia.

In turbulent flow particles of differing density may be brought into contact due to the inertia of the larger particle; the heavier particle does not follow the fluid motion as closely as the smaller. This is most effective when particles are very different in size. Again the kernel may be compared with that for turbulent shear, however the relation varies with the particle size distribution. A comparison of I and T is plotted in Fig. 2.6 (plot X1 in Appendix X) using the density-size relation from McCave [1984]. The greatly increased collision rate when flocs of greater than 500 µm are present with small particles is apparent.

The plots in Fig. 2.6 were produced by evaluating the kernels of equations 2.17 for values of d_i, $d_j \in \{$ *1µm, 2µm, 5µm, 10µm, 20µm, 50µm, 100µm, 200µm, 500µm, 1mm* $\}$ and corresponding densities from McCave [1984]. Contour plots of $log_{10}\ K_{ij}$ against $log_{10}\ d_i$ and $log_{10}\ d_j$ were made for T and I for two dissipation rates *1000* cm^2/s^3 and *1* cm^2/s^3. The sum of T *and* I is also plotted, *viz.* $log_{10}(T_{ij}+I_{ij})$. The distinctive form of I highlights the dependence of turbulent inertial aggregation (and differential settling) on size differences.

2C1.5 Differential Settling.

The collision kernel is similar in form to that for turbulent inertia. Different sized particles settle at different rates and the largest 'sweep up' the smaller. G_{ij} is proportional to the difference in settling velocities so that when widely dissimilar sized particles are present differential settling can be a major contributor to aggregation. Comparison of the kernels for gravitational capture and turbulent inertial capture shows that they are equally important in high energy environments ($\varepsilon \approx 1000$ cm^2/s^3) while under quiet conditions ($\varepsilon \approx 1$ cm^2/s^3) differential settling is approximately 200 times more effective. The plot of

aggregation kernels (Fig. 2.6 Appendix X) can be interpreted as showing that knowledge of the turbulent shear aggregation rates gives the correct order of magnitude of aggregation processes over the range of particle sizes, although gravitational settling must be taken into account during quiet periods when large and small particles are present - such conditions exist in the Tamar at HW springs in the region of maximum deposition.

2C1.6 Summary.

As far as estuaries are concerned turbulent shear is the most important mechanism of aggregation since it is relatively fast at all scales. However in quiet conditions differential settling gives the maximum aggregation rates.

Consider a suspension of particles having mass concentration C, If all the particles are in the form of flocs of diameter d and density ρ then the number density will be $n(i)= C/\rho d^3$. If the concentration is C=100 mg/l and all the particles are microflocs of diameter 10 μm, and density 1.4 g/cm^3 (see section 2B3.1), then the number density is $n(i)\approx 7\times10^4$ [per cm^3]. If these particles are flocculated to give flocs of diameter 500 μm (density 1.01 g/cm^3) the number density is $n(i)\approx 0.8$ [per cm^3].

If the suspension were 90% microflocs of diameter 10 μm and 10% flocs of diameter 500 μm then the kernel $G_{10\mu m,500\mu m}$ for gravitational settling (small with large flocs) is of the order *1*, giving an initial aggregation rate of order $(0.9\times7\times10^4 \times(0.1\times0.8)\times1 \approx 5\times10^3$ [small particles swept up per second per cm^3]. If this rate of aggregation is continued all the smaller particles ($\approx 7\times10^4$) are scavenged by the larger particles in less than a minute. The initial aggregation rate is, of course, not maintained since it is proportional to the number of small particles remaining and hence decreases exponentially with time. However the vast majority (~99% using $n\sim e^{-\lambda t}$, λ the initial rate) of all particles will be removed in one hour, over which time the larger particles settle through about 3 m. These figures are representative of conditions at HW conditions in the upper Tamar.

2C2 Break-up

2C2.1 Disruption Kernels.

Collision kernels can be used to describe empirically the breakup of flocs although little is yet known of the theoretical form or applicability of such functions. The general form of the disaggregation equation, corresponding to equation 2.16, involves the probabilties that particles breakup due to the action of turbulence, and the probabilities that particles breakup after collisions with other particles. The terms involving turbulent breakup are linear in the concentrations n_i, while the terms involving collisions between particles from bands i and j involve quadratic terms $n_i n_j$. Burban et al. [1989], observing that experiments show median floc diameter to decrease with increasing concentration, show that there must be cubic terms, $n_i n_j n_k$, involved in the rate equation. These terms they account for by three-body collisions causing disaggregation at high concentrations.

For a distribution that is limited by floc breakup in the largest sizes, the most useful parameter is the maximum floc diameter d_{max}. This may be defined rigourously as the diameter below which, say, 90% of floc diameters fall [Alani 1987], although it is of most use for distributions which are highly skewed towards large sizes where d_{max} approximates a cut-off in the distribution. Since particles of many different sizes and origins are present an estuary, d_{max} is not an absolute cutoff size. However it has been found in this work that it can usually be approximated by inspection of the laser sizer histograms.

2C2.2 Floc Model.

As indicated in 2A1.3 flocs can be expected to remove energy from their surroundings during breakup - it is this energy which causes fracture. A floc which is about to rupture is first distorted so that the internal bonds, electrostatic or organic, are stretched to the limit of their tensile strength. During this distortion the fluid within the floc also dissipates energy. Van de Ven and Hunter [1977] use their model of floc structure (Fig. 2.4) to estimate the amounts of energy dissipated in the three processes illustrated in Fig. 2.7. Part of the energy is dissipated in stretching the internal bonds to breaking point: as the constituent microflocs, or flocculi, are stretched apart their motion is resisted by the viscosity of the water contained within the floc: this drag is estimated from

Stokes' equation; the internal fluid must also move to accommodate the change in shape of the floc, and viscous dissipation within the fluid accounts for further energy loss. Van de Ven and Hunter [1977] concluded that the viscous dissipation within the internal water was the most important of these mechanisms.

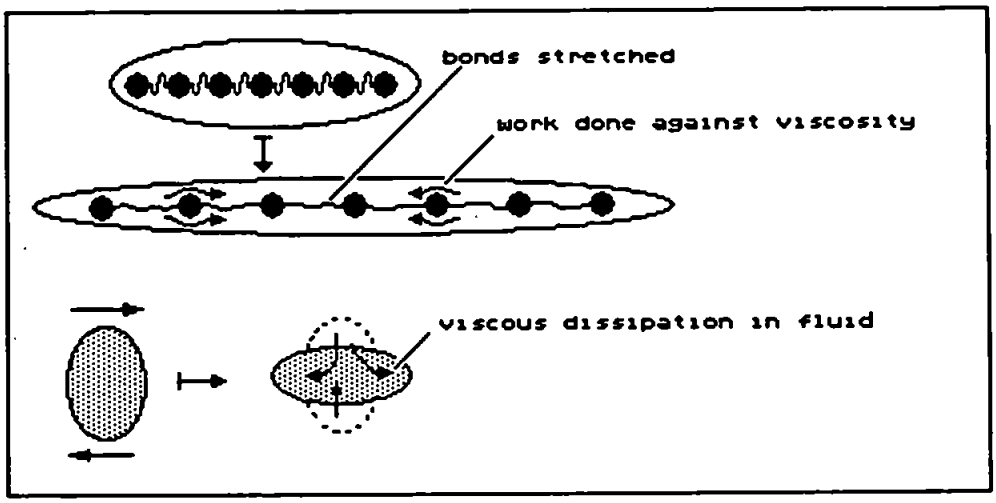

Fig. 2.7 Energy dissipation mechanisms during rotation of floc in shear flow.

2C2.3 'Bulgy Fracture'.

When turbulent eddies are large, the floc is carried along by the eddy. As the size of eddy decreases, the flow varies with position over the surface of the floc, and this results in pressure fluctuations across the floc. For oil droplets this can result in rupture and Thomas [1964] proposed that a similar process might be the cause of floc breakup. The magnitude of the pressure difference across the floc may be estimated from the turbulent dissipation rate using Batchelor's result [Hinze 1975]

$$\langle (p_a - p_b)^2 \rangle = \langle (u_a - u_b)^2 \rangle^2$$

and

$$\varepsilon = 15\nu u^2/\lambda_g^2 . \qquad \lambda_g \text{ the Taylor microscale.} \qquad (2.19)$$

Tambo and Hozumi [1979] use this with estimates of the number of bonds within a floc to predict the maximum stable floc size in a given turbulent regime. Alani [1987] (see section 2D2 below) refined the experimental verification of Tambo and Hozumi [1979] results (*T&H*) and gave the result (for $d < \eta$)

$$d_{max} = A\varepsilon^{-\gamma}, \quad \begin{matrix} 0.33 < \gamma < 0.38 & d \ll \eta & \text{[Alani, T\&H]} \\ 0.4 < \gamma < 0.5 & d \gg \eta & \text{[T\&H]} \end{matrix} \qquad (2.20)$$

2C2.4 Surface Stripping.

If the turbulent eddies are small compared with the floc then the floc as a whole cannot respond to each influence but, if the local shear is strong enough, particles or flocculi may be stripped from the surface of the floc. Parker et al. [1972] estimate d_{max}, and the rate of erosion from the surface of (fractal dimension $D=3$) flocs, by considering the maximum fluid shears produced by turbulence; the fluid velocities are obtained for both inertial range and viscous dissipation range turbulence. 'Filament fracture' is an alternative mechanism, similar in principle to 'bulgy fracture', where it is the viscous shear stress difference across a floc which causes fracture. The results of Parker et al. [1972] for floc disruption exponent γ, are:

$$\gamma = \begin{cases} 2 & d \ll \eta \\ 1 & d \gg \eta \end{cases} \Big\} \text{ surface stripping} \qquad \begin{cases} 1/2 & \text{filament fracture} \end{cases} \tag{2.21}$$

2C2.5 Summary.

The 'bulgy fracture' breakup mode seems to agree best with the experimental determination of floc breakup exponent γ for macroflocs [eg Bache and Alani 1989], although both mechanisms give similar qualitative behaviour. Note that Adler and Mills' [1979] porous sphere, which predicts a difference in breakup mode depending on turbulent scale (2B2.3), is discussed in terms of viscous flow equations and does not pre-select either mode of break up. Sonntag and Russel [1986] use it to predict the radius at which the sphere will rupture — their results show the two modes of fracture dependent on how far into the floc the external fluid motion penetrates.

Both 'bulgy' and 'stripping' models predict inverse power law dependencies of floc maximum diameter on turbulent dissipation rate, with surface stripping having the strongest effect on d_{max}. Experimental work, however, points to an exponent in the range 0.3 to 0.5 [Tambo and Hozumi 1979, Bache and Alani 1989].

Part (D) Flocs and Turbulence

2D1 Floc-size Distributions in Turbulence

2D1.1 Equilibrium Distribution.

The particle size distribution in a turbulent flow is brought about by the processes of aggregation and disruption working against each other. At the smallest scale are the primary particles which are not broken down even under the highest turbulent dissipation rates. At the largest scale are the flocs whose growth is limited by the turbulence - any further aggregation at this scale results in floc rupture. At each intermediate scale the size distribution is controlled by turbulence - a balance between aggregation and disruption is maintained.

Parker et al. [1972] present a distribution for a process controlled by surface stripping of primary particles and their subsequent re-aggregation. As expected this distribution is bi-modal with peaks in the primary particle range and at the size of maximum stable floc. Where fracture dominates, a less pronounced distribution is expected. However Burban et al. [1988, 1989], in laminar shear flows, obtain peaked distibutions with the mode size controlled by the shear rate. In turbulent flow, shears at many rates affect each floc and distributions are expected to be flatter.

Hunt [1982] used a dimensional argument, similar to that of Kolmogorov for inertial transfer of turbulent energy, to obtain a self-similar size distribution, and presents supporting experimental data. In Hunt's argument the (constant) particle volume flux (E) through the size distribution is analogous to the turbulent dissipation rate ε. Hunt [1982] expresses his results in terms of particle volume distribution: $dV/d(\log d)$ - the suspended volume in a logarithmic particle volume interval. $|B|$, $|L|$ and $|G|$ parametrize the coagulation mechanisms and are independent of particle size; $a(.)$ are dimensionless constants.

$$\frac{dV}{d(\log d)} = \begin{cases} a_{(B)}\sqrt{(E/|B|)}.\, d^{3/2} & \text{Brownian motion} \\ a_{(LS)}\sqrt{(E/|L|)}. & \text{laminar shear} \\ a_{(DS)}\sqrt{(E/|G|)}.\, d^{-1/2} & \text{diff. settling} \end{cases} \qquad (2.22)$$

These results are verified experimentally by Hunt [1982] for Brownian motion and laminar shear using kaolinite particles and, by computer simulation of particle collisions, by Pearson et al. [1984].

Maximum stable floc size, d_{max}, is the parameter of distributions most useful in describing aggregating/disaggregating systems, as it forms a cut-off scale above which there are few flocs; the floc distribution near d_{max} is not affected by the breakup of larger particles. Several laboratory studies have been made of the variation of d_{max} with turbulence dissipation rate (and in some cases shear rate - though Cleasby [1984] argues that dissipation rate is the more relevant parameter) resulting in a relation of the form $d_{max}=A\varepsilon^{-\gamma}$ (eqn. 2.20), where the exponent takes values in the range 0.3 to 0.5 [Parker et al. 1972, Tambo and Hozumi 1978, Bache and Alani 1989].

2D1.2 Timescales.

The time taken to reach a stable distribution after altering the local shear rate was also investigated by Burban et al. [1989] (under conditions not too dissimilar to estuarine). A time of the order of ten minutes was needed for stabilisation of the median diameter at the new value and fluctuations from the stable median diameter were observed over similar times. Turbulent intermittency of the flow is therefore expected to affect the final distribution since intermittency has shorter timescales than floc distribution alterations.

Gibbs et al. [1989] observed flocculation processes in muds from the Gironde estuary and give a time scale over which a steady distribution is built up of 30 to 120 minutes. For clay particles flocculated in the laboratory Gibbs [1983] found particle-number half-lives of between 10 and 40 minutes, comparable with the above characteristic timescales.

2D2 Floc strength

2D2.1 Vibrating column experiment.

In the experiments of Bache and Alani [1989, Alani 1987] flocs were disrupted as they settled in a column through increasing turbulence. The turbulence was maintained by a vibrating plunger at the base and the turbulent dissipation rates throughout the column were calibrated both calorimetrically and using tracer particles.

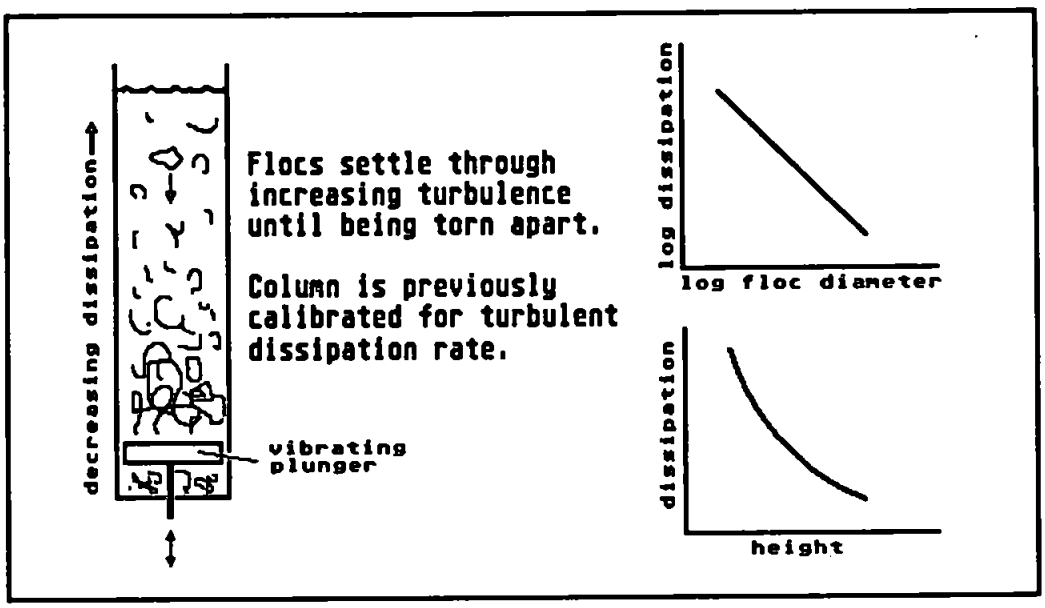

Fig. 2.8 Principle of laboratory floc-strength experiments.

As individual flocs were introduced at the top and settled they were recorded on a video camera and their size and the position at which they fragmented were noted. This enabled a d_{max} versus dissipation rate relation to be derived. Note that flocs were disrupted individually in clear water and so a possible disaggregation mechanism due to floc collisions [Burban et al. 1989] was not involved.

2D2.2 Tamar mud strength

Experiments were performed with the vibrating column apparatus using flocs sampled from the surface water of the Tamar at Calstock [Alani et al. 1990]. The results are shown in Fig. 2.9, and indicate the type of interaction between floc-size and turbulence to be expected. Turbulent dissipation rates in the vibrating column are in the range 10 to 3000 cm^2/s^3, comparable with the very highest rates expected in an estuary, (and measured in this fieldwork).

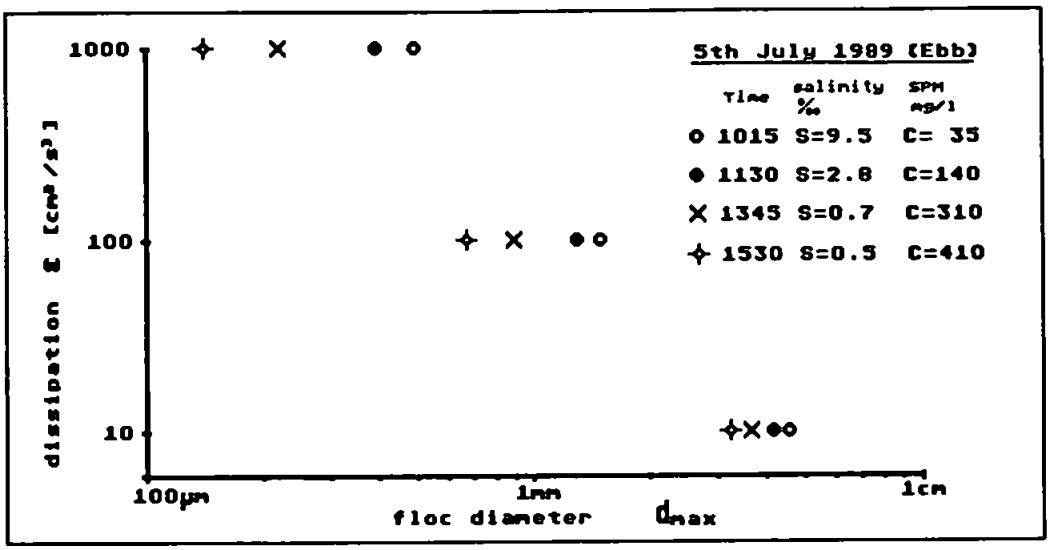

Fig. 2.9 Strength/size relationship for flocs sampled directly from Tamar.

In similar experiments using mud which had been reflocculated in the laboratory under various conditions of concentration and salinity, floc strength was found to be dependent on the salinity and the concentration at which the flocs were produced. Removal of the biological coating on the particles followed by reflocculation resulted in flocs of approximately 25% of the density of the unstripped flocs [Alani et al. 1990].

An *in-situ* version of this apparatus has been used by Alldredge et al. [1990] to measure the strength of marine snow and similar size-dissipation relations have been found, although with lower turbulent energies.

2D3. Estuarine Flocs and Turbulence

2D3.1 Particle Size Distributions.

Floc size distributions have only recently begun to be measured with any accuracy [Bale and Morris 1987]. Previous estimates have been biased by damage to flocs during sampling, as in Coulter counting, or have used settling velocity data to characterise the size distribution. Since the particle distribution is expected to vary with turbulence, and settling velocity also varies with concentration [Owen 1971, Bale et al. 1988, West et al. 1990], it is necessary to measure each of these factors to quantify deposition rates.

Information on particle populations in estuaries has also been obtained from studies of the bacterial and organic chemical properties of sediments. Plummer et al. [1987] measured the bacterial activity associated with two types of

particles at points along the Tamar estuary (during a neap tide). Permanently suspended particles were identified as those that remained in suspension 12 hours after sampling; periodically resuspended particles settled out within 12 hours. The permanently suspended particles had sizes in the range 20-60 μm (larger than the periodically resuspended fraction), and in the turbidity maximum were completely covered by bacteria. It should be noted that the samples were collected using a submersible pump and transported to the laboratory, so that the larger particles are unlikely to be flocculated material.

Reeves and Preston [1991] made a similar study (in the Tamar, during a neap tide) of the distribution of lignin in suspended particles and found that the permanently suspended particles contained on average three times more lignin than periodically resuspended particles.

These results suggest that the larger particles, those favoured by bacteria, are those with the highest vegetation content and hence most bouyant. This aspect is discussed further in section 4C4 along with discussion of the assignment of the phrase 'permanently suspended' to these particles.

2D3.2 Turbidity Maximum.

The turbidity maximum is a feature of many estuaries [Allen 1980, Postma 1980]. High concentrations of suspended material are formed when the net suspended solids flux is directed to seaward in the upper reaches of the estuary while in the lower reaches the net transport is landward. Many factors contribute to the formation and maintenance of a turbidity maximum; geometry, stratification and sediment characteristics being major influences [Postma 1980, Dyer 1989]

The turbidity maximum is also important in the cycling of chemicals between the sediments and water. Anderson [1986] found the abundance of bacteria in the turbidity maximum zone to be reponsible for removal of silicic acid from the riverine water and its incorporation into diatoms which later reach the sediment. Cloern [1991], although not presenting any data on turbidity, has linked phytoplankton populations in an estuary to the spring/neap cycle, which is suggestive when taken in conjunction with the results of Plummer et al. [1987]. Morris et al. [1982a,b] have observed the link between estuarine chemistry and the turbidity maximum, and Ackroyd et al. [1986] found the turbidity maximum to

be a region of removal of dissolved metals, which are transported with the sediments and which dissolve into the water in the mid estuary region.

Bale et al. [1985] have studied the mobility of muds, reporting the turbidity maximum to lie between Calstock and Morwellham during the summer months, and associated transport of mud onto the mudbanks in this region. Uncles and Stephens [1989] have observed and modelled the turbidity maximum, in the upper Tamar estuary. This forms just upstream from the salt intrusion and concentrations within it vary with the spring/neap cycle. The main cause is tidal pumping of eroded sediment due to the strong flood and weaker ebb in the upper part of the estuary. At High water (during summer and with low freshwater runoff) the turbidity maximum is just below the upper limit of tidal flow at Weir Head and travels approximately 10 km downstream during the ebb [Bale et al. 1988]. The concentrations within the turbidity maximum vary with the spring/neap cycle and its position varies with the freshwater runoff.

The model of Uncles and Stephens [1989], based on resuspension under the asymmetrical and longitudinally varying tidal flows of the Tamar, predicts a broader turbidity maximum than their fieldwork observed and this was thought to be related to the presence close downstream of the freshwater/saltwater interface which did not feature in their model. Festa and Hansen [1978] predict a turbidity maximum based on tidally averaged residual circulation and without erosion, and find its strength dependent on particle size - via fall velocity - with larger particles producing a stronger maximum. Many observers report that the turbidity maxima of various estuaries select small particles of the order 5-20 μm for retention [Postma 1980, Gibbs et 1989, Hamblin 1989] which is to be expected since erosion from the bed is their source. However the chief observable effect of the existence of a turbidity maximum is the accumulation of mudbanks [Bale et al. 1985] and this requires that settling particles are large enough to reach the bed when currents reduce; Allen et al. [1980] consider the influence of the spring neap cycle, and van Leussen and Winterwerp [1990] note the importance of HW slack flows as an opportunity for aggregation and settling to take place.

The timescales for the variation of turbulence, following a variation in production, are discussed by Nunes Vaz et al. [1989]. Vertical stratifcation,

resulting from an initial longitudinal density gradient, has a typical estuarine timescale of the order of 5 minutes (obtained from a horizontal Brunt-Vaisala frequency calculation), while the decay of turbulence has timescale of the order of 15 minutes. Thus there is ample time for the establishment of stratified, quiescent flow at the HW stand.

2D3.3 The Tamar Estuary.

The Tamar drains the high ground of NE Cornwall and Dartmoor, and flows into the English Channel at Plymouth. The estuary in its present form was formed when the sea began to rise after the retreat of the last ice age 10,000 years ago, and the drowned river valleys have been silting up ever since; mining activities accelerated the silting up over the last 200 years [Perkins 1971].

The estuarine Tamar begins at Weir Head, Gunnislake, where a weir halts the tidal influence. Between Weir Head and Hole's Hole, 17 km below the weir, the estuary is narrow and runs through a steep sided valley; below Hole's Hole the valley widens and there are extensive mudflats. Below the Brunel Bridge, 24 km below Weir Head, the estuary deepens and is joined by the Lynher river, to form the Hamoaze - used as a naval port. The estuary flows into Plymouth Sound through the Narrows, off Cremyll, 31 km below Weir Head.

The Tamar is a partially mixed estuary; Uncles et al. [1985], and Uncles and Stephens [1990] present data on stratification and circulation for various stations in the Tamar, showing significant stratification in the upper estuary during the ebb. During conditions of low runoff the salt intrusion reaches almost to Weir Head. Münchow and Garvine [1991] model the flow in channel shaped estuaries based on three parameters, ε specifying the tidal forcing at the mouth, φ the ratio of friction scale to estuary length, and γ the ratio of tidal wavelength to estuary length. Substitution of values for the Tamar (and taking the 'mouth' to be at the Brunel bridge where the estuary deepens) gives $\varepsilon \approx 0.6(sp)\ 0.3(Np)$, $\varphi \approx 0.3(sp)\ 0.4(np)$, $\gamma \approx 0.1$. The qualitative behaviour of the estuary can be obtained from their diagram "Fig.11", and varies between that of a weak tidal bore at spring floods and of a damped tidal wave at neaps. Asymmetry between flood and ebb currents and duration is observed in the data presented here and is modelled by Uncles and Stephens [1989]. An important consequence of this asymmetry is the production of a turbidity maximum which forms because the tidal currents set up a net landward flux of eroded sediments in the mid-estuary region [Uncles and Stephens 1989].

Objectives of the Experimental Work

Settling velocity is an important input to sedimentation models. When cohesive sediments are present settling velocity is strongly dependent on floc density and size. Laboratory experiments show that (i) floc size distribution is limited by turbulence, with the turbulent dissipation rate being a controlling parameter, and (ii) floc density is modified by the turbulence experienced during floc formation. It is proposed that turbulence plays a similar role in estuaries [Dyer 1989].

If the influence of turbulence on floc size distributions in the estuary could be predicted then deposition rates could be obtained using settling velocity results. Suspended solids concentrations can be obtained relatively easily, either by observation or from models, and partitioning this matter by size would enable better values of cohesive sediment deposition rates to be obtained. Turbulence parameters can be estimated from mean velocities so that this last step of linking floc sizes to turbulence would greatly improve tidal models and the estimation of settling rates from easily obtained field data. This chain of reasoning is illustrated in Fig. 2.1.

In order to test the Owens [1971] hypothesis, ,(confirmed in the laboratory work of Alani [1987, Alani et al. 1990]), that increased dissipation rates reduce maximum floc size (and conversely that decreased dissipation rates promote floc growth), the turbulent dissipation rate and particle size distribution are measured and compared for a site in the Tamar estuary.

The measurements of floc size distributions are themselves interesting as few surveys of this type have yet been undertaken. Flocs form the home of many marine organisms [Plummer et al. 1987] so that their size variations over the tidal cycle may shed light on ecological, and also chemical, aspects of the estuary.

The near bed region was chosen for study since this is where the greatest turbulence is experienced. During deposition the near bed region presents a 'barrier' through which flocs must settle intact if they are to be incorporated into the bed; flocs which are disrupted will remain in suspension. During erosion

particles close to the bed will indicate the mechanism by which they were resuspended - that is whether they were resuspended as aggregates or as primary particles - since aggregation processes will not have had time to work. Also erosion rates are determined by the bed shear stress which is more readily estimated where the velocity gradient is steepest.

Introduction.

The object of this experiment was to obtain turbulence and particle-size data in one region of the flow, during a variety of flow conditions. This data would then be used to test the hypothesis that floc-growth is (strongly) limited by the local turbulence. Theory suggests that it is the turbulent dissipation rate that is the relevant parameter of the flow; however this cannot be measured directly but must be obtained from the high frequency fluctuating velocity components (see 2A2.4 above).

The size of particles ranges from silt particles and microflocs of up to about 20 μm, to large flocs of maybe 1 mm diameter. Whilst the size distribution of the primary particles could be obtained in a variety of methods most of these would destroy the larger flocs and bias the distributions. The sizer system used for these experiments measures the scattering of a laser beam as the flow passes through the sampling volume and is the least disruptive of available techniques.

The measurements were taken from as close to the bed as practicable as this is where the greatest turbulence is expected.

In order to relate the turbulence and flocculation to the tidal cycle the large scale flow was monitored by profiling salinity, current velocity, salinity and temperature.

3A Instrumentation

3A1 Electromagnetic Current Meters.

3A1.1 EM Flowmeters.

In order to measure the high frequency turbulent velocity fluctuations two 10 cm diameter annular 'Colnbrook' [Valeport Scientific Marine Ltd, Dartmouth, Devon] electromagnetic flowmeters were used. These instruments measure the voltage produced across the annulus when the flow cuts the magnetic field produced by coils in the annulus. The induced voltage is a linear function of the component of flow parallel to the annulus and perpendicular to the electrodes. Each instrument has two pairs of electrodes across one coil and measures two perpendicular components of a three dimensional flow.

The field is alternated at high frequency in order to minimise electrolytic effects at the electrodes and the induced (alternating) voltage output is rectified and low-pass filtered. The resulting frequency resolution of the output is 5 Hz and produces approximately 1 mV *per* cm/s. The spatial resolution is determined by the size of the annulus. The induced voltage across each pair of electrodes is a volume averaged response to the flow in the region between the electrodes. Soulsby [1980] discusses possible transfer functions: here the smallest resolvable eddies are taken to be of the order of the electrode spacing, this gives a lower limit of 10 cm in diameter.

3A1.2 Calibration.

The two EM current meters were calibrated in the towing tank at IOS Deacon Laboratory (Wormley) both shortly after building, and again after the first period of fieldwork during late June 1988.

The two instruments were labelled with serial numbers '26' and '27', and the two channels labelled 'X' and 'Y' on each. The data was labelled *u0,..,u3* as indicated in Table 3.1 below and their relation to the flow is shown in Fig. 3.11.

Each of the two components on each instrument was towed at nominal speeds from 0 cm/s to 120 cm/s in both positive and negative directions. The EM output, filtered and converted to digital signals, was recorded on an 'Opus' microcomputer (the data logging system is described in section 3B). The speed of the towing frame was recorded when it had reached a steady value for each run and this was later compared with the steady section of the EM record to provide a calibration. Calibration curves are plotted in Fig. 3.1 (plot X2 in Appendix X) and linear regression coefficients tabled below:

Table 3.1

		EM response *(mV)* to flow *u (cm/s)*			
		June 1988		July	
26x	*u0*	511.2	- 1.0u	514.1	- 1.03 u
26y	*u1*	511.7	- 1.0u	513.8	- 1.03 u
27x	*u2*	512.6	- 1.0u	512.2	- 1.02 u
27y	*u3*	511.5	+ 1.0u	513.5	+ 1.02 u

(The sign of the calibration depends on the electrical wiring. An offset of 512 mV is introduced in the data storage process.)

In processing the field data a nominal calibration of *V=512-u (V[mV], u [cm/s])* was used on each channel in order to speed up processing: mean speeds are affected by up to 3% and have an offset error of up to *2 cm/s*, spectra will be affected by up to 6%. This nominal calibration corresponds to the designed output of the system - the actual output is thus found to be very close to this. Using the nominal calibration enables the processing to be speeded up.

3A1.3 Noise.

Previous to, and twice during, the field work the rig was 'bucket tested' in still water in order to assess the noise limits of the instruments in as close to working condition as possible.

In the laboratory the instruments were immersed in a glass sided tank of water approximately 4 ft. square and 3 ft. deep, taking care to orientate the flowmeters so that their magnetic fields did not interact. During the field work, at slack water, a large GRP tank was floated into position between the hulls of the barge and submerged by filling from the river. When full the rig was lowered into the tank and suspended without touching the tank floor or wall. The leading edge of the tank was held under water during the test to avoid electrically isolating the rig from the river - this did have a noticeable quieting effect on the EMs, the effect was particularly obvious if waves were allowed to slop over the leading edge.

The results of 'bucket' tests in the laboratory using just the EM flowmeters (run J15–2), and at Calstock using the complete experimental rig (runs B04, C04) are shown in Table 3.2. Power spectra from run 'C04' (recorded at 24 Hz) are shown in Fig. 3.2 below. A comparison of data and 'bucket test' spectra is also made in Fig. 3.2: the difference between 'bucket test' C05 (recorded at 12 Hz), and run N13 is shown shaded. Run N13 (1130 on 5th July) provided a particularly low dissipation estimate and so exhibits the poorest signal to noise ratio.

It can be seen that the noise levels are low (r.m.s. values of order 1 cm/s are indicated in Table 3.2) and that the filters are removing most of the energy above 5 Hz. Channel 1 (EM26Y) however exhibits a pronounced peak at about 7.5 Hz which suggests that one of the anti-aliasing filters is unreliable. The same peak (aliased to ~4.5Hz) appears in channel 1 of N13.

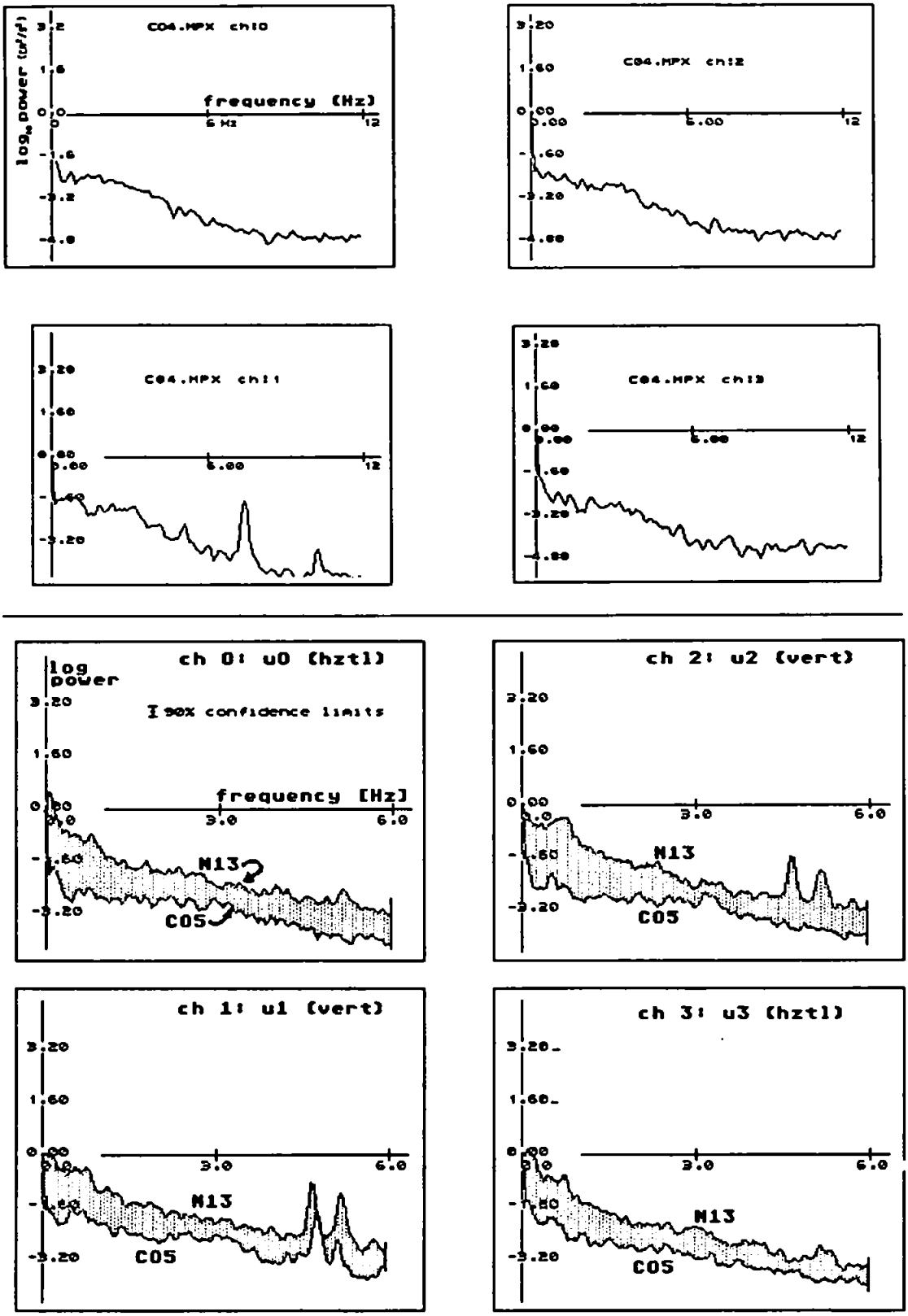

Fig. 3.2 EM current meter noise tests. C04 and C05 bucket tests at Calstock, N13 low dissipation data run. The shaded area highlights the difference between N13 and C05: the signal N13 is significantly higher than the noise of C05.

Table 3.2

	Means (mV)				Variances $(mV)^2$				
	26x	26y	27x	27y	26x	26y	27x	27y	
J15–2	1.22	6.39	-8.56	10.93	0.40	0.29	0.61	0.30	(Lab. 15June)
B04	6.03	2.59	0.48	6.55	6.39	13.56	4.49	6.14	(Bucket 3Juiy)
C04	7.20	3.27	-0.08	5.84	0.49	0.69	0.35	0.36	(Bucket 6July)
C05	8.00	3.25	0.00	10.25	1.06	2.87	1.28	1.42	(Bucket 6July)
N13	48.50	1.25	1.00	10.00	45.69	25.22	22.61	30.29	(Calstock 5July)

3A2 Optical BackScatter Sensors.

3A2.1 OBS

Two Optical BackScatter sensors (OBS) were used to study the high frequency suspended solids concentration structure, and to obtain concentration gradients near the bed. The instruments used were OBS-1 [Downing and Associates, Washington State, USA]

OBS work by measuring the light scattered backwards from a light source within the instrument by a suspension of particles. The source, an infra-red LED, is pulsed very rapidly (500Hz), and the return signal detected at that frequency and then smoothed at 30 Hz.

The instruments themselves consist of a cylinder approximately 5 cm in length and 2 cm diameter connected to electronics, which are housed in a pressure case, by 2 m of cable. A flattened face houses the light source and is surrounded by the sensor (see Fig. 3.3). Their size makes them very versatile as they can be taped into position, and removed, very easily. The sampling volume extends to about 3 cm from the instrument under estuarine conditions (and during the calibration described below).

Fig. 3.3 Photograph of OBS sensor.

3A2.2 Calibration.

A working calibration was obtained for each OBS sensor using mud taken from the surface of the mud layer at the bottom of the slipway at Calstock. This was used to make a slurry of known concentration which was progressively stirred into a large black plastic dustbin of clear water. At each addition the OBS voltages were recorded and the new concentration in the dustbin worked out. The resulting calibrations are shown in Fig. 3.4 (plot X3 in Appendix X). A calibration of *voltage [mV] = concentration/4 [mg/l]* was used for data processing (this simplified calibration speeds up processing). The regression lines shown in Fig. 3.4 are given by -

		OBS response(mV) to concentration(mg/l)	
C5	OBS I	$(42 \pm 8) + (0.26 \pm 0.01) \times C$	$r^2=0.99$
C4	OBS II	$(18 \pm 10) + (0.27 \pm 0.01) \times C$	$r^2=0.99$

3A3 Laser Sizer.

A 'marinised' version of the 'Malvern Instruments' laser particle sizer has been developed at Plymouth Marine Laboratory for the *in-situ* sizing of estuarine particles [Bale et al. 1987, Bale et al. 1989].

A 'Malvern Instruments' 3600E type laser sizer is mounted in a pressure case and incorporates optics to enable laser and sensors to be mounted together. Fraunhoeffer diffraction of the laser beam by suspended particles results in light being detected at an array of concentric circular photocells. The intensity of light diffracted at each angle depends upon the particle size distribution in the sampling volume. The sizer computes the size distribution by comparing the scattering produced by successive trial distributions to the observed scattering pattern. Size distributions are presented as percentage weight of particles in each of sixteen size bands (Table 3.3). It should be noted that the weight is calculated on the assumption that particles are solid (have dimension *D=3*), and thus measures floc volume.

The underwater part of the system consists of a cylindrical pressure case of diameter 50cm and length 80cm. Power and data are carried by cable to the surface where a microcomputer controls the system and processes the data.

The sampling volume is 2 cm wide, to reduce the reduce the possibility of shearing flocs during measurement, and situated at one end of the pressure case. Perspex fairings reduce the turbulence produced by edges of the casing.

The Sizer system was calibrated against particles of known size prior to each deployment [Bale, personal communication]. The reliability of sizer distributions is indicated by the *obscuration* and *log error* statistics produced by the sizer software; these are discussed in section 3B4.

Table 3.3 Laser Sizer Bands

Band	lower dia.	upper dia.	Band	lower dia.	upper dia.
1	less than 5.8 µm diameter		9	30.3 µm	39.0 µm
2	5.8 µm	7.2 µm	10	39.0	50.2
3	7.2	9.1	11	50.2	64.6
4	9.1	11.4	12	64.6	84.5
5	11.4	14.5	13	84.5	112.8
6	14.5	18.5	14	112.8	160.4
7	18.5	23.7	15	160.4	261.6
8	23.7	30.3	16	261.6	564.0

3A4 Bead Thermistor.

A rapid response bead thermistor was available, with associated electronics, courtesy of D Sturley [Sturley 1990]. The thermistor system obtains the temperature of the water passing the thermistor bead by measuring the varying resistance of the bead as the temperature varies. The bead is approximately 0.5 mm in diameter and is mounted at the tip of a 3 inch long, ½ inch diameter cylinder, see Fig. 3.5. The thermistor system output produces a signal of 50 mV per °C and is accurate to 0.1 °C with a resolution of better than 0.01 °C.

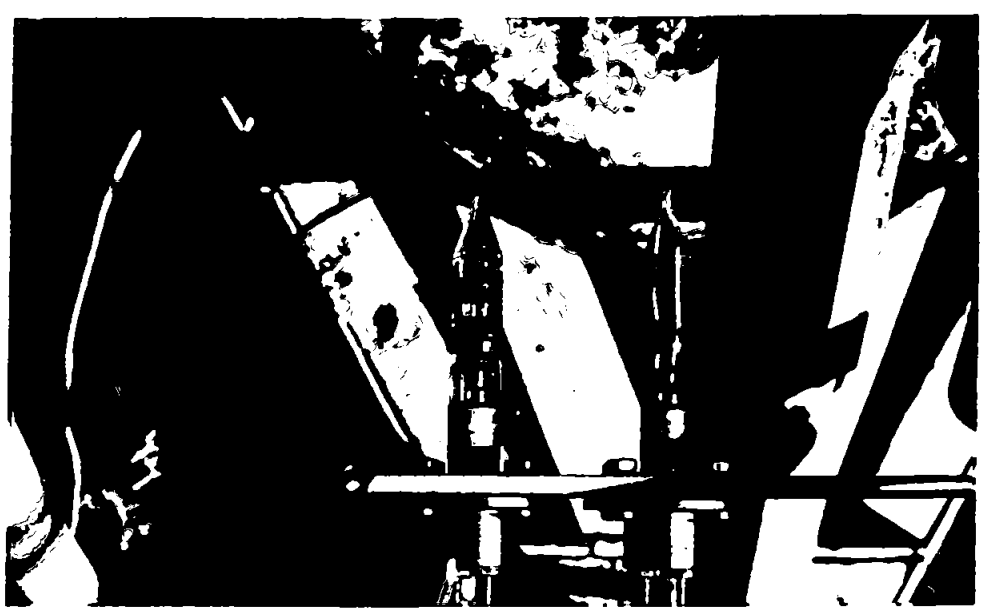

Fig. 3.5 Photograph of thermistors

In order to monitor the noise levels in the system the thermistor is run in parallel with a 'dummy' thermistor which has a very stable known resistance. The time series of the dummy shows noise rarely exceeding one bit (0.25 mV) from the mean. The electronics also provide anti-aliasing filters at 5 Hz.

3A5 Siltmeter.

The 'Partech' [Partech (Electronics) Ltd., Charlestown, Cornwall] suspended solids meter measures the attenuation in intensity occuring when a beam of light passes through a suspension. The instrument consists of a box, about 5 x 10 x 20 cm, open at each end through which the suspension passes. A cable to the surface carries power and data. Gravimetric calibrations of SPM as measured by 'Partech' instrument were made throughout the fieldwork, with the results below [Bale, personal communication]: where C is the 'Partech' siltmeter reading. No corrections were made in using the concentration readings.

$$SPM = \begin{cases} 12C/19 & C \leq 380\ mg/l \\ 6C/7 & C > 380\ mg/l \end{cases}$$

3A6 Current meter.

An 'NBA' [NBA (Controls) Ltd., Farnborough, Hampshire] DNC-3 current meter provided mean current speeds and directions. Speed is proportional to the rate of rotation of the rotor and the vane ensures that the instrument is aligned with the flow. An internal compass provides direction information. Speeds in the range 0 to 2.5 m/s are measured to +/- 2% and directions are accurate to +/- 10°.

3A7 T-S Bridge.

The 'Electronic Switch Gear Ltd.' MC-5 T-S bridge measures the temperature of the water by matching the sensor resistance with the bridge resistance. The salinity is then measured by balancing the resistance of the water with the bridge. Salinity is accurate to +/- 0.1‰ and temperature +/- 0.1 °C. Salinity calibrations were made regularly throughout the fieldwork and the instrument calibration found to be correct [Bale, personal communication].

3A8 Pitch and Roll Sensor.

The pitch and roll sensor provides information on the attitude of the rig by producing a voltage in proportion to the deflection of an internal pendulum from the zero position. The output was:

	Tiltmeter Output [Volts]
Pitch	1.1 + 0.025×(degrees upward pitch)
Roll	1.25 + 0.025×(degrees tilt to starboard)

3A9 Rig.

The instrumentation was mounted on a steel tetrahedral frame standing 75 cm in height and having a pole added at the forward corner of the base to carry the current meters. The layout of the rig is shown in Fig. 3.6. Details of the positioning of individual instruments on the frame are discussed in section 3C2.

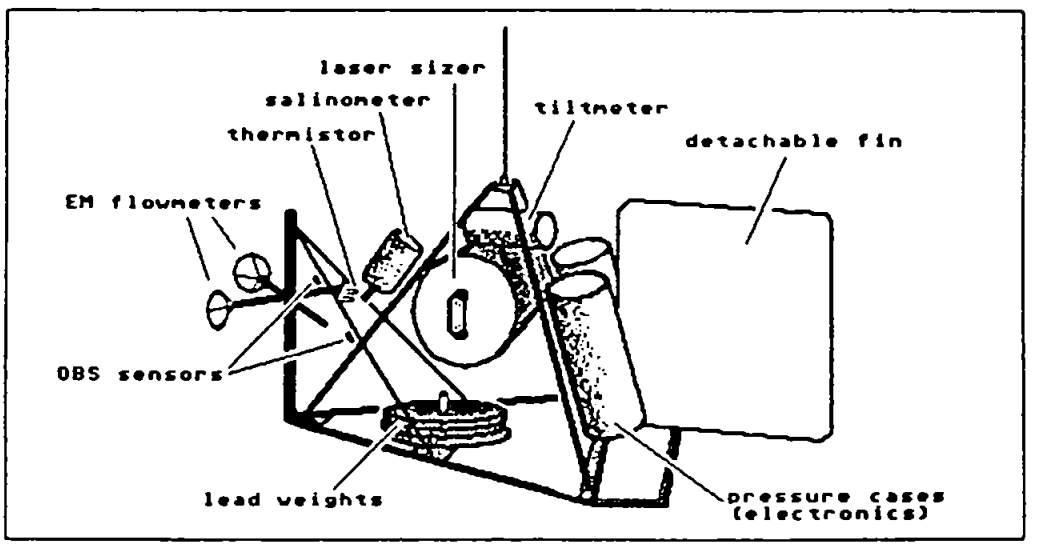

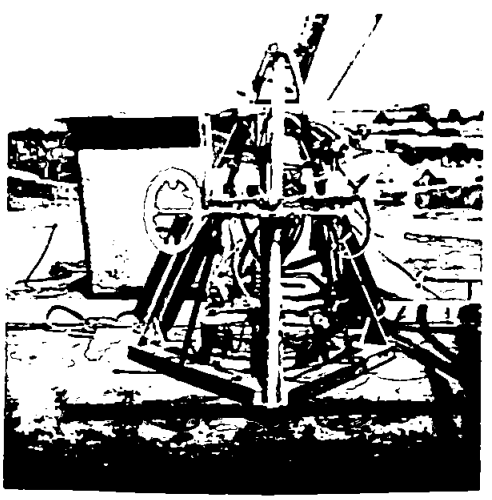

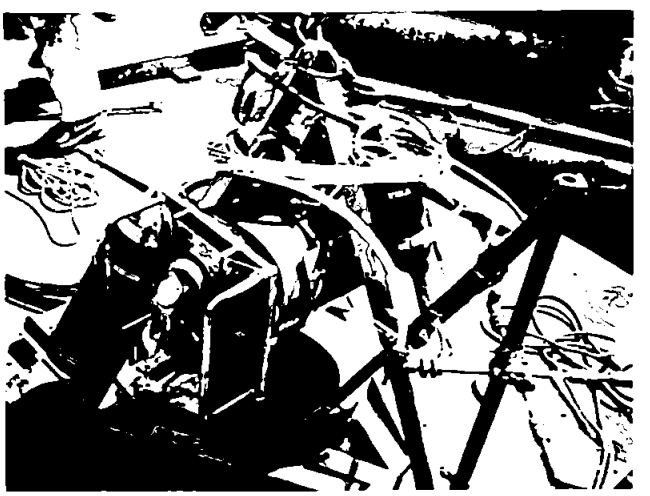

Fig. 3.6 Layout and Photographs of Experimental Rig.

3B Data Processing

General.

Since the data is to be processed digitally the continuous velocity record must be sampled at discrete intervals to produce a time series of velocity measurements; this means that events happening on time scales of less than the sampling interval will not be observed; nor will events be recorded that take longer than the total record length. The upper frequency limit is known as the Nyquist frequency (f_q) and is entirely determined by the sampling interval (Δt), with $f_q = 1/2\Delta t$. The process of approximating the continuous Fourier transform by a discrete Fourier transform assumes that there is no energy at frequencies higher than f_q. If high frequency energy is present it will be 'aliased' into lower frequency bands. This is avoided by low-pass filtering the continuous data before digitising.

The turbulence statistics to be used depend for their reliability on observing large enough regions of turbulence. The reliability of an estimation of the energy in a given frequency band of a spectrum is quoted in terms of its 90% confidence limits which indicated the probable error range of that energy estimate. Confidence limits are discussed in section 3B3.1.

3B1 Analogue to Digital Conversion.

Analogue to digital conversion of rig data was performed at the surface using a Microlink [Biodata Ltd, Manchester] 12 bit A/D converter controlled from an 'Opus PC V' microcomputer running 'Microlink Applications Software' 'HSDC' data collecting software.

The EM and OBS channels were passed through 5 Hz digital low-pass anti-aliasing filters immediately prior to A/D conversion. The thermistor and dummy channels were internally filtered at 5 Hz before passing to the A/D system. The frequency response of the filters was obtained by comparing the input and output, using an oscilloscope, while applying a low frequency signal from a signal generator. The filter response is shown in Fig. 3.7. Filter characteristics were roll-off of 35 dB per decade and 5 Hz half-power point.

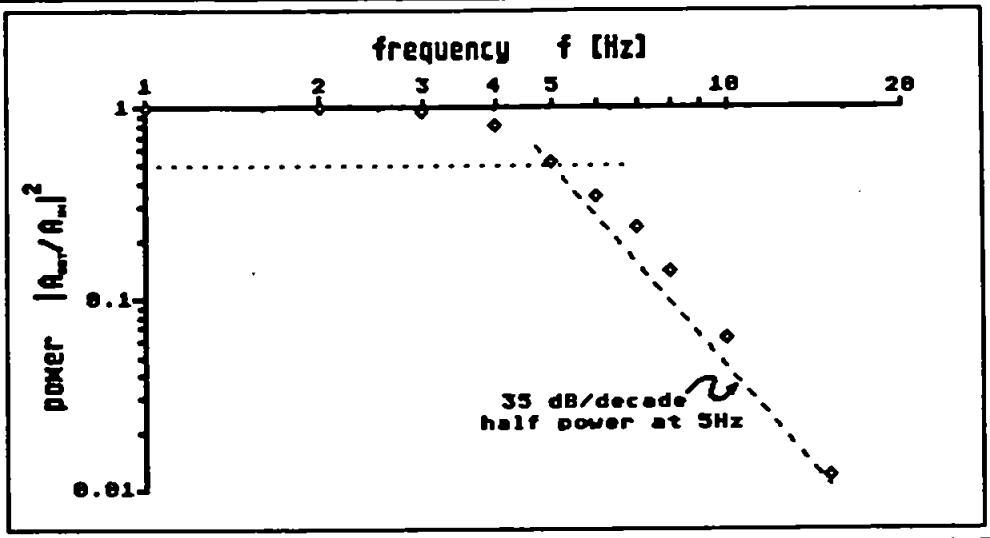

Fig. 3.7 Filter response.

382 Data Storage.

The eight channels (*u0,.., u3, c4, c5, temp., dummy*) were multiplexed and converted for passing to the microcomputer and storage on hard disc. Data was stored as the bit pattern obtained from the A/D unit - each sampled voltage was stored in two bytes with the lo byte first; channels were cycled from high to low starting with the highest channel (*viz. 7lo, 7hi. 6lo, 6hi ,...., 0lo, 0hi, 7lo,...*). Each file contained 4096 samples of each of the 8 channels: total filesize was 65539 bytes including an ASCII header of 24 lines.

Data was backed up onto floppy disc regularly and these discs processed on an 'Atari 1040 ST' computer.

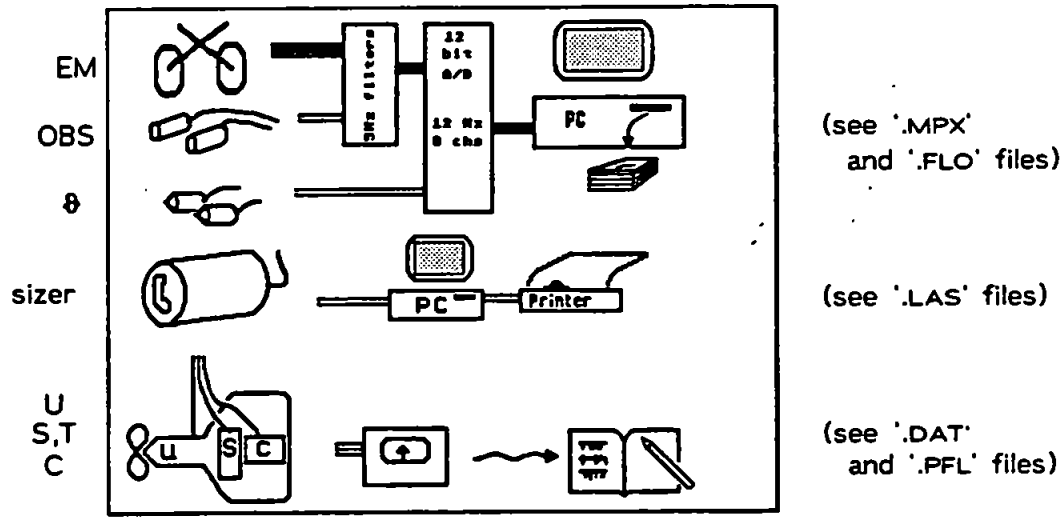

Fig. 3.8 Schematic of data collection and storage. Rig data was stored as a bit pattern on computer; sizer data was printed and later tabulated; profile data was recorded on paper and tabulated. Computer filenames are indicated and these (except '*.DAT' and '*.MPX')are shown in Appendix Y.

3B3 Processing.

Processing was performed in three stages. The operations used to convert stored EM current meter data to dissipation estimates are shown in Table 3.4. Data was read into RAM from floppy disc, calibrated (for convenience of de-bugging), and the mean for each channel obtained.

The use of 'nominal' calibrations ($u=x/4-512$, $c=x/4$, $\vartheta=x/4$) enables the processing to be faster than if the experimentally obtained calibrations were used as bit-shift operations may be used. As shown in 3A1.2 the accuracy of resulting spectra is acceptable - this calibration may introduce an error of up to 6%. The OBS calibrations in the laboratory and in the field differ by a factor of about four and this is thought to be due to different properties of the mud used in the two calibrations - see 4A2.2. The thermistor system was calibrated electronically to produce the stated output [Sturley 1990].

The discrete Fourier transformation of 256 samples from two channels was evaluated using a FFT routine documented by Brigham [1974]. Daniell windowing was performed over each 3 adjacent frequency estimates in order to improve the stability of the estimate. The resulting power spectrum (Sk) was converted to a 'dissipation' spectrum (ψ^k) which was plotted against k so that an inertial dissipation range of frequencies, (showing the characteristic '-5/3' spectrum), showed up as a range of k with constant ψ^k.

'Dissipations' obtained from each 256 point block in one channel's time series (of total length 4096 points) were averaged and this spectrum smoothed by averaging neighbouring frequencies. The turbulent dissipation rate (ε) could then (when present) be obtained from the constant range of the plot.

Note that all averaging was done by software in order to increase the repeatability of the dissipation estimates. The only non-automated part of the operation was in finding the limits of an observed inertial range.

Table 3.4 Data Processing Program.

$x^l = z.lo + 256*z.hi$ where z is read from disc.

$u^l = \begin{cases} (x^l - 2048)/4 & \text{EM channels} \\ x^l/4 & \text{OBS, } \vartheta \end{cases}$ (approx. calibration)

$u^l = u^l - \mu$ where $\mu = \frac{1}{N}\sum_{l=0}^{N-1} u^l$ (remove mean)

$\hat{u}^k = \frac{1}{N}\sum_{j=0}^{N-1} u^j \exp(-2\pi ijk/N)$ (by FFT) $k = 0..N-1$ (DFT)

$S^k = (|\hat{u}^k|^2 + |\hat{u}^{N-k}|^2)/2$ where $k=0..K-1$ and $K=N/2$ (Power)

$S^k = S^{k-1}/4 + S^k/2 + S^{k+1}/4$ (Daniell window)

$S^k = \frac{1}{12}\sum_{b=1}^{12} S^k(b)$ (segment averaging)

$x_k = 2\pi f_q k/K$ converting to (radian) wavenumber $x_k = 2\pi f_k/U$ with f_q the Nyquist frequency and U the mean current.

$E(x^k) = \left(\frac{UK}{2\pi f_q}\right) S^k$ (so that $\int E dx = \Sigma S^k = \langle u^2 \rangle$)

[so that $\left(\frac{2\pi f_q}{KU}\right)^{-1} S(f_k) = E(x) = \alpha \varepsilon^{2/3} x^{-5/3} = \alpha \varepsilon^{2/3} k^{-5/3} \left(\frac{2\pi f_q}{KU}\right)^{-5/3}$ where α is the Kolmogorov constant]

$\varepsilon_k = \sqrt{\left(S_k^3 k^5\right)} \cdot \left(\frac{2\pi f_q}{KU\alpha^{3/2}}\right)$

$\psi^k = 3/2 \log_{10} S^k + 5/2 \log_{10} k$

$\psi^k = (\psi^{k-1} + \psi^k + \psi^{k+1})/3$ (plot smoothed 'dissipation' spectrum)

$\log_{10}\varepsilon = \Psi - \log_{10} U + C$ where $C = \log_{10}(2\pi f_q/\alpha^{3/2} K)$

$\log_{10}\varepsilon$ gives 'log dissipation' when the dissipation spectrum is constant, Ψ over a valid inertial range of k. Values used were $f_q = 6$ Hz, $\alpha = 0.5$, $K = 128$ giving $C = -0.08$]

3B3.1 Reliability of Spectra.

The data was processed in segments of $N=256$ points using a fast Fourier transform routine [Brigham 1974] and transforming two channels simultaneously. The resulting power spectrum, S^k, partitions the variance, $\langle u^2 \rangle$, among the $K=N/2$ power estimates of bandwidth f_q/K, each having 2 degrees of freedom. The Nyquist frequency f_q for the sampling rate used was 6 Hz giving an initial bandwidth of $f_q/K = 0.05$ Hz: the block length of 21.3 seconds limits the detection of low frequency variations of frequency less than 0.05 Hz. Daniell

windowing over three adjacent frequencies increases the bandwidth by a factor of 2 [Jenkins and Watts 1968] and increases the number of degrees of freedom to 4. Segment averaging over 12 blocks raises the degrees of freedom to 48. The confidence limits for the spectra can be obtained from tables of χ^2 distributions [eg. Newland 1984].

Following Newland [1984] the number of degrees of freedom ν, is related to the total record length T, and effective bandwidth B_e, by $\nu=2B_eT$: for the program outlined above using 12 blocks of 256 points at 12 Hz, $B_e= 2f_q/K= 0.094$ [Hz] and $T=12N/(2f_q)= 256$ [s] so that $\nu=48$. From tables of the distribution of χ^2 for $\nu=48$ we find that $p(\chi^2 > X^-)=0.95$ and $p(\chi^2 > X^+)=0.05$ gives $X^-=33.098$ and $X^+= 65.171$. That is, 90% of the values of the χ^2 distribution with mean $\nu=48$ lie within $33.098 < \chi^2 < 65.171$. Supposing S to be distributed as χ^2 about the true spectral density E, then 90% of the values of S lie within $X^-/\nu < S/E < X^+/\nu$. Rearranging gives $\nu S/X^+ < E < \nu S/X^-$ and substituting from the tables gives the 90% confidence limits for the spectrum as $0.74S<E<1.45S$. On log axes these limits are given by $\log_{10}S-0.13< \log_{10}E < \log_{10}S+0.16$.

Smoothing the 'log dissipation' plot further increases the bandwidth with the estimate being a geometric average of three adjacent frequencies: however the estimate is only used where the spectrum is constant. The 90% confidence limits for the 'log dissipation' values are given approximately by $\log_{10}\varepsilon$ +/- 0.25.

Several programs were developed at different stages for analysing the data. All are compiled from *Pascal* source to run on an 'Atari 1040ST' which, although slower at running the programs than an IBM type PC or mainframe, reduced the time spent in transfering files. Program *Calstock* views the time series for one channel and obtains mean, variance and the power or dissipation spectrum of one block of 256 points, and adds spectra to produce an average spectrum from several blocks. Program *Batch* processes one disc (of ten data files) and saves the averaged 'dissipation' spectrum, with means and variances for inspection later (using *Calstock*). Program *Tamar* prints the full time series of each channel, averaged power spectra, and mean, variance and other statistics (eg Fig. 3.9 (a)-(d), plot X21 in Appendix X). Various *Pascal* and *FORTRAN* routines, using *NAG* graphics were written for plotting data and results.

3B3.2 Test of data logging system.

In order to check that the data processing routines and electronics were performing correctly the frequency response of the data processing system was tested. This was done by supplying an oscillating signal from a signal generator to the input of the anti-aliasing filters and logging the output *via* the A/D converter and microcomputer. The files produced were analysed using the program *Calstock* and the resulting spectra shown in Fig. 3.10 and Table 3.5 below. Note that the energy of the input signal is faithfully reproduced in a peak at the correct frequency and that in each case at least 90% of the output energy is in the peak. Some broadening of the peak is apparent in run J9—2 although this was not thought to be important in the analysis of smooth inertial range turbulence records.

3B4 Sizer Data.

The 'Malvern Instruments' program which runs the laser particle sizer outputs volume distributions, in roughly logarithmically spaced bands, as percentages. Also output are the obscuration and log error which indicate the reliability of the data. The log error measures the difference between the calculated diffraction pattern and the observed pattern - values of less than 5.0 are considered good, and less than 5.5 are usable. The obscuration measures the fraction of light that fails to penetrate directly through the suspension. Data may be used with obscurations of up to 95% but above this sizes are underestimated [West et al. 1990].

During the fieldwork obscurations exceeded 95% only during the periods 4/1642-1701 and 5/1721-1745. Obscurations exceeded 90% only during 4/1621-1701 and 5/1702-1804 and concentrations near the bed during these periods were greater than 1000 mg/l on the 4th and 630 mg/l on the 5th.

Table 3.5 Frequency response of system

Run	Input f Hz	Input A mV	Input mean mV	Input variance $(mV)^2$	Output (in peak) f Hz	Output $\log_{10}A$ ‡	Output width Hz	Output area $(mV)^2$
J9-1	3.0	20	−0.20	183	3.03	1.63	0.24	91.6
J9-2	2.5	20	−0.20	182	2.53	1.46	0.52	84.6
J9-3	5.0	20	−0.13	179	5.00	1.58	0.42	85.9
J9-4	4.0	20	−0.18	177	3.99	1.63	0.28	88.0

‡ Output amplitude, A, is from "raw" spectrum for which units are $(mv)^2$ per band, where the bandwidth is 10/128 Hz. Peak width is measured at A=1, area is area under peak. NB Area ≈ variance/2.

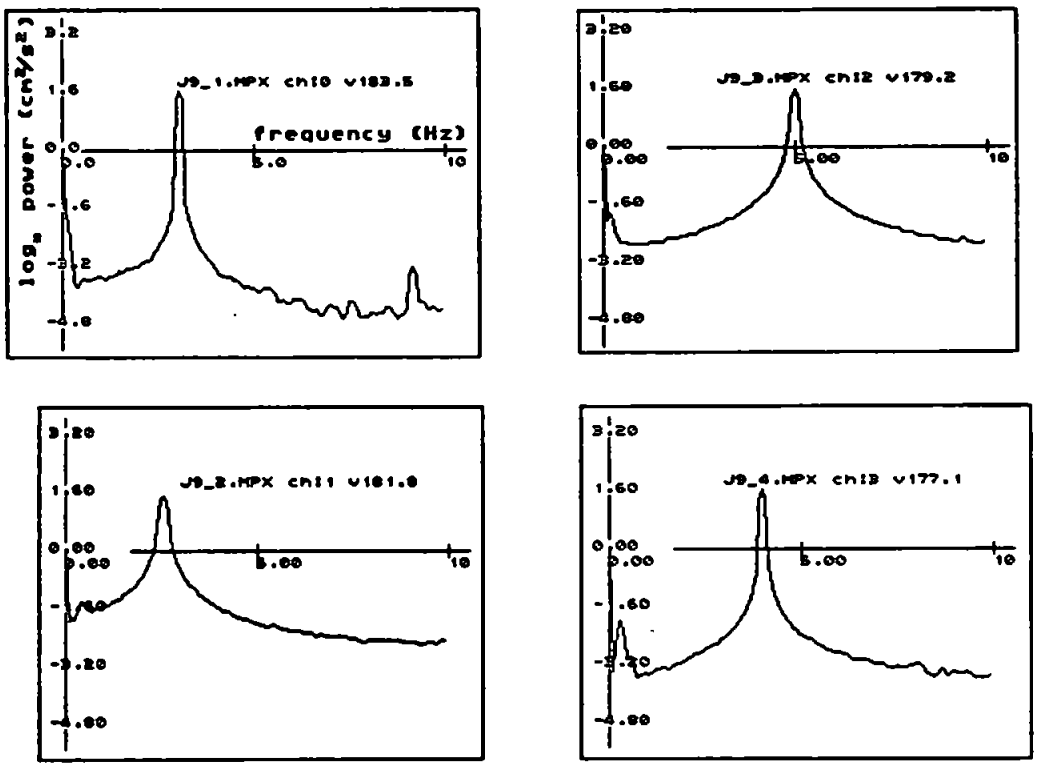

Fig. 3.10 Frequency response of system. The input signals are shown in Table 3.5.

3C Deployment of Gear

3C1 Theoretical Constraints on Positioning of Instruments.

In order to derive turbulence statistics from the data use is made of Taylor's frozen turbulence hypothesis; this requires the turnover time of eddies to be much greater than the time for them to be advected past the sensor - the eddies must appear to the sensor to be frozen into the mean flow. Frozen turbulence requires that $k \gg \varepsilon/U^3$, which can be shown as follows.

Supposing an eddy to be spherical of diameter λ, mass m and spinning with angular velocity ω its energy can be estimated as $T = \frac{1}{2} I\omega^2 \sim m\omega^2 k^{-2}$ where $k \sim 1/\lambda$ and I is the moment of inertia of a sphere about its axis. The energy spectrum $E(k)$ gives the energy in a volume of mass m due to eddies of wavenumber $\frac{1}{2}k$ to $\frac{3}{2}k$ as $mE(k)k$. Equating the two estimates gives $\omega^2 \sim Ek^3$ and substituting the inertial range spectrum gives $\omega^2 \sim \varepsilon^{2/3} k^{4/3}$ or equivalently an eddy turnover time $1/\omega \sim (\varepsilon k^2)^{-1/3}$. The time taken for such an eddy to advect past a point in a flow of mean speed U is λ/U and Taylor's frozen turbulence hypothesis requires this to be small compared to the eddy turnover time, thus $1/kU \ll (\varepsilon k^2)^{-1/3}$ or $k \gg \varepsilon/U^3$.

Upper limits on the wavenumbers for which inertial ranges may be observed are imposed by the sensor sampling volume (if sensor diameter is D then $k < 1/D$), and by the sensor sampling frequency f_q ($k < f_q/U$). Together with the frozen turbulence requirement these give a minimum mean speed for which an inertial range may be observed: $U \gg \sqrt[3]{(\varepsilon/k_D)}$ with $k_D = 1/D$. The sampling volumes for each of the instruments are indicated in section 3A above. The lower limit on k is imposed by requiring the turbulence to be isotropic: for this to be so $k > 1/H$ where H is the height of the sensor above the bed [Huntley and Hazen 1988].

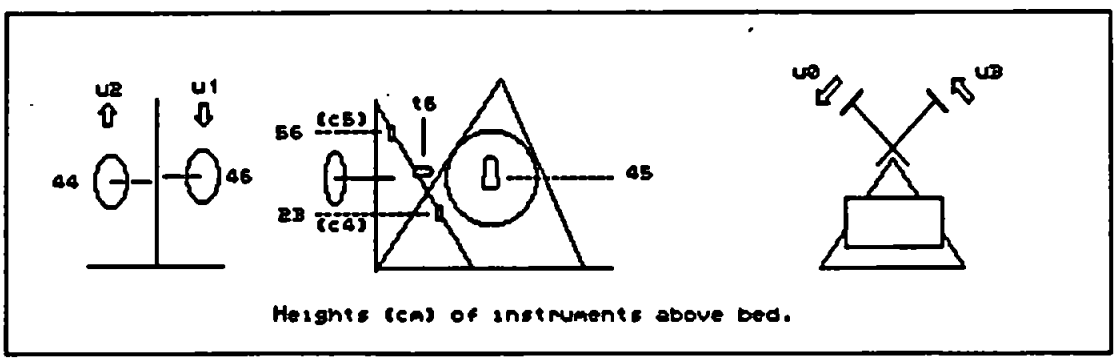

Fig. 3.11 Positions of instruments and assignment of labels.

For the EM current meters the range of valid inertial ranges is shown against wavenumber and speed in Fig. 3.12. Note that the upper wavenumber limit of the inertial range of turbulence, the Kolmogorov (wavenumber) microscale, $1/\eta$, is much larger than that of the sensors, except possibly the thermistor bead [$\eta \approx 300$ μm for $\varepsilon = 1$ cm^2/s^3].

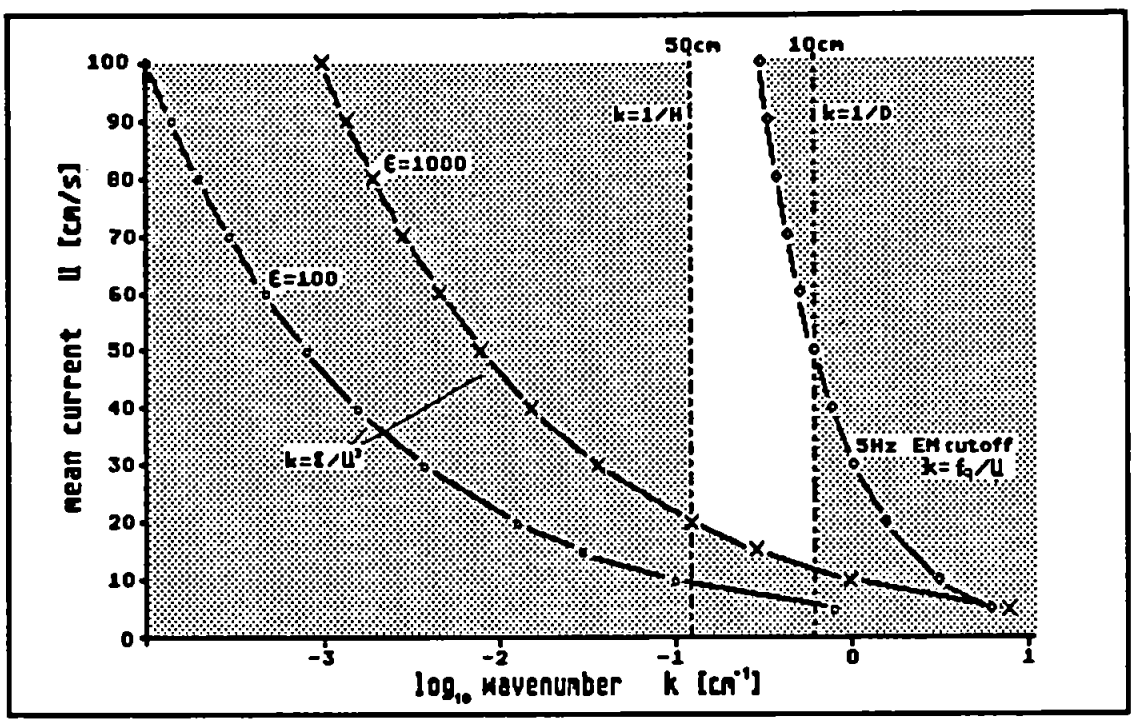

Fig. 3.12 Range of wavenumbers and currents for valid inertial range spectrum. For a given current speed the range of wavenumbers in which a valid inertial range may be found is indicated by the unshaded region.

The limits for which a valid inertial range may be expected are plotted in Fig. 3.12 against mean flow velocity. Spectra obtained from the observed time series were compared against the diagram to find the relevant wavenumber range - the unshaded region. It can be seen that below about 15 cm/s the dissipation estimates are likely to be less reliable and that at very high flow rates the filter roll-off at 5 Hz masks any inertial range.

3C2 Practical Constraints.

Other considerations involved ensuring that the flow reaching the EMs and sizer was affected as little as possible by the presence of the rig, and reducing the risk of trapping weed and debris on the frame. These resulted in the rig shown in Fig. 3.6 with the EMs on a pole at the front of the rig and

measuring vertical velocities, and components of horizontal velocities at 45° to the longitudinal direction. The pole was stayed to reduce movement and all obvious causes of excessive vibration, such as loose cabling and large flat surfaces, were removed or secured.

The sizer was mounted horizontally with the sampling volume at the same height as the EMs but offset to be in clear flow. The sizer casing is buoyant when submerged and so had to be placed centrally. The delicacy of the thermistor bead precluded pointing it into the flow and it was placed in behind a strut at the sampling height; although this strut certainly produced turbulence it was felt that the temperature information could still be useful.

The OBS presented no problems and were taped to the frame, facing outwards, and at heights above and below the other measurements. A 'Partech' suspended solids meter and a salinity meter were secured to the frame where they would not interfere with the primary measurements and as close to the sampling height as possible. A pitch and roll sensor was incorporated in order to check that the rig was on a flat bed and to warn if movement occured during deployment.

This arrangement had a definite forward direction and it was necessary to point the rig into the flow during both flood and ebb. The whole rig thus had to be heavy to keep it in position and also recoverable at least every six hours for turning. In order to achieve this a mooring-lifting barge was hired from 'Tozer and Sons' at Calstock (Fig. 3.13) who also provided head and stern moorings. The barge carried a diesel powered hydraulic winch for recovery of the rig. Housing and power for logging and monitoring equipment was provided on board m/v 'Tamaris' (PML).

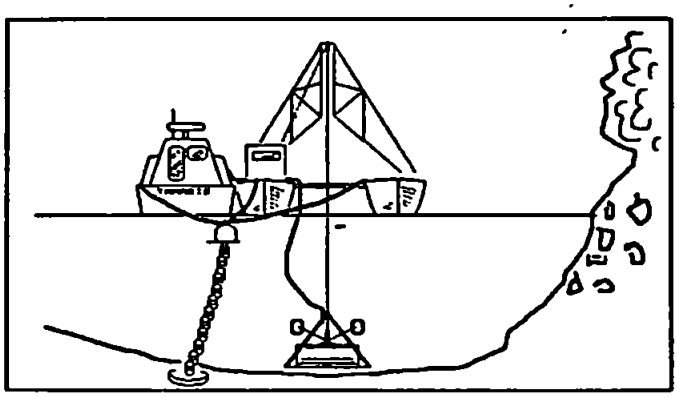

Fig. 3.13 Deployment of rig.

A plywood fin was fitted to the rig prior to each deployment and the rig lifted under power from on deck and swung under the lifting frame. Deployment was made soon after the flow at the bed had turned, as measured with the NBA current meter. The vane aligned the rig along the river as it grounded and, when the pitch and roll sensor had been checked, the vane was released and recovered after it had floated clear. The only deployment problems with this arrangement were met at low water when it was possible for the barge to have ridden over the rig and damaged it; veering the barge downstream on the mooring lines solved this.

3C3 Site of Experiment.

In order to sample flocs and turbulence from as wide a variety of conditions as possible, a site within the excursion of the turbidity maximum was chosen. As the turbidity maximum forms just upriver from the tip of the salt intrusion this site gives high salinities at HW, while at LW freshwater is experienced. In summer the turbidity maximum is located between Cotehele and Morwellham [Bale et al. 1985]. In order to minimise the effect of bed topography on the turbulent character of the flow, a relatively straight stretch of river was needed, and so that the rig could sit level and not move, the bed needed to be level and firm. These considerations were met reasonably well at a site 0.5 km upstream from the Calstock viaduct (see Fig. 3.14). There are gentle curves above and below the site and the bed is level, although the bank is steep and rock covered on the Devon side, while consisting of mud banks on the Cornish side. Water depths at LW of over a metre enabled sampling to continue throughout most of the day. The availability of head and stern moorings at the site reduced the likelihood of damaging consolidated bed by anchoring, and the disruption to the flow by boats moored further upstream was thought to be small and confined to the surface.

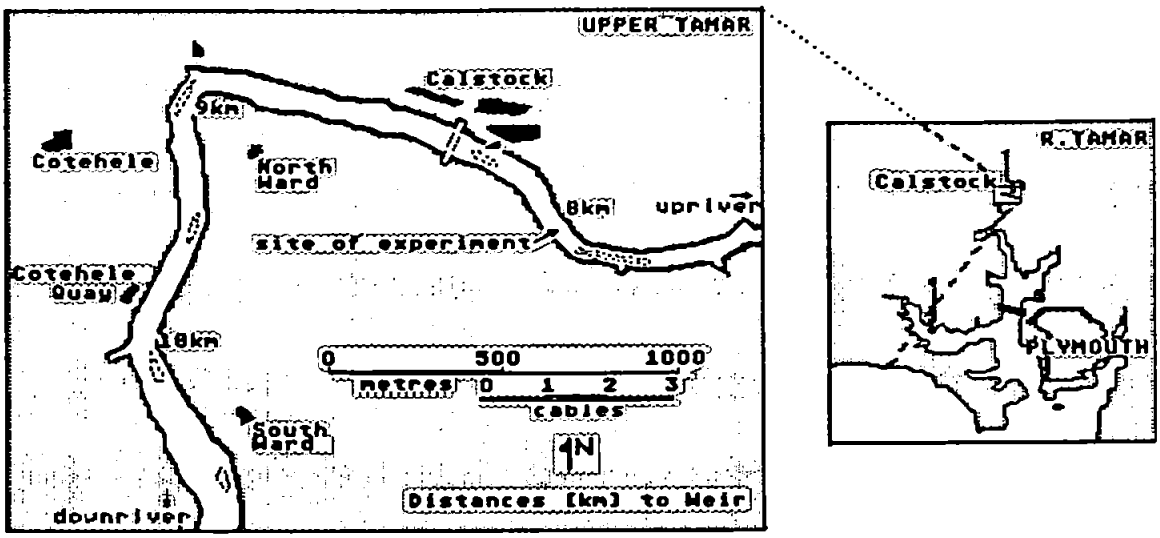

Fig. 3.14 Location of experiment site.

3D Sampling Strategy

Turbulence and size data were required from differing periods throughout the tidal cycle and although it was expected that slack water and maximum flood or ebb might provide the greatest contrast in turbulence it was useful, with regard to assessing the reliability of the results, to have a nearly continuous record of the turbulence. Less was known about the expected particle size distribution changes which again pointed to the need for a continual sampling scheme.

The data aquisition package used in the Calstock experiment could have sampled continuously for six hours (only limited by the space available on hard disc), however for ease of handling of the data for processing, and for flexibility in operation, a standard length of record of 4096 samples on each channel was chosen, giving a record length of just under six minutes when sampling at 12 Hz.

In order to record as continuously as possible the rig was deployed at the start of the ebb or flood, and remained on the bed until the mean flow at the bed became slack. The rig was then raised for cleaning and calibration of the sizer. While the rig was submerged sampling continued at twenty minute intervals on all instuments. Six-minute turbulence records started on the hour, and at twenty and forty minutes after, and were in many cases augmented by records starting ten minutes later. Sizer samples consisted of two thirty-second runs, starting every twenty minutes. Concentration and salinity from the rig were recorded at the time of sizer runs. (Also recorded were pitch and roll readings - these in no case varied after deployment). Profiling at half-metre depths from just below the surface to within half a metre of the bed continued at twenty minute intervals during the whole period that we were afloat.

The preliminary experiment at Cotehele in June/July 1988 showed that the six minute, 12 Hz turbulence records provided usable spectra for the derivation of dissipation rates. The Cotehele experiment also highlighted the need for back-up data of salinity and concentration variations in order to relate the differing velocity records to physical processes in the estuary. A twenty minute profiling scheme has been used in other work in the Tamar and proved satisfactory [Sturley 1990].

While the rig was submerged, output from the EMs was monitored using a chart recorder, in case weed became entangled or the pressure cases leaked, or any malfunction occured, as the data acquisition package gave no real-time indication of what was recorded. It was interesting to note that there was a large variability evident while the instuments were apparently behaving well, and this gave confidence when confronted by seemingly very noisy records during the processing stage.

Table 3.6 Instuments used, parameters measured, and sampling strategy.

4×	EM	U, u	12Hz	5 mins. ev. 20 mins.
2×	OBS	C, c	12Hz	5 mins. ev. 20 mins.
1×	thermistor	ϑ	12Hz	5 mins. ev. 20 mins.
Sizer		$Z\%$	30s	2 runs ev. 20 mins.
Profiles		S, C, Θ U, dir?	at 0.5m depths from 0.5m below surface to bed. ev. 20 mins.	
Pitch/Roll sensor			at rig	ev. 20 mins.
Salinity			at rig	ev. 20 mins.

General.

This Chapter is in three parts dealing successively with: (A) the observed data, which is presented in the figures of Appendix X; (B) the interrelations of the data sets acquired from each instrument (and which are found to be best characterized with reference to the averaged size distributions); and (C) in which the implications of the observations of part B are considered.

Part 4A Measurements.

4A1 Auxiliary Data.

The experimental work took place over a period of a fortnight during late June and early July of 1989 and resulted in the acquisition of four full tidal cycles of data. The first week of deployment was just after neap tides, during which data was obtained from two tidal cycles (28th June and 29th June). The second week began with spring tides and two further tidal cycles of data were obtained (July 4th and July 5th). Intervening days were used for setting up the system and making tests. An axial profile of the section of estuary above Calstock was made at HW on the morning of 6th July.

An abridged log of the fieldwork is given in Table 4.1. Tidal information, obtained from the Admiralty Tide Tables, is shown in Table 4.2 along with the measured maximum and minimum water depths observed from the mooring barge at Calstock. Table 4.3 is a brief description of the weather at Calstock. It is worth noting that wind waves never became larger than ripples of about 5 cm height. Table 4.4 shows the attitude in which the rig was sitting on the bed for each set of EM current meter records.

Table 4.1 1989 Experiment at Calstock.

Xnn: 5½ minute runs recording 4 EM current meter components
2 OBS concentrations
1 thermistor + 1 'dummy'
at 12 Hz, 4096 samples each channel.

Salinities, temperatures and concentrations as measured at rig ('*.PFL' files).
Height is total water depth at rig. Tide times and heights for Devonport.

Tuesday 27th June 1989

AM: *Tamaris* moored alongside barges 3 cables above Calstock bridge.
PM: Trial deployments of rig. Runs T01 - T05.

Wednesday 28th June 1989

0734 1.6
1348 4.6
2006 1.7 range 2.9m

Weather: SW 3/4, overcast with occasional light rain.

Hr	S	T	C	Ht	Remarks
9	0.5	17.4	120	2.0	0906 W00. 0908 commence profiling.
10	0.5	17.8	350	2.8	Setting up system. Experimenting with
11	3.0	18.5	370	3.9	earthing and interference.
12	8.1	18.9	80	4.5	1248-1308 rig raised.
1	9.5	18.9	50	4.7	1350 W17. 1355 rig raised.
2	13.2	19.0	35	5.0	1443 rig deployed.
3	13.6	19.1	25	4.6	1500 V00. Standard earthing config.
4	13.1	19.1	20	4.0	
5	7.9	18.8	40	3.5	
6	0.6	17.7	210	3.0	
7	0.5	17.4	220	2.5	1920 ceased profiling. 1927 rig raised.

V: 28 records, 0 unusable, 8 poor.

Thursday 29th June 1989

0845 1.6
1500 4.7
2120 1.7 range 3.0m

Weather: SW 4, intermittent light rain, clearing and becoming E 2/3, cloudy.

Hr	S	T	C	Ht	Remarks
10	0.5	16.5	150	1.8	1005 comm. profiling. 1015 rig deployed.
11	0.5	16.8	240	2.6	1119 H07, rig raised to clean. 1140 H08.
12	2.0	17.8	400	3.8	
1	7.5	18.4	180	4.3	
2	11.8	18.8	35	4.9	
3	13.4	18.9	30	5.0	1500 H32. 1511 rig raised for turning.
4	14.1	18.9	10	4.9	1630 rig deployed, vane left on. 1632 G00.
5	12.9	18.8	10	4.3	1720 G05. 1728 rig realigned, vane removed.
6	10.4	18.7	30	3.8	1730 G06.
7	1.8	18.2	140	3.1	
8	0.5	17.7	240	2.4	2032 G32 cease profiling. 2045 rig raised.

H: 33 records, 4 unusable, 5 poor.
G: 33 records, 3 unusable, 3 poor.

Monday 3rd July 1989

'Bucket' tests of EM flowmeters. Runs B04, B05, B07.

Tuesday 4th July 1989

0736 5.1 Weather: Light Airs, partly cloudy.
1334 1.0
1952 5.4 range 4.4m

Hr	S	T	C	Ht	Remarks
8	.	.	.	.	0840 comm. profiling. 0850 rig deployed. 0854 S00.
9	12.3	19.5	50	4.6	0920 S03. Rig raised to clean. 0954 S04.
10	9.7	19.4	35	4.0	1019 S08. Rig raised to install transducer. 1034 S09.
11	2.8	19.3	140	3.3	
12	0.6	19.2	430	2.3	
1	0.6	19.0	460	1.8	
2	0.5	19.1	310	1.5	1420 S33. 1430 rig raised for turning.
3	0.5	19.6	250	1.4	1538 rig deployed. 1541 R00.
4	0.5	20.2	410	1.8	
5	2.0	21.1	M+	4.0	[M+ indicates concentrations exceeding 1000 mg/l]
6	10.6	21.0	430	5.0	
7	15.2	20.9	140	5.5	
8	16.4	20.8	90	5.5	2020 R34, cease profiling. 2026 rig raised.

S: 34 records, 1 unusable, 3 poor.
R: 35 records, 2 unusable, 6 poor.

Wednesday 5th July 1989

0819 5.1 Weather: E 3/4, partly cloudy, showers later
1417 1.1
2031 5.4 range 4.3m

Hr	S	T	C	Ht	Remarks
9	.	.	.	.	0940 rig deployed, comm. profiling. 0947 N00 rig not level. 0955 rig redeployed. 1000 N01.
10	7.2	20.1	50	4.7	
11	6.8	20.2	55	3.9	
12	1.7	20.1	230	3.1	
1	0.7	20.0	410	2.4	
2	0.6	19.5	450	1.9	
3	0.5	19.2	340	1.5	1501 N33. 1506 rig raised for turning.
4	0.5	19.2	290	1.3	1630 rig deployed. 1632 D00.
5	0.6	20.0	M+	2.5	[M+ indicates concentrations exceeding 1000 mg/l]
6	5.9	20.4	630	4.6	
7	14.0	20.4	350	5.2	1947 D24. 1959 D26.
8	16.9	20.4	20	5.6	2000 cease profiling. 2005 rig raised.

N: 34 records, 5 unusable, 3 poor.
D: 27 records, 2 unusable, 3 poor.

Thursday 6th July 1989

AM: 'Bucket' tests C04 (24Hz), C05 (12Hz). Axial profile above Calstock.
PM: *Tamaris* return to Plymouth.

Comments (11/89)

Profiles for 4 full tidal cycles were recorded. Rig was deployed during 3½ tidal cycles. 224 runs obtained and disssipations evaluated for horizontal channels. 17 (8%) records provided no identifiable inertial range, 31 (13%) provided poor spectra; this occured mostly when low turbulent energies coincided with low mean flows (below ≈10 cm/s). 79% of runs were usable.

Table 4.2 Tides (Admiralty Tide Tables)

		Predicted				Observed	
		Devonport		Cotehele		Calstock	
June	28	0734	1.6	0800	0.8	(0900	2.0)
		1348	4.6	1420	3.8	1340	5.0
		2006	1.7	1940	1.0	(1920	2.0)
	29	0845	1.6	0900	0.9	(1000	1.8)
		1500	4.7	1500	3.7	1500	5.0
		2120	1.7	2200	1.1	(2040	2.1)
July	4	0736	5.1	0740	4.0	0840	4.8
		1314	1.0	1400	0.7	1520	1.3
		1952	5.4	2000	4.2	1940	5.8
	5	0819	5.1	0836	4.1	(0940	4.7)
		1417	1.1	1440	0.7	1520	1.3
		2031	5.4	2100	4.3	2000	5.4

(Calstock depths are as measured at the barges)
(Bracketted readings are not at HW or LW)

Table 4.3 Weather. (Beaufort notation)

27	pm:	*1400 W 4/5 pr/o/c, 1645 W4 bc*
28	am:	*0920 S 3/4 o, 1000 SW 3/4 c/o/c, 1110 SW 3/4 o/dz*
	pm:	*1430 SW 4 c/dz, 1720 SW 4 o, SW 4 dz*
29	am:	*0940 SW 4 dz/o, 1235 W 4 o/c*
	pm:	*1300 lt. airs c/bc, 1720 lt. airs bc, 1945 E 2/3 bc/c*
4	am:	*0830 lt. airs b, 1120 E 3 b/bc/b*
	pm:	*1400 E 1 b, 1525 SW 2 b, 1645 lt. airs b, 1820 calm bc*
5	am:	*0930 E 3/4 c, 1115 NE 4 b/bc/c, 1235 NE 3 c/o*
	pm:	*1410 NE 4 o, 1600 E 4 o/c, 1740 NE 3 c/o,*
		1800 pr, 1840 pr, 1900 calm ir

Rainfall over the previous month was slight [PSW METENQ]

Table 4.4 Pitch and Roll.

Date	Time	Runs	Pitch	Roll
28	0905-1240	W00-W15	0	1 Pt
	1310-1350	W16-W17	-6	16 St
	1450-1920	V00-V27	-4	0
29	1020-1120	H00-H07	+4	1 St
	1140-1500	H08-H32	+6	6 St
	1630-1720	G00-G05	-3	2 St
	1730-2000	G06-G33	-4	3 St
4	0852-0920	S00-S03	-2	2 St
	0940-1020	S04-S08	-1	2 St
	1034-1440	S09-S33	-3	4 St
	1540-2000	R00-R31	-1	6 St
5	0955-1500	N00-N33	0	2 St
	1632-1920	D00-D23	-2	0
	1940-2000	D24-D26	0	3 Pt

Pitch is given as degrees tilted up at forward corner.
Roll is given as degrees tilted to port (Pt) or starboard (St).
All changes in attitude correspond to redeployments of rig.

4A2 Boundary Layer.

4A2.1 Velocity. (Fig. X4)

The mean current (6 minute average from each EM current meter record) shows a short, rapid flood followed by a stand and longer lasting ebb (with the flood less pronounced during neap tides). This is expected in the upper Tamar, which narrows and shelves rapidly in its upper reaches. The ebb, near the bed, begins with a rapid increase in mean current at both springs and neaps; the acceleration of the flood is dependent on the tidal range. Approximate mean flow maxima are, at 50cm above the bed:

	Flood	Ebb	
Spring	80	50	cm/s
Neap	45	45	

The relative angle of attack (defined as $\alpha = \tan^{-1}(u_0/u_3)$) was generally between 60° and 80° - indicating a flow arriving at the rig from 15° to 35° left of ahead; this applied on both flood and ebb, with the current tending to come more ahead as the mean speed increased.

The vertical mean velocities lie within +/- 4 cm/s of zero, with maximum inclination to the horizontal of about 10°, and with the two channels fairly well correlated (see Fig. X4 (a)-(d)). The pitch-and-roll sensor indicated the rig to be sitting on a flat bed at each deployment (with no shifting during deployment) so that the non-zero mean flows and angle of attack are thought to be due to secondary flows; the experiment site was on a slight curve of the river and the bed was steeper on the Devon side than the Cornish side. The rig was deployed at slack water, when only the weak main flow influenced the vane.

For angles of attack near to 90° (or 0°) turbulence data is suspect due to blanking and vortex shedding by the upstream flowmeter, however such records were not used for dissipation estimates as mean flows were too small; mean current speeds were used as recorded.

4A2.2 Suspended Solids Concentration. (Fig. X5)

The two OBS sensors (mounted at 23 and 56 cm above the bed) record similar concentration variations to the 'Partech' SPM meter (section 4A3 below). However in order to get approximate agreement of magnitude between 'Partech' and OBS, the OBS data needed further division by a factor of four. This

is thought to be due to the different reflective characteristics of the mud at the sampling site to that used in the original calibration. Adjusted OBS concentrations reached approximately 1600 mg/l in the spring turbidity maximum. The divergence of the two concentrations with time (*eg* 29/1300 4/1200 5/1400 [notation is DAY/TIME]) is thought to be due to differing rates of silting over of the OBS sensor windows; the effect does not persist over periods when the rig is raised and cleaned. If the effect were due to settling out of sediment on decreasing currents both series would be expected to fall but at differing rates. There was occasional fouling of the sensors by strands of weed, showing up as a large oscillating signal on one instrument; however this was readily detected and was not a major problem. The OBS windows were cleaned with a detergent solution before each deployment although silting up was not apparent at the time. Spectra obtained from the OBS data were generally good with little contamination by spurious frequencies. An inertial range, with '-5/3' slope, was easily discernible in most records, and a possible viscous convective range, with '-1' slope, was observed in several.

4A2.3 Temperature. (Fig. X4)

Temperature is well correlated with salinity, (see Fig. X16) with temperatures highest at HW. The increase in temperature over the flood tide of the 4th July is thought to be due to solar heating during the day which was almost cloudless, unlike the other days which were more or less overcast. The obvious explanation, that the sun heats the drying mudbanks which in turn heat the incoming flood, is backed up by the observation that temperature starts to increase with the flood. Heating may also be occuring while the mud banks are draining; however each of the four days shows the same temperature fall over low water.

4A2.4 Turbulent Intensities. (Fig. X6)

The turbulent intensities, $\sqrt{(variance)}/mean$, of EM current meter and OBS sensor records provide an indication of the quality of the data. Estuarine turbulent intensities are generally in the range 0.0 to 0.3 [Anwar 1981; West et al. 1986; Bowden and Ferguson 1980; see section 2A3]. Excessive intensities are presumed to be due to instrument noise or fouling rather than to turbulence. Figs. X6 (a)-(d) show the intensities recorded; values of above 1.0 are deemed noisy

and these records are only used for the derivation of mean values. This interpretation of large intensities is borne out by inspection of the time series which show an obviously different character and which begin and end abruptly.

There are periods in each day during which the turbulent intensity is recorded as 0.5 and above, and these are in some cases coincident with flow events, such as the change in salinity on the ebb or the flood turbidity maximum, but there is no consistency between each of the days. There are also occasions when all four EM channels show peaks in intensity at the same time but of different magnitude. However inspection of the time series reveals that the variance increases instantaneously and it seems very unlikely that such a change in the flow would not show up in increased signal on, for instance, the OBS channels. Since the EM heads are separated by about 40 cm, only long strands of weed would be likely to affect both instruments at the same time; only short strands of weed were ever apparent on the rig on recovery. The cause of these periods of high noise is thus unknown. However such periods are identifiable from inspection of the time series and discarded from further processing.

It is somewhat surprising that the ratio of vertical to horizontal intensity is greater than unity over most of the sampling period whereas other surveys have found a typical ratio $w':u' \approx 0.7$ [Anwar 1981, West et al. 1986]. It should be noted that a ratio closer to unity is expected in this case since each horizontal channel is measuring $(u \pm v)\cos \pi/4$. Similarly the ratio of vertical to horizontal dissipation rates is expected theoretically to be $(4/3)^{1.5}:1$ [since the horizontal Kolmogorov constant has been used for both vertical and horizontal dissipation calculations] but is measured here as greater. It is known from the laboratory tests of noise levels that the channel *u2* (EM27X) was noisiest and for this reason this channel was oriented to measure one of the two vertical components. Field 'bucket tests' however show *u2* as no noisier than other channels. See Fig. 3.2.

If it is assumed that the intensitity and dissipation ratios measured here are correct, then they indicate either increased vertical fluctuations - possibly due to internal wave activity - or decreased longitudinal or transverse fluctuations. Neither of these possibilities is indicated by the proximity of bed, bank or barge hulls, nor by the stratification of the flow.

Inspection of velocity time series reveals a different character to the vertical fluctuations rather more clearly than the spectra do. It should be noted that the horizontal dissipations *e0* and *e3* have been 'cleaned' by recalculating 'dissipation spectra' block by block and removing sections of the time series with excessive variances. No dissipation value is obtained for vertical channels with large variances.

Temperature variances were too small too show up with the program used to derive the other components, howevever inspection of the time series reveals that the largest turbulent fluctuations of temperature occur while the temperature is changing most rapidly; this is partly due to the fact that turbulent mixing only shows up where there are temperature gradients but inspection of the temperature records reveals wavelike fluctuations on the ebb tide. No further work has been done on the temperature records except to note that they may provide information on mixing on the ebb.

4A2.5 Turbulent Dissipation Rates. (Fig. X4)

Turbulent dissipation rates were obtained as described in section 3B3 and those with no valid inertial range discarded, with the exception of those indicating low dissipation rates on low mean flows: the dissipation estimate is not accurate but is still correctly indicating low turbulence.

The turbulent dissipation rate values (ε) that remain after removing records with noise are shown as time series in Fig. X4. There seems to be little structure to the time series except for the period during which the top of the salt wedge passes the sensors and which shows up as a period of increased dissipation with a pronounced brief drop at its centre. This period has a marked influence in each data set.

Plots of dissipation rates against mean current are shown in Fig. X17 and comparisons of the two horizontal channels can be made in Fig. X4, where reasonable agreement is found.

'Dissipation rates' were obtained from the fluctuating concentration data but time series of 'dissipations' revealed little; the concentration spectra were generally good and little contaminated by spurious peaks. An inertial dissipation range is discernible in most OBS spectra.

4A3 Sizer. (Figs. X7 to X11)

4A3.1 Histograms.

The laser sizer partitions the floc data into sixteen (very) roughly logarithmically spaced size bands which may be plotted as histograms of percentage weight (assuming floc density to be constant) in each band. These provide information on the floc distribution at one time.

In order to appreciate the variation of the size distribution over time the size bands are plotted together in Fig. X7; the width of each band corresponds to the percentage weight in that band, with largest flocs at the top of the plot. Obvious features are the large percentage of small particles in the flood turbidity maximum during springs (and less so at neaps), and the retreat of the salt intrusion which is accompanied by a pronounced change in the size distribution.

Absolute band weights, shown in Fig. X8, are obtained by proportionately distributing SPM concentrations obtained from the 'Partech' siltmeter profiles according to the sizer results. (Note that the siltmeter effectively measures the cross-sectional area of a floc by light obscuration; *ie* $(vol.)^{2/3}$).

The 'weight' obtained from the sizer is based on the assumption that the particles all have the same density and is thus more a measure of floc volume than mass. A correction may be made to the distribution if a size/density relation is assumed and this considerably reduces the mass contained in the larger size bands which is important in considering deposition and erosion rates. In Fig. X9 the size/density relation of Table 2.2 is used to obtain a mass distribution. In order to maintain comparability with the 'Partech' SPM concentrations it is assumed that flocs of 50 μm diameter have "Partech density" - that is that the 'Partech' siltmeter is calibrated correctly for a suspension of 50 μm flocs. (This correction is not applied to other sizer plots since it tends to obscure the larger size bands).

[The notation $\mathbb{Z} = (\mathbb{Z}1, \mathbb{Z}2, \ldots \mathbb{Z}16)$ is used to denote the particle size distribution, with $\mathbb{Z}1$ being the (absolute) weight in the smallest size band (≤5.8μm) and $\mathbb{Z}16$ that in the largest size band. $\mathbb{Z}\%$ is similarly the relative size distribution. It is useful to split the distribution into two populations ($\mathbb{Z}_P$ and $\mathbb{Z}_A$), divided by the

diameter 50.2 μm, so that $\mathbb{Z}_P$=($\mathbb{Z}$1, $\mathbb{Z}$2, .. $\mathbb{Z}$10) and $\mathbb{Z}_A$=($\mathbb{Z}$11, $\mathbb{Z}$12,..$\mathbb{Z}$16). This decomposition is justified in section 4B2, and plotted in Fig. X10].

4A3.2 Quality.

The quality of the observations is indicated by the distributions being mostly centered within the range of the sizer, and by the fact that pairs of observations taken concurrently are closely matched. The particle sizer program provides two statistics to indicate the reliabity of the sizer data: (i) the *log error* indicates how well the calculated distribution fits the observed diffraction, values for the *log error* of less than 5.0 are considered good, and are usable if less than 5.5; (ii) the *obscuration* indicates how little light passes through the suspension; values for *obscuration* of between 0.10 and 0.60 are good, and up to 0.95 gives reduced accuracy, above 0.95 results are unreliable.

Most of the time both *obscuration* and *log error* were in the acceptable range; however at times of high turbidity the *obscuration* rose to between 0.60 and 0.95 with 0.97 being reached in the spring flood turbidity maximum. The sizer results from the peak of the spring flood turbidity maximum show distributions strongly biased to the smallest size bands and the 'Malvern Instuments' manual suggests that these sizes should be doubled (see also West et al. 1990).

This problem could be avoided by reducing the optical path length (different path-length lens sytems may be bolted on); this would have meant raising the rig just before a strong flood started - this in fact occurs very shortly after LW and would have presented no problem. Replacing the longer path lenses after the passage of the turbidity maximum would have been less acceptable as continuity of data would have to be lost and rapidly decreasing bed currents could make alignment of the rig difficult on redeployment.

4A4 Profile Data.

4A4.1 Profiles.

Vertical profiles of current, salinity, concentration and temperature provide information on the flow at twenty minute intervals and at half metre depths from 50 cm below the surface. (Profile plots are not included here - see contour plots Fig. X12).

Current direction information has been used only to provide a sign for the mean velocity: all currents with an upstream component are recorded as positive regardless of the cross-stream strength. Depths are less accurate for currents above about 40 cm/s due to drag on the cable and current meter. Maximum deflection of the current meter cable from the vertical was around 30°, giving an error in depth of up to 15%, or about 0.4 m, during periods of strongest flow. No attempt has been made to correct for this in the plots.

Note that the concentration gradient is inverted at high water when muddier, less saline water begins to ebb at the surface before the flood of clearer salty water ceases at the bed.

4A4.2 Contour Plots. (Figs. X12)

In order to show the time variation of the profile data the components are plotted against depth and time and contoured (Fig. X12 (a)-(d)). (Note that the time is on the horizontal axis so that care must be taken in interpreting the plots as a spatial description of the salt intrusion).

4A4.3 Features.

The salt intrusion is an obvious feature of the salinity plots. Salinity, with its low molecular diffusivity, is a very good marker of the water body, which advances up the river as a 'wall' on the flood and then drains out of the upper reaches during the ebb. The stratification of the river as the ebb begins is also apparent, resulting in a sharp interface between fresh and saline water which lasts for three to four hours.

In the velocity plots the interface between ebbing and flooding water corresponds to the fresh- salt water interface, showing the fresh water riding over the salt intrusion. The interface is also, more weakly, apparent in the concentration contours.

Concentration plots show the turbidity maximum as it passes the station twice each cycle. The turbidity maximum is closely related to the maximum current speeds and also shows some settling of suspended solids in the rear (later) of the maximum. The concentration maximum lags behind the current maximum slightly (approx. 20-40 mins.) on the ebb but not at the flood; this suggests that the ebb turbidity maximum is a 'passive' feature formed from the decaying flood turbidity maximum.

Part 4B Results.

4B1 Average Tide Model.

The profile data for each of the four days show many common features. In order to compare measurements obtained on different days the data are related to a model of a 'typical tidal cycle' at Calstock, which is based on the contoured profile data.

4B1.1 Flood.

The main feature of the model is the salt intrusion which pushes up the estuary to varying distances dependent on the tidal range. On the flood the narrowing of the estuary above Cotehele steepens the advancing tidal wave which continues upriver as a wall of vertically well mixed water of increasing salinity - see salinity contours (Fig. X12) for 28/1100, 29/1200, 4/1700, 5/1800.

As the salt intrusion advances upstream, outflowing (low salinity) river water is slowed and pushed back upriver. By the time the intrusion reaches Calstock the front of the tidal wave is formed of fast moving, low salinity water which has recently ceased to be part of the ebb.

The current accelerates rapidly after low water reaching its maximum about 1 hr. after LW at springs, 2 hrs. at neaps. The tide continues to rise for another 2 hrs. with gradually slackening current speeds until the stand occurs and the salt intrusion is halted - or almost so. The velocity profiles are modified by bed friction and are roughly parabolic during the flood. Greatest shears occur near the bed at the time of maximum current (and maximum rate of rise of tide).

There is a background of suspended solids in the river water of between 100 mg/l and 200 mg/l. Suspended solids concentrations on the flood reach their maximum at the same time as maximum shears are measured suggesting that much of the material involved in the turbidity maximum is resuspended on each flood. After the turbidity maximum has passed the clearer water of the salt intrusion itself passes and concentrations reduce as the salinity increases.

Note that continuity requires that the region of greatest velocity - the front of the advancing salt intrusion - is moving upstream faster than the water particles.

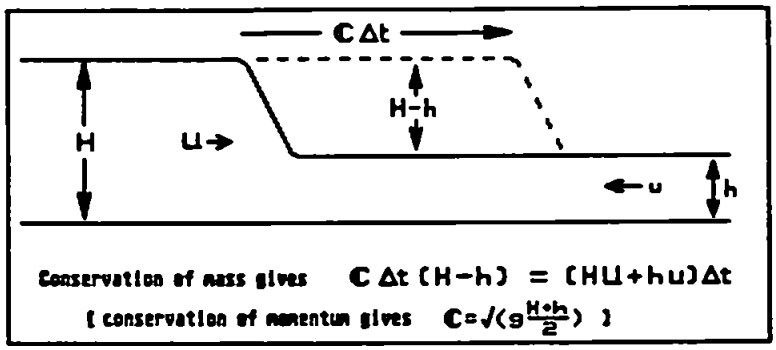

Fig. 4.1 Speed of advance of tidal wave.

In Fig. 4.1 the flood is flowing with speed U and depth H, stopping and turning back the ebb which has speed u downriver and depth h; the speed of advance of the front of the flood is given by C and mass conservation over the region containing the front requires $C = (HU+hu)/(H-h)$. Substituting observed (spring) values of $H=300\,cm$, $h=100\,cm$, $U=100\,cm/s$, $u=10\,cm/s$, $C=160\,cm/s$; the region of maximum current - at the salinity front - is thus travelling about 50% faster than the water itself. This means that the position of the turbidity maximum must be moving faster than its constituent particles. The leading region of the turbidity maximum therefore consists only of recently resuspended material plus the background river SPM concentration.

As the current slows the SPM profiles show greater concentrations near the bed indicating settling out of particles or limited resuspension. Note that this is not due to shearing of the turbidity maximum by vertical velocity gradients as the salinity contours would then also show stratification. The slopes of the concentration contours after the turbidity maximum indicate settling velocities of between 2 mm/s and 0.5 mm/s (large flocs and dense particles) at springs and neaps respectively; sizer data shows large particles at neaps but small particles at springs - see section 4B2.2. If this is assumed due to settling out then the depositional flux may be estimated from the contour plots X12(a)-(d), as follows.

Supposing that the sediment is completely mixed at the time of resuspension into the turbidity maximum and that after its passing sediments settle out with their respective settling velocities, then each contour records the settling of those particles which were at the surface when the turbidity maximum passed. For the 500 mg/l contour at springs the settling velocity is 2 m in 3 hrs

(allowing C= 1.5 m/s, U=1 m/s), that is $w_s \approx 1.9 \times 10^{-4}$m/s (0.2 mm/s), corresponding to a particle size of 50-100 μm. The depositional flux is then $Cw_s \approx 10^{-4}$ kg/m²/s. Neap values are for the 200 mg/l contour give $w_s \approx 3 \times 10^{-4}$, corresponding to 100-200 μm flocs, and depositional flux $Cw_s \approx 6 \times 10^{-5}$ kg/m²/s. These being reasonable results (eg Oduyemi 1986) suggests that the SPM distribution is dominated at this time by settling out of particles resuspended during the current maximum.

Temperature followed salinity in general (see Fig. X16), with the salt intrusion warmer than the river water. The largest temperature variations over a tidal cycle were of about 2 °C so that any temperature effects on density were less than 3% of those due to salinity.

There are several likely mechanisms whereby the time of low water might have a considerable effect on erosion and floc strength. The effect of temperature (due to solar heating of the mud banks) on the biology of the estuary may alter the strength of mucal bonding; light also could affect the growth rates of organisms in the estuary and this would be strongly dependent on the time of day during which the mudbanks were uncovered. At the spring low water the mud banks could be seen to be covered by a greenish-yellow film. It seems likely that a complete description of resuspension and erosion should include 'time of exposure' of mud bank effects, however this work will concentrate on the erosional and floc-strength properties of the muds as observed; future work may shed light on the variability of these properties of mud beds.

4B1.2 Ebb.

The ebb begins at the surface earlier than at the bed; that is, fresher water from upstream begins to overide the salt water which is still moving upstream at the bed. An interface is apparent in each component of the contour plots and divides the fresher, ebbing, muddier, (cooler) water upstream from the saltier, flooding/stationary, clearer, (warmer) water below and downstream.

The height above the bed of the interface reduces steadily over a period of about 3 hours. During the stand over HW the lower layer is stationary and is eroded from above by entrainment into the surface layer (section 4C2.3 below). As the tide begins to drop the lower layer begins to ebb so that

eventually, at about half tide, the tip of the salt wedge retreats downstream, at a rate rather more slowly than the 30 to 40 cm/s of the surface layer.

As the tip of the salt wedge passes, the near bed current speed increases rapidly to that of the upper layer and the ebb continues as one layer with roughly parabolic current profiles and increased velocity.

The increase of current after the salt wedge retreats (to a speed greater than that of the initial upper layer) is probably due to the surface water slope increasing as the mud banks downstream drain. (Less water is trying to get out of the estuary. There are no mud flats above Calstock so that the ratio of water volume above Calstock to that below Calstock changes when the mud flats above Cargreen begin to dry).

About 20 to 40 minutes after the current speed and bed shear maximum the SPM concentration reaches its maximum. After this both current and concentration decrease slowly to approximately 20 cm/s and 100 to 200 mg/l respectively. The SPM concentrations here represent a 'background' of suspended matter which is present in the fresher end of the estuary.

Note that the river water has become muddy in its journey from Weir Head where it enters the estuary. Water at the very top of the estuary is clear although the turbidity maximum reaches to within a quarter of a mile of Weir Head, see axial profile at HW (Fig. X18 (a)). Fresh water flowing downstream from the weir at LW erodes the bed and acquires the background suspension.

4B1.3 Comparisons.

Using the above model, features of each day may be compared.

At spring tides the salt intrusion pushed further up the estuary and bed salinities reached 17‰ compared with 14‰ at neaps. This is expected with the larger spring tidal range but will also be related to the freshwater input; the second half of June was dry and the only rain during the experimental period was on 5th July.

Larger tidal ranges produced greater current speeds on the flood, but had no effect on the ebb, and with higher current speeds the SPM concentrations increased (see Table 4.5).

Table 4.5 Variability of Turbidity Maximum.

Date	EBB Concentration C	Zp	ZA	U	Salinity	FLOOD Concentration C	Zp	ZA	U	Salinity
28	240	60	160	41	0.5	520	160	360	47	0.7
29	250	50	200	44	0.6	520	160	370	48	0.7
4	430	260	270	49	0.6	1000+	1000	460	72	0.8
5	450	230	290	53	0.6	1000+	950	330	77	0.9

[Current speeds(cm/s) and concentrations (mg/l) are the ebb or flood maximum; salinities (‰) are for maximum concentration. NB ZA and Zp reach their maxima at different times.]

The major difference between the flood and ebb is brought about because during the flood the velocity distribution is acting to reduce stratification whereas during the ebb the velocity distribution is acting to increase stratification. (On the flood, bed friction acts on a longitudinal salinity gradient to create an unstable salinity profile as more saline water is carried upstream faster near the surface than near the bed. On the ebb the velocity profile acts to carry lower salinity water downstream faster near the surface than near the bed, thus creating stable stratification.) This gives a well mixed flood and a stratified ebb. The ebb velocity time series are very similar in magnitude and form whereas the flood velocities are influenced by the tidal range.

4B1.4 Fluxes.

Longitudinal fluxes of salt, SPM and heat (Fig. X13) are readily obtained from the profile data. Tidal average fluxes are not obtained as it is not possible from the few days of observation to reliably define the start and end of each tidal cycle. Null-velocity times are not a suitable reference point when tidal ranges are varying and this is especially true when the processes under investigation are due to tidal range dependent flux differences. A net upstream flux of sediment is apparent during spring tides and this is due to the asymmetric tides experienced at Calstock. The spring flood erodes material from the bed and carries it upstream; no erosion, or little, occurs on the weaker ebb. Little of the eroded material returns downstream.

The sizer data shows the spring turbidity maximum to be composed of predominantly fine particles (however see comment on *obscuration* in 4A3.2) Particles which have settling velocities of less than about 1 m in 8 hrs. ($d \sim 20\mu m$)

will remain in suspension until the ebb carries them out again. The upstream SPM flux indicates that a proportion of the eroded material must be settling out upstream: either eroded particles are much larger than the sizer has recorded or are flocculating further upstream.

Salt is pumped upstream as tidal ranges increase, and downstream as ranges decrease. The upstream heat flux at springs and not at neaps is explained by the fact that the mud flats were covered over midday at neaps while being exposed over midday at springs. The temperature/salinity plots (Fig. X16) show this occuring on July 4th which was fine while the mud banks were exposed. July 5th was cloudy and there was little temperature change on the flood.

4B2 Size Distributions.

4B2.1 Z_A and Z_P. (Fig. X10)

As noted in 4A3.1 there is a difference in the behaviour of the largest and smallest size bands. From the relative size plots (Fig. X7) it can be seen that the distributions are roughly bimodal with the two peaks separated by bands 8 to 10; there are two populations - large particles with diameters greater than approximately 50 μm, and small particles with diameters less than approximately 30 μm. Sternberg et al. [1988], using nephelometer profiles, similarly found that particles of greater than about 10 μm diameter were likely to be flocs in San Fransisco Bay.

The smaller sized population is dominated by the smallest sizer band consisting of particles with diameters less than 5.8 μm. Note that this smallest size band might better be plotted in the histograms with a width of at least 5 bands if the same roughly logarithmic scale were used throughout, and that this would considerably alter the appearance of the histograms. However particles smaller than 5.8 μm will be primary particles and microflocs and their structure is thought to be stable under the conditions we are investigating (the initial flocculation processes, which form the microflocs from freshwater input, occur at the head of the estuary).

Particles of diameter less than approximately 50 μm have settling velocities of the order tenths of millimetres per second which enables them to remain in suspension over periods greater than 6 hours, and which consequently

remain suspended indefinitely as tides ebb and flow. Plotting the absolute weights of Fig. X8 as two populations, $\mathbb{Z}_P$=$\mathbb{Z}$1..10 and $\mathbb{Z}_A$=$\mathbb{Z}$11..16, shows the differing behaviour of large and small particles (Fig. X10).

The larger bands are more closely linked to the mean current and $\mathbb{Z}$11..16 correlates well with near bed velocities, except at spring flood, suggesting that these large particles and flocs are being eroded from the bed rather than aggregating whilst in suspension.

The smaller size bands $\mathbb{Z}$1..10 have a maximum at the peak of the spring flood whilst at the ebb these small particles form a broad maximum at the upstream end of the turbidity maximum.

Based on this the two populations may be considered as: a permanently suspended load, $\mathbb{Z}_P$ (~$\mathbb{Z}$1..10 consisting of primary particles and microflocs), and a periodically resuspended load, $\mathbb{Z}_A$ (~$\mathbb{Z}$11..16 consisting of aggregates).

4B2.2 Behaviour of $\mathbb{Z}_A$ and $\mathbb{Z}_P$.

The larger particles, $\mathbb{Z}_A$, follow the mean velocity at 50 cm above the bed fairly closely at periods other than in the spring turbidity maximum (Fig. X15). At current speeds above about 45 cm/s the numbers of large particles fall off rapidly This suggests that flocs (and perhaps other large, low density materials) are being easily resuspended by the action of the near bed shear, but that at higher velocities these flocs are broken up on resuspension. Lavelle et al. [1984] used similar observations of cohesive sediments resuspended at low shear stresses to argue against the concept of a critcal erosion velocity.

The smaller particles, $\mathbb{Z}_P$, are almost entirely absent at neap tides, and at spring tides are associated most obviously with the flood turbidity maximum; this is likely to be due to erosion deeper into a more consolidated bed during periods of high current and/or breakup of larger resuspended particles. Based on the near bed velocities during the turbidity maximum on the 4th and 5th July, a critical erosion speed of about 50 cm/s is suggested (see Table 4.5) - in broad agreement with other observers [Oduyemi 1986, Uncles and Stephens 1989]. On the ebb these fine particles reach their highest concentration up to 2 hours later than the larger particles. Without knowing the longitudinal distribution of particle sizes there are two obvious explanations for these observations, one an advective effect and the other local, and these are discussed below.

4B2.3 Time Variation of Z%.

Assuming erosion of fine particles on the flood, these remain in suspension during the remainder of the flood and over the start of the ebb, but the action of velocity shear will broaden out the longitudinal distribution. Larger particles will settle out earlier, and not reach so far upstream. When the current picks up again on the ebb (just after the retreat of the salt wedge) the large particles will be resuspended and form the first section of the turbidity maximum; the smaller particles having travelled further upstream, and not now being tied to the current speed maximum, will return later as the later part of the ebb turbidity maximum.

Alternatively, ignoring advective effects, the gradual increase of smaller particles at the expense of the larger during the ebb could be due to the turbulent disruption of flocs; this would apply also on the flood. Dissipation rate data, however, does not support this second mechanism as the primary cause of the observed variations. (See Fig. X11 where dissipations are plotted with d_{max} - defined in section 4C3).

A striking feature of the relative size distributions (Fig. X7) is the smooth way in which they vary with time. The only exceptions to this are the spring flood turbidity maxima - which pass in a relatively short time, and the retreat of the salt wedge.

Overall the distributions change relatively slowly during the tidal cycle: this suggests that typical distributions may be attached to periods of the flow.

In order to compare size data for different days, and to relate it to hydrodynamic processes, periods during which the relative distributions varied little were identified for each day and labelled by reference to the idealised model of section 4B1. The averaging periods used are shown in Table 4.6; note that during 'max.ebb' the smallest size band is increasing at the expense of the largest band.

The time averaged distributions are shown in Figs. X19 (a)-(d) and their relation to the 'model' is shown in Fig. 4.2. There was only one observation of a 'last.ebb' distribution as the rig was lifted just before low water for turning and cleaning ready for deployment on the incoming tide.

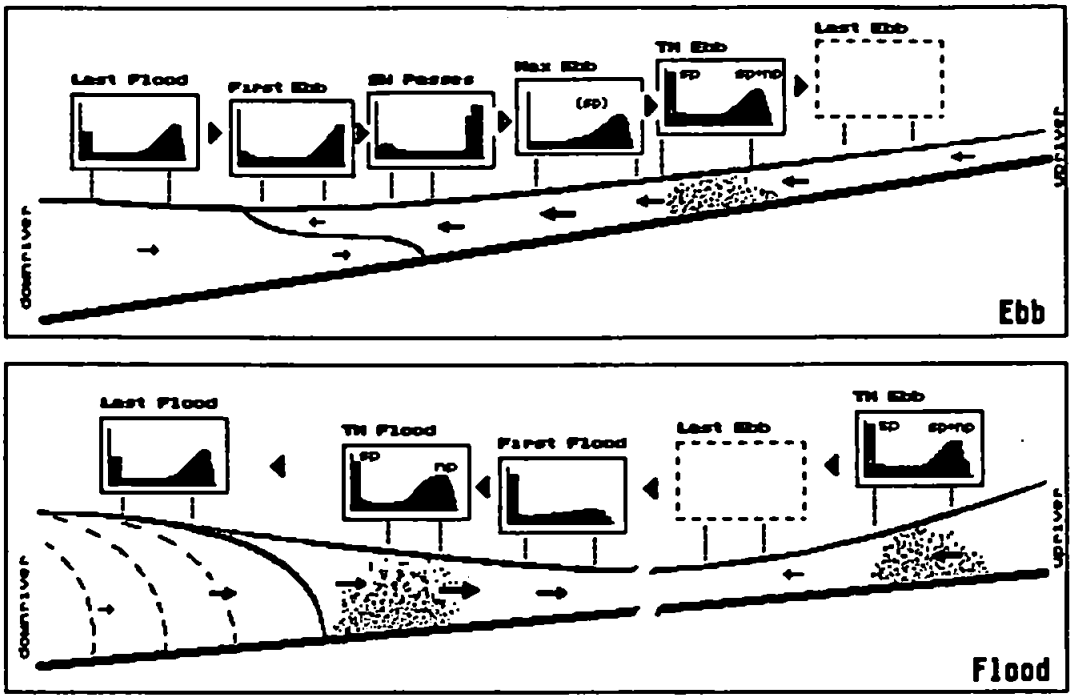

Fig. 4.2 Relation of Averaged Sizer Data to Average Tide. This diagram indicates the flow conditions (surface slope, current and water depth) experienced during each of the sizer averaging periods. The diagram may be interpreted as showing the variations in size distributions as the salt intrusion and turbidity maximum are advected past the sizer on the flood (bottom left - well mixed rapid flood), and ebb (top - stratified followed by long ebb of low salinity water). Note that the surface slope determines the current and that the position of the bed is determined by the surface and the water depth - the bed slope is not intended to indicate a longitudinal section of the river bed.

Table 4.6 Sizer Averaging Periods.

	June 28th	June 29th	July 4th	July 5th
First Flood	--	--	1541-1620	1640-1700
TM Flood	1035-1140	1119-1220	1638	1719
Last Flood	--	1401-1500	1822-1841	1947-1959
First Ebb	1520-1600	1720-1800	1940-2020	--
SW Passes	1639-1720	1821	1019	0947-1100
Max Ebb	--	--	1059-1201	1150-1320
TM Ebb	1741-1900	1839-2039	1240-1320	1340-1359
Last Ebb	--	--	1340-1420	--

B3 Averaged Size Distributions.

These descriptions apply to the time averaged histograms Fig. X19(a)-(d).

First Flood Fig. X19(a). The first of the flood occupies a period of duration between 30 mins. (sp) and 90 mins. (np) immediately after low water and before the passage of the turbidity maximum. Salinity is less than 2‰. SPM concentrations are 100 mg/l (np) to 200 mg/l (sp) - 'background' levels. Currents are low and increasing to between 20 and 30 cm/s. This water has recently been flowing downstream and is 'backing-up' ahead of the salt intrusion. Z is biased towards the smallest band.

TM Flood Fig. X19(a). The passage of the turbidity maximum (a period of about 30 mins. (sp) to 90 mins. (np)). Salinity is less than 2‰. Concentrations are high and range from about 400 mg/l (np) to over 1000 mg/l (sp). OBS (calibrated aginst the 'Partech' siltmeter at lower turbidities) give concentrations to about 1600 mg/l at springs. Currents are high: 100 cm/s (sp) and 60 cm/s (np). River water is being pushed upriver and is resuspending sediment. This distribution shows the greatest difference between springs and neaps. At neaps the distribution is biased towards the larger bands and there appears to be a maximum diameter of about 400 μm. At springs almost all the particles are in the smallest band (<5.8 μm) and nothing larger than 150 μm appears (but note remarks on obscuration in section 4A3.2.

Last Flood Fig. X19(b). The tail end of the flood, after the turbidity maximum has passed. Salinity is about 10‰ and increasing. The flow is beginning to stratify. Concentrations are low 150-300 mg/l (sp), 50 mg/l (np). Current speeds are about 15-20 cm/s. Z contains large flocs with max. diameter exceeding 600 μm.

First Ebb Fig. X19(b). The surface ebb begins although salt water may still be flooding near the bed. Maximum salinities are reached at the bed: 14‰ (np) to 17‰ (sp) with surface salinity about 2 to 3‰. less. Turbidity is low with concentrations largest nearer the surface: 20-100 mg/l. Currents are small, either upatream or downstream. The size distribution is still biassed towards large flocs. (The rig was out of the water here on the 5th)

Salt Wedge Passes Fig. X19(c). This period lasts from 30 minutes to an hour (and lasts longest at springs) during which the water is stratified and the the tip of the salt intrusion retreats downstream. The salinity at the end of this period is about 7‰. Concentrations are about 50 mg/l and OBS records show fluctuations over timescales of seconds. Current speeds increase to approximately 20 cm/s. At least 50% of the particle volume is of greater diameter than 260 μm. and there is very little less of than 100 μm. In the time series of sizer data (Fig. X7) this period stands out from those before and after due to the rapid changes in distribution.

Max. Ebb. Fig. X19(d) (NB Fig. out of sequence). The period of maximum ebb current speed. This section is only discernible during springs and is marked by a steadily increasing proportion of particles in the smallest band. Salinity is low at 2 to 3‰. Turbidity is high: 300-400 mg/l, and current speeds reach their ebb maximum of 60 cm/s. Floc sizes are reduced and a maximum diameter of around 300 μm is indicated.

TM Ebb. Fig. X19(c) (NB Fig. out of sequence). The turbidity maximum passes downriver. Salinity drops below 2‰. Concentrations are about 400 mg/l (sp) and 200 mg/l (np). Currents are falling slowly from 60 cm/s at springs and 40 cm/s at neaps. Distributions are similar to 'max.ebb' with somewhat higher percentages of smallest particles at spring tides; there is a continuous variation from 'max.ebb' to 'TM.ebb' at springs.

Last Ebb. Fig. X19(d). River water continues to flow downstream. Profiles show the flow to be about 20 cm/s and moderately turbid at about 200 mg/l. (The rig was raised during this period for turning ready for the flood).

Part 4C Interpretation.

This section attempts to describe the observed features of the data in terms of the processes thought to be occuring in the estuary. Many of the features are expected, on the basis of previous work, to be related to the spring/neap cycle [Bale et al. 1985; Uncles and Stephens, 1989]. It must be stressed that this experiment covers just four tidal cycles during one period of a fortnight in the summer of 1989.

4C1 FLOOD Formation of turbidity maximum.

4C1.1 Resuspension.

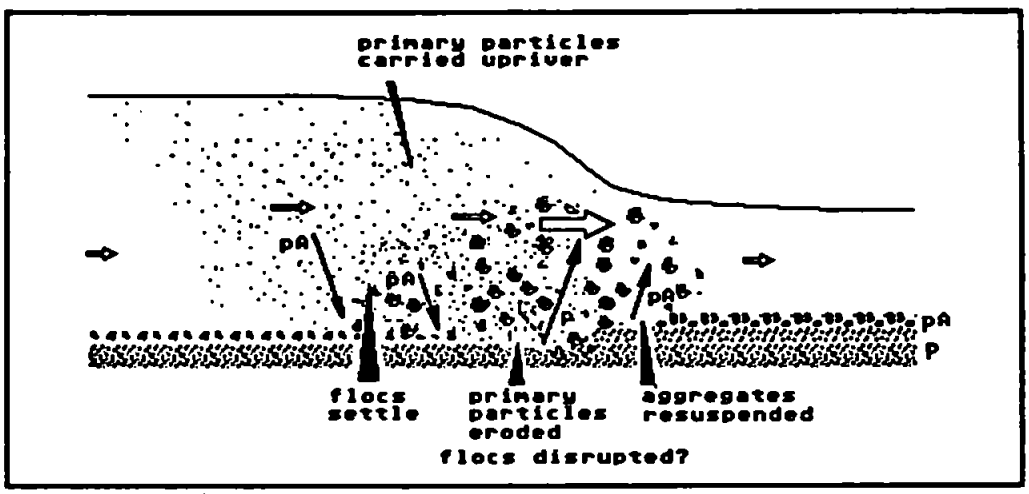

Fig. 4.3 Formation of turbidity maximum.

Suppose that the bed of the river is lined with two types of mud - large flocs (pA) which settled out only recently and have not become consolidated into the bed, and the bed itself consisting of consolidated mud which becomes stronger and less erodible with depth. Fig. X15 indicates a critical erosion velocity for large particles of between 20 and 30 cm/s. Recently settled aggregates are expected to have a range of (low) critical erosion stresses.

Applying the observed tidal currents to the bed would result in a pulse of all the available large particles being resuspended beneath the region of maximum current and settling out when the current slackened. This pulse would continue up the river on the flood with flocs being resuspended at the upriver end and flocs settling out at the rear.

During the spring flood, when near bed current speeds exceed the critical erosion velocity (~50 cm/s), smaller particles (p) would be eroded from the bed and remain suspended after the passage of the current maximum.

On the ebb the flocs will be resuspended just after the salt wedge retreats and carried out at the rear as the current maximum reached ahead of the incoming flow.

4C1.2 Settling.

The profiles show stratification of the suspended solids as the currents slacken in the rear of the spring flood and particles begin settling out (see 4B1.1); the sizer shows that these are large particles and that the small particles have all been advected upstream, (or removed by flocculation). Plotting the percentage of large particles, ΣA, against dissipation, $\varepsilon 0$, failed to show any obvious limitation of floc size by turbulence (Fig. X17b).

These processes would result in a long turbidity maximum with a bias towards smaller particles at its upstream end and more flocs at the downstream end. This does not explain the distribution at the spring turbidity maximum (entirely in the less than 5.8 μm band) nor the floc dominated distribution as the salt wedge recedes.

Turbulent dissipation rates in the maximum currents of the flood at springs are high and this may cause the breakup of large particles here. However measured dissipations are not higher than at other times when flocs are present so this cannot be the full explanation. The *obscuration* measured by the sizer at these periods is very high and the complete lack of larger sized particles is somewhat suspect.

4C2 EBB Salt Wedge.

4C2.1 Salt Wedge.

The passing downstream of the tip of the salt wedge is one of the major features of the data and appears to sharpen the downstream edge of the turbidity maximum by accentuating the effect of differing particle settling velocities.

Several features of the salt wedge show up in this data. From the contour plots (Figs. X12) it can be seen that there is a period of 2 to 3 hours during which the lower layer of saltier water is stationary or moving very slowly up- or down- stream. The thickness of the salt wedge reduces over the first half of the ebb and eventually becomes zero.

The presence of the tip of the salt wedge near the rig has a characteristic effect upon each set of measurements. The sizer data (Fig. X7) shows an increasing percentage of large particles followed by an abrupt change to a more evenly spread distribution. The turbulence data records (Fig. X4) show a peak in dissipation rates followed by a lull. The time of passing of the salt wedge can be found separately from each of the data sets and the coincidence of all three times indicates a common cause. The times of occurence of these features on each day are presented in Table 4.7.

Table 4.7 Time of passing of salt/fresh interface.

Date	HW Calstock	Profiles S=6‰	Dissipations Peak	Dip	Sizer From	To
28	1340	1720	1720	1730	1640 -	1720
29	1500	1820	1815	1825	1820	
4	0840	1020	1030	1040	0900 -	1020
5	0940	1050	1100	1120	0950 -	1100

Partch and Smith [1978] have observed somewhat similar abrupt onset of turbulence in the Duwamish Waterway on the ebb, when an internal hydraulic jump was thought to be the cause of intense mixing. Our results indicate that the turbulence peaks observed at Calstock are associated with the tip of the salt wedge. In our case there is also evidence of velocity shear within the interface which was not present in the Duwamish results. Mixing due to the breaking of internal waves has however been observed lower in the Tamar estuary at Cargreen [Sturley 1989].

4C2.2 Lowering of Interface.

The salinity difference across the interface averaged about 6‰ but reached 10‰ at 2 hours after HW on the 28th and 29th of June; this gave a density difference of between 5 and 8 mg/l. The thickness of the interface goes from 1.5 m soon after high water to 2.5 m as the bottom of the interface reaches the bed. The interface thickens with time and drops at a rate of about 1.5 m/hr.

Two processes could be reducing the height of the lower layer: the body of the salt wedge might be advecting slowly downriver and decreasing in thickness near to the tip, or the surface layer might be entraining water from the

top of the salt wedge. The latter possibility is investigated in the following section, followed by consideration of the effects of the advection of the salt wedge.

4C2.3 Entrainment Rate.

If the height of the interface is given by $\eta(x,t)$ then the longitudinal slope is $\partial\eta/\partial x$ and the rate of entrainment (rate at which height of interface is reduced due to entrainment) is $\partial\eta/\partial t$. If the salt wedge is bodily retreating with speed u then the rate at which the height of the interface changes is

$$(d/dt)\eta = \eta_{,t} + u\eta_{,x} \qquad (4.1)$$

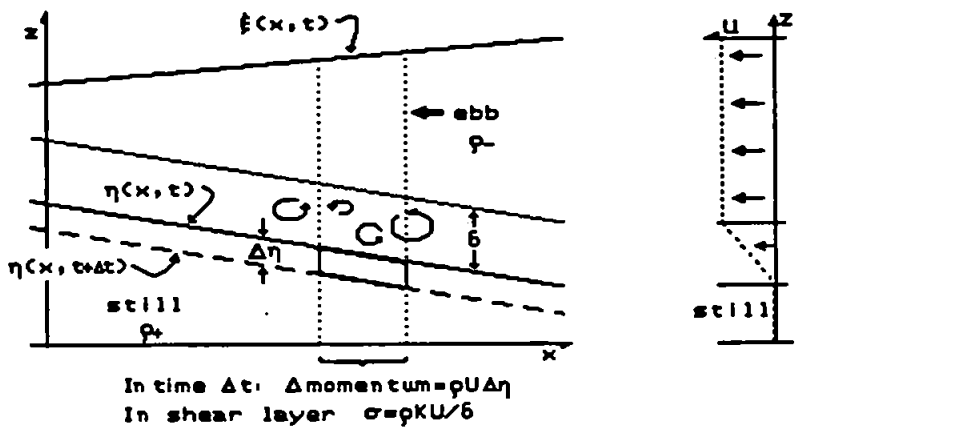

Fig. 4.4 Definition of variables for section 4C2.3. Densities of upper and lower layers are ρ_- and ρ_+ respectively. Interface thickness is δ. Shear stress in interface is σ. Kinematic vertical eddy viscosity is K.

Considering the forces acting on a column of water and starting at the bed we observe that:

(i) There is no current near the bed, and consequently no shear nor shear stress. The absence of a bed shear stress must be balanced by an absence of pressure gradient at the bed. Since the lower layer is homogeneous the pressure gradient produced because of the interfacial slope must be balanced by an opposing surface slope. (A reversed longitudinal salinity gradient in either layer is not observed.)

(ii) The surface slope $\partial\xi(x,t)/\partial x$ drives a flow in the upper layer which is limited by the friction (or wavemaking or entrainment) at the interface. With a steady flow in the upper layer the pressure gradient at the height of the interface is balanced by the interfacial shear stress.

Considering the lower layer, a balance must be made between the pressure gradients due to the slopes of the surface and interface. Thus $\rho_+\eta_{,x} + \rho_-(\xi_{,x}-\eta_{,x}) = 0$ and so $\eta_{,x} = -(\rho_-/\Delta\rho)\xi_{,x}$, substituting $\Delta\rho \approx 0.005$ and $\rho \approx 1.002$ gives an interfacial slope $\eta_{,x} \approx -200\,\xi_{,x}$.

The rate of supply of momentum to the saltier water is readily obtained as the mass of water which is entrained and accelerated to the speed of the upper layer, *viz.* $\rho U\eta_{,t}$ per unit (horizontal) area and time. This is effected by the working of the shear stress σ, which may be written $\sigma = \rho KU/\Delta z$, where K is the kinematic vertical eddy viscosity, and Δz the interface thickness, so that $K = \eta_{,t}\Delta z$. Substituting the observed values $\Delta\eta$=150 cm, Δt=3600 s, Δz=150 cm gives an estimate of $K \approx 6$ [cm²/s], (or in SI units $K \approx 6\times10^{-4}$ m²/s) This value is comparable to those of between 0.5 and 6 cm²/s observed during mixing by Partch and Smith [1978] in the Duwamish Waterway, Seattle and 2 to 10 cm²/s by Oduyemi [1986] in the Tamar.

Balancing the vertical gradient of shear stress in the upper layer against the surface slope pressure gradient gives $\rho g\xi_{,x} = \rho U\eta_{,t}/\Delta z$. Substituting $U = 40\,cm$ and the above values gives $\xi_{,x} \approx 1.1\times10^{-5}$ a not unreasonable surface slope. The interfacial slope is now $\eta_{,x} \approx 2.2\times10^{-3}$, which would put the furthest upstream reach of the tip of the salt wedge about 2 kilometres upstream from the barges (assuming a HW depth of 5 m).

The alternative to entrainment of the lower layer as the reason for decreasing salinity is advection. If the salt wedge is now assumed to be advecting bodily downstream with speed u the slope of the interface may be found; with u=5 cm/s (an absolute maximum limit on the currents which might have been recorded as zero) the slope is $\eta_{,x} \approx 1/100$. Smaller advection speeds will give a steeper slope. Since we assume no mixing, conservation of mass requires the river to double its breadth over the distance in which the depth of the upper layer halves, this distance is (less than) 1500 m. There is no widening at Calstock so that entrainment must be the cause of the apparent motion of the salt interface. In the above analysis a (small) velocity in the lower layer affects $d\eta/dt$ only in the term $u\,\partial\eta/\partial x \approx 0.01$ [cm/s]; this leaves the shear stress estimate unaffected.

The lowering of the interface is thus due to entrainment and is not an advective effect.

4C2.4 Mixing and Turbulence.

The turbulence in the lower layer is low, but increases towards the interface. At the interface the 'dissipations' are high and then drop as the current speed increases. The wave number turbulent velocity spectra show a change at this time becoming closer to the -5/3 inertial range spectrum, having been flatter earlier. The earlier rise in 'dissipation' may therefore not be due to inertial range turbulence but to internal wave or mixing activity. In any case the turbulence is not expected to be isotropic in the region of large salinity and current gradients.

The period during which the rig sensors are within the entrainment layer is revealed by the various instruments as follows:

(ϑ) the temperature time series becomes very noticeably more variable over the period of passage of the interface.

(C) the concentrations rise rapidly in the fresher, faster water and in the time series this can be seen to occur over less than half a minute, preceeded by a smooth rise in concentrations over two or three minutes. In each case the concentrations change character with current speed of close to 30 cm/s and coincide with the peak in the dissipation rate (see Fig. X4).

(S) the time at which the salinity decreases most rapidly coincides each day with this onset of increased concentration variance.

The peak in turbulent dissipation occurs in the middle of the period of rapidly increasing current at the rig and corresponds to the middle of the interface where the shear is greatest (Fig. X4 for 28/1720, 29/1815, 4/1030, 5/1100). The peak thus reflects the increased production of turbulence in the shear zone. See also Fig. 4.5 which shows how the stability of the lower 50 cm layer varies as the tip of the salt wedge is eroded.

At the time of the peak in dissipation, there will be approximately 50 cm of shear layer still above the current meters; this will be eroded away in approximately twenty minutes (the peak is roughly 20-30 mins wide). The tip of the interface meanwhile is somewhat less than 100 m ($\eta_{,x} \approx 2 \times 10^{-3}$ from previous section) upstream and water passes the tip (and is lifted off the bed) three to four minutes before passing the rig.

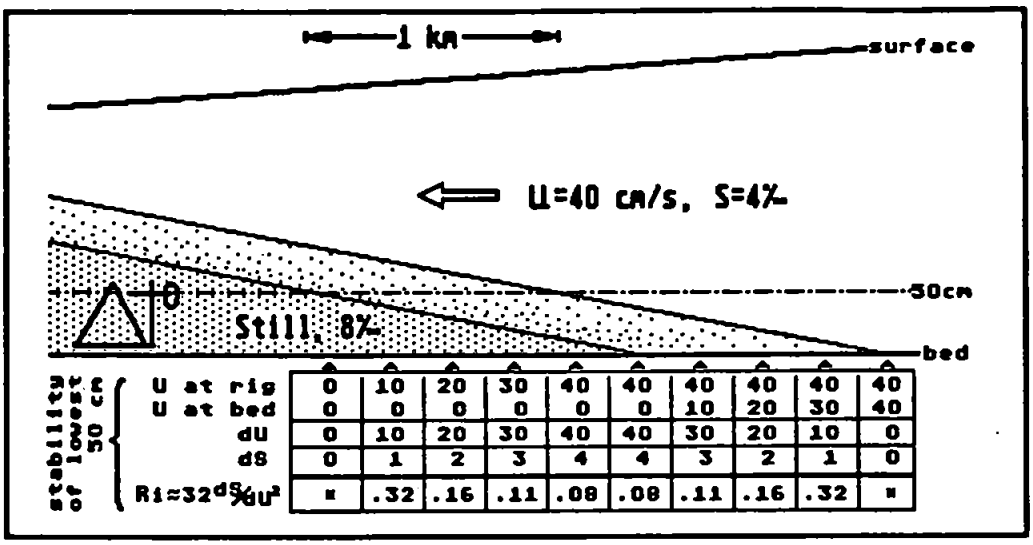

U at rig	0	10	20	30	40	40	40	40	40	40
U at bed	0	0	0	0	0	0	10	20	30	40
dU	0	10	20	30	40	40	30	20	10	0
dS	0	1	2	3	4	4	3	2	1	0
Ri=32dS/dU²	∞	.32	.16	.11	.08	.08	.11	.16	.32	∞

Fig. 4.5 Salinity and velocity at rig during final erosion of stratification. The layer below the level of the EM current meters is most unstable near the centre of the interface.

The turbulence becomes quiet, after the peak, for about 20 to 30 minutes and then begins to rise again. This is accompanied by a gentle rise in concentrations. The argument that the peak in estimated dissipation rate is due to internal wave activity contradicts the evidence that turbulent mixing is occuring, although it has been suggested that breaking internal waves may be responsible. Another possibility is that large suspended solids concentrations are damping the turbulence near the bed; neither the profiles nor the OBS concentrations support this however. The dip starts as the very last of the stratification disappears and it may be that the rig is now leaving the region of higher shear in which salt water is accelerated. Mean currents increase gradually after this and could account for the later, less accentuated dissipation increases.

Consideration of the sources of turbulent energy and of stratification suggest the following explanation for the observed dissipation rate time series. Dissipation rates are low in the stationary layer and high in the fresher water above the salt tip, where bed friction is producing turbulence. Turbulence is suppressed beneath and above the interface by stratification, but production is occurring in the central region of the interface (see Fig. 4.5). Turbulence during the period immediately after the passing of the tip, when the EM current meters are in the surface layer, is reduced because the surface layer is isolated from the bed by the remains of the salt tip.

4C2.5 Sizer Data in Salt Wedge.

The particle size distributions over the period labelled 'Salt Wedge Passes' are different in character from the periods either before or after, being highly skewed towards the two size bands of particles larger than 160 μm in diameter, and with very little in the smaller sizes. The SPM concentrations are low, between 30 and 50 mg/l, and have been increasing slowly since HW. Concentrations near in the surface layer are about 20 mg/l higher.

The settling velocity of a 200 μm floc is 0.46 mm/s (see Table 2.2) or 165 cm/hr, and the speed at which the top of the salt wedge is eroded is between 150 and 200 cm/hr so that only the larger flocs are 'out-settling' the mixing layer; those particles that are overtaken by the mixing layer are swept downstream, while remaining in the fresher water, or aggregate to form larger flocs which settle out of the mixing layer and reach the bed within the salt wedge. Consideration of the paths taken by variously sized tracer particles starting at various heights and times is used in the following section to show how the size distributions become increasingly skewed to larger sizes as the tip of the salt wedge approaches.

4C2.6 Modelling of Particle Settling during Stratification.

A straightforward computer model of a (laminar) two layer flow with a linear velocity gradient over the interface, with a constant entrainment rate and interfacial slope, provides qualitative confirmation of the different transport characteristics of small and large particles through the region of stratification.

A model of the observed stratified flow was set up having a stationary lower layer and an upper layer having a constant speed of 40 cm/s (1440 m/hr). The interface between the two layers had slope 2.2×10^{-3} and thickness 1.5 m. The velocity profile was linear over the thickness of the interface and the interface was lowered at the rate of 1.5 m/hr. The model is started with the salt tip well upstream of the origin so that initially there is still water above $x=0$. Five particles, with diameters 50 μm, 100 μm, 200 μm, 500 μm and 1 mm, were released at time zero from each grid point (see Fig. X20) and tracked as they settled (with their respective settling velocities obtained from Table 2.2) through the flow. The flow was updated at intervals of three minutes and tracking of each

particle continued for three hours, or until the particle reached the bed or passed downstream of *x=0*. The particle tracks are presented in Fig. X20 where, in order to preserve clarity, horizontal and vertical track scales are reduced by a factor of ten.

Fig. X20 clearly shows how smaller particles are carried by the surface layer while larger particles quickly settle out. Initially particles of all sizes are reaching the bed near the origin, however as the swiftly moving upper layer flow begins to appear above the origin the lighter particles nearer the surface are swept downstream - the particle size distribution near the bed loses some of the smallest particles. As the upper layer thickens, more of the smallest particles are removed downstream and some of the larger particles, which were released near the surface, are also removed - the size distribution near the bed becomes still more biassed towards the larger sizes. When the lower layer is almost completely removed only the largest particles are reaching the bed.

This model illustrates the likely mechanism for the production of the characteristic particle size distributions observed during the period leading up to, and including, the period 'Salt Wedge Passes'. It should be noted that this description depends on the observation that the fresher water of the upper layer has less weight in the larger size bands. Future versions of this model should include size distribution data at each grid point and should also derive explicitly the size distribution at the origin at successive times; this requires rather more sophisticated programming however.

4C2.7 Possible Spring/Neap Variation.

The distributions 'Max.Ebb' and 'TM.Ebb' are also skewed to the larger sizes so that flocs in the overriding fresher water will also add to the count of large particles arriving at the rig, as will any flocculation occuring in the mixing zone; the increasing absolute concentration of flocs over this period suggests that at least one of these processes is occurring. The lower cut-off of sizes reaching the bed should depend on the rate at which the interface is dropping; it can be seen from the sizer data that there is a cut-off but with just four observations it is not possible to test this.

4C2.8 Overall Effect of Salt Wedge.

Once the flocs have reached the bed they lie undisturbed under still water until the tip of the salt wedge reaches them, when the current increases rapidly and the flocs are resuspended, and possibly broken up. The particles, both large and small, that were within the salt wedge are now all in suspension in the lower end of the turbidity maximum.

This sweeping up of smaller particles by the mixing layer means that large flocs travel downstream more slowly than smaller particles: a floc and primary particle together at the surface at HW will be separated by a distance of at least $h/\eta_{,x}$ *(≈2 km)* by the time that the floc is resuspended. The smaller particle and the water surrounding it will be mixed on the flood with more saline water; in effect the smaller particle is escaping to seaward (this has implications for the maintenance of the turbidity maximum during neap tides). The floc on the other hand has passed into less saline water and on the flood might expect to be resuspended into water of approximately its original salinity. In any case its downstream excursion has been limited, tending to keep it near the downstream end of the turbidity maximum.

As the turbidity maximum is advected past on the ebb it can be seen that the lower end is dominated by a maximum in the concentration of larger particles.

4C3 Turbulence and Particle Sizes.

The processes described above provide qualitative explanation of the observed particle size distributions. A strong dependence of suspended particle characteristics on the spring/neap cycle is shown which is linked with the greater mean bed shears experienced during spring tides. Turbulent dissipation rates are expected to be linked with mean flow rates and maximum dissipation rates occur on the spring floods. However the observed dissipation data is much more variable than the sizer data or the mean flow data.

During the ebb, particle sizes are mainly large and not dependent on dissipations to any noticeable degree. On the flood, when stratification and longitudinal effects are less important because of the rapid mixing, there is a more noticeable tendency for smaller flocs to be associated with large dissipations.

The theoretical relation (Eqn. 2.20) relates d_{max} to the turbulent dissipation rate. In order to test this relationship an estimate of d_{max} is needed for the sizer data. The procedure used was to fit a line to the upper end of the cumulative percentage size distribution, and then quote d_{max} as the diameter at which this line intercepted a given percentile, usually 95%. The 11th to 15th terms of the cumulative distribution were used and the line fitted by least squares regression (percentage on band number). The band number for which the given percentile was cut was converted to diameter as $d_{max} = 10^{band/6.1}$, which ensures a moderately good assignment of band numbers to band upper limit diameters. Time series of d_{max} values are presented in Fig. X11 along with dissipations.

In order to investigate the effect of the dissipation rate, ε, on the maximum floc size, d_{max}, a power law dependence of d_{max} on the parameters C, U, S, and ε was tested. Multi-linear least squares regression of $\log_{10}(d_{max})$ on $\log_{10}(C)$, $\log_{10}(U)$, $\log_{10}(S)$ and $\log_{10}(\varepsilon)$ was performed on two subsets of the data; one from the freshwater flow over LW, and the other from the more saline water around HW. The correlation coefficients (R^2), obtained by omitting each of the parameters in turn from the regression, are shown in Table 4.8. The R^2 value using all four components is shown under '*'. It can be seen that the inclusion of a relationship of the form $d_{max} \sim A\varepsilon^{-\gamma}$ makes the least contribution to R^2.

Table 4.8 Linear regression for d_{max}.

Correlations (R^2 as %) obtained from linear fit using C U S ε and omitting –

		*	C	U	S	ε
(file SW\ε)	S ≥ 6‰	61.7	60.5	53.7	57.1	61.6
(file FW\ε)	S ≤ 2‰	47.4	33.8	43.9	46.9	47.1

For S≥6 ‰ $d_{max}/650 = (C/66)^{-0.1} \times (U/3.5)^{0.2} \times (S/1.7)^{0.5} \times (\varepsilon/1.7)^{0.0}$

For S≤2‰ $d_{max}/213 = (C/360)^{-1.4} \times (U/3.5)^{0.2} \times (S/0.4)^{-0.2} \times (\varepsilon/19)^{0.0}$

Correlations (R^2 as %) obtained from linear fits using –

variables used in regression	SW	SW\ε	FW	FW\ε
C U S	58.7	61.6	37.7	47.1
C U	57.1	55.7	37.7	46.8
C	54.8	51.8	34.7	43.4

SW – file containing data with $S \geq 6$‰ from all four days. SW\ε – as SW and with reliable ε. FW – all data with $S \leq 2$‰. FW\ε – as FW and with reliable ε.

In the fresher water C and U are seen to be the most important factors in determining floc size. In the more saline water U and S are the most important factors. It must be remembered that C and U are related through erosion and that the turbidity maximum is present in low salinity water, while the saltier water contains less suspended sediment. The power laws obtained from this analysis are thus unlikely to be very realistic but do serve to show that the laboratory floc-size/turbulence relationship is masked (or invalid) in the estuary.

These results are inconclusive as to whether a relation of the form $d_{max} \sim A\varepsilon^{-\gamma}$ exists and the value of γ if it does. It seems likely that, while theoretical relation may control individual floc breakages, the number and strength of the flocs which are in suspension at any time are controlled by the 'bulk' parameters of mean speed and salinity.

4C4 Processes during tidal cycle.

At Calstock at LW the river is shallow and freshwater is flowing downstream carrying moderate concentrations of suspended matter in the form of primary particles and microflocs: the remains of the upstream end of the turbidity maximum. Measured dissipation values are not high, but the method of estimating dissipation is not really satisfactory in shallow water as isotropy cannot be assumed and the energy containing eddies will occur at too high frequencies. This water is the smeared out end of the turbidity maximum. The turbidity maximum reaches almost to Weir Head at HW, this water will be pushed back up on the flood.

LW occurs at Calstock 45 minutes later than at Devonport; and when the water starts to rise at Calstock it consists of muddy fresh water that has recently been flowing downstream. The particle distribution (unsurprisingly) still consists of small particles.

The flood current rapidly increases, although because of the backing-up effect, the salinity is still low. The high bed shears erode loosely bound material, and at springs erode small particles which had been consolidated into the bed since earlier spring tides. The formation of the spring turbidity maximum is an active event, with erosion of the bed occuring when the current at a height of 50 cm exceeds about 45 to 50 cm/s, a sharp pulse of small particles is produced

which is advected upstream and augmented as the bed continues to be eroded. The neap turbidity maximum is formed of larger particles which are resuspended on each flood and ebb.

There is a need to explain why the larger particles remain in suspension in the rear of the turbidity maximum after the fine particles have gone. Turbulent disruption may be responsible for breaking up the loosely consolidated large aggregates that settled during the ebb, and which now re-aggregate; this is what the sizer data appears to show, although the large obscurations experienced in the turbidity maximum make this slightly suspect. Dissipations reach their maximum values here but more observations are needed to show whether this occurs in general during the turbidity maximum. The larger particles may get left behind by the turbidity maximum because they settle more rapidly into the lower velocities nearer the bed, or it may be that flocculation is taking place in the reduced turbulence after the current maximum (again there are not enough tidal cycles to investigate this further).

After the turbidity maximum has passed, the mean currents gradually decrease while well-mixed, increasingly saline water pushes up river. This water has larger concentrations nearer the bed and the distributions are skewed towards the larger sizes. With time a decreasing proportion of the decreasing sediment load is in large particles and this points to settling as being the main process occuring over this period. The content of largest particles does not decrease to zero in the salt water though, and this may be due to the presence of low density biological debris (such particles will be escaping to sea in much the same manner as the finest particles).

As HW is reached, stratification begins to take place with a low speed, less salty ebb beginning at the surface while the flow lower down is almost stationary. The fresher surface water erodes the salt intrusion away for the next three hours. The size distribution at HW may be considered the background size distribution for salt water: particles having been settling out over the last two to three hours. The salt/fresh interface increasingly restricts the supply of smaller particles reaching the rig as described above, and when the interface is at the level of the rig only the largest particles are reaching the sizer.

The tip of the salt intrusion is now downstream from the rig and the current increases rapidly to its ebb maximum; concentrations rise in the fresher water with the particles being of the larger sizes. These are particles which reached the bed since the last flood maximum; the 'cleaning' effect of the entrainment layer has preferentially allowed the larger particles to reach the bed. Sanford et al. [1991] suggest a similar erosion process occurring in Chesapeake Bay and refer to the coating of 'estuarine dust' or 'fluff' on the bed which is easily eroded. As the ebb continues the currents do not increase and there is no further erosion of small particles from the bed. At springs the remains of the (Z_p) turbidity maximum advect past the rig having been diffused by the vertical current shears further up the river (that is, in the 8 km to Weir Head) and some of the material having settled out (possibly after being incorporated into aggregates).

During the last of the ebb, moderately high concentrations exist in water that has formed the top end of the turbidity maximum where mixing with the river input occurs. There appears to be a background of larger particles which is augmented by smaller particles at springs, but the sizer data stops here at neaps so it is not possible to be certain. This region is important for the production of microflocs although water depths are too low for the experimental set-up used; at high water the upstream region of the turbidity maximum could be studied nearer to Weir Head. It is also possible that erosion is taking place in the shallow fresh water flow; again with low water levels the profiling scheme is not accurate enough to provide reliable SPM flux data for this period - in particular we have no cross-sectional area information.

4C5 Comparisons with other Indicators of Particle Size Distribution.

The particles considered in the previous sections have been formed of flocculated clay sediments and the settling and breakup properties based on that structure. However other particles are present in the estuary having differing sizes and densities such as bacteria and vegetable detritus (indicated by the presence of lignin).

Owens [1986] made a study of the axial distribution of nitrification and NH_4-oxidising bacteria in the Tamar and found that both maxima of nitrification and of bacteria coincided closely with the turbidity maximum. (The survey was repeated during May, June, July and August 1982; samples were taken by pumping from 0.5m below the surface). It was suggested that bacteria were attached to the *'periodically resuspended'* particles which formed the turbidity maximum. The trapping of particles in the turbidity maximum increased the residence time of the particles so that the population of slow-growing nitrifying bacteria could develop, and the periodic resuspension ensured an adequate supply of growth substrates.

Plummer, Owens and Herbert [1987] in a similar study in the Tamar partitioned the bacteria amongst *'free-living bacteria'*, bacteria attached to *'permanently suspended particles'* and bacteria attached to *'periodically resuspended particles'*.

The assignment of the terms *'permanently suspended'* and *'periodically resuspended'* was based on settling rates, with *'permanent'* suspension referring to particles which remained suspended in the collecting container for over twelve hours after agitation. The terms seem likely to be misapplied in view of the high probability of floc breakage during sampling and analysis, but results are still indicative of increased microbial activity within the turbidity maximum.

The maximum bacterial activity was found to be associated with the *'permanently suspended'* fraction. The turbidity at springs was due mainly to *'resuspended'* particles, with the *'permanently suspended'* particle concentration being relatively unaffected over a period of 14 days. The *'permanently suspended'* particles were found to be larger than the *'resuspended'* particles and had diameters in the range 10 to 60 μm. The small diameters of these particles, measured in the laboratory, suggest that larger sized flocs may well have been disrupted. It is interesting to note that Cloern [1991] found the blooming of phytoplankton in south San Fransisco Bay to be strongly dependent on tidal range, with biomass increasing during neap tides and decreasing at springs. Also, Logan and Hunt [1987] found the flocculation of microbes to form permeable aggregates to be to their advantage, by increasing the net flow of water, and nutrients, past individuals.

Reeves and Preston [1991] made axial profiles of the Tamar and measurements at Halton Quay of the amounts of lignin present. Samples were pumped from three depths at Halton Quay, and from 0.5 m below surface during axial profiles; suspended particles were partitioned as by Plummer et al. [1987]. The axial profile, taken during a spring tide, shows that the turbidity maximum consists mainly of *'resuspended'* particles. Lignin was more concentrated in the *'permanently suspended'* particles and was thought to be the reason for their buoyancy. The *'resuspended'* particles had an almost constant composition (based on carbon and lignin concentrations) reflecting their long residence time in the turbidity maximum. The *'permanently suspended'* fraction was more variable, varying by a factor of three over a tidal cycle, indicating a rapid change in the composition of the organic fraction possibly due to microbial activity. Axial profiles show the bulk of the lignin present in the turbidity maximum to be associated with *'resuspended'* particles - although containing less lignin they are resuspended in large quantities during spring tides - the small amount of lignin in the turbidity maximum due to *'permanently suspended'* particles was thought to originate in land runoff.

These results are summarised in Table 4.9.

Table 4.9 Biological aspects

	Sp/Np	Size	Bacterial Activity	Lignin Content
Permanently Suspended	relatively unaffected	10 to 60 μm	high	high & varies over tidal cycle
Periodically Resuspended	form Sp. TM	smaller	low	low & constant (but most of TM lignin)

It can be seen that there must be other processes occuring since the *'permanently suspended'* particles will be those escaping to seaward fastest; there must be a continual flux of resuspended sediment becoming *'permanently'* suspended or the sampling process misleadingly produces the *'permanently suspended'* fraction by breaking up periodically resuspended aggregates into buoyant and non-buoyant parts. Note that the influx of sediment over Weir Head is not large enough to account for this [Bale et al. 1985].

The effects on the two types of particle, Z_P and Z_A, of the salt intrusion and turbidity maximum are summarised in Fig. 4.6.

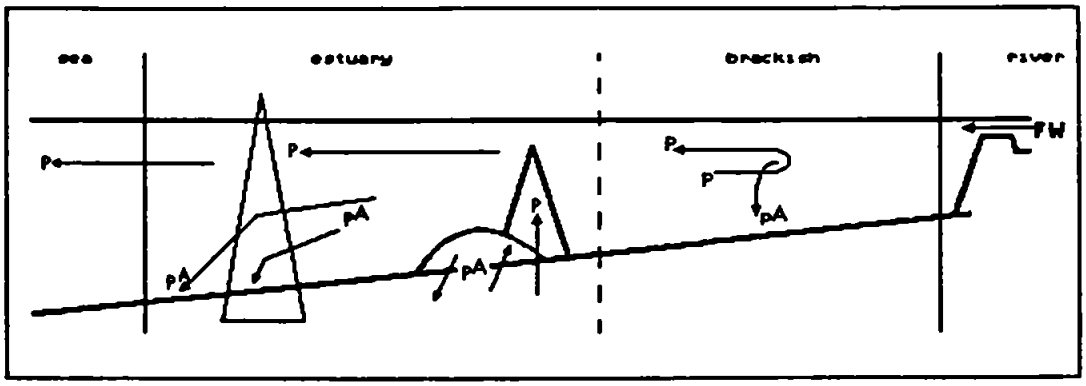

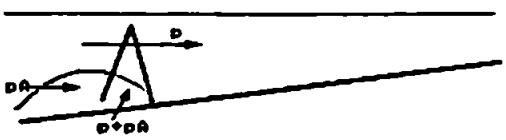

On the flood particles are resuspended into the turbidity maximum and carried upriver. On neap tides only aggregates are resuspended; on springs erosion occurs.

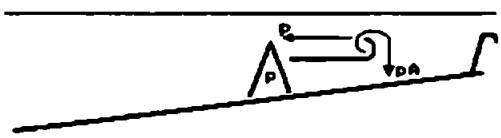

At HW aggregates form and settle out, sweeping up primary particles, which have remained in suspension.

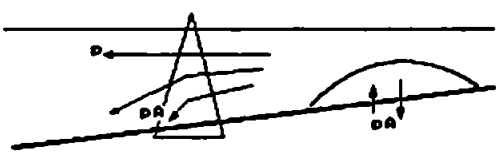

The salt wedge acts to retain aggregates while letting primary particles escape to seaward. The ebb turbidity maximum is formed of resuspended aggregates.

Fig. 4.6 Overall effect of salt intrusion in upper estuary. The large prism represents the action of the salt intrusion in retaining aggregates (pA) further upstream than primary particles (p). During spring tides the bed is eroded to form the turbidity maximum (peaked shape) from primary particles. These particles are advected upstream where they either flocculate and settle as aggregates (pA), or remain un-flocculated, (p) to pass downstream. The remnant of the turbidity maximum (humped shape) consisting of aggregates is advected downstream. Aggregates resuspended by the ebb current maximum are retained in low salinity water by the action of the salt wedge. On neap tides the turbidity maximum is formed of aggregates which are resuspended at low current speeds. The position of the 'hump' (pA) downstream from the 'peak' (p) reflects the interpretation of the neap turbidity maximum as the remnant of the spring event and hence residing in more saline water.

A survey of floc size distribution variations over the tidal cycle has been made for a station in the Tamar estuary which lies within the excursion of the turbidity maximum and salt intrusion. The observed variations have been related to specific periods of the tidal cycle and described in terms of measured flow properties on the assumption that suspended particles may be partitioned into two populations with different settling and resuspension properties.

This work has highlighted the need to consider estuarine flocculation processes as inseparable from the tidal variations in flow. Flocculation processes are essentially Lagrangian while the flow is largely determined by the geometry of the estuary so that there is a complex interplay of resuspension, flocculation and sedimentation varying over the whole tidal cycle.

Flocculation Processes

Floc size distributions vary appreciably in the observed range (6 μm to 500 μm) during the tidal cycle, with periods when the distribution mode appears to be smaller than 6 μm (during the spring flood turbidity maximum) or larger than 500 μm (during the first part of the ebb). Variations occur over timescales of the order one hour except that there is a rapid change over the transition from salt to fresh water on the ebb.

There are periods of up to an hour during which the size distributions vary little or slowly; averaging of distributions over these periods allows portions of each tidal cycle to be characterised according to the particle sizes. By considering the common features of the tidal flow on each day, in particular the salinity structure, it is possible to compare size distributions obtained on different days.

The most distinctive feature of the size distribution time series is the passing of the tip of the salt wedge downstream past the station. From a consideration of the flow as measured it is found that turbulent entrainment of the salt intrusion by the surface layer is responsible for the downstream movement of the salt tip during the ebb. Turbulence data supports this interpretation. The generation of turbulence is damped by stratification below and

above the interface but is increased in the interfacial mixing layer. The observed changes in the size distribution during the first part of the ebb are explained by noting that the entrainment rate exceeds the settling velocity of the smaller particles; thus the smaller particles are selectively removed before reaching the bed, or the rig, in the region beneath the salt wedge.

Averaged distributions can be identified with specific periods of the tidal cycle; variability between observations on different days can be attributed mainly to the spring/neap cycle, with particle size modes being reduced during spring tides. The flood turbidity maximum distribution is most responsive to the spring/neap cycle while distributions at other stages of the tidal cycle vary remarkably little over the period of observation (two spring and two neap tidal cycles).

Consideration of settling velocities suggests differing behaviour of particles smaller than about 50 μm in diameter and those larger; the smaller particles are likely to remain in suspension over several tidal cycles. Observations confirm that a diameter of 50 μm divides two floc populations with different concentration variations over the tidal cycle.

The variations in each population may be explained on the assumption that the smaller fraction consists of primary particles - clay particles, microflocs - which are eroded from the consolidated bed during periods of high bed shear stress; the larger particles are assumed to be flocs of low effective density, possibly colonised by bacteria and incorporating detrital matter, which are readily resuspended on each flood and ebb.

Small particles are introduced into the turbidity maximum on the spring flood by erosion from the bed: a critical erosion velocity of 50 cm/s is indicated by the (limited) data shown here.

The turbidity maximum advects up and down the river, being diffused by the action of the velocity shear and deposition, and reinforced by subsequent erosion. Small particles may be removed from the turbidity maximum by aggregating and settling out or by escaping to seaward, assisted by the action of the salt wedge.

From longitudinal suspended solids fluxes it can be seen that the upriver pumping of sediment occurs predominantly at spring tides and is due to erosion of mudbeds seaward of the station followed by advection upstream as small particles. Some of the small particles return downstream on the ebb but the majority are retained upriver. These are presumed to settle out after being 'swept up' by the larger flocs during the quieter conditions at HW. There is, however, no direct evidence for this.

The neap turbidity maximum consists entirely of large particles and aggregates which are eroded on each flood, settle out as currents decrease and which are resuspended in the turbulent flow following the erosion of the salt tip downstream. The action of the ebb stratification is to keep these large flocs within the low salinity waters: once incorporated into the turbidity maximum large flocs tend to remain just upstream of the salt intrusion.

The main features of the observed floc size distributions can be explained without reference to floc breakup mechanisms (except that they are involved in eroding small particles from the consolidated bed), although aggregation must be assumed to occur near the head of the estuary. Large particles are present on the ebb at both spring and neap tides. Maximum particle sizes (d_{max}) show a decrease with increased dissipation on the flood, though it cannot be shown that turbulent disruption of flocs is responsible.

Evaluation of Experimental Work

Laser particle-sizing at intervals of 20 minutes is suitable to provide information on the time variations of the floc size distribution. The lens system used is adequate for concentrations up to 800 mg/l, above which the high obscuration affects the detection of larger sizes.

Profiling with the sizer was not carried out in the present series of measurements but can be expected to provide useful information during stratification and during the passage of the turbidity maximum, and should be tried in future field work.

Electromagnetic current meters provide usable turbulence data although electronic and fouling problems reduced their usefulness at times: the sampling rate was ideal for ensuring that a turbulent inertial range could be distinguished from sensor and filter roll-off ranges. Mean data obtained from the EM current meters is excellent and future processing strategy should include analysis of the low frequency (~1 cycle/minute) variations of velocity, which would enable any internal wave events and concentration/velocity correlations to be investigated. This could be done by using records of up to 30 minutes in length and processing them as single blocks after linear trend removal.

The OBS sensors proved excellent for this work and were less prone to fouling and electronic problems than the EM current meters. Future work should include analysis of both low frequency and high frequency concentration variations. OBS spectra are remarkably free from spurious noise peaks and it may be possible to derive turbulence and diffusion data from them. It would also be useful to investigate the reflective properties of suspended sediments from different sources and in different states of flocculation in order to calibrate the OBS sensors more effectively.

The thermistor itself worked without problems although the data is limited by the lack of temperature variation in the water throughout most of the tidal cycle. Some interesting time series, suggestive of internal waves, were obtained at 'max.flood' and 'SW.passes'.

Profiling of salinity, concentration and velocity is essential in trying to interpret the other data sets. A useful comparison of advection and local effects could be made by profiling at two points separated by about ½ km, possibly using only a salinometer.

The rig layout used, and system of deployment, seem ideal, combining convenience with experimental requirements, although care needed to be taken to keep the barges and 'Tamaris' (which are sources of contaminating turbulence) downstream of the rig.

The 'Atari 1040ST' computer is quite capable of performing all the processing required for extracting turbulence data.

Further Work

The experimental work summarised above has successfully delineated the variations in floc distributions to be observed in the upper Tamar and the data has been used as the basis for a description of sedimentation processes. The major deficiency is that few tidal cycles have been observed.

In order to confirm that there is a critical erosion velocity (of approximately 50 cm/s) for small particles and to discover the behaviour of the larger size fraction over the spring/neap cycle, the experiment should be repeated over a two week period. A repetition of the fieldwork could be improved by shortening the optical path length of the sizer for use on spring floods so that the apparent absence of large particles in the spring flood turbidity maximum can be investigated. A second profiling station upstream of the sizer would also contribute to identification of advective effects. So far as a repetition of the survey aspect of the experiment is concerned less emphasis need be placed on the turbulent fluctuations of velocity and concentration. However the OBS sensor and thermistor data have not been analysed in full and there are indications in the spectra of these instruments that much more information about the turbulent structure could be obtained.

This work has suggested that flocculation is occuring in the region just upstream of the furthest advance of the salt intrusion, (where turbulence is weaker, and differential settling, coupled with high concentrations of sediment and bacteria, enhance flocculation rates) resulting in sedimentation of recently eroded particles. It should be useful to obtain time series and vertical profiles of particle size distributions in this upper estuary region in order to study the rate at which flocculation and deposition occurs.

An axial profile with the particle sizer over the region of the turbidity maximum is needed to confirm the proposed spatial separation of large - and small - particle maxima. This should be performed on both flood and ebb, near HW, and cover the region of the 'decay' of the turbidity maximum; that is the region including, and downstream from, its HW position. Sizer data should be combined with profiles of current, salinity and concentration.

Vertical variations of particle size distribution have been observed indirectly over the first part of the ebb, and concentration profiles indicate greater concentrations near the bed after the passage of the turbidity maximum. Since this experiment has failed to find a strong turbulence/particle-size dependence there is now the option of separating the sizer and turbulence measurements so that profiling could include profiling of sizer data.

(Turbulence measurements require fixed sensors and a steady mean flow while the sizer is more mobile. During the 1988 fieldwork it was attempted to drift with the current while deploying the sizer/turbulence rig then in use, however interpretation of the velocity data was problematic due to the presence of large scale eddies and variable orientation of the rig.)

It is necessary to investigate the *in-situ* settling properties of aggregates since it is possible that some of the larger particle load is substantially more buoyant than laboratory studies of clay flocs indicate, due to the inclusion of biological material. This work is already underway in the Institute of Marine Studies, Plymouth.

Some simple modelling of the processes described here, using two particle populations with different erosion and settling characteristics, and based on existing one dimensional estuary models, but including the filtering effect of the salt wedge, might provide confirmation that the physics involved in these descriptions is correct.

REFERENCES

Ackroyd DR, AJ Bale, RJM Howland, S Knox, GE Millward, AW Morris 1986. Distributions and Behaviour of Dissolved Cu, Zn, Mn in the Tamar Estuary. Estuarine and Coastal Shelf Science 23 621-640.

Adler PM and PM Mills 1979. Motion and Rupture of Porous Sphere in a Linear Flow Field. Journal of Rheology 23(1) 25-37.

Alani SH 1987. Developement of a Vibratory System for Evaluating Floc Strength. PhD thesis, Univ of Strathclyde.

Alani SH, KR Dyer, DA Huntley (1990). Effect of Salinity on the Physical Properties of Estuarine Flocs. To be published.

Alldredge AL, TC Granata, CC Gotschalk, TD Dickey 1990. The Physical Strength of Marine Snow and its Implications for Particle Disaggregation in the Ocean. Limnology and Oceanography 35(7) 1415-1428.

Allen GP, JC Solomon, P Bassoulet, Y du Penhoat, C De Grandpre 1980. Effects of Tides on Mixing and Suspended Sediment Transport in Macrotidal Estuaries. Sedimentary Geology 26 69-90.

Anderson GF 1986. Silica, Diatoms and a Freshwater Productivity Maximum in Atlantic Coastal Plain Estuaries, Chesapeake Bay. Estuarine and Coastal Shelf Science 22: 183-197.

Anwar HO 1981. A Study of the Turbulent Structure in a Tidal Flow, Estuarine, Coastal and Shelf Science 13: 373-387.

Bache DH and SH Alani 1989. Developement of a System for Evaluating Floc Strength. Water Science and Technology 21: 529-537.

Bale AJ, CD Barrett, JR West, KOK Oduyemi 1989. Use of *In-situ* Laser Diffraction Particle Sizing for Particle Transport Studies in Estuaries. In J McManus and M Elliot (eds) 'Developements In Estuarine and Coastal Study Techniques', EBSA 17 Symposium, Olsen and Olsen, Fredensborg, Denmark, pp133-137.

Bale AJ and AW Morris 1987. *In-situ* Measurements of Particle Sizes in Estuarine Waters. Estuarine, Coastal and Shelf Science 24: 253-263.

Bale AJ, AW Morris, RJM Howland 1985. Seasonal Sediment Movement in the Tamar Estuary. Oceanologica Acta 8(1): 1-6.

Bale AJ, Morris AW, West JR, Darbyshire E, Barton M 1988. Measurement of Cohesive Sediment Transport Parameters in Estuaries. Paper given at the Chapman Conference on Sediment Transport Processes in Estuaries (Bahia Blanca, Argentina, June 1988).

Bowden KF and SR Fergusson 1980. Variations in the Turbulent Mixing Processes in a Tidally Induced Bottom Boundary Layer. In: JCJ Nihoul (ed) 'Marine Turbulence', Proc. 11th International Colloquium on Ocean Hydromechanics, pp259-286.

Brigham EO 1974. The Fast Fourier Transform. Prentice-Hall, New Jersey.

Burban P-Y, W Lick, J Lick 1989. The Flocculation of Fine Grained Sediments in Estuarine Waters. Journal Geophysical Research 94 C6: 8,323-8,330.

Burban P-Y, YJ Xu, J McNeil, W Lick 1990. Settling Speeds of Flocs in Freshwater and Seawater. Journal of Geophysical Research 95 C10: 18,213-18,220.

Burt TN 1984. Field Settling Velocities of Estuarine Muds. In AJ Mehta (ed) 'Estuarine and Cohesive Sediment Dynamics', Springer-Verlag, pp126-150.

Champagne FH 1978. The Fine-Scale Structure of the Turbulent Velocity Field. Journal of Fluid Mechanics 86(1): 67-108.

Cleasby JL, 1984, Is Velocity Gradient a Valid Turbulent Flocculation Parameter, American Society of Civil Engineers Journal of Environmental Engineering 110 (5): 875-897.

Cloern JE 1991. Tidal Stirring and Phytoplankton Bloom Dynamics in an Estuary. Journal of Marine Research 49: 203-221.

D&A Instuments 1989. Optical Methods for Measuring turbidity and Suspended Particles in Water - Some Notes for Users of OBS Sensors. Technote (3/89). Downing and Associates, Washington State, USA.

Dyer KR 1986. Coastal and Estuarine Sediment Dynamics. John Wiley and Sons.

Dyer KR 1989. Sediment Processes in Estuaries: Fututre Research Requirements. Journal of Geophysical Research 94 C10: 14,327-14,329.

Eisma D 1986. Flocculation and De-flocculation of Suspended Matter in Estuaries. Netherlands Journal of Sea Research 20: 183-199.

Eisma D, J Boon, R Groenewegen, V Ittekkot, J Kalf, WG Mook 1983. Observations of Macro-Aggregates, Particle Size and Organic Composition in the Ems Estuary. SCOPE/UNEP Sondeband Heft 55 Hamburg: 295-314.

Festa JF and DV Hansen 1978. Turbidity Maxima in Partially Mixed Estuaries: a Two Dimensional Numerical Model. Estuarine and Coastal Marine Science 7: 347-359.

Garrett C 1989. Mixing Length Interpretation of Fluctuations in Passive Scalar Concentrations in Homogeneous Turbulence. Journal of Geophysical Research 94 C7: 9,710-9,712.

Gibbs RJ 1983. Coagulation Rates of Clay Minerals and Natural Sediments. Journal of Sedimentary Petrology 53 (4): 1193-1203.

Gibbs RJ 1985. Estuarine Flocs: Their Size, Settling Velocity and Density. Journal of Geophysical Research 90: 3,249-3,257.

Gibbs RJ, DM Tshudy, L Konwar, JM Martin 1989. Coagulation and Transport of Sediments in the Gironde Estuary. Sedimentology 36: 987-999.

Glasgow LA and YH Kim 1989. A Review of the Role of the Physico-Chemical Environment in the Production of Certain Floc Properties. Water, Air and Sea Pollution 47: 153-174.

Gordon CM 1974. Intermittent Momentum transport in a Geophysical Boundary Layer. Nature 248 (March 29 1974): 392-394.

Gordon CM 1975. Sediment Entrainment and Suspension in a Turbulent Tidal Flow. Marine Geology 18 M57-M64.

Gore RA and CT Crowe 1989. The Effect of Particle Size in Modulating Turbulent Intensity. International Journal Multiphase Flow 15 (2): 279-285.

Grant WD, AJ Williams, SM Glenn 1984. Bottom Stress Estimates and their Prediction on the Northern California Continental Shelf during CODE-1: The Importance of Wave-Current Interaction. Journal of Physical Oceanography 14: 506-527.

Gust G and E Walger 1976. The Influence of Suspended Cohesive Sediments on Boundary Layer Structure and Erosive Activity of Turbulent Seawater Flows. Marine Geology 22: 189-206.

Hamblin PF 1989. Observations and Model of Sediment Transport near the Turbidity Maximum of the Upper St. Lawrence Estuary. Journal of Geophysical Research 94 C10: 14,419-14,428.

Heathershaw AD 1974. Bursting Phenomena in the Sea. Nature 248: 394-395.

Hicks GF 1988. Sediment Rafting: a Novel Mechanism for the Small Scale Dispersal of Intertidal Estuarine Meiofauna. Marine Ecology - Progress Series 48: 69-80.

Hinze JO 1975. Turbulence, 2nd Edn, McGraw-Hill, New York.

Hou HC and JR Kuo 1987. Gyarmati Principle and Open Channel Velocity Distribution, American Society of Civil Engineers Journal Hydraulic Engineering. 113(5): 563-572.

Hunt JR 1982. Self-similar Particle-size Distributions During Coagulation: Theory and Experimental Verification, Journal Fluid Mechanics 122: 169-185.

Hunter KA and PS Liss 1982. Organic Matter and the Surface Charge of Suspended Particles in Estuarine Waters. Limnology and Oceanography 27 (2): 322-335.

Huntley DA 1988. A Modified Inertial Dissipation Method for Estimating Seabed Stresses at Low Reynolds Numbers, with Applications to Wave/Current Boundary Layer Measurements. Journal of Physical Oceanography 18: 339-346.

Huntley DA and DG Hazen 1988. Seabed Stresses in Combined Wave and Steady Flow Conditions on the Nova Scotia Continental Shelf: Field Measurements and Predictions. Journal of Physical Oceanography 18: 347-362.

Jackson RG 1976. Sedimentological and Fluid Dynamic Implications of the Turbulent Bursting Phenomenon in Geophysical Flows. Journal of Fluid Mechanics 77: 531-560.

Jeffrey DJ 1982. Aggregation and Breakup of Clay Flocs in Turbulent Flow. Advances in Colloid and Interface Science 17: 213-218.

Jenkins GM and DG Watts 1968. Spectral Analysis and its Applications. Holden-Day, San Fransisco.

Kranck K and TG Milligan 1988. Macroflocs from Diatoms: *In-situ* Photography of Particles in Bedford Basin , Nova Scotia. Marine Ecology - Progress Series 44: 183-189.

Krone RB 1978. Aggregation of Suspended Particles in Estuaries. In Kjerfve (ed) 'Estuarine Transport Processes', Univ. S.Carolina Press, pp177-190.

Lavelle JW, HO Mofjeld, ET Baker 1984. An *In-situ* Erosion Rate for a Fine Grained Marine Sediment. Journal of Geophysical Research 89 C4: 6,543-6,552.

LI DH and J Ganczarczyk 1988. Flow Through Activated Sludge Flocs. Water Research 22 (6): 789-792.

Lick W and J Lick 1988. On the Aggregation and Disaggregation of Fine Grained Lake Sediments. Journal of Great Lakes Research 14 (4): 514-523.

Logan BE and JR Hunt 1987. Advantages to Microbes of Growth in Permeable Aggregates in Marine Systems. Limnology and Oceanography 32 (5): 1,034-1,048.

Ludwick JC and GW Domurat 1982. A Deterministic Model of the Vertical Component of Sediment Motion in a turbulent Fluid. Marine Geology 45: 1-15.

Mandelbrot B 1983. The Fractal Geometry of Nature. WH Freeman and Co.

McCave IN 1984. Size Spectra of Aggregates of Suspended Particles in the Deep Ocean, Deep Sea Research A 31(4): 329-352.

Morris AW, Bale AJ, RJM Howland 1982a. Chemical Variability in the Tamar Estuary, South-West England. Estuarine and Coastal Shelf Science 14: 649-661.

Morris AW, DH Loring, AJ Bale, RJM Howland, RFC Mantoura, EMS Woodward 1982b. Particle Dynamics, Particulate Carbon and the Oxygen Minimum in an Estuary. Oceanologica Acta 5 (3): 349-353.

Munchow A and RW Garvine 1991. Nonlinear Tides and Bores in Estuaries. Tellus 43A: 246-256.

Muschenheim DK, PE Kepkay, K Kranck 1989. Microbial Growth in Turbulent Suspension and its Relation to Marine Aggregate Formation. Netherlands Journal of Sea Research 23 (3): 283-292.

New AL, KR Dyer, RE Lewis 1986. Predictions of the generation and Propagation of Internal Waves and Mixing in a Partially Stratified Estuary. Estuarine and Coastal Shelf Science 22: 199-214.

Newland DE 1984. Random Vibrations and Spectral Analysis (2nd Edition). Longman.

Nunes Vaz RA, Lennon, JR De Silva Samrasinghe 1989. The Negative Role of Turbulence in Estuarine Mass Transport. Estuarine and Coastal Shelf Science 28 (4): 361-377.

Oduyemi KOK 1986. Turbulent Transport of Sediment in Estuaries, PhD Thesis, Univ. Birmingham Department of Civil Engineering.

Offen GR and SJ Kline 1975. A proposed Model of the Bursting Process in Turbulent Boundary Layers. Journal of Fluid Mechanics 70 (2): 209-228.

Owen MW 1971. The Effect of Turbulence on the Settling Velocities of Silt Flocs. Proc. 14th Congress International Assoc. Hydraulic Research, Paris, pp27-32.

Owen MW 1976. Problems in the Modelling of Transport, Erosion and Deposition of Cohesive Sediments. In: Goldberg (ed) 'The Sea: Ideas and Observations on Progress in the Study of the Seas', John Wiley and Sons, Chapter 12: 515-537.

Owens NJP 1986. Estuarine Nitrification: A Naturally Occuring Fluidised Bed Reaction? Estuarine and Coastal Shelf Science 22: 31-44.

Parker DS, WJ Kaufman, D Jenkins 1972. Floc Breakup in Turbulent Flocculation Processes. American Society of Civil Engineers Journal of Sanitary Engineering Division 98 SA1: 79-99.

Partch EN and Smith JD 1978. Tide Dependent Mixing in a Salt Wedge Estuary. Estuarine and Coastal Shelf Science 6: 3-19.

Partheniades E 1986. The Present State of Knowledge and Needs for Future Research on Cohesive Sediment Dynamics. 3rd International Symposium on River Sedimentation, Mississippi, pp3-25.

Paterson DM 1989. Short Term Changes in the Erodibility of Intertidal Cohesive Sediment Related to the Migratory Behaviour of Epipelic Diatoms. Limnology and Oceanography 34 (1): 223-234.

Pearson HJ, IA Valioulis, EJ List 1984. Monte-Carlo Simulation of Coagulation in Discrete Particle Size Distribution, Part 1: Particle Motion and Fluid Shearing. Journal of Fluid Mechanics 143: 367-385.

Perkins JW 1971. Geology Explained in South and East Devon. David and Charles, Newton Abbot 192pp.

Plummer D, NJP Owens, RA Herbert 1987. Bacteria-Particle Interactions in Turbid Estuarine Environments. Continental Shelf Research 11/12: 1,429-1,443.

Postma H 1980. Sediment Transport and Sedimentation. In: E Olausson and I Cato (eds) 'Chemistry and Biogeochemistry of Estuaries', John Wiley and Sons, pp154-186.

Rarity J 1989. Colloids Stick to Fractal Rules. Nature 339: 340-341.

Reeves AD, MR Preston 1991. A Study of the Composition and Distubution of Lignin in Resuspended and Permanently Suspended Particles in the River Tamar Estuary. Estuarine and Coastal Shelf Science 32: 11-25.

Sanford LP, W Panageotou and JP Halka 1991. Tidal Resuspension of Sediments in Northern Chesapeake Bay. Marine Geology 97: 87-103.

Scarlatos PD and AJ Mehta 1990. Some Observations on Erosion and Entrainment of Estuarine Fluid Muds. In: RT Cheng (ed) 'Residual Currents and Long-term Transport, Coastal and Estuarine Studies (38)', Springer-Verlag, New York, pp321-332..

Schroder M and G Siedler 1989. Turbulent Momentum and Salt Transport in the Mixing Zone of the Elbe Estuary, Estuarine, Coastal and Shelf Science 28: 615-638.

Sonntag RC and WB Russel 1986. Structure and Breakup of Flocs Subjected to Fluid Stresses. Journal of Colloid and Interface Science 113 (2): 399-415.

Soulsby RL 1980. Selecting Record Length and Digitazation Rate for Near Bed Turbulence Measurements, Journal of Physical Oceanography 16: 208-219.

Sreenivasan KR and C Meneveau 1986. The Fractal Aspects of Turbulence. Journal of Fluid Mechanics 173: 357-386.

Sternberg RW, K Kranck, DA Cacchione, DE Drake 1988. Suspended Transport under Estuarine Tidal Channel Conditions. Sedimentary Geology 57: 257-272.

Sturley DRM 1990. Topographically Induced Internal Waves and Enhanced Vertical Mixing in an Estuary. PhD Thesis, Polytechnic South West, Plymouth.

Tambo N and Y Watanabe 1979. Physical Characteristics of Flocs (1): The Floc Density Function and Aluminium Floc. Water Research 13: 409-419.

Tambo N and H Hozumi 1979. Physical Characteristics of Flocs: (2) Strength of Floc. Water Research 13: 421-427.

Thomas DG 1964. Turbulent Disruption of Flocs in Small Particle Size Suspensions. American Institute of Chemical Engineers Journal 10(4): 517-523.

Tsai CH and W Lick 1988. Resuspension of Sediments from Long Island Sound. Water Science and Technology 20 (6/7): 155-164.

Turner JS 1973. Buoyancy Effects in Fluids. Cambridge University Press 368pp.

Uncles RJ, Bale AJ, RJM Howland, AW Morris, RCA Elliott 1983. Salinity of Surface Water in a Partially Mixed Estuary, and its Dispersion at Low Run-off. Oceanologica Acta 6 (3): 289-296.

Uncles RJ, RCA Elliott, SA Weston 1985. Observed Fluxes of Water, Salt and Suspended Sediment in a Partly Mixed Estuary, Estuarine, Coastal and Shelf Science 20: 147-167.

Uncles RJ and JA Stephens 1989. Distribution of Suspended Sediment at High Water in a Macro-Tidal Estuary. Journal of Geophysical Research 94 C10: 14,395-14,405.

Uncles RJ and JA Stephens 1990. Salinity Stratification and Vertical Shear Transport in an Estuary. In: RT Cheng (ed) 'Residual Currents and Long-term Transport, Coastal and Estuarine Studies 38, Springer-Verlag, New York, pp137-150.

van de Ven TGM and RJ Hunter 1977. The Energy Dissipation in Sheared Coagulated Sols. Rheologica Acta 16: 534-543.

van Leussen W 1988. Aggregation of Particles; Settling Velocity of Mud Flocs- a Review. In: J Dronkers and W van Leussen (Eds.) 'Physical Processes in Estuaries', Springer-Verlag, Berlin Heidelburg New York, pp347-403.

van Leussen W and JC Winterwerp 1990. Laboratory Experiments on Sedimentation of Fine Grained Sediments: A State of the Art Review in the Light of Experiments with the Delft Tidal Flume. In: RT Cheng (ed) 'Residual Currents and Long-term Transport', Coastal and Estuarine Studies 38, Springer-Verlag, New York, pp241-259.

van Olpen H 1976. An Introduction to Clay Colloid Chemistry (2nd Edn) Wiley Interscience, New York.

Wei T and WW Willmarth 1991. Examination of v-Velocity Fluctuations in a Turbulent channel Flow in the Context of Sediment Transport. Journal of Fluid Mechanics 223: 241-252.

West JR and K Shiono 1988. Vertical Turbulent Mixing Processes on Ebb Tides in Partially Mixed Estuaries, Estuarine and Coastal Shelf Science 26: 51-66.

West JR and KOK Oduyemi 1989. Turbulent Measurements of Suspended Solids Concentration in Estuaries, American Society of Civil Engineers Journal of Hydraulic Engineering. 115(4): 457-474.

West JR, KOK Oduyemi, AJ Bale, AW Morris 1990. The Field Measurement of Sediment Transport Parameters in Estuaries. Estuarine and Coastal Shelf Science 30: 167-183.

West JR, KOK Oduyemi, K Shiono 1991. Some Observations on the Effect of Vertical Density Gradients on Estuarine Transport Processes. Estuarine and Coastal Shelf Science 32: 365-383.

West JR and AYA Sangodoyin 1991. Depth-Mean Tidal Current and Sediment Concentration Relationships in Three Partially Mixed Estuaries. Estuarine and Coastal Shelf Science 32: 141-159.

West JR, DW Knight, K Shiono 1986. Turbulence Measurements in the Gt. Ouse Estuary, American Society of Civil Engineers Journal of Hydraulic Engineering 112(3): 167-180.

Williams RM and CA Paulson 1977. Microscale Temperature and Velocity Spectra in the Atmospheric Boundary Layer, Journal of Fluid Mechanics 83 (3): 547-567.

Yang CT and Song CSC 1986. Theory of Minimum Energy and Energy Dissipation Rate. In NP Cheremisinoff (ed) 'Encyclopaedia of Fluid Mechanics, Vol 1 Chapter 11, ed NP Cheremisinoff, Gulf Publishing Co., pp353-399.

X1 (Fig. 2.6) Log aggregation kernels.

Each plot shows contours of log_{10}*(aggregation kernel)* for turbulent shear, T_{ij}, and for turbulent inertia, I_{ij}, for particles of diameter d_i and d_j. Blue contours are for $\log_{10}(T)$ and green contours are for $\log_{10}(I)$, black contours are for $\log_{10}(T+I)$. The upper plot evaluates kernels for a dissipation rate ϵ=1000 cm^2/s^3 and the lower plot uses ϵ=1 cm^2/s^3. Units of T and I are *collisions per second per cm^3*.

Fig 2.6

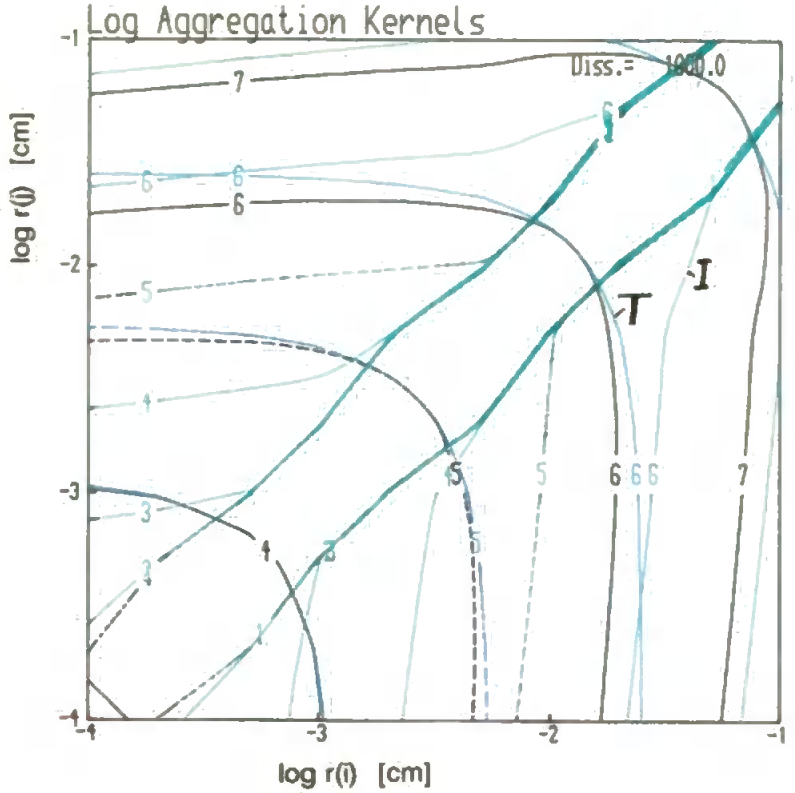

$\log_{10} K(r_i,r_j)$	
1	-12.00
2	-10.00
3	-8.00
4	-6.00
5	-4.00
6	-2.00
7	0.00
8	2.00

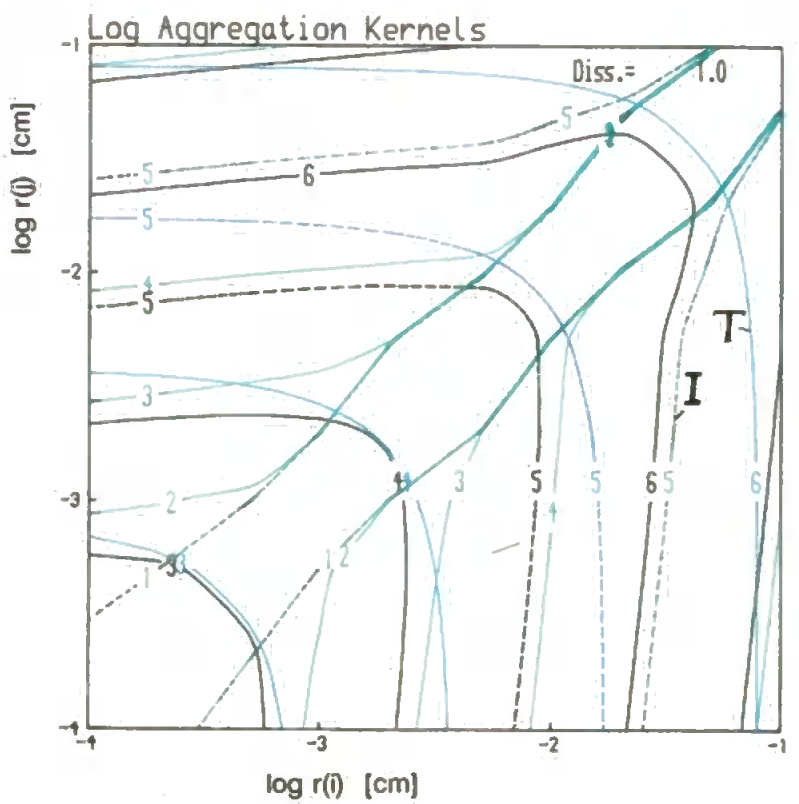

$\log_{10} K(r_i,r_j)$	
1	-12.00
2	-10.00
3	-8.00
4	-6.00
5	-4.00
6	-2.00
7	0.00
8	2.00

X2 (Fig. 3.1) EM current meter calibrations.

Each plot shows the two calibrations performed for one EM channel. Pre-fieldwork calibrations (June 1988) are shown with solid markers in blue, and post-fieldwork calibrations use open markers in green. The equations of the fitted lines are shown in Table 3.1.

X 2
Fig 3.1

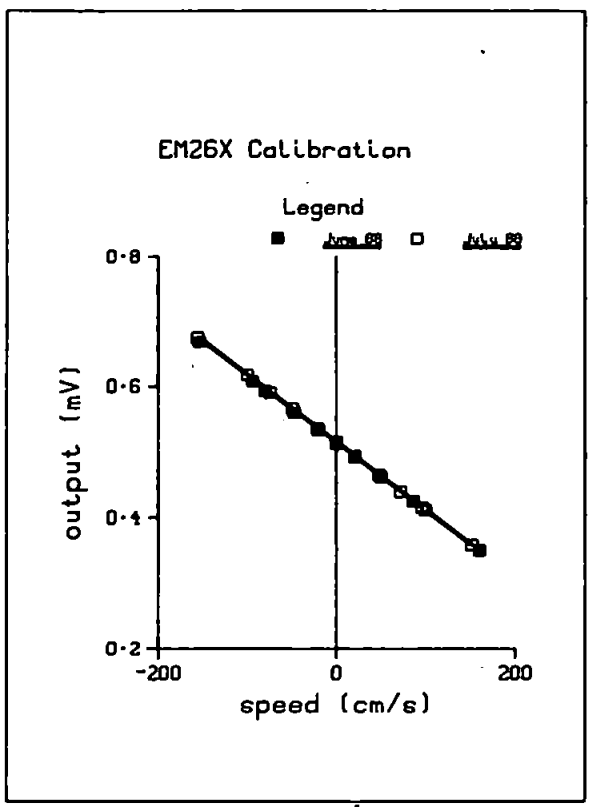
EM26X Calibration
Legend
June 89
July 89
output (mV)
0·8
0·6
0·4
0·2
-200
0
200
speed (cm/s)

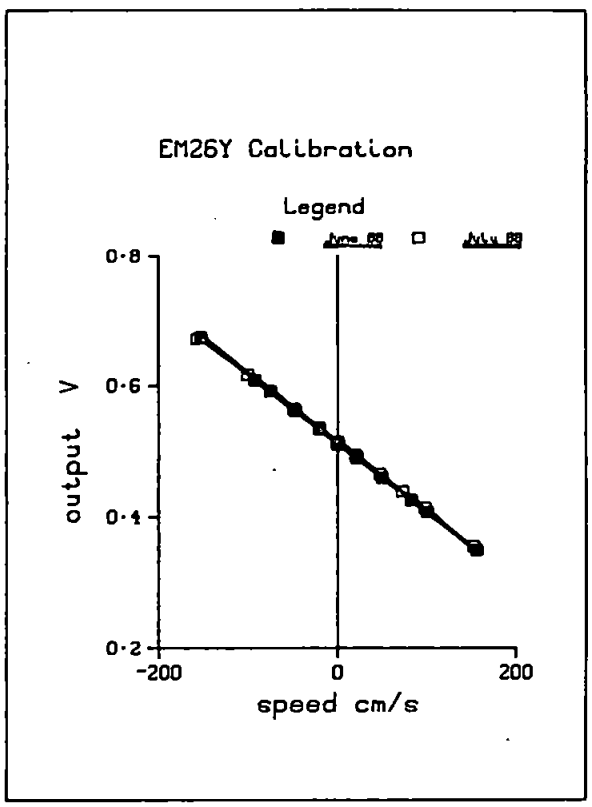
EM26Y Calibration
Legend
June 89
July 89
output V
0·8
0·6
0·4
0·2
-200
0
200
speed cm/s

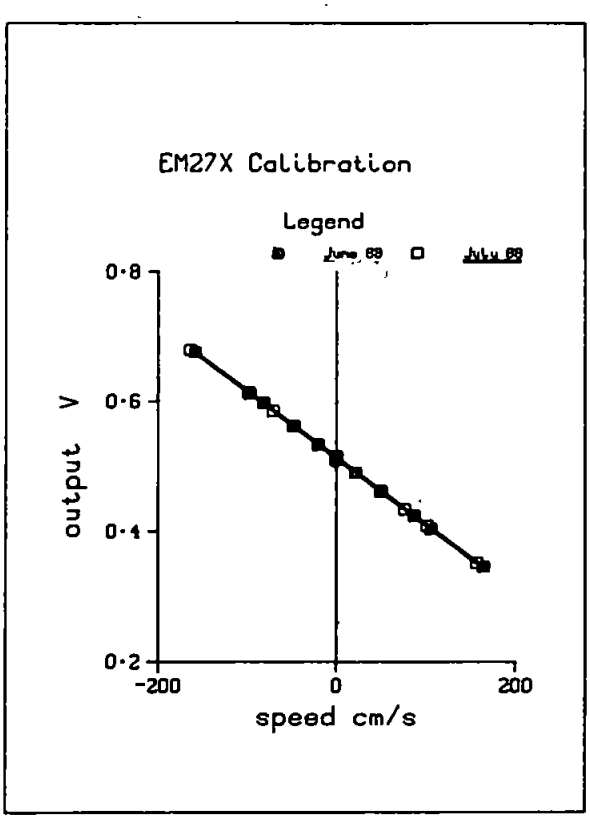
EM27X Calibration
Legend
June 89
July 89
output V
0·8
0·6
0·4
0·2
-200
0
200
speed cm/s

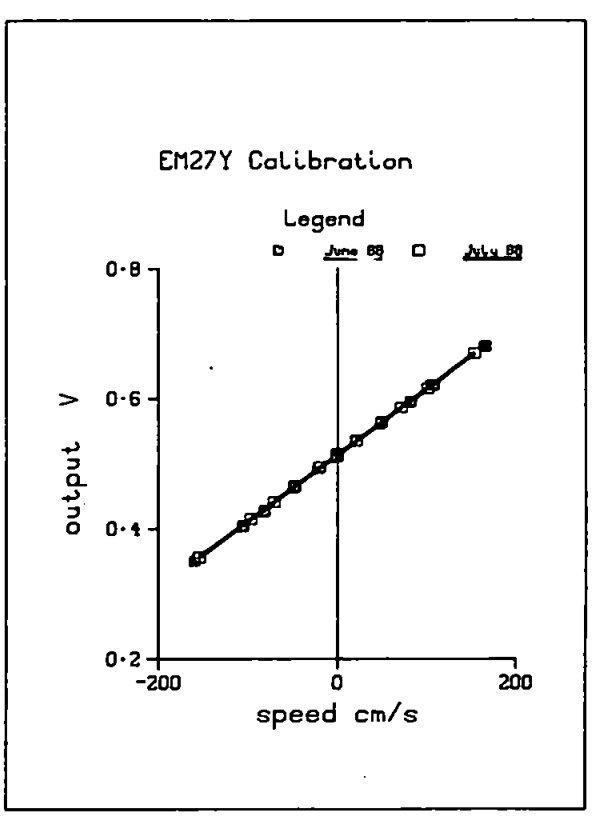
EM27Y Calibration
Legend
June 89
July 89
output V
0·8
0·6
0·4
0·2
-200
0
200
speed cm/s

X3 (Fig. 3.4) OBS calibrations.

The plot shows the calibrations for both OBS sensors obtained as described in section 3A2.2. OBS I calibration is shown by solid markers in blue, OBS II calibration uses open markers in green.

X 3
Fig 3.4

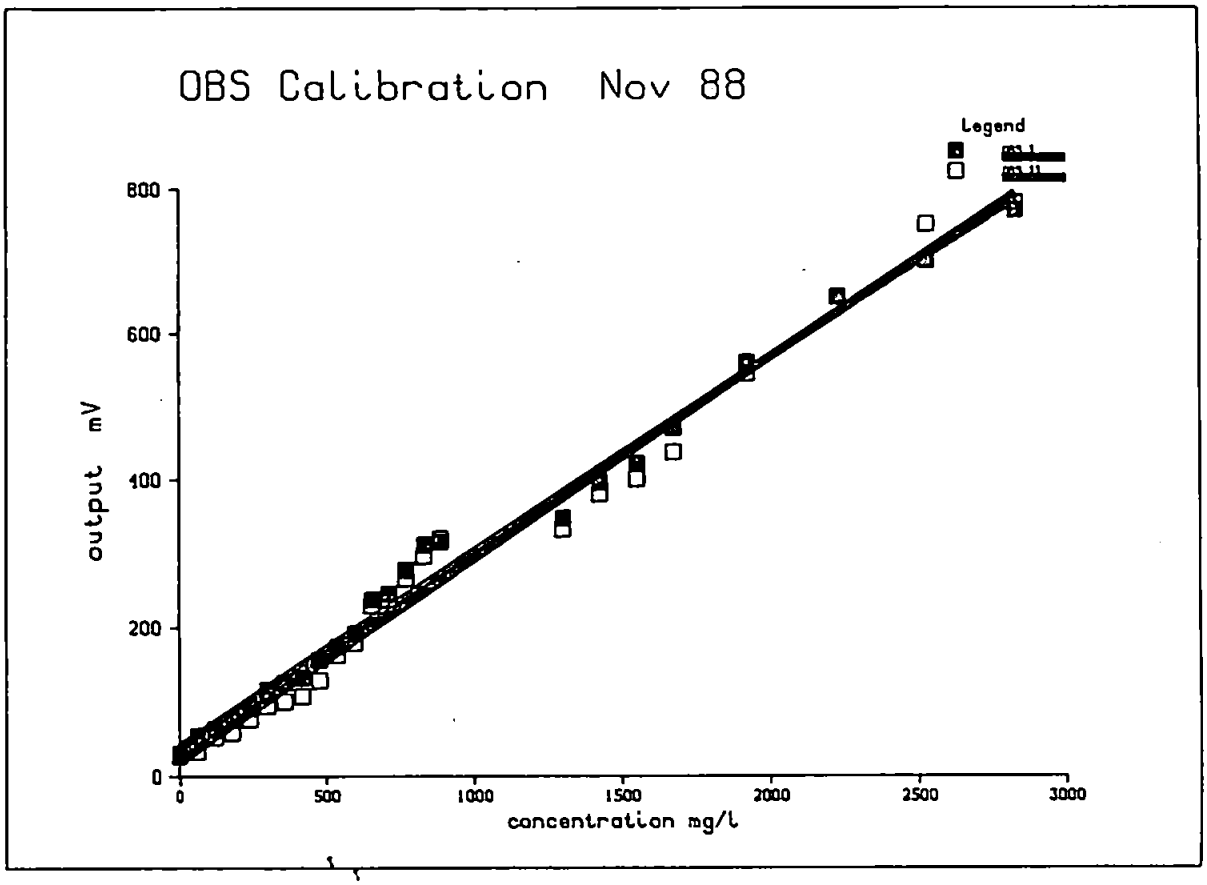
OBS Calibration Nov 88
Legend
output mV
800
600
400
200
0
0
500
1000
1500
2000
2500
3000
concentration mg/l

X4 (a)-(d) Boundary layer measurements.

Each page (labelled in top right corner) relates to one day's measurements of conditions on the bed. Each point is the mean value of the parameter over one record (approx. 5½ mins.). Each plot shows data of two related parameters which are labelled in the upper left corner: the first label refers to the coloured points and the second label to the black points. The colour used for plotting the first parameter is irrelevant. The horizontal axis is time (BST) with tick marks at twenty minute intervals. The vertical axes are in c.g.s. units with the logarithm to the base ten of dissipations being plotted. Data is read from "*.FLO" files.

label	parameter	units
U,	mean current	cm/s
a	angle of attack	degrees
-m1, m2	vertical speeds (+ve. up)	cm/s
e0, e3	$\log_{10}$(hztl. dissipation)	$\log_{10}$ cm^2/s^3
e1, e2	$\log_{10}$(vert. dissipation)	$\log_{10}$ cm^2/s^3
c4, c5	OBS concentrations	mg/l
temp.	from thermistor	°C

Boundary layer measurements.
Units are c.g.s.
e0..3 on log10 scale

X4a
June 28

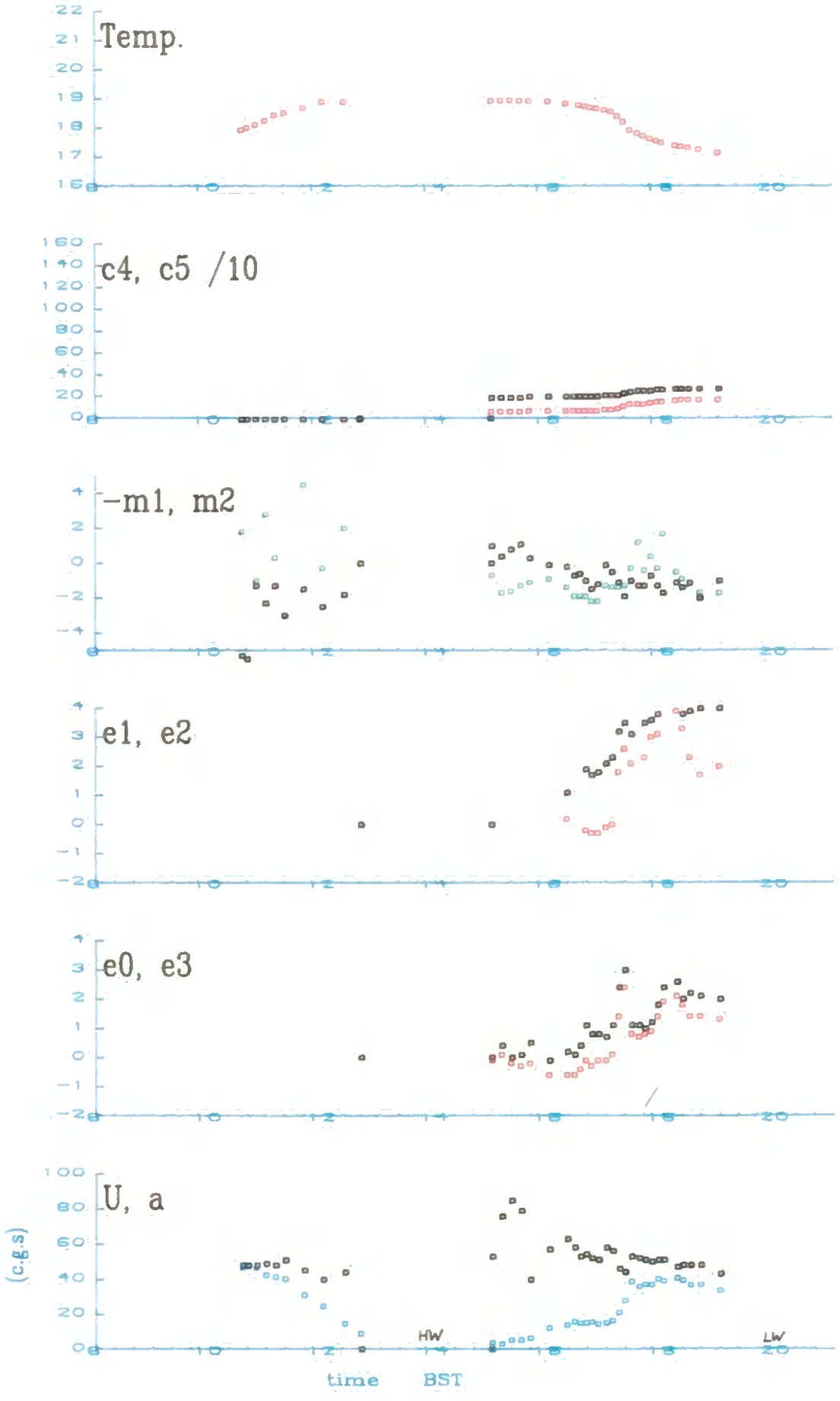

Boundary layer measurements.
Units are c.g.s.
e0..3 on log10 scale

X4b
June29

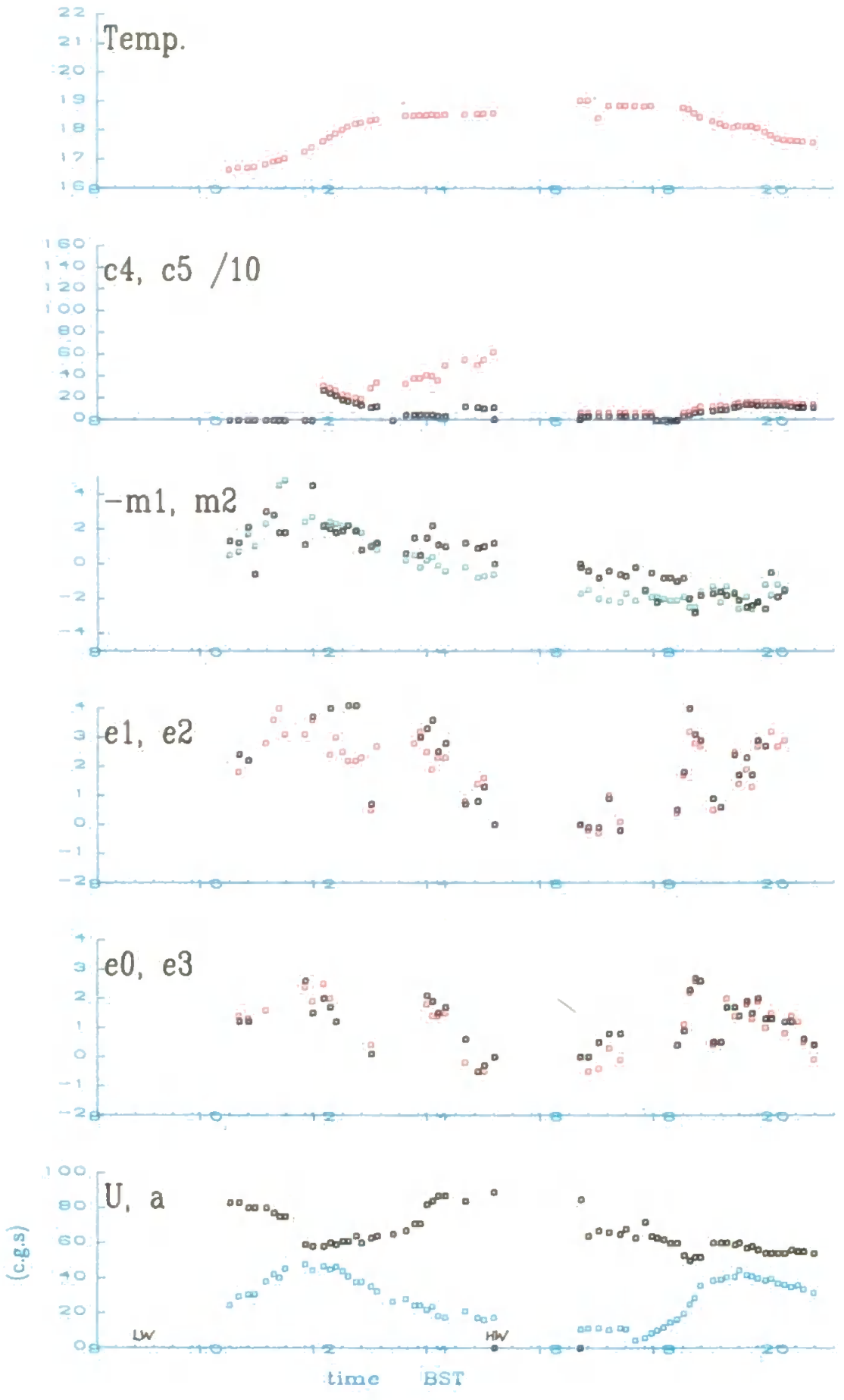

Boundary layer measurements.
Units are c.g.s.
e0..3 on log10 scale

X4c
July4

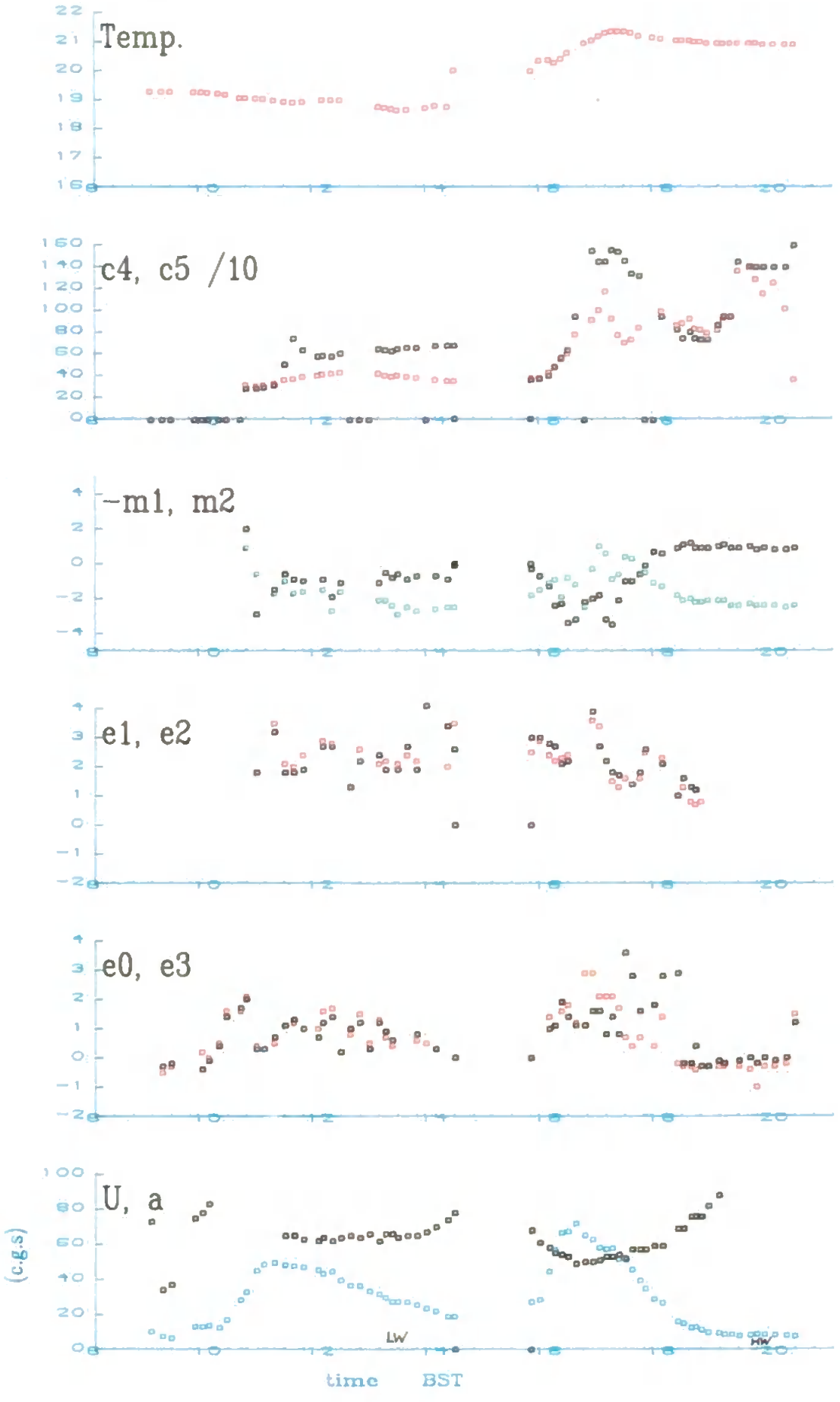

Boundary layer measurements.
Units are c.g.s.
e0..3 on log10 scale

X4d
July5

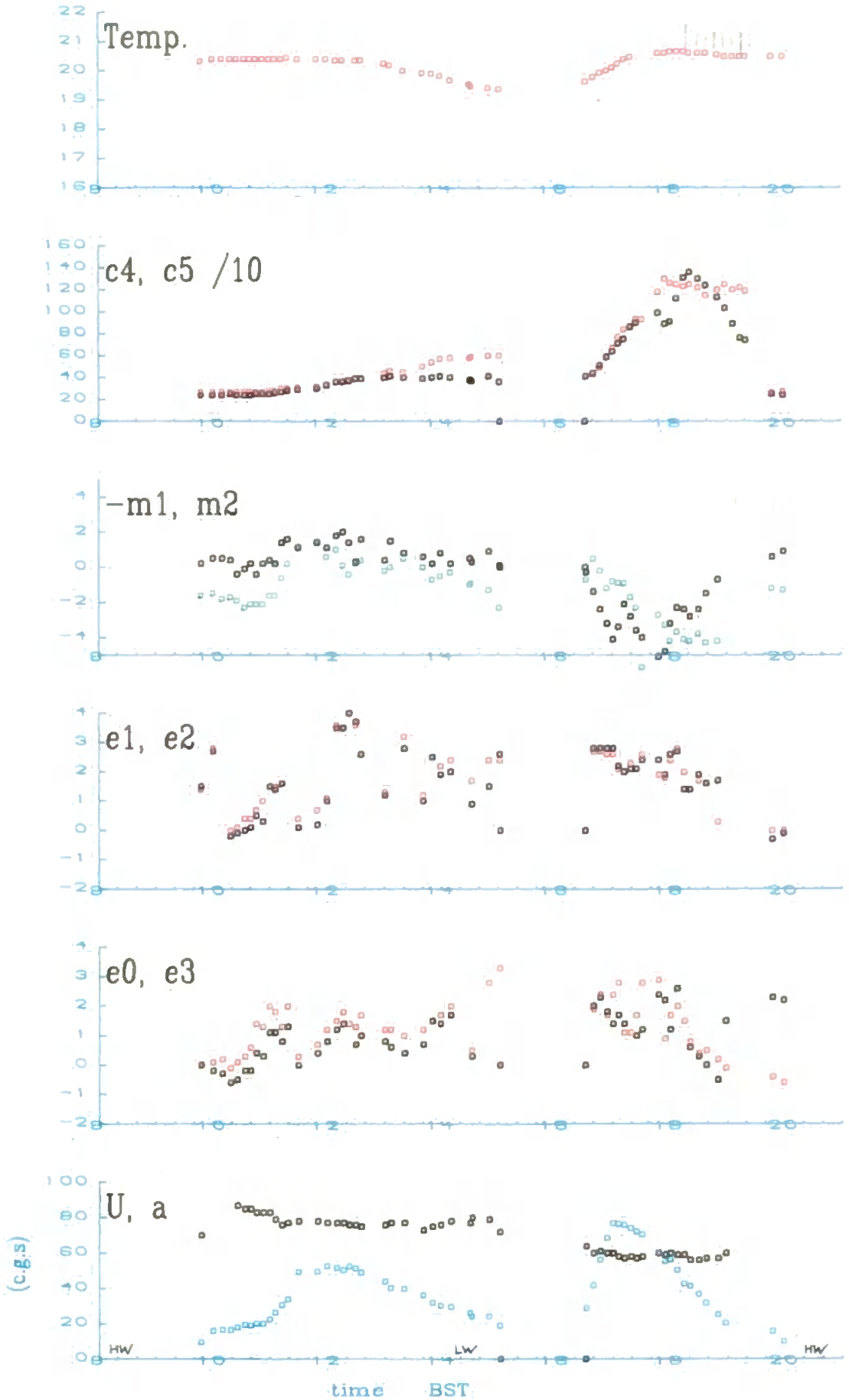

X5 Comparison of OBS and 'Partech' concentrations.

Each plot refers to one day (labelled in upper left). OBS concentrations *c4* (red) and *c5* (black) are run averages. 'Partech' concentrations (line) are values from the lowest profile depth. Horizontal axis is time (BST). Vertical axis is marked as SPM concentration (g/l). Note that in order to roughly calibrate the OBS sensors with the 'Partech' instrument the OBS concentrations are reduced by a factor of four from the calibration of section 3A2.2. Data is read from "*.PFL" and "*.FLO" files.

C, c4, c5 [g/l]

C (line) from profiles

c4 (▲) lower OBS (approx.calib.)

c5 (▪) upper OBS (–"–)

X5

SPM

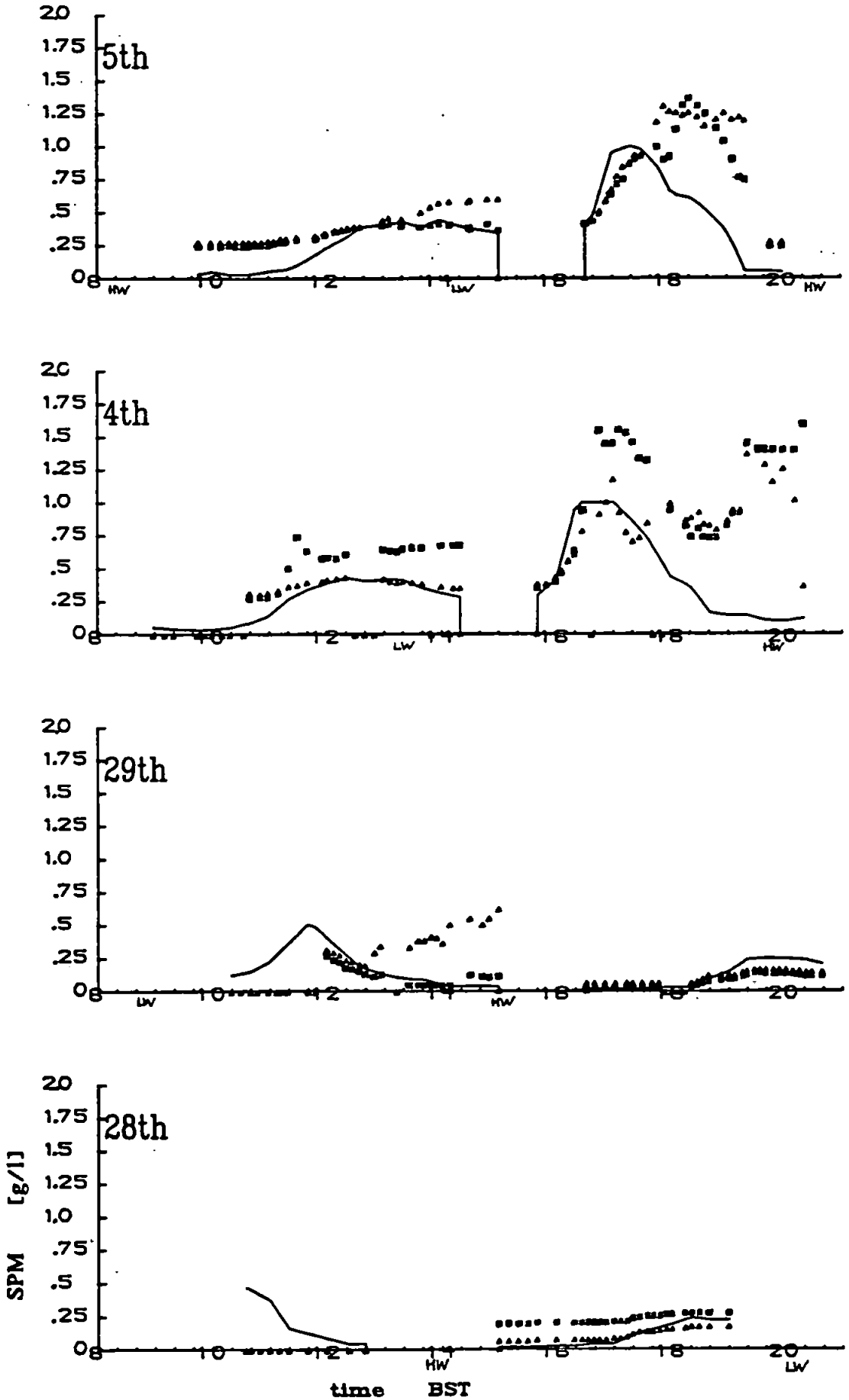

X6 (a)-(d) Turbulent intensities.

Each page (labelled in top right corner) relates to one day. Each plot relates to one parameter (labelled in upper left). Horizontal axis is time (BST), vertical axis is the intensity ratio. Intensity is obtained as the square root of the variance in the relevant channel, divided by the mean current, *i.e.* $\sqrt{\langle u^2 \rangle}/U$. Note that *c4* and *c5* are also divided by U. Variances are taken from "*.VAR" files.

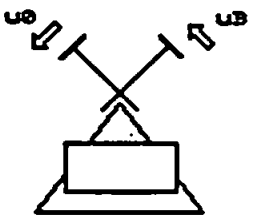

u0, u3 horizontal

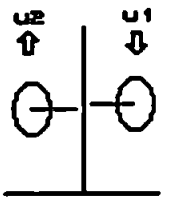

u1, u2 vertical

Turbulent Intensities:

sqrt<variance>/U

(marked line) u'/U

(line) w'/u'

X6a
June 28

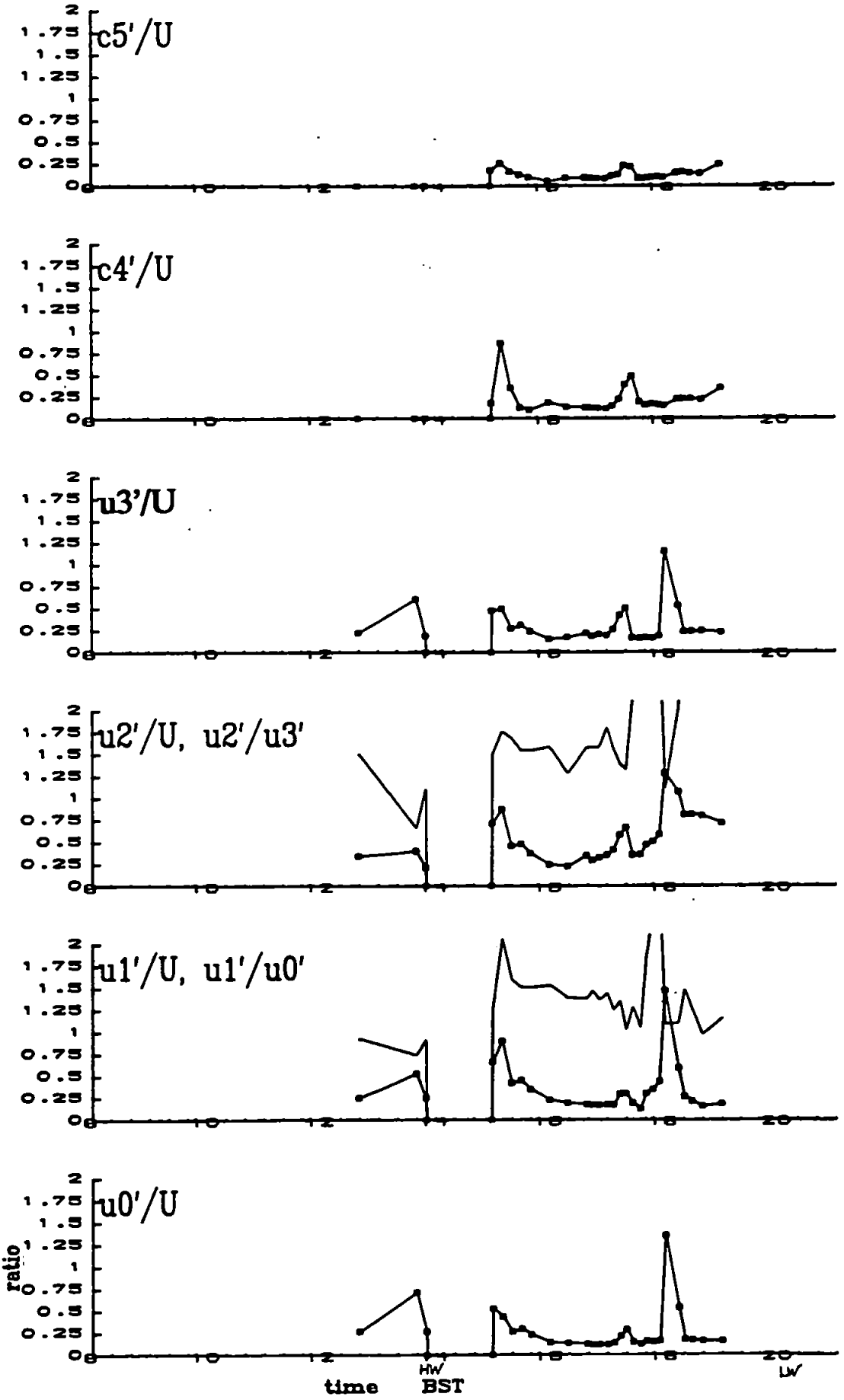

Turbulent Intensities.
sqrt<variance>/U
(line) w'/u'

X6b
June 29

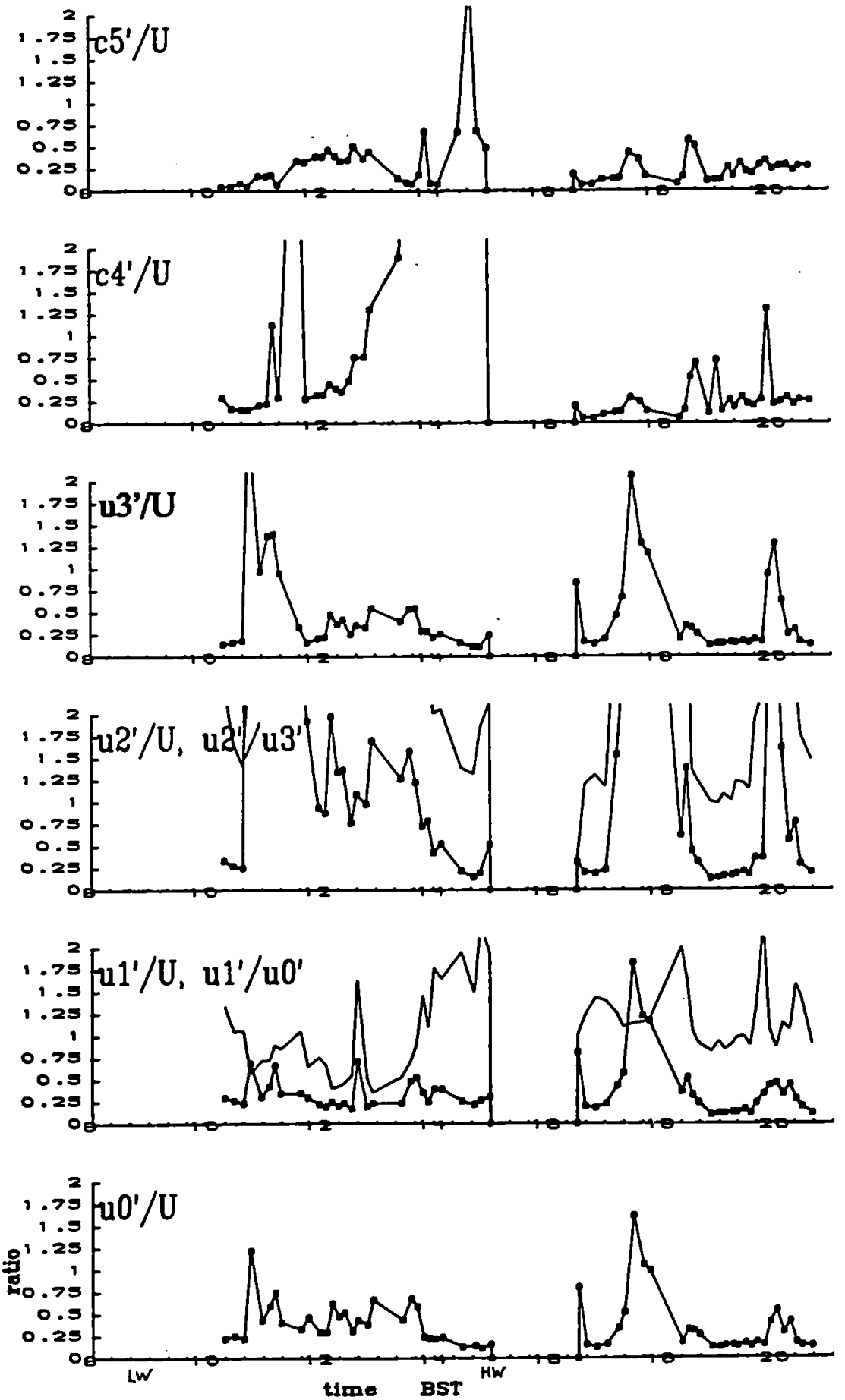

Turbulent Intensities.

sqrt<variance>/U

(line) w'/u'

X6c

July 4

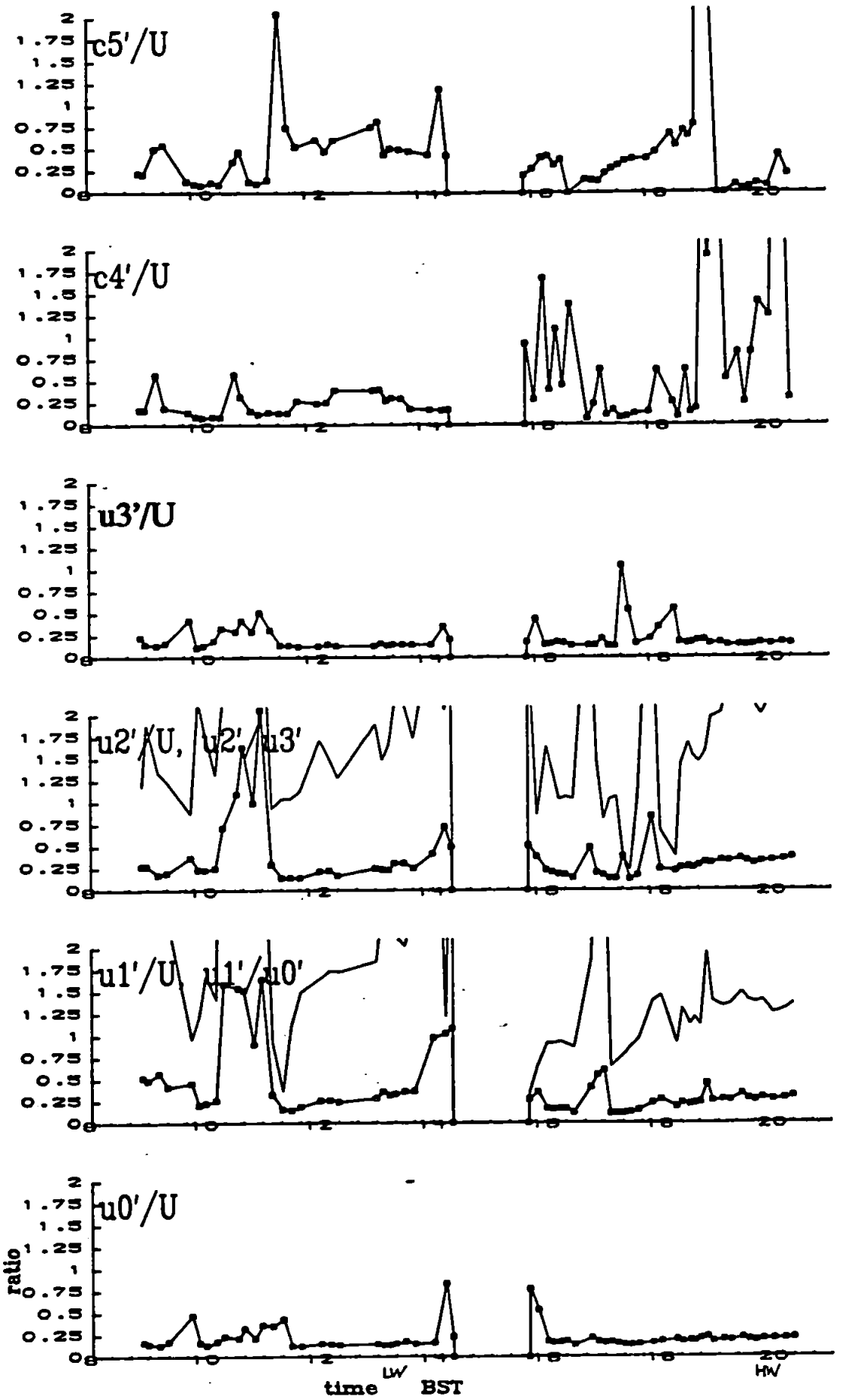

Turbulent Intensities.
sqrt<variance>/U
(line) w'/u'

X6d
July 5

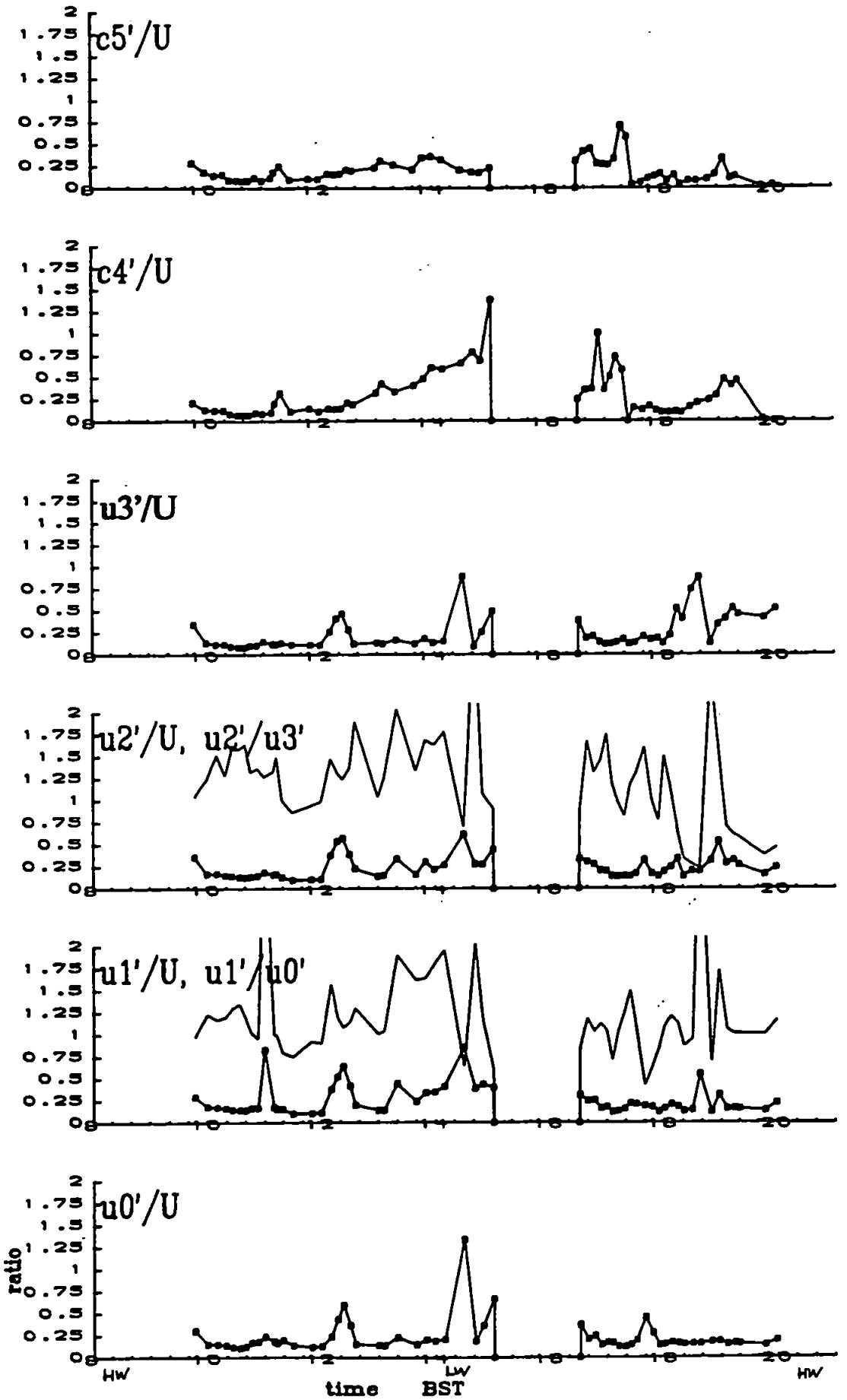

X7 ZX Relative sizer data.

Each plot relates to one day (labelled in upper left). Horizontal axis is time (BST), vertical axis is percentage of total weight (volume). Relative weights (strictly volume) of particles in each of sixteen size bands are plotted cummulatively, with the smallest band at the bottom and the largest band at the top. The percentage weight of particles in the *i* th band is represented by the vertical distance between the *i* th and *i-1*th plotted lines. Bands Z1..10=Z_P are plotted in green and bands Z11..16=Z_A are plotted in red. Data is read from "*.LAS" files.

Relative weights in bands.
(Red) bands 11 to 16
(Green) bands 1 to 10

X7

Z%

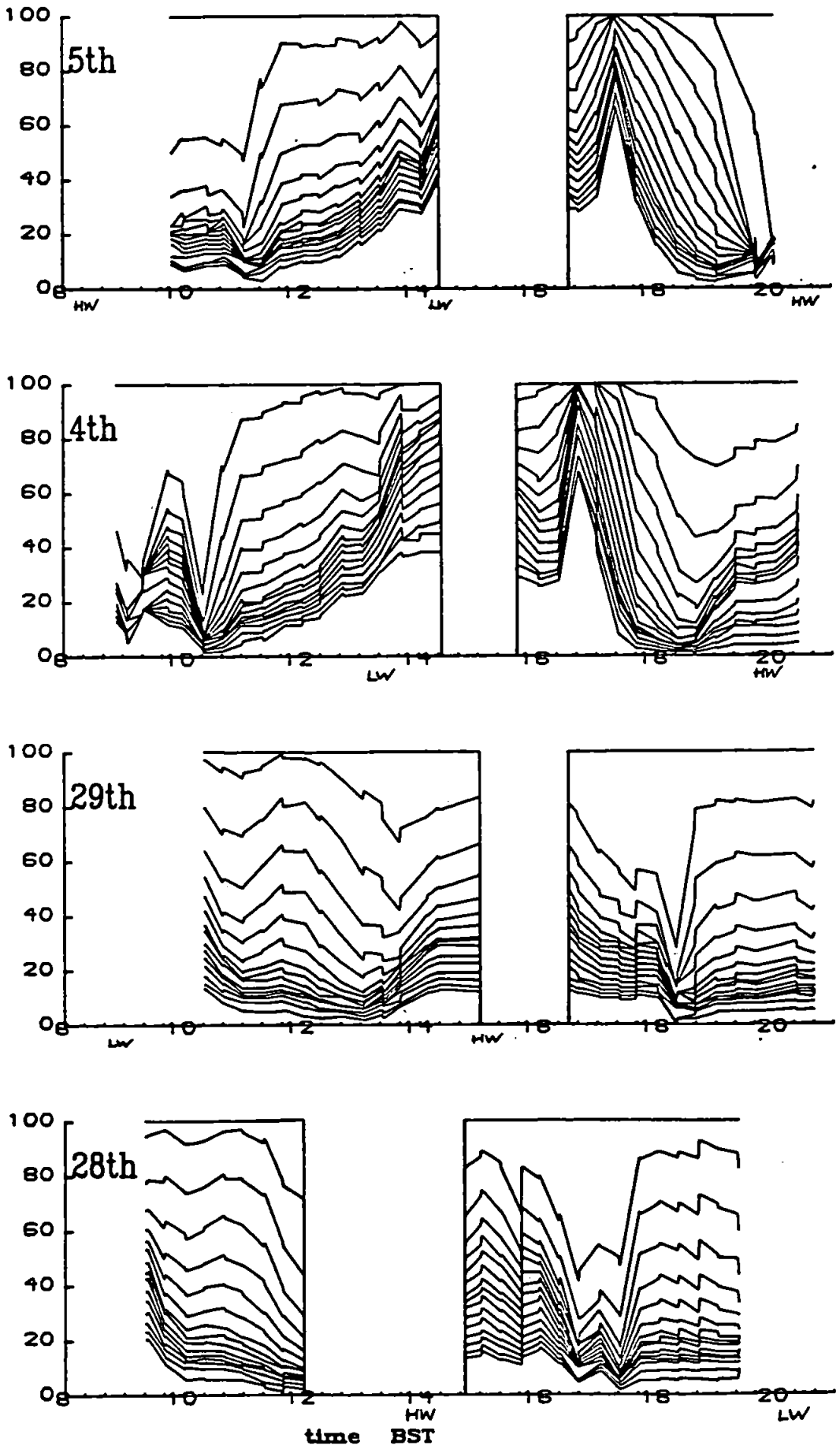

X8 Z Absolute sizer data.

Each plot relates to one day (labelled in upper left). Horizontal axis is time (BST), vertical axis is SPM in mg/l. Total SPM ('Partech') is plotted in black, Z_A in red, Z_P in green. Data is read from "*.LAS" and "*.PFL" files.

Absolute weights in bands.
(Red) Bands 11 to 16
(Green) Bands 1 to 10
(Black) Total SPM (partech)

Z X8

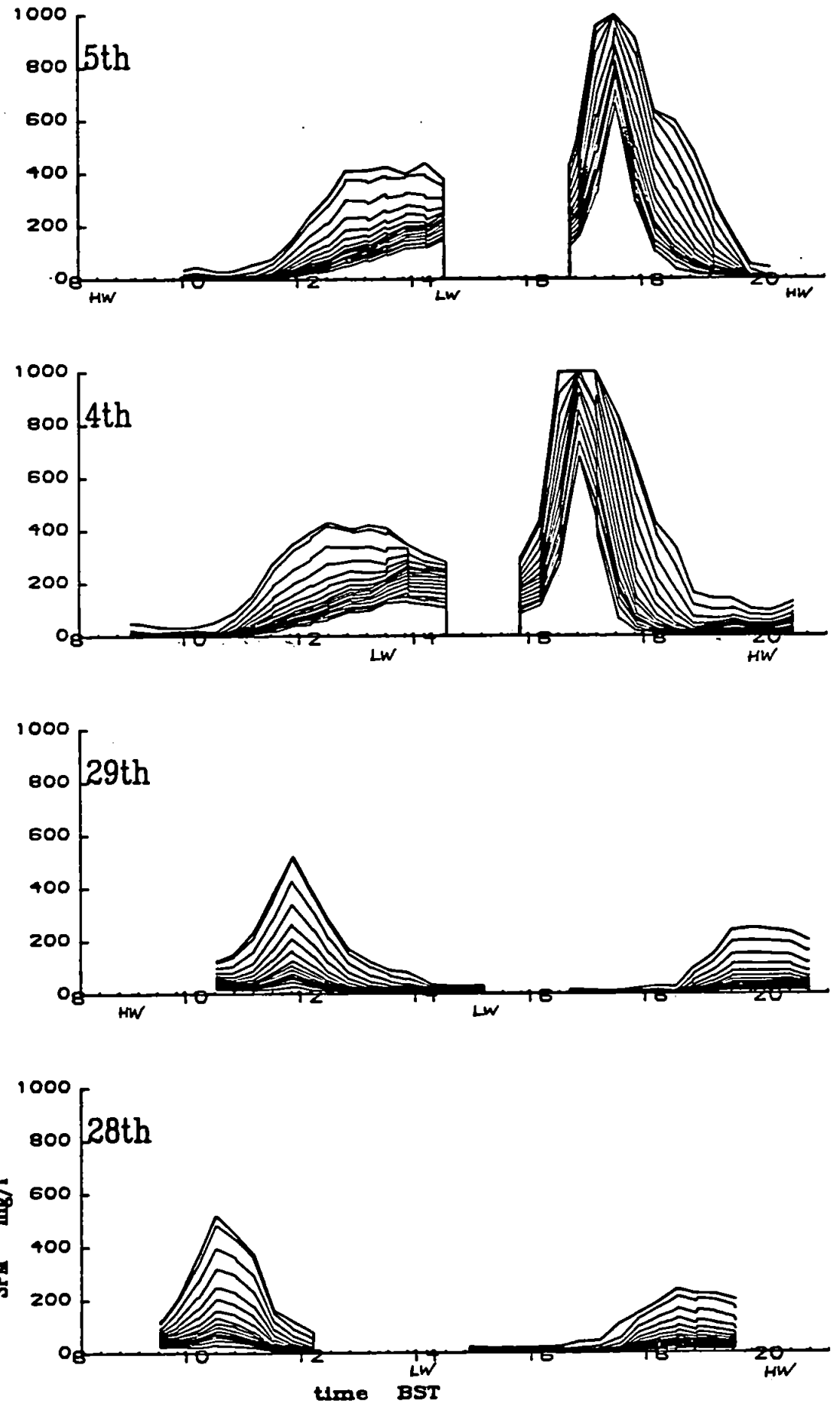

X9 Z(D) Sizer data 'corrected' for floc density.

Plot X8 is redrawn allowing for a size dependent floc density function using the model of McCave 1984 (Table 2.2), see section 4A3.1. Note that no correction has been applied to the 'Partech' concentration (black).

Corrected weights.
Floc density function from McCave 1984.
50um flocs taken to have 'partech density'.
(Rd) ZA. (Gn) Zp. (Bk) total.

X9
Z(D)

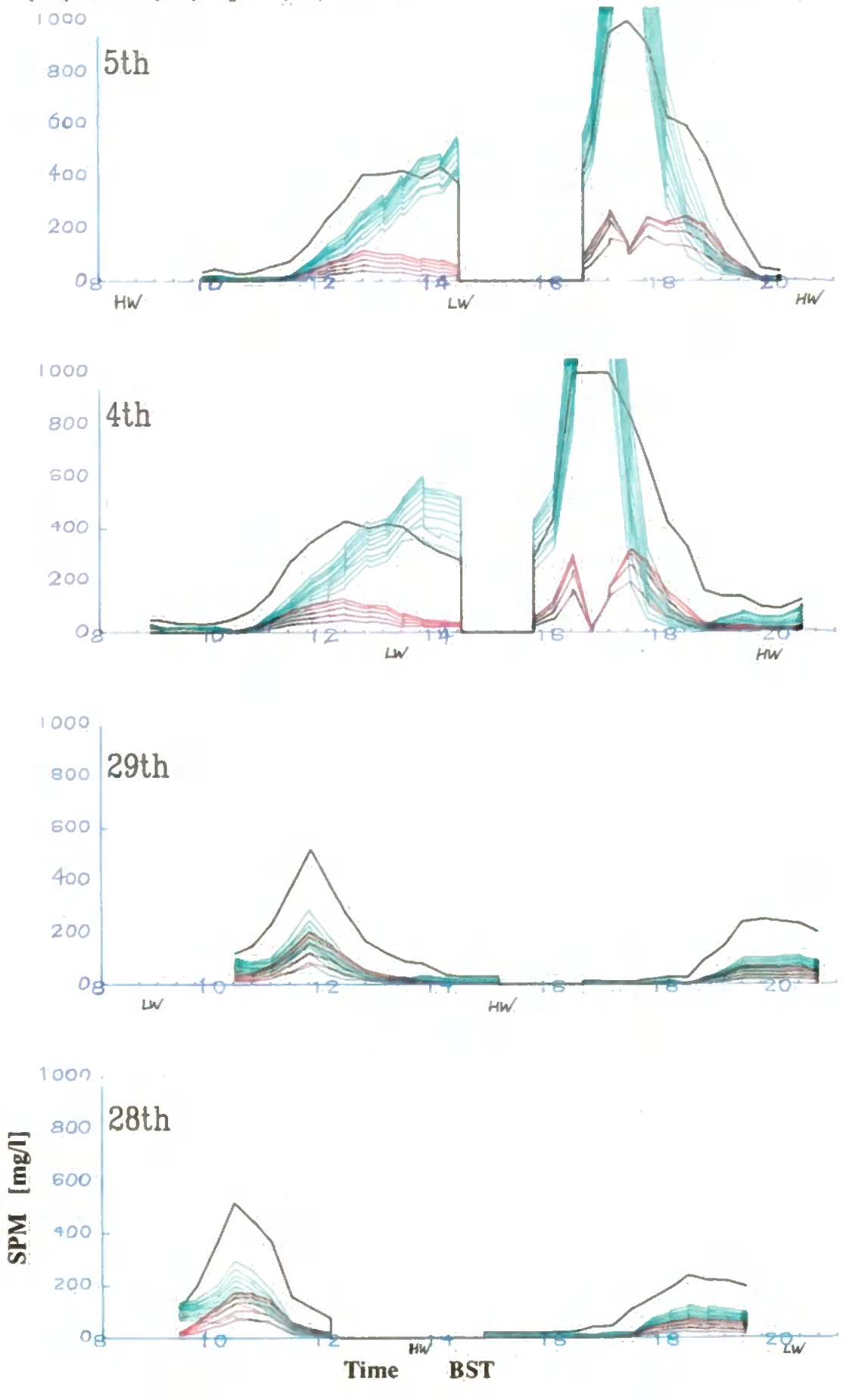

X10 Z_P, Z_A

This plot is the same as X8 except that Z_P and Z_A are plotted independently. Z_P is shown in green, Z_A is shown in red. Total concentration, C, is shown in black.

Absolute weights.
(Red) Z11..16 not incl. Z1..10
(Green) Z1..10
(Black) Total SPM (partech)

X10
Zp, ZA

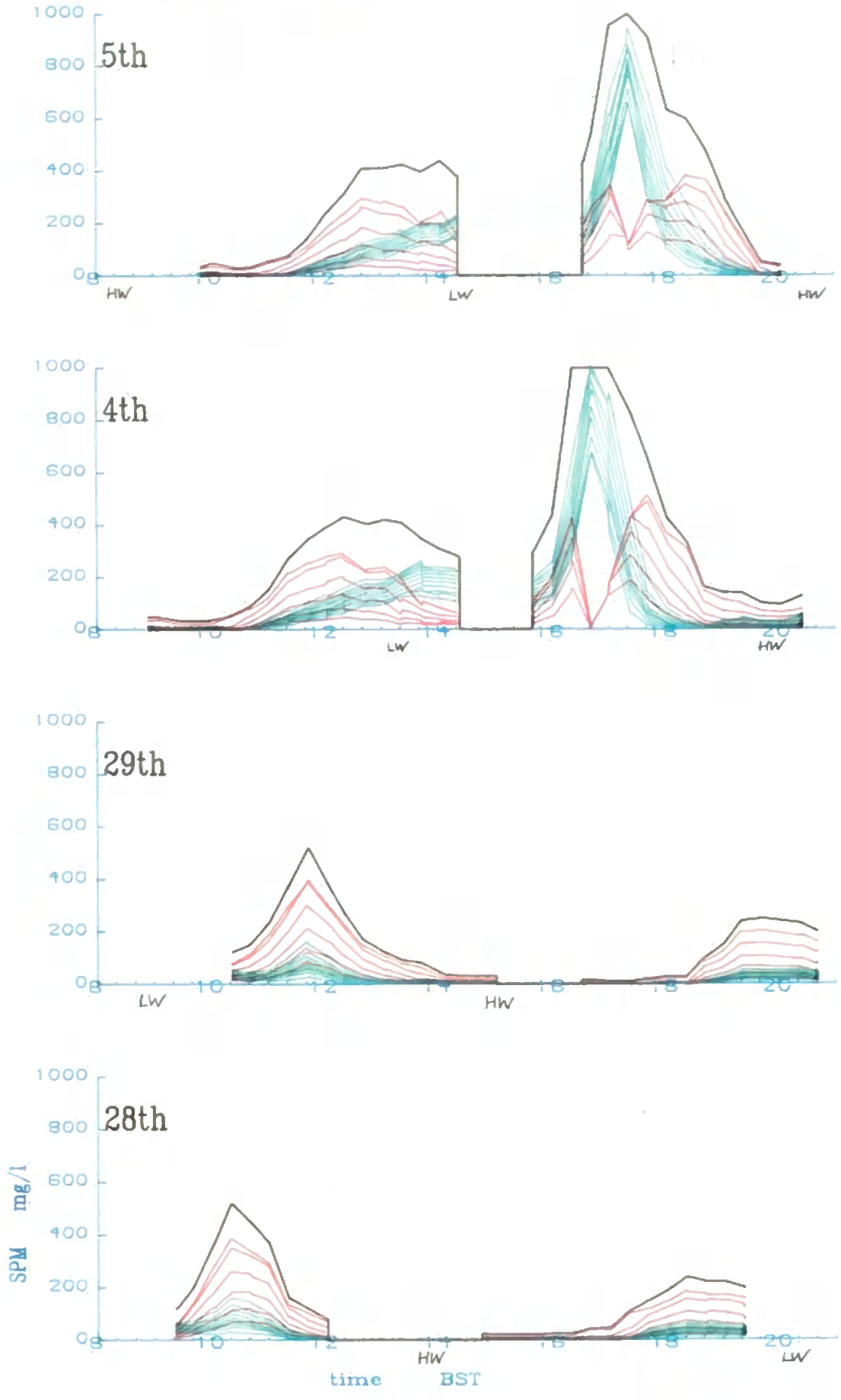

X11 Time series of d_{max} and ε.

Values of d_{max} were obtained as in section 4B2.2 and are plotted here for the 90, 95, 99 percentiles. Also plotted are time series of turbulent dissipation rates, ε, from the EM current meters. Note that 950 μm particle diameter is an arbitrarily imposed upper limit on d_{max}.

Dmax for 90%(Bk), 95%(Rd), 99%(Bk)
using Z12..15.
Also (blue markers)
100.log(e0)+500

X11
d max

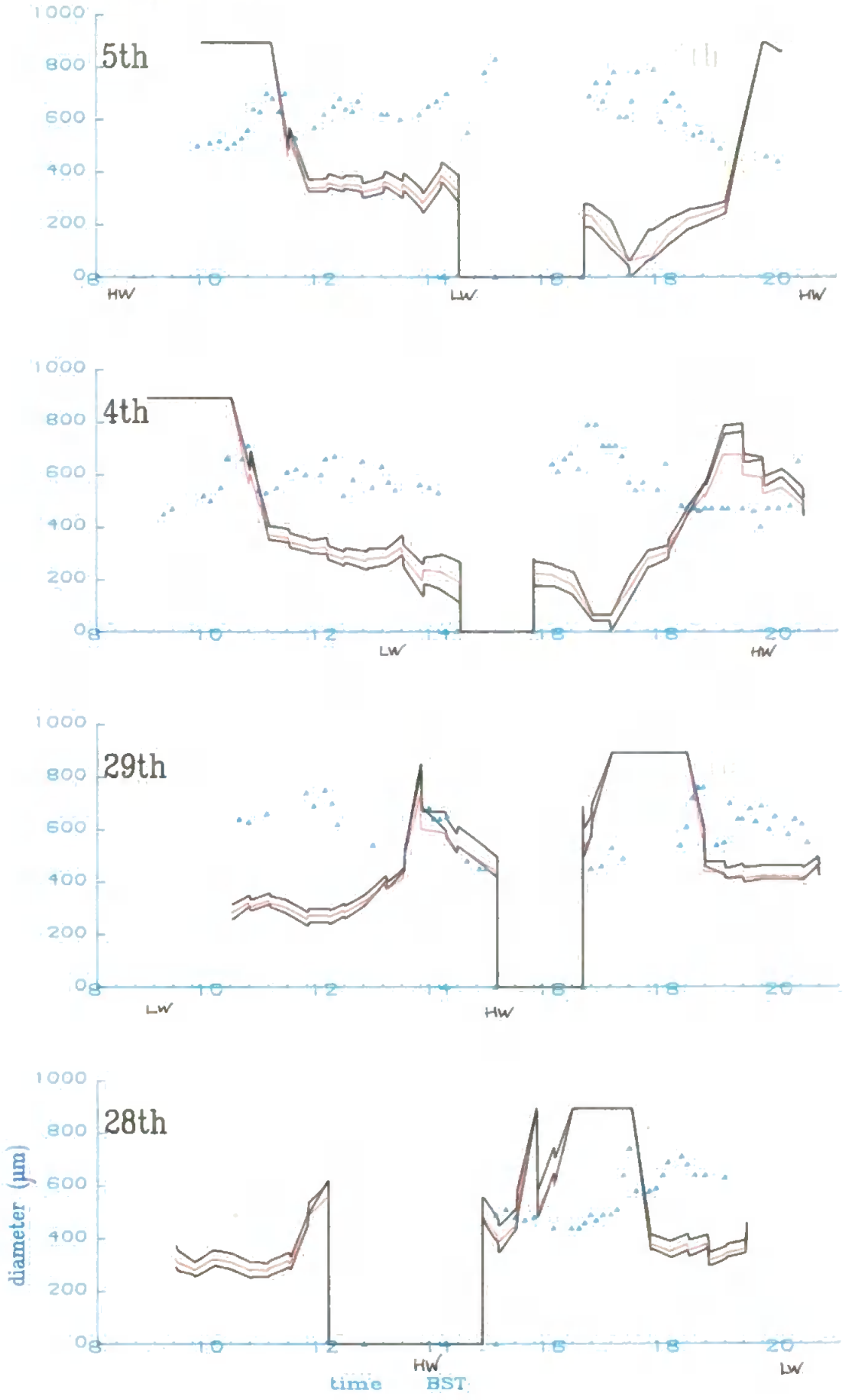

X12 (a)-(d) Contour plots.

Profiled current, salinity, concentration and temperature data is presented as a time series and contoured. The vertical axis is marked in metres such that the surface is at a height of 6 m for each profile. The bed (marked by a black line) was obtained as the depth at which the current meter touched the bed. Positive velocities indicate flood currents.

X12a

CONTOUR KEY	
1	0.00
2	2.00
3	4.00
4	6.00
5	8.00
6	10.00
7	12.00
8	14.00
9	16.00
10	18.00
11	20.00

S ppth.

CONTOUR KEY	
1	0.00
2	20.00
3	30.00
4	50.00
5	70.00
6	100.00
7	200.00
8	300.00
9	500.00
10	700.00
11	999.00

C mg/l

CONTOUR KEY	
1	-1.20
2	-1.00
3	-0.80
4	-0.60
5	-0.40
6	-0.20
7	0.00
8	0.20
9	0.40
10	0.60
11	0.80
12	1.00
13	1.20

U m/s

CONTOUR KEY	
1	17.00
2	17.50
3	18.00
4	18.50
5	19.00
6	19.50
7	20.00
8	20.50
9	21.00
10	21.50
11	22.00

T degC

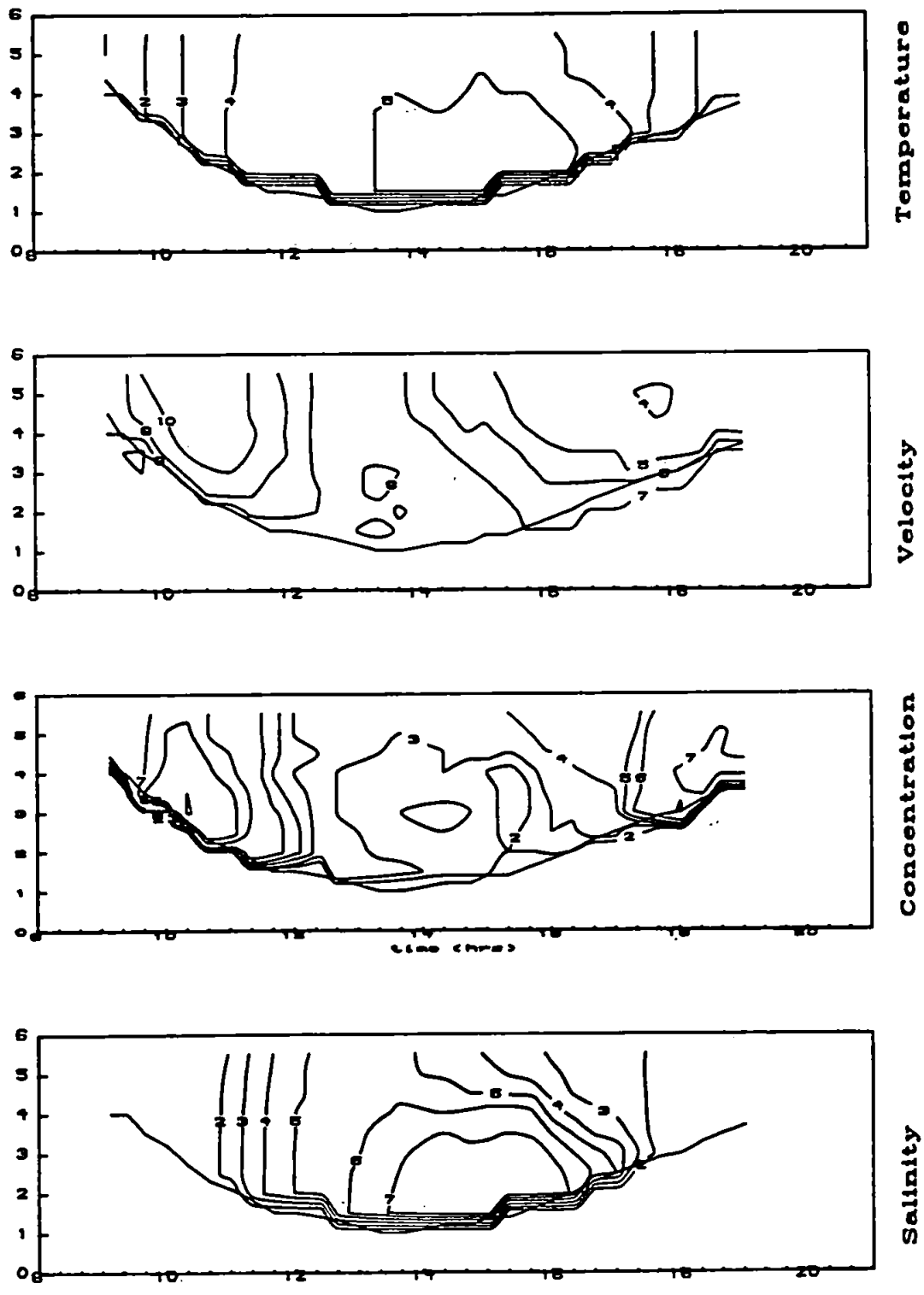

JUNE28

X12b

CONTOUR KEY	
1	0.00
2	2.00
3	4.00
4	6.00
5	8.00
6	10.00
7	12.00
8	14.00
9	16.00
10	18.00
11	20.00

S ppth.

CONTOUR KEY	
1	0.00
2	20.00
3	30.00
4	50.00
5	70.00
6	100.00
7	200.00
8	300.00
9	500.00
10	700.00
11	999.00

C mg/l

CONTOUR KEY	
1	-1.20
2	-1.00
3	-0.80
4	-0.60
5	-0.40
6	-0.20
7	0.00
8	0.20
9	0.40
10	0.60
11	0.80
12	1.00
13	1.20

U m/s

CONTOUR KEY	
1	17.00
2	17.50
3	18.00
4	18.50
5	19.00
6	19.50
7	20.00
8	20.50
9	21.00
10	21.50
11	22.00

T degC

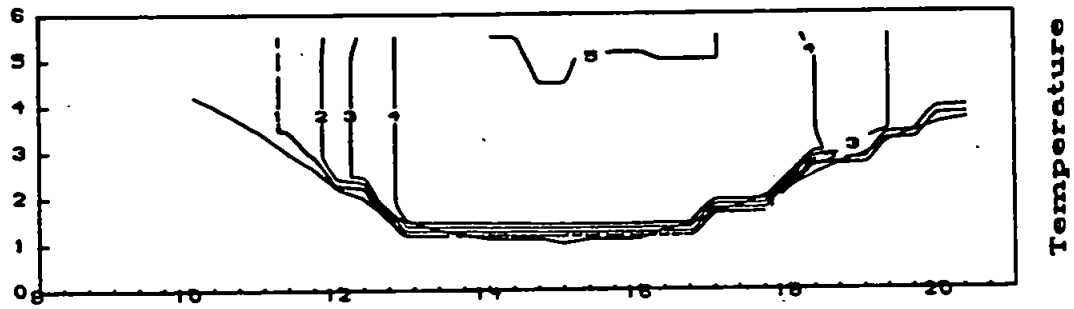

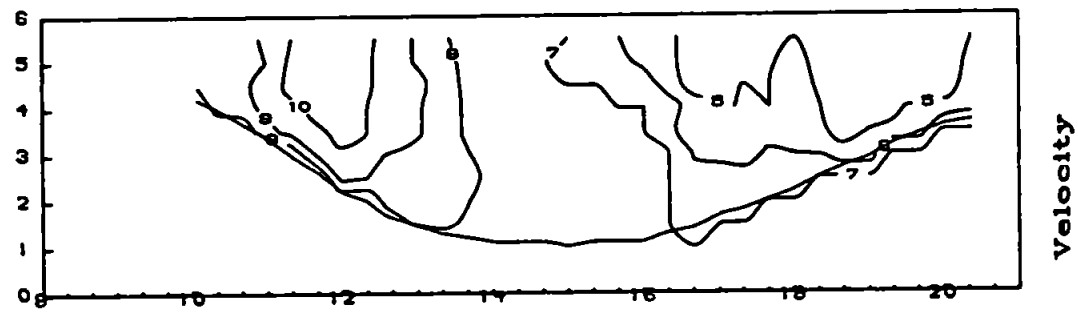

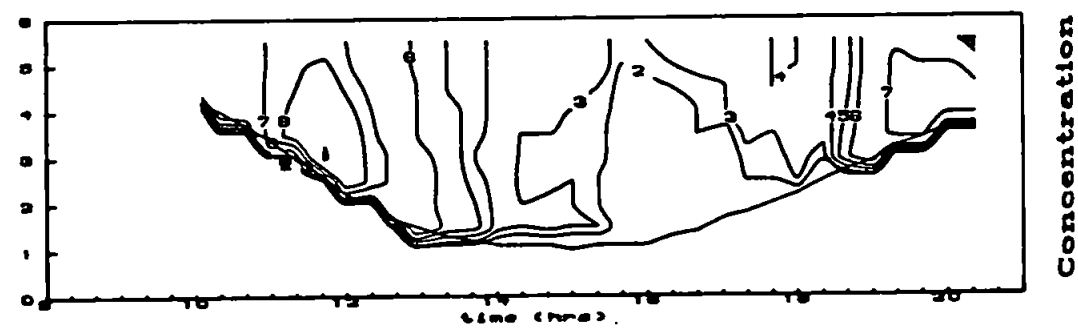

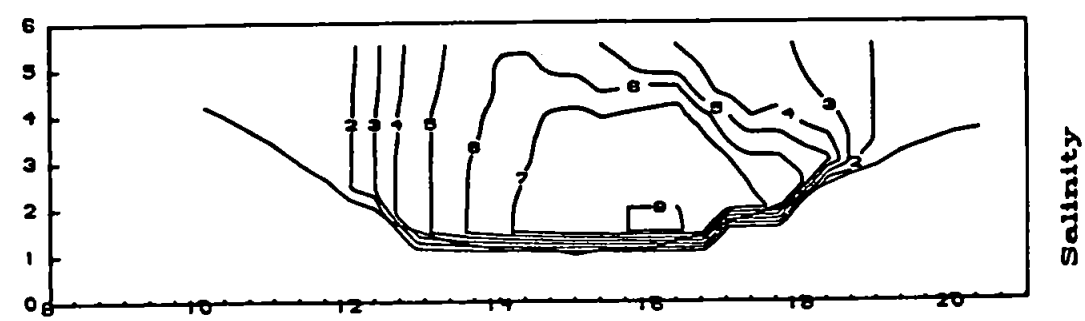

JUNE29

CONTOUR KEY	
1	0.00
2	2.00
3	4.00
4	6.00
5	8.00
6	10.00
7	12.00
8	14.00
9	16.00
10	18.00
11	20.00

S ppth.

CONTOUR KEY	
1	0.00
2	20.00
3	30.00
4	50.00
5	70.00
6	100.00
7	200.00
8	300.00
9	500.00
10	700.00
11	999.00

C mg/l

CONTOUR KEY	
1	-1.20
2	-1.00
3	-0.80
4	-0.60
5	-0.40
6	-0.20
7	0.00
8	0.20
9	0.40
10	0.60
11	0.80
12	1.00
13	1.20

U m/s

CONTOUR KEY	
1	17.00
2	17.50
3	18.00
4	18.50
5	19.00
6	19.50
7	20.00
8	20.50
9	21.00
10	21.50
11	22.00

T degC

X12c

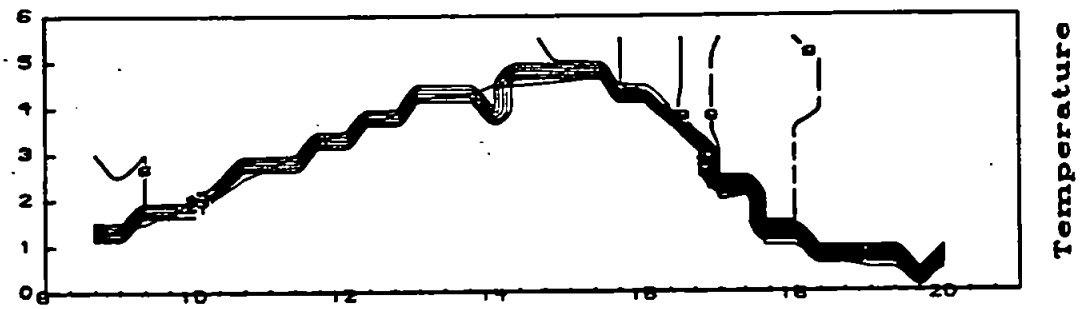

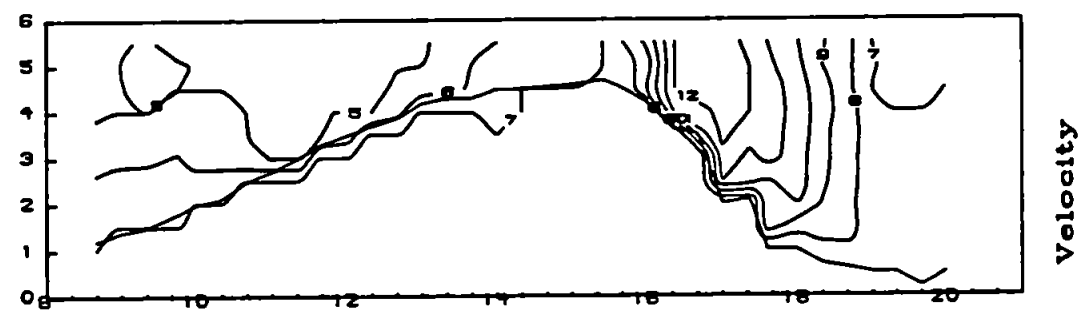

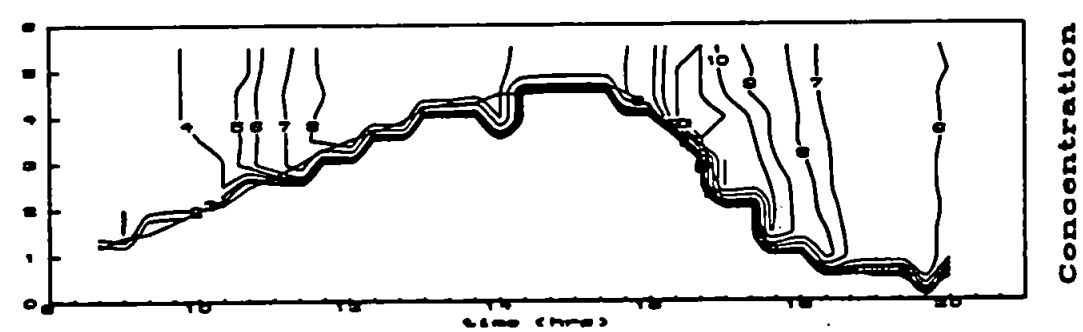

JULY4

X12d

CONTOUR KEY	
1	0.00
2	2.00
3	4.00
4	6.00
5	8.00
6	10.00
7	12.00
8	14.00
9	16.00
10	18.00
11	20.00

S ppth.

CONTOUR KEY	
1	0.00
2	20.00
3	30.00
4	50.00
5	70.00
6	100.00
7	200.00
8	300.00
9	500.00
10	700.00
11	999.00

C mg/l

CONTOUR KEY	
1	-1.20
2	-1.00
3	-0.80
4	-0.60
5	-0.40
6	-0.20
7	0.00
8	0.20
9	0.40
10	0.60
11	0.80
12	1.00
13	1.20

U m/s

CONTOUR KEY	
1	17.00
2	17.50
3	18.00
4	18.50
5	19.00
6	19.50
7	20.00
8	20.50
9	21.00
10	21.50
11	22.00

T degC

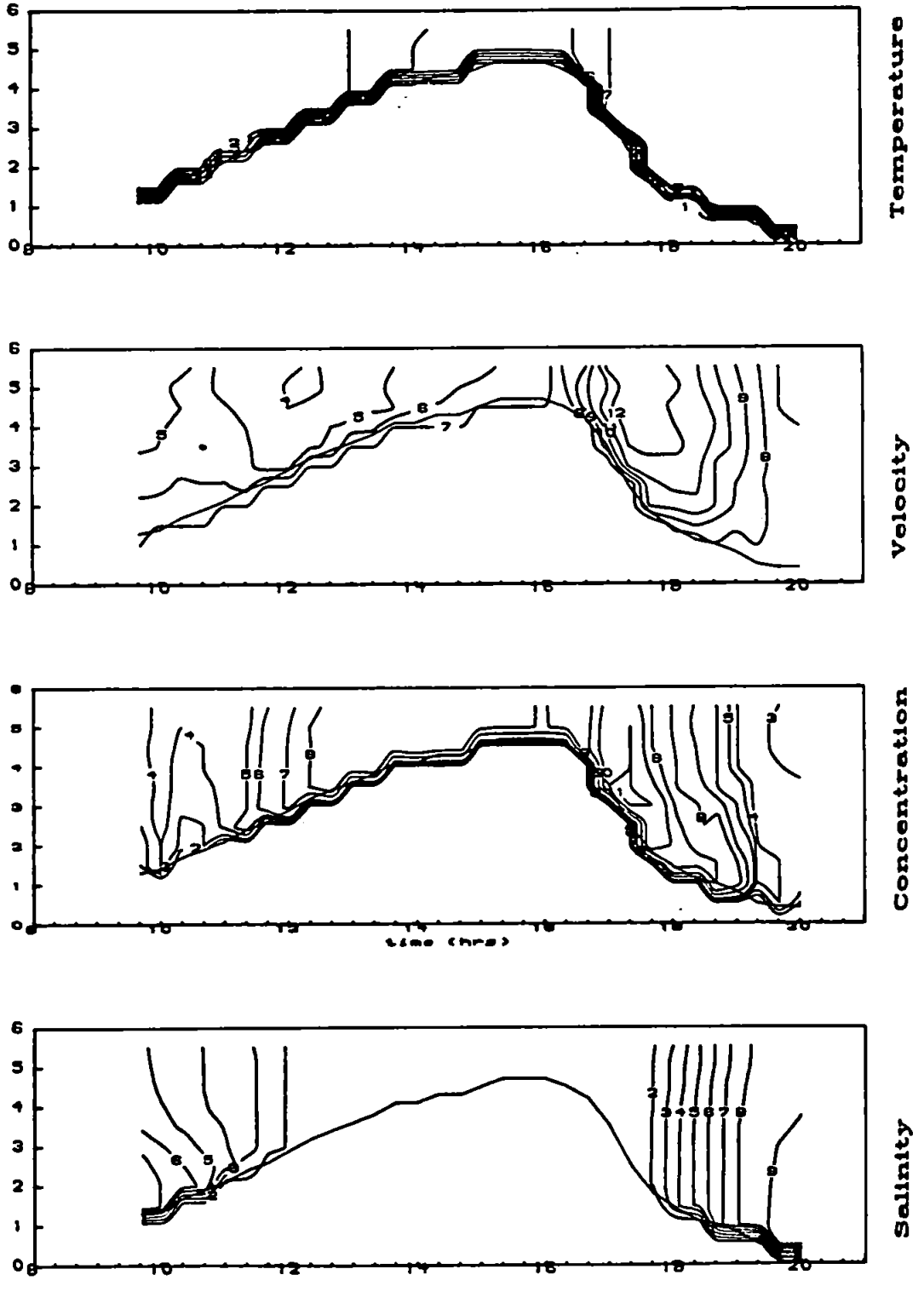

JULY5

X13 Fluxes.

Longitudinal fluxes (positive up-river) are obtained from each profile by integrating over height. Time series of fluxes are plotted. Units are indicated on the plot.

(Bl) mass/10 (kg/m/s)
(Rd) heat (C.m.m/s)
(Gn) salt (ppt.m.m/s)
(Bk) SPMx100 (g/m/s)

X13
Fluxes

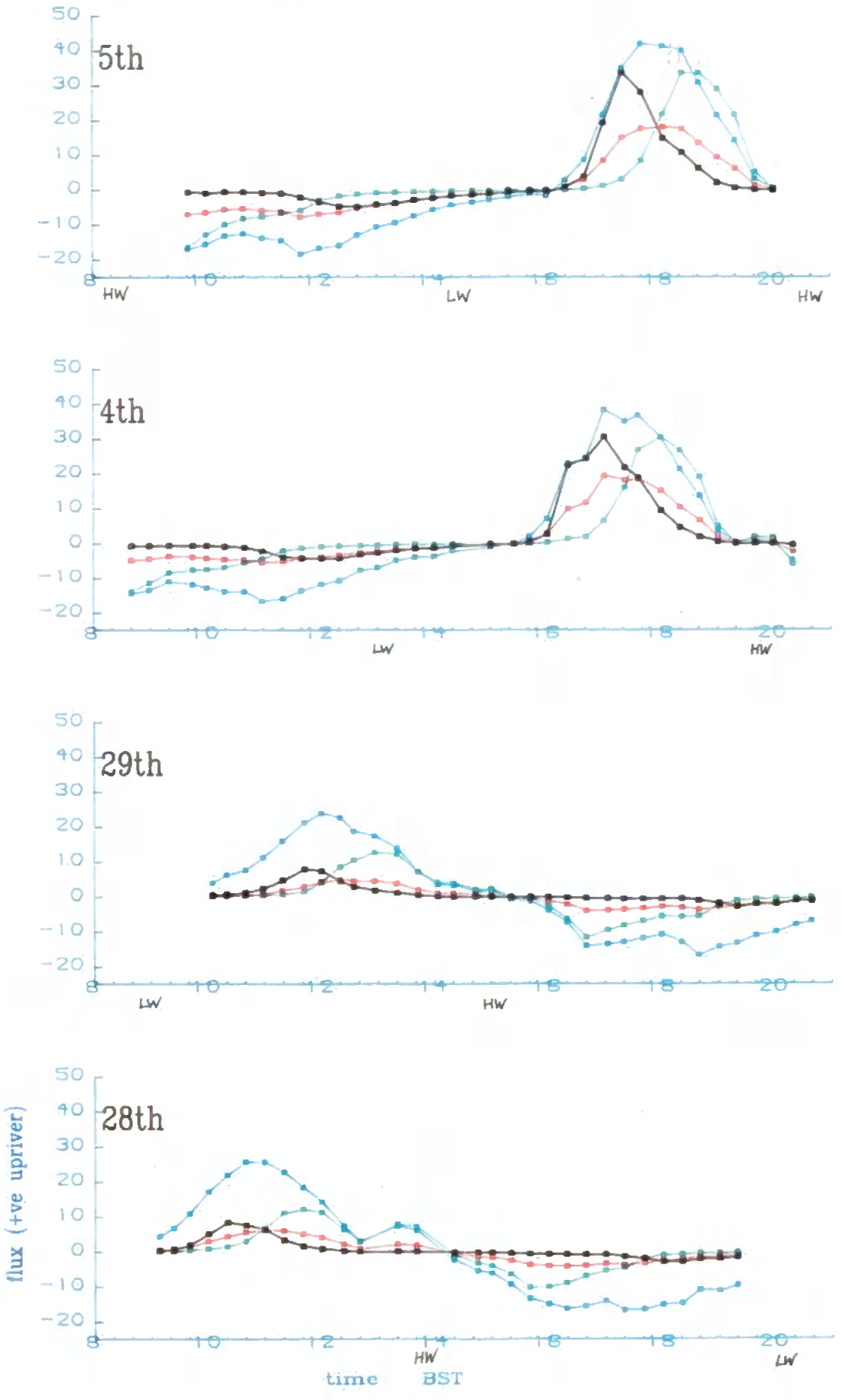

X14 Richardson numbers.

A layer Richardson number is obtained from each profile and the time series plotted. Also plotted are time series of terms relevant to the Richardson number: water depth, surface/bed salinity difference, and depth averaged flow. Units are indicated on the plot.

X14

(Rd) Ri×10
(Bl) depth averaged current x10 [m/s]
(Gn) salinity difference, $S_{sfce} - S_{bed}$ [‰]

Ri

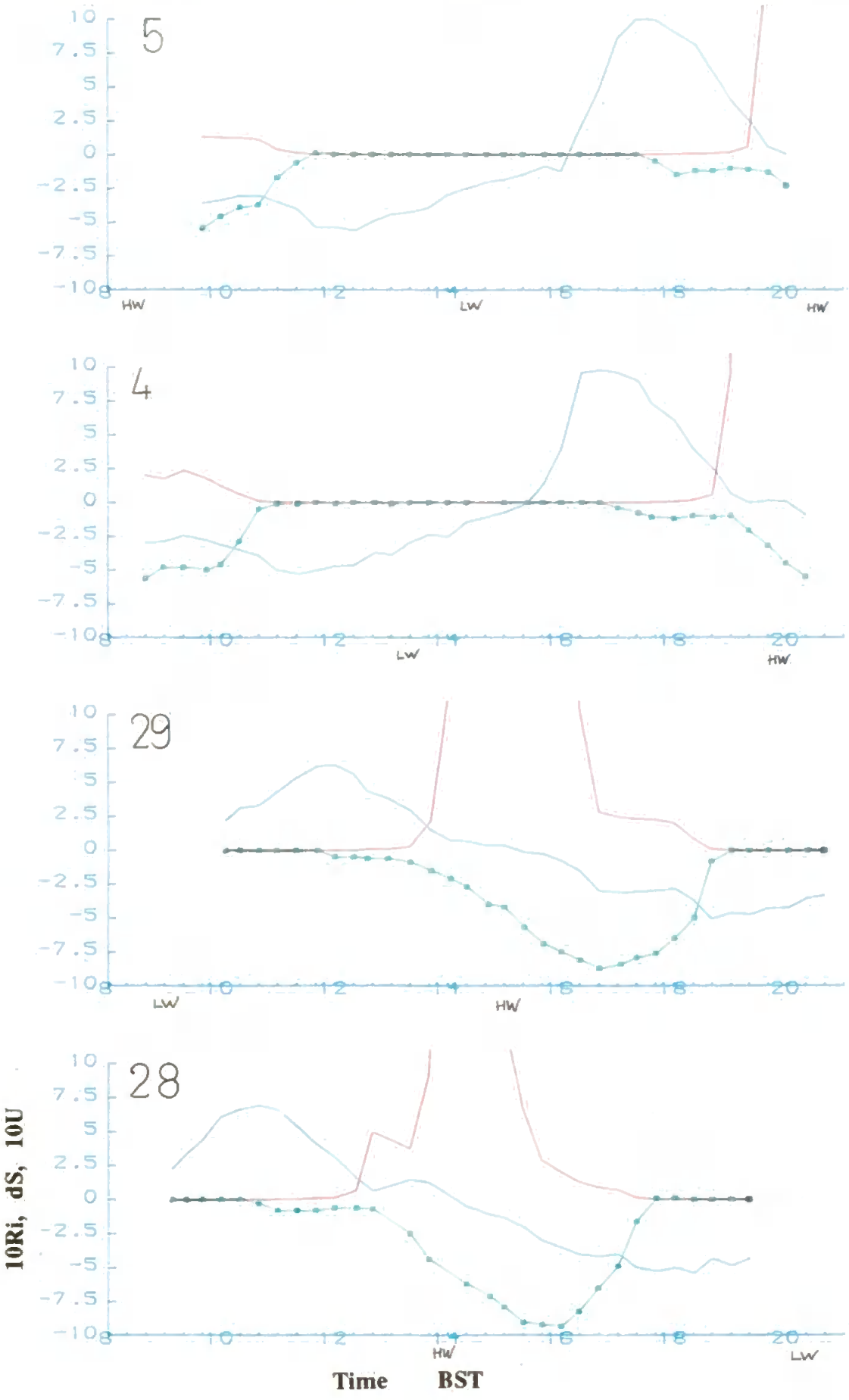

X15 C, Z_P, Z_A against mean current.

Time series of total SPM concentration, C, and Z_P and Z_A are plotted against current speed, U (flood positive). Note that the time series for the 28th and 29th June begin with negative speeds, and those for 4th, 5th July begin with positive speeds.

C, Z1..10, Z11..16 [mg/l]
against U [cm/s].

X15
Z|U

C (Bk), Z1..10 (Gn), Z11..16(Rd).

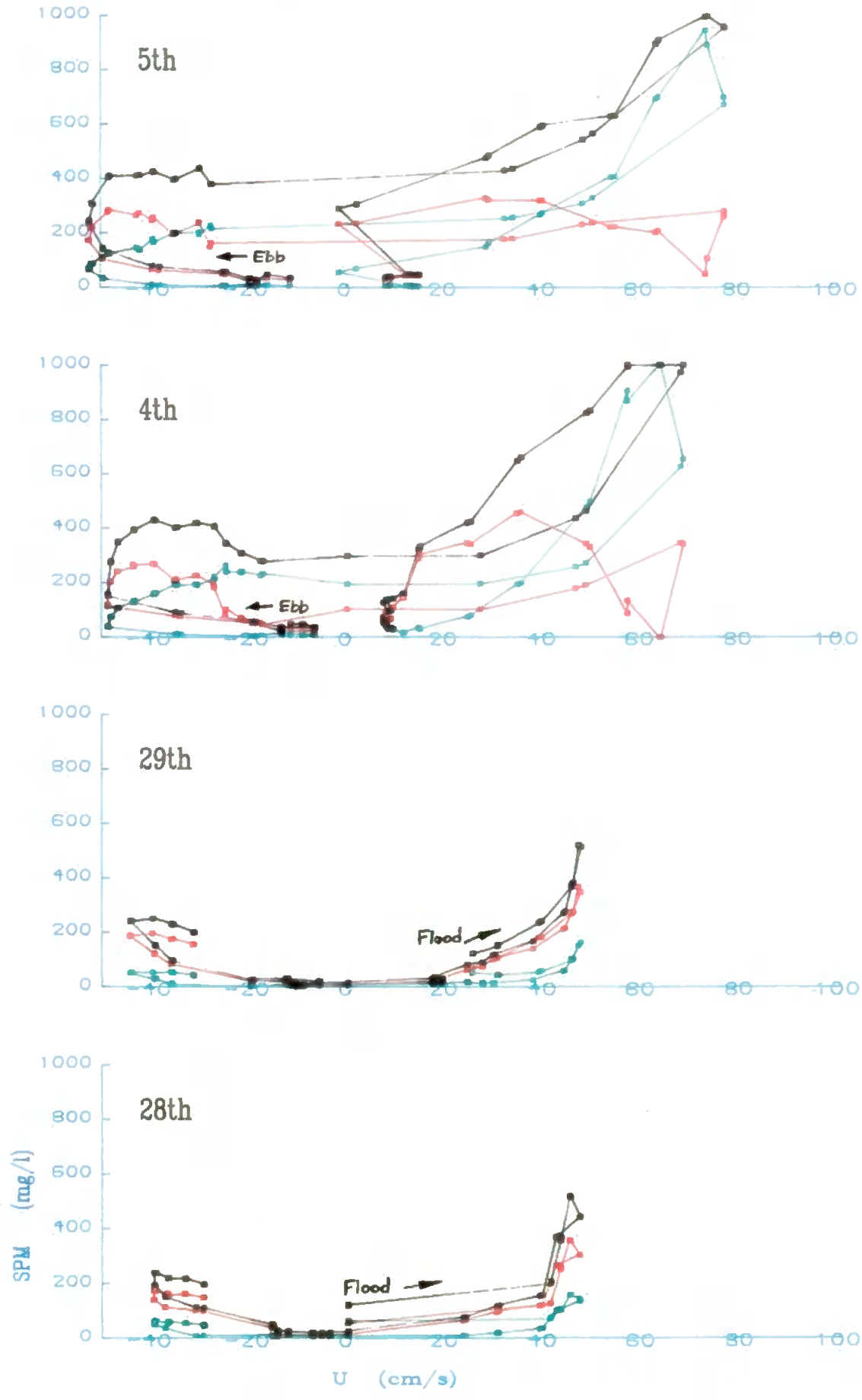

X16 (a)-(d) Environment of rig.

Various parameters (U, C, S, ϑ) of the flow near the bed are plotted against each other to indicate typical variations over the tidal cycle. Values were obtained from '*.PFL' files.

X16a

28th June 1989

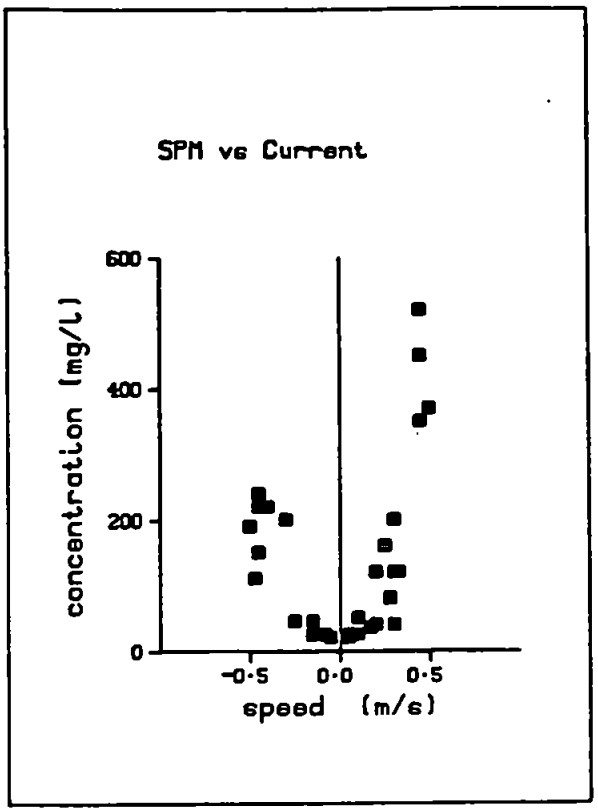

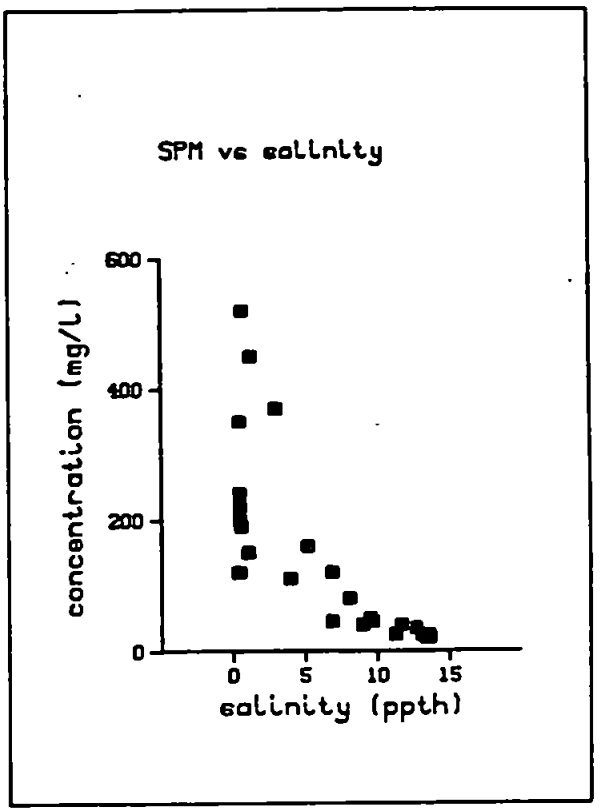

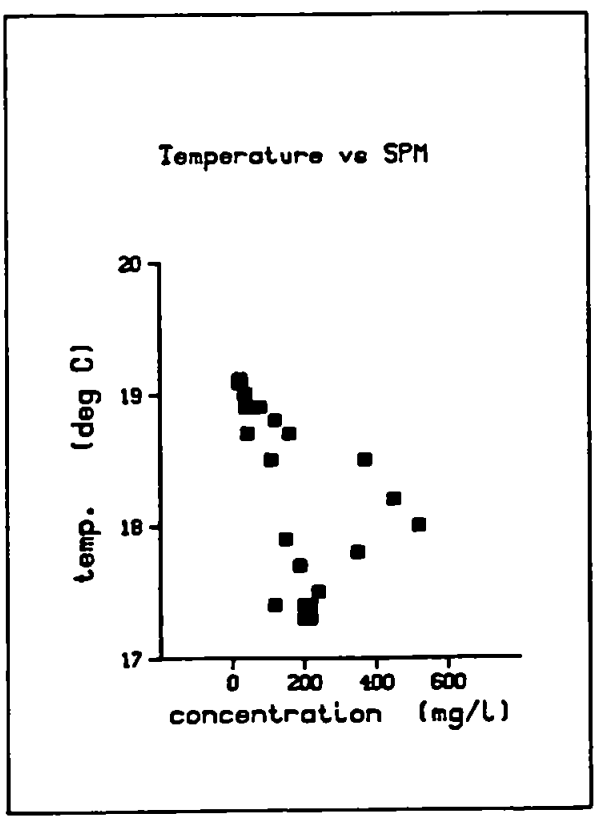

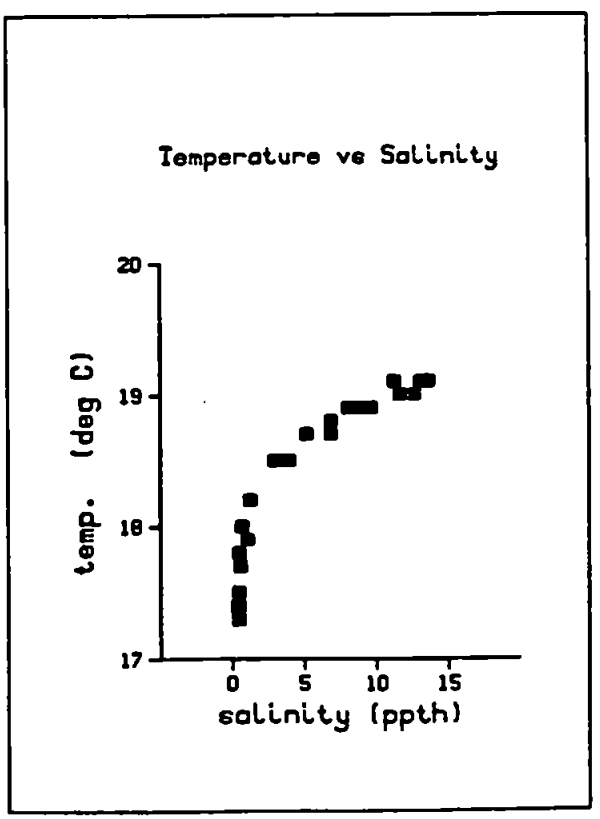

X16b

29th June 1989

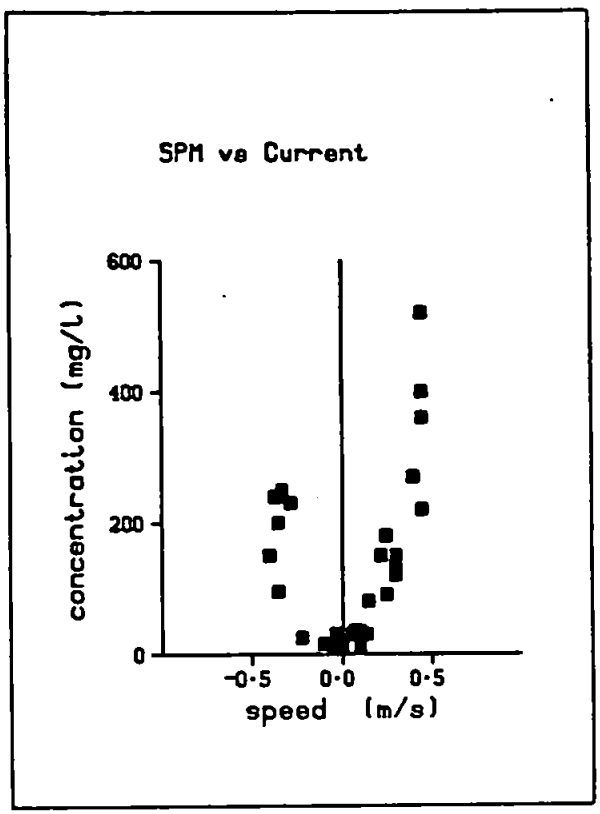

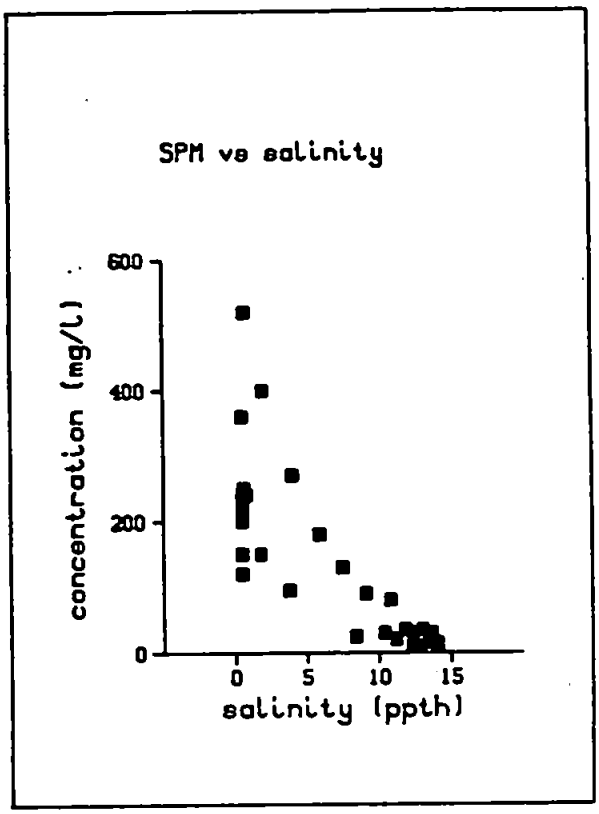

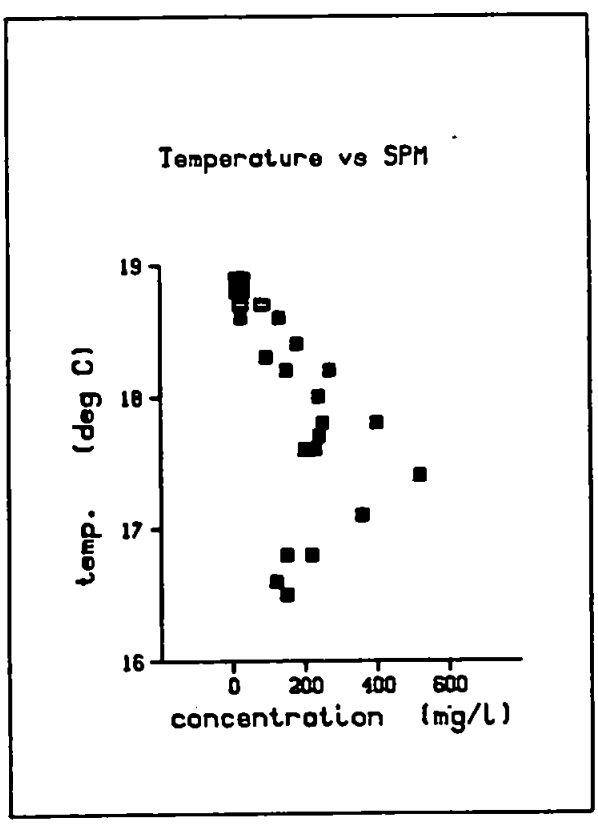

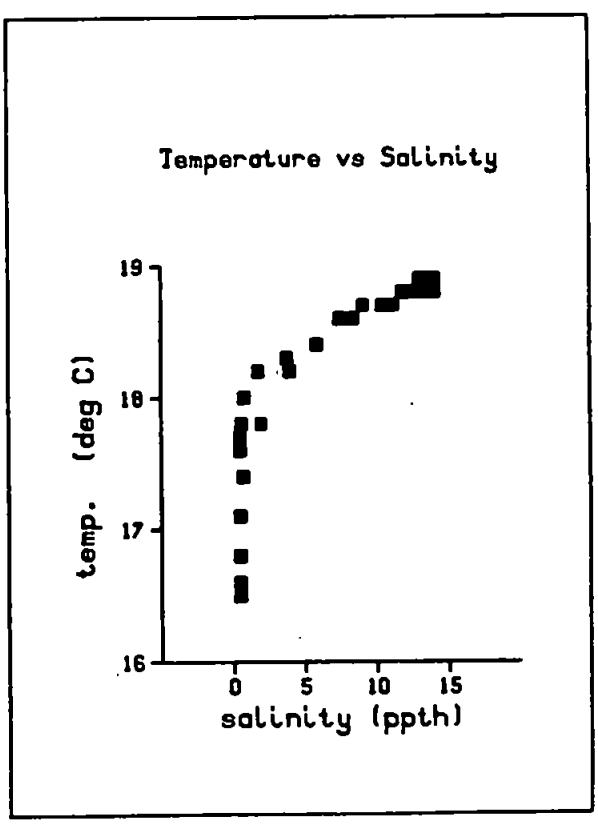

X16c

4th July 1989

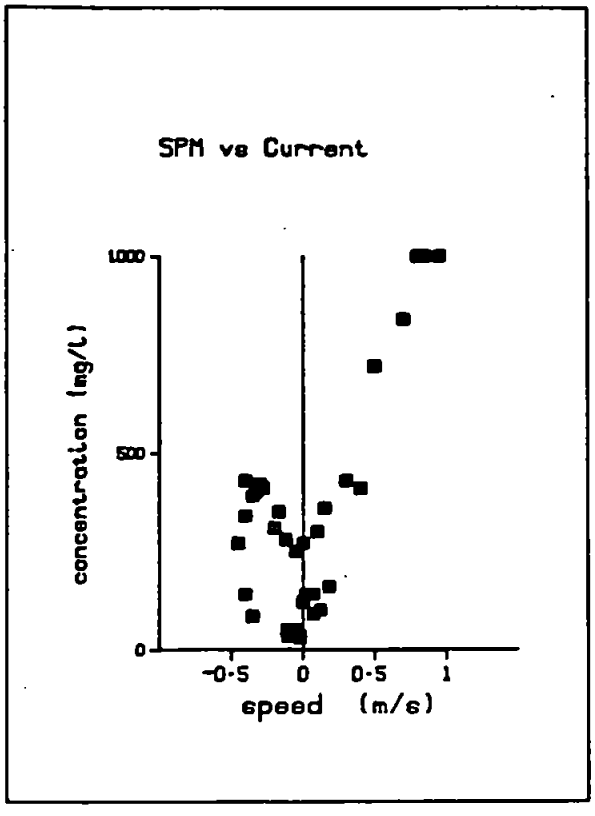

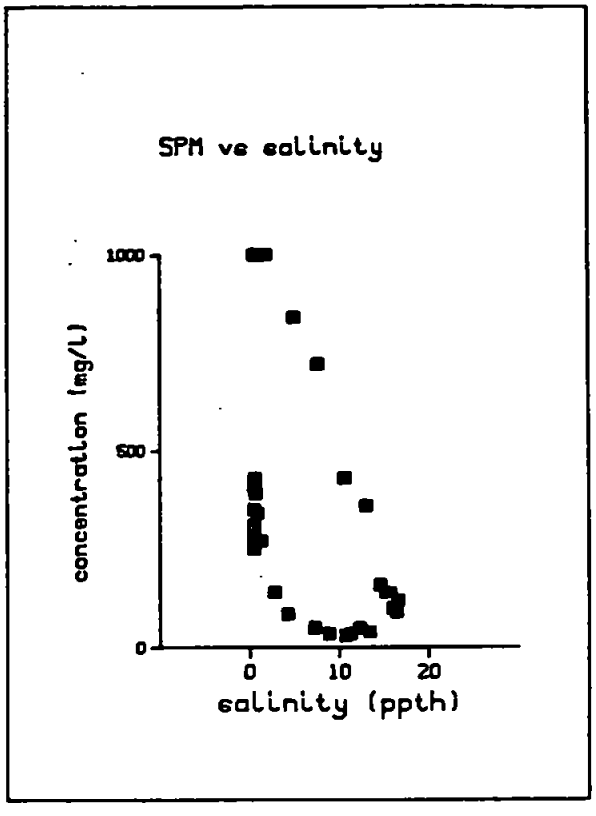

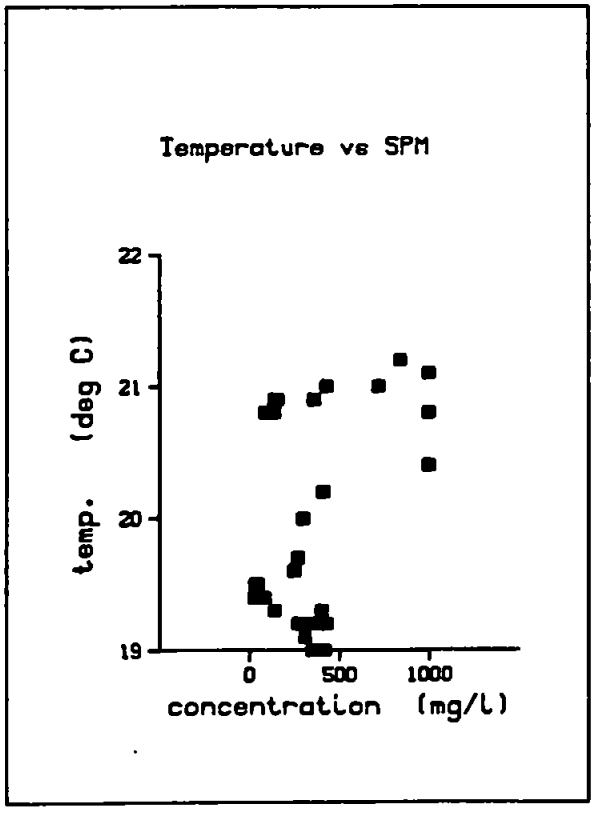

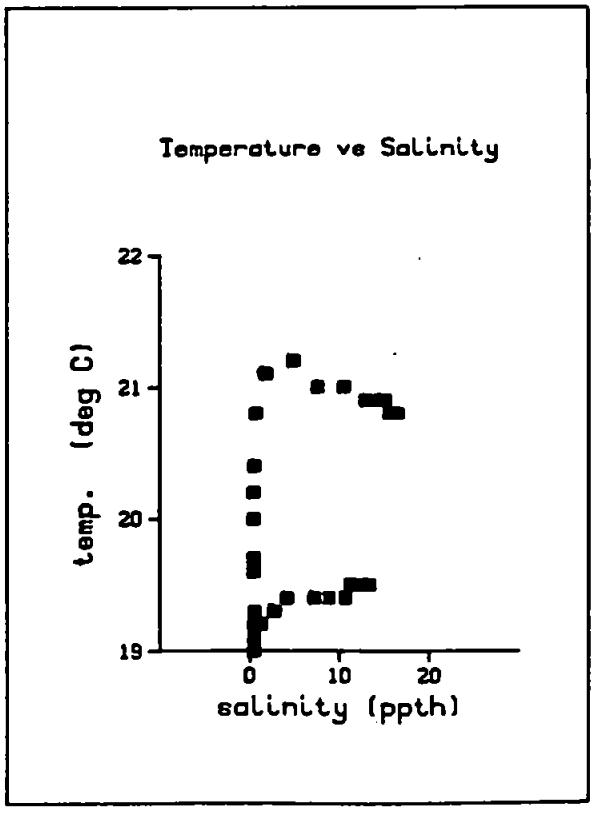

X16d

5th July 1989

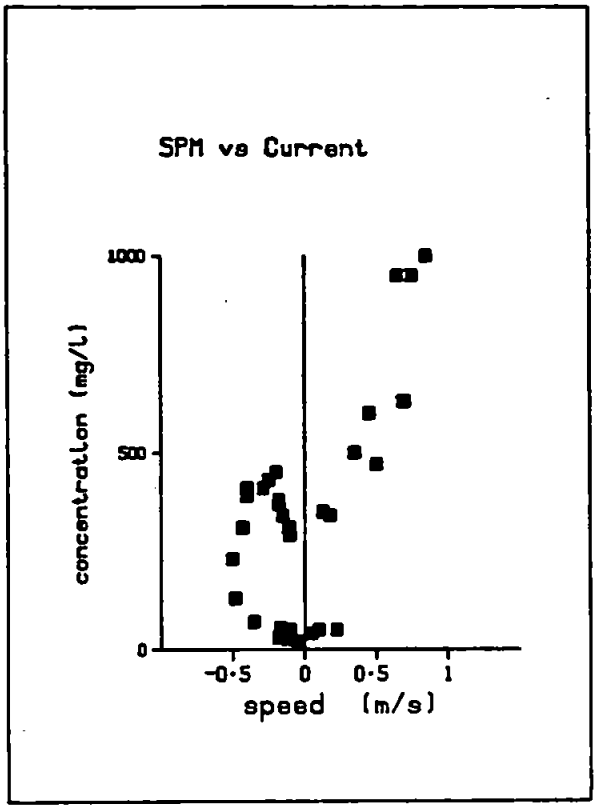

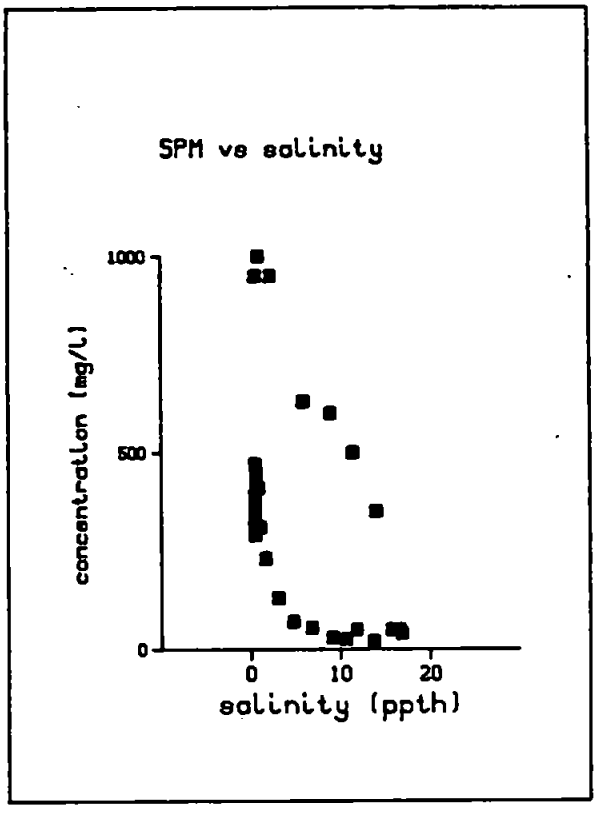

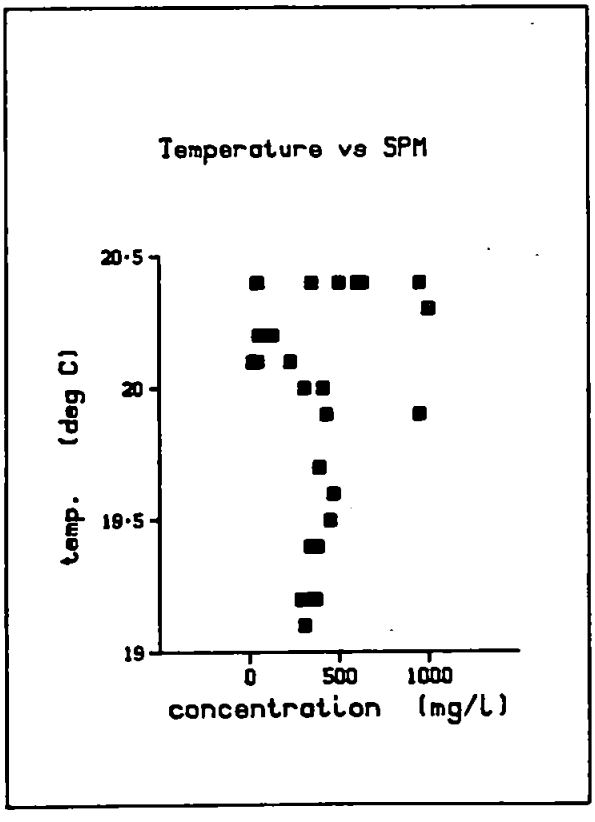

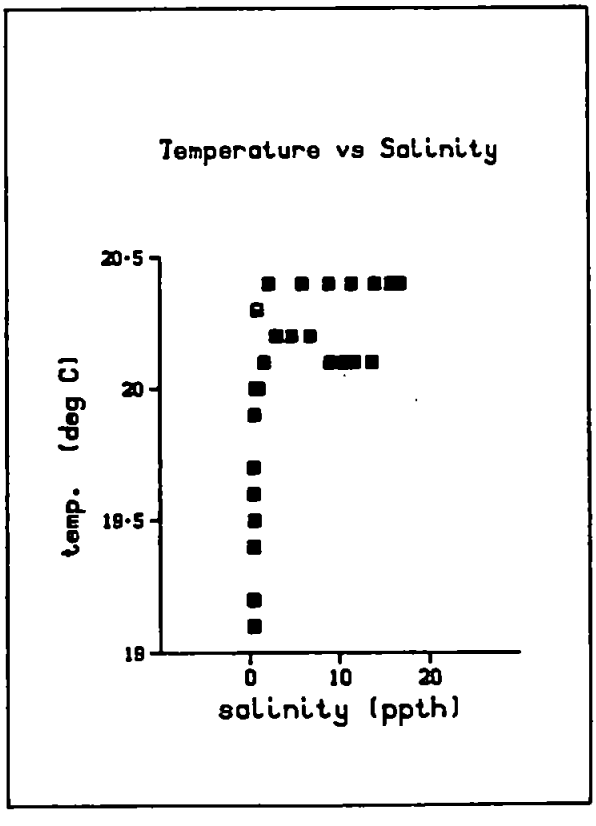

X17 Dissipation rates *e0*, *e3* against mean current, and $Z\%_A$.

In Fig. X17(a) log dissipation rates, *e0* and *e3*, are shown aginst the mean current, *U*, obtained from the same EM current meter record. Both *e0* (red), and *e3* (black) are plotted together. The upper plot uses data obtained on the ebb, and the lower plot uses flood data. Data from all four days is used.

Fig. X17(b) shows , in red, the percentage weight in bands 11 to 16, $Z\%_A$, against turbulent dissipation rate, ε. Also plotted, in green, are percentage weights $Z\%_p$, in the bands 1 to 10. NB $Z\%_p = 100\% - Z\%_A$. Upper plot uses ebb data, lower plot uses flood data. Data from all four days is used.

z%|e0

Ebb

%

log10 dissipation ε

Flood

%

x17b

e0,e3|U

Ebb

log10 diss.

U

Flood

x17a

X18 (a)-(c) Axial Profiles of R. Tamar.

Fig. X18(a) shows the results of surface observations of the upper Tamar at HW on the 5th July 1989. Sample stations are approximately evenly spaced along the estuary above Calstock.

Figs. X!8 (b) and (c) were obtained during the fieldwork of 1988 and result from use of the sizer at the surface. Observations on both days began at about half tide and continued over about three hours to arrive at Morwellham at HW. Only the weights in bands 1 (*≤5.8μm*) and 16 (*261.6-564.0μm*) are indicated. Total SPM concentration is shown by the black line.

X18a

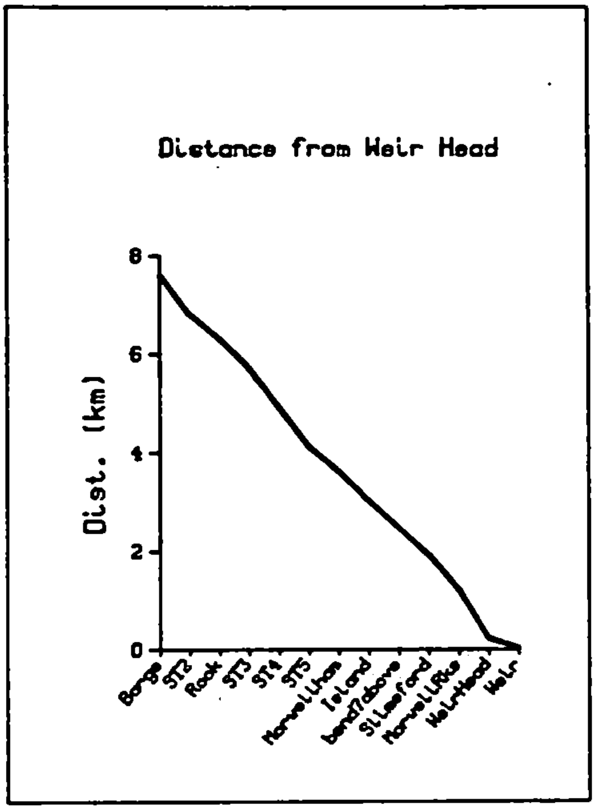
Distance from Weir Head
Dist. (km)
8
6
4
2
0
Barge
ST2
Rock
ST3
ST4
ST5
Island
Weir

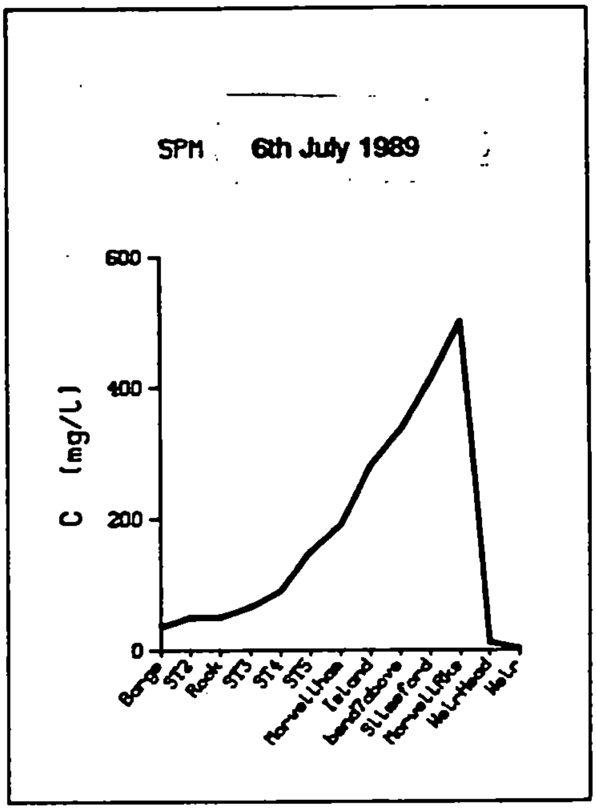
SPM 6th July 1989
C (mg/L)
600
400
200
0
Barge
ST2
Rock
ST3
ST4
ST5
Island
Weir

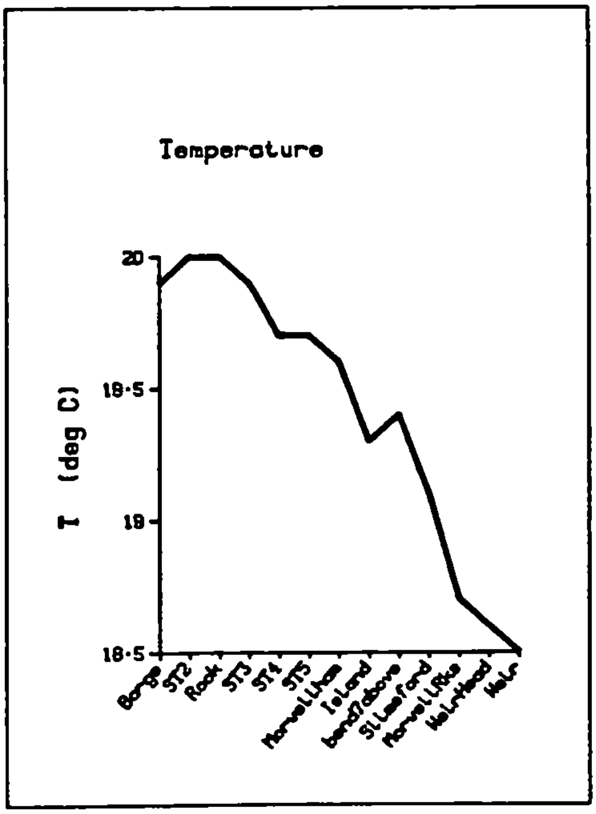
Temperature
T (deg C)
20
19.5
19
18.5
Barge
ST2
Rock
ST3
ST4
ST5
Island
Weir

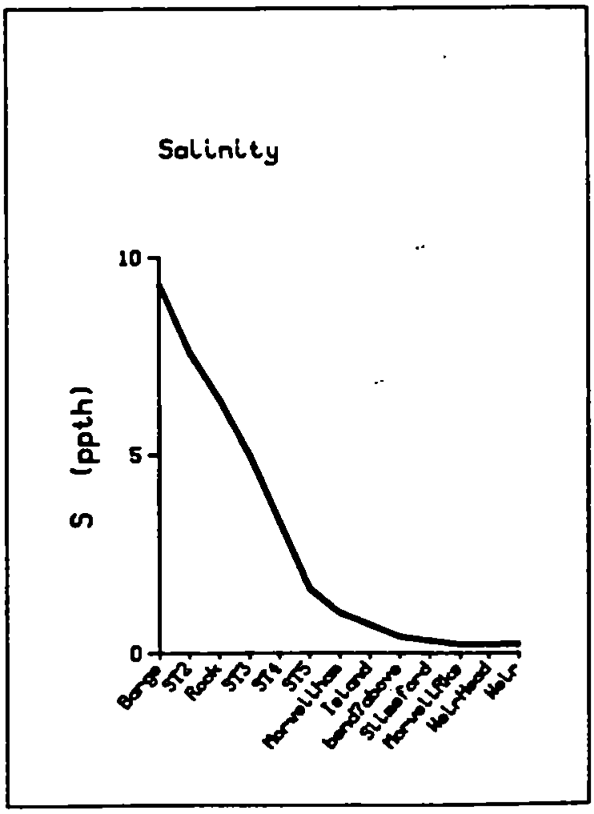
Salinity
S (ppth)
10
5
0
Barge
ST2
Rock
ST3
ST4
ST5
Island
Weir

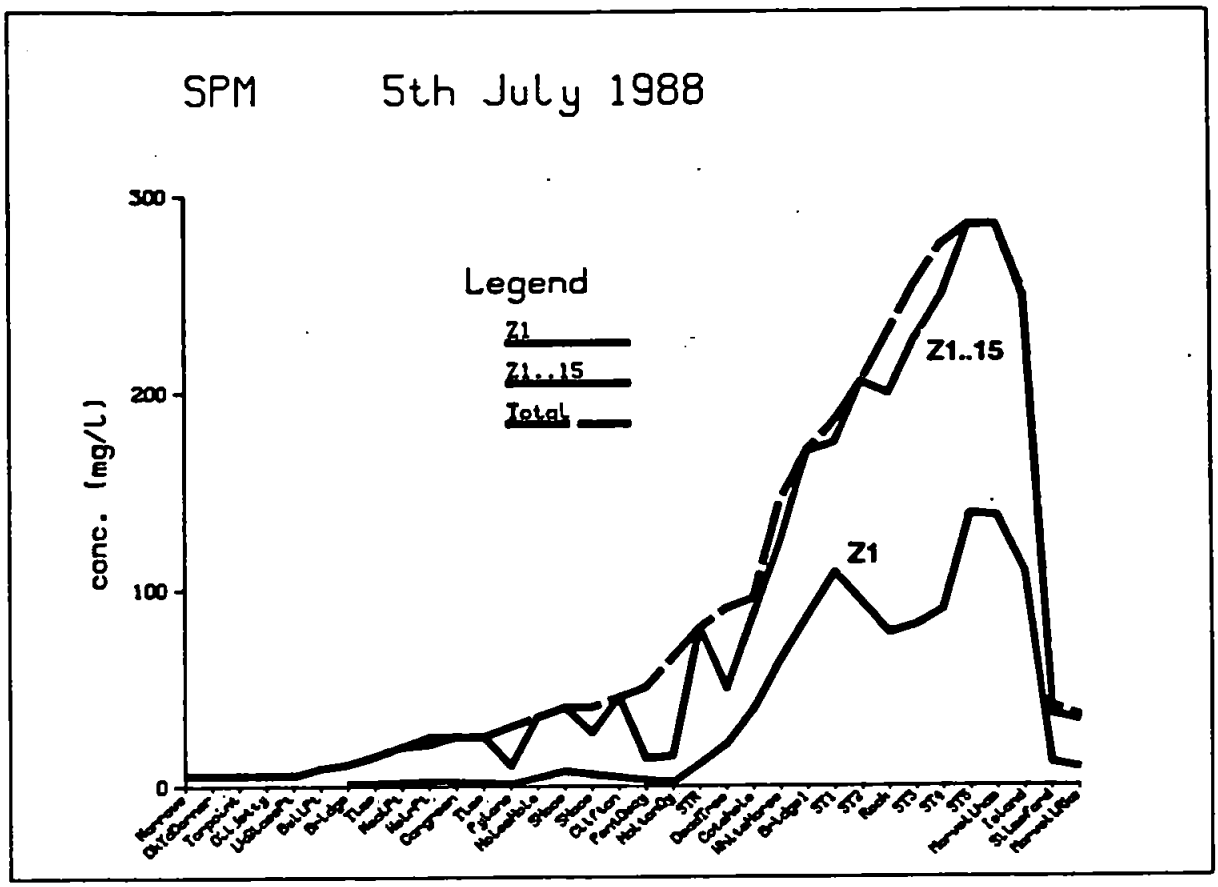
SPM 5th July 1988
conc. (mg/L)
300
200
100
0
Legend
Z1
Z1..15
Total
Z1..15
Z1

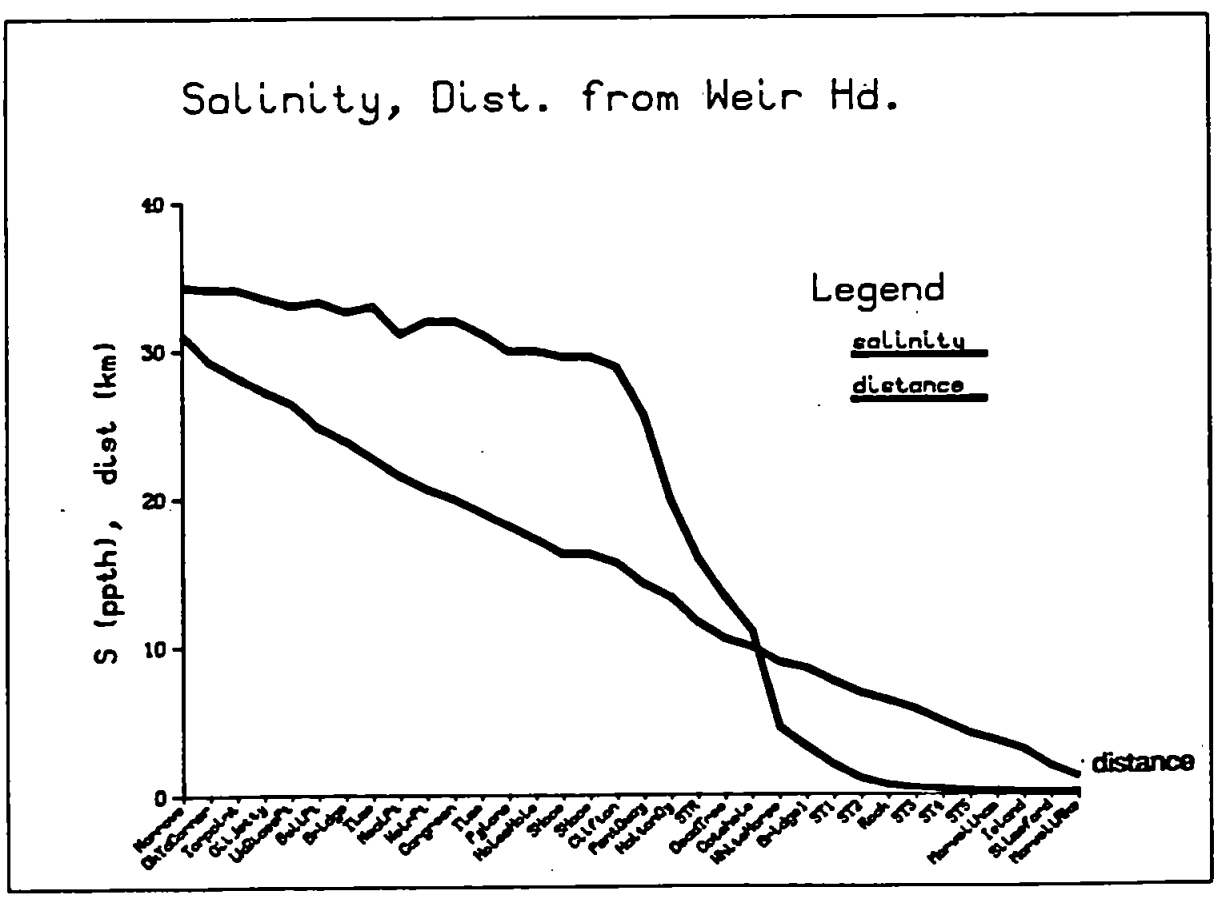
Salinity, Dist. from Weir Hd.
S (ppth), dist (km)
40
30
20
10
0
Legend
salinity
distance
distance

X18c

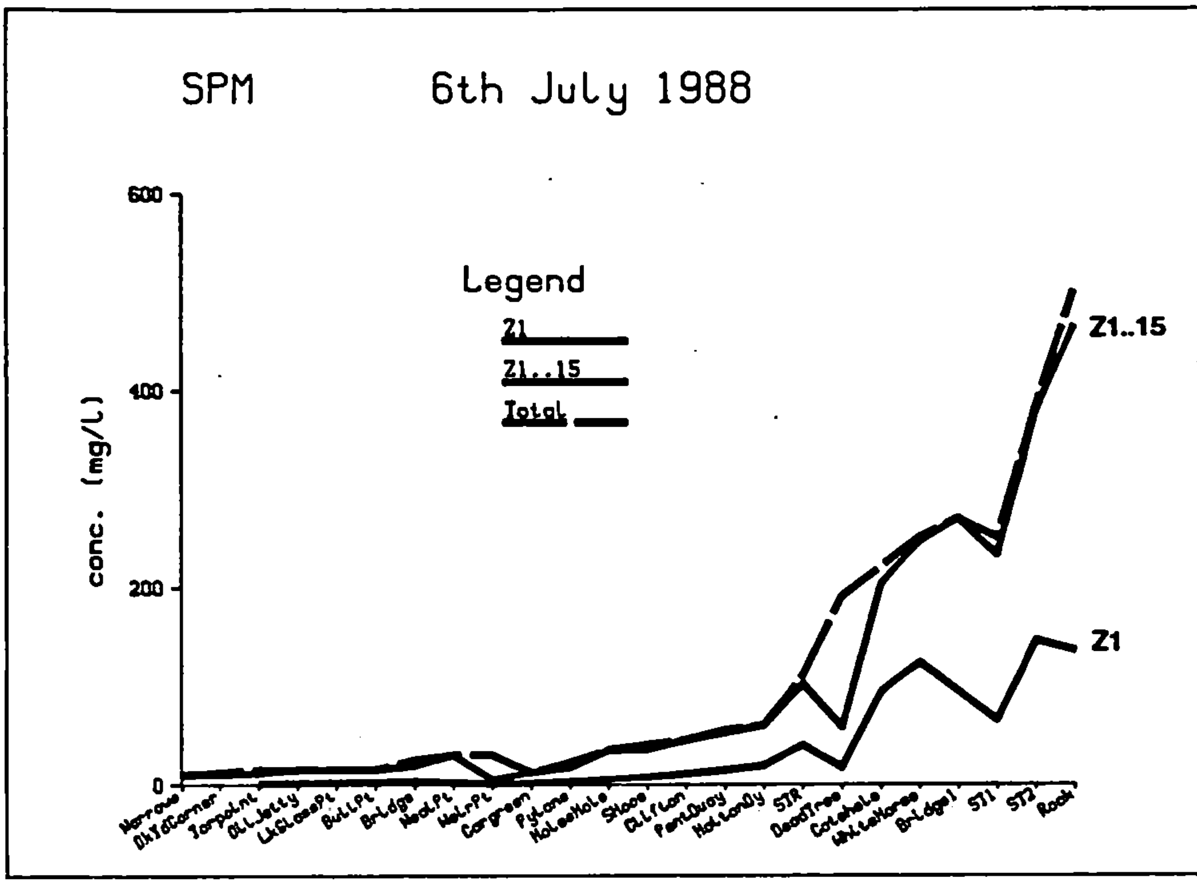
SPM 6th July 1988
Legend
Z1
Z1..15
Total
conc. (mg/L)
600
400
200
0
Z1..15
Z1
Narrows
OldCorner
Torpoint
OilJetty
LkGlassPt
BullPt
Bridge
NealPt
WeirPt
Cargreen
Pylons
HolesHole
SHoos
Clifton
PentQuay
HaltonQy
STR
DeadTree
Cotehele
WhiteHorse
Bridge1
ST1
ST2
Rock

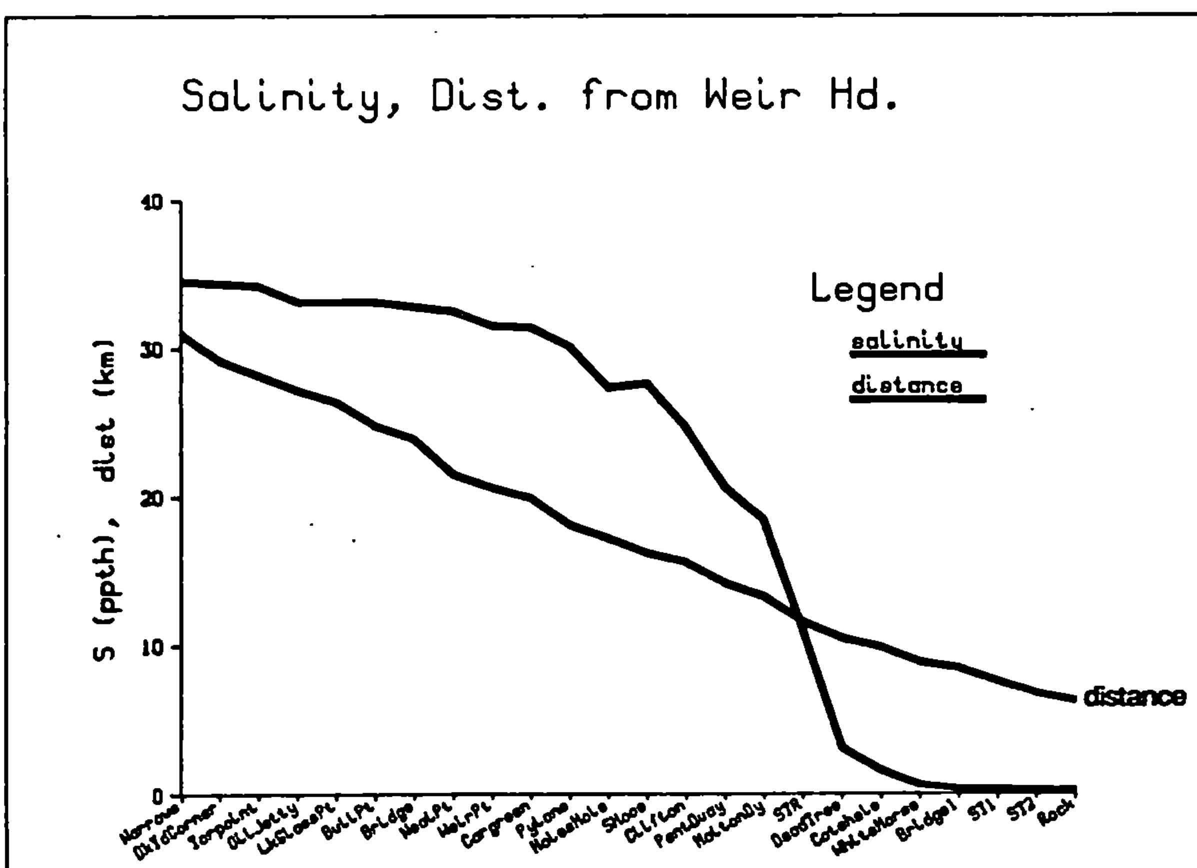
Salinity, Dist. from Weir Hd.
Legend
salinity
distance
S (ppth), dist (km)
40
30
20
10
0
distance
Narrows
OldCorner
Torpoint
OilJetty
LkGlassPt
BullPt
Bridge
NealPt
WeirPt
Cargreen
Pylons
HolesHole
SHoos
Clifton
PentQuay
HaltonQy
STR
DeadTree
Cotehele
WhiteHorse
Bridge1
ST1
ST2
Rock

X19 (a)-(e) Averaged Sizer Data.

For each of the periods described in Table 4.6 the time-averaged size distributions are shown. (Note that 'Max.Ebb' should precede 'TM.Ebb'.) Figure X19(e) compares the averaged size distributions for both flood and ebb turbidity maxima. Neap distibutions are plotted in blue, and spring distributions in red.

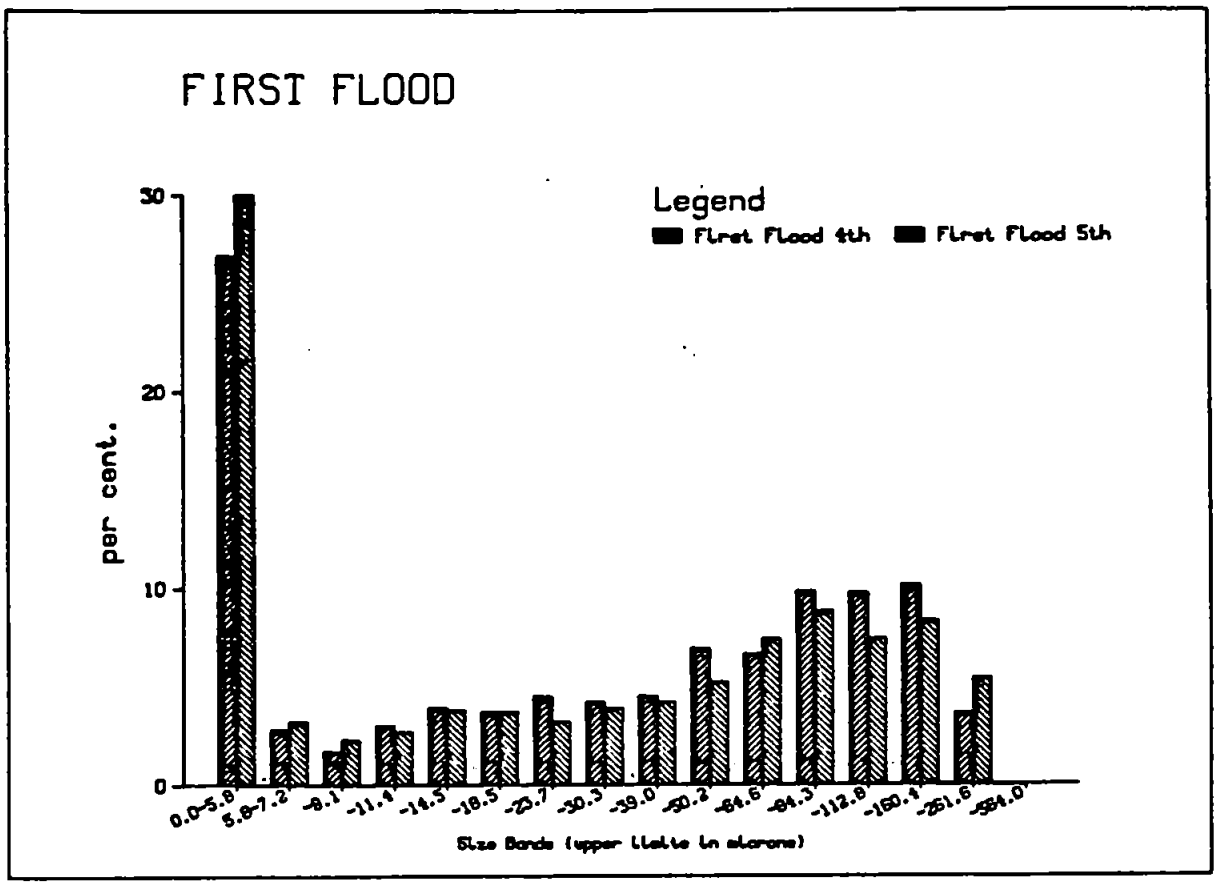
FIRST FLOOD
Legend
First Flood 4th
First Flood 5th
per cent.
30
20
10
0
0.0-5.8
5.8-7.2
-8.1
-11.4
-14.5
-18.5
-25.7
-30.3
-39.0
-50.2
-64.6
-84.3
-112.8
-160.4
-251.6
-584.0
Size Bands (upper limits in microns)

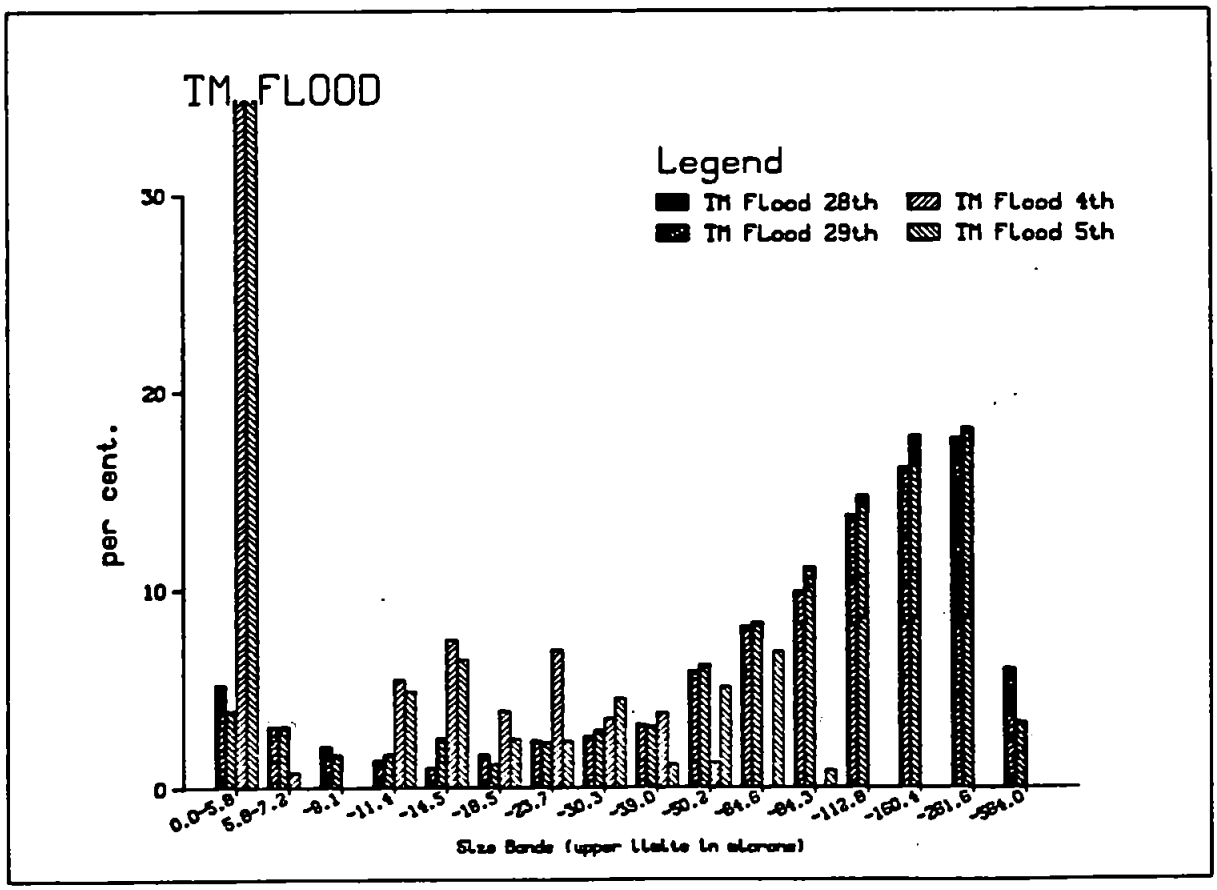
TM FLOOD
Legend
TM Flood 28th
TM Flood 29th
TM Flood 4th
TM Flood 5th
per cent.
30
20
10
0
0.0-5.8
5.8-7.2
-8.1
-11.4
-14.5
-18.5
-25.7
-30.3
-39.0
-50.2
-64.6
-84.3
-112.8
-160.4
-251.6
-584.0
Size Bands (upper limits in microns)

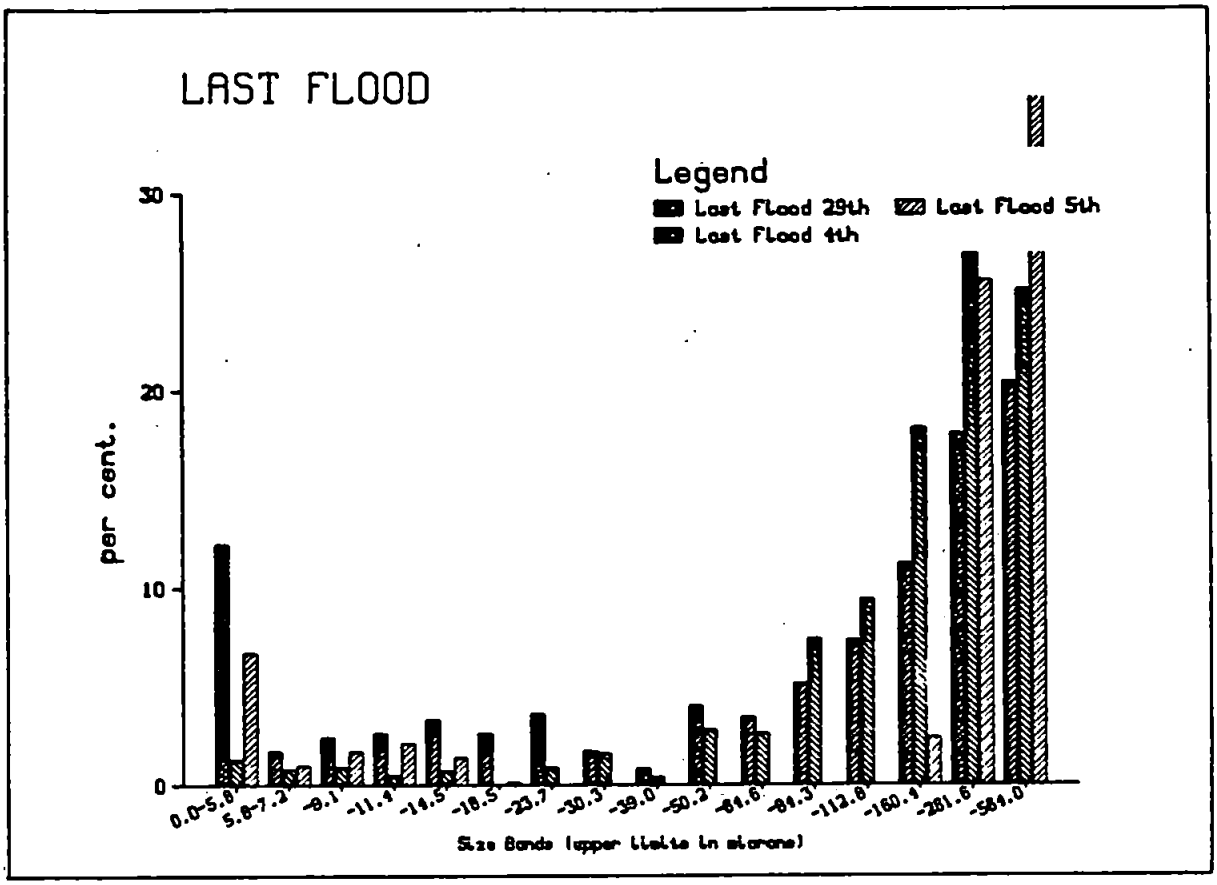
LAST FLOOD
Legend
Last Flood 29th
Last Flood 5th
Last Flood 4th
per cent.
30
20
10
0
0.0-5.8
5.8-7.2
-8.1
-11.4
-14.5
-18.5
-23.7
-30.3
-39.0
-50.2
-64.6
-84.3
-112.8
-160.4
-281.6
-584.0
Size Bands (upper limits in microns)

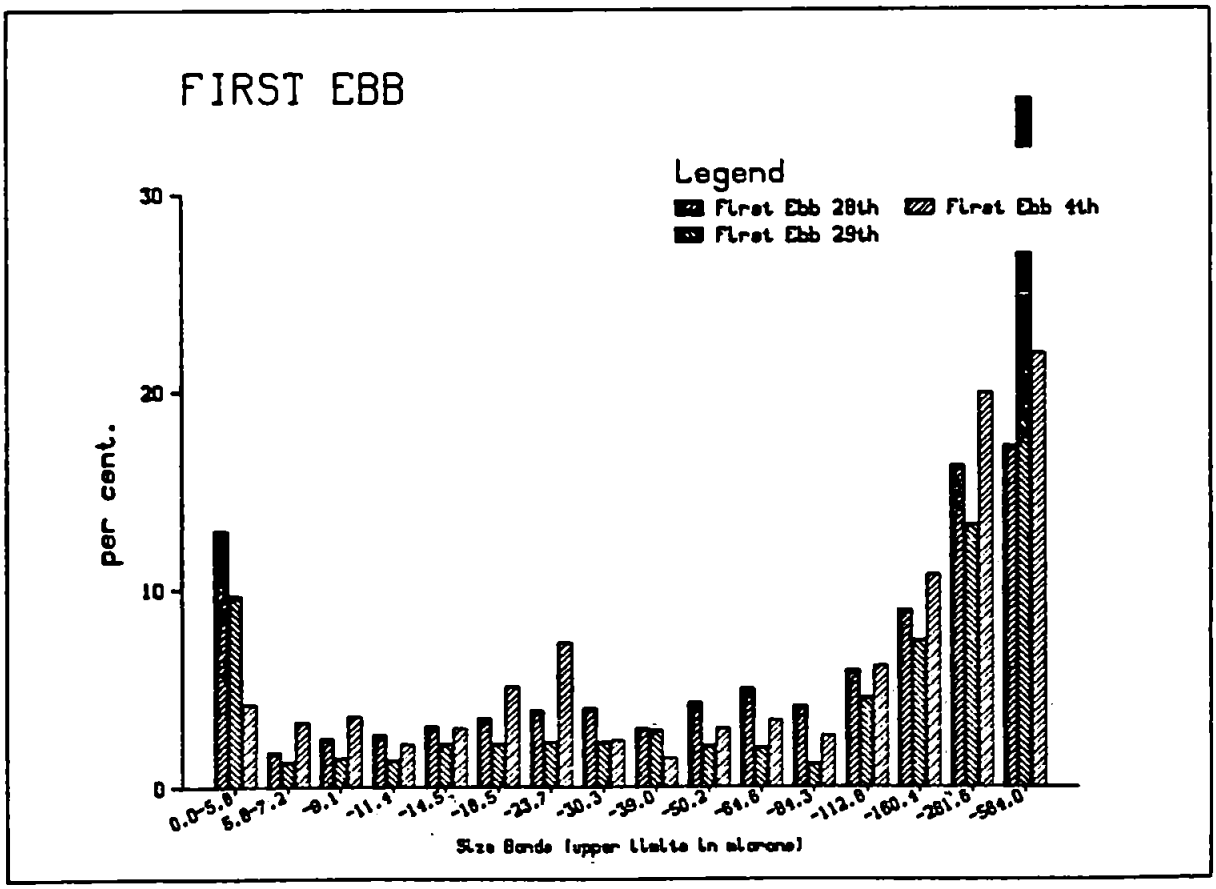
FIRST EBB
Legend
First Ebb 28th
First Ebb 4th
First Ebb 29th
per cent.
30
20
10
0
0.0-5.8
5.8-7.2
-8.1
-11.4
-14.5
-18.5
-23.7
-30.3
-39.0
-50.2
-64.6
-84.3
-112.8
-160.4
-281.6
-584.0
Size Bands (upper limits in microns)

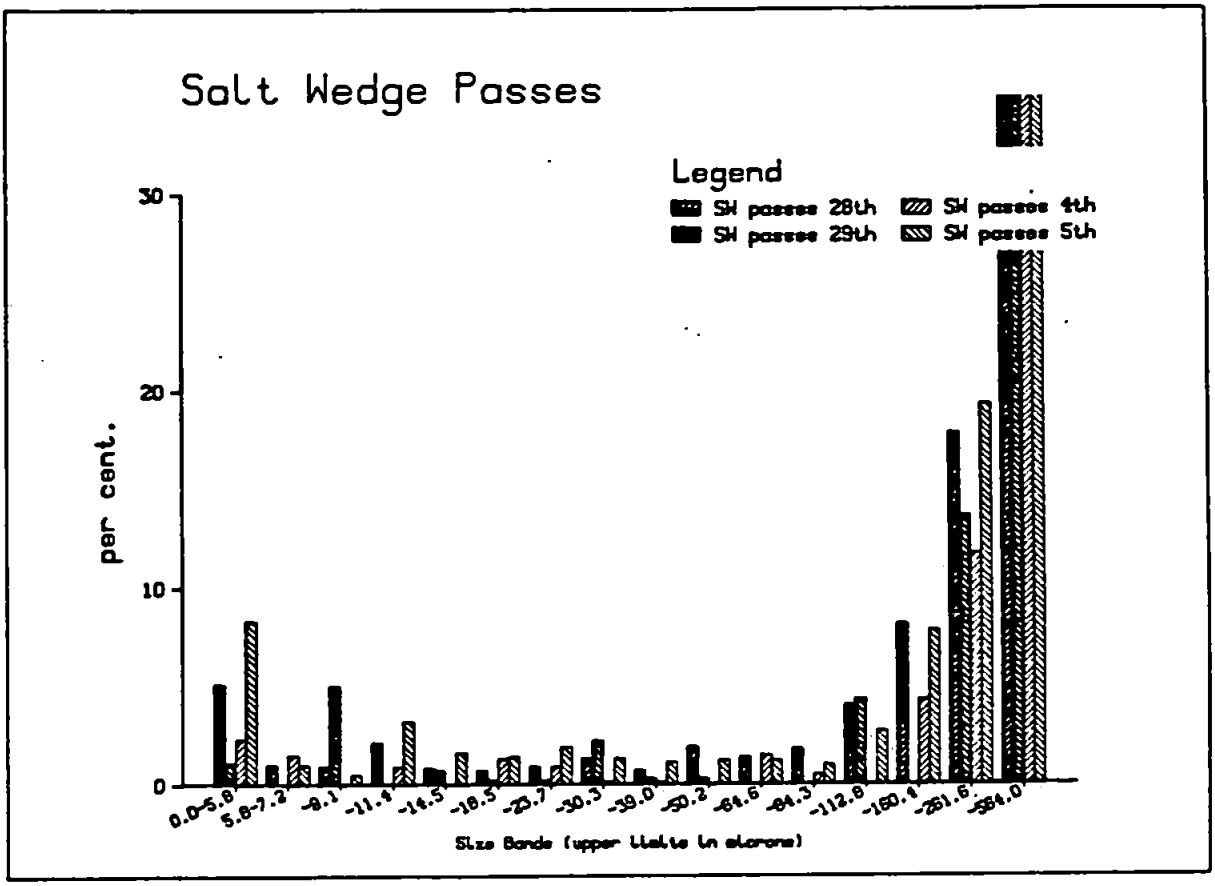
Salt Wedge Passes
Legend
SW passes 28th
SW passes 4th
SW passes 29th
SW passes 5th
30
20
10
0
per cent.
0.0-5.8
5.8-7.2
-8.1
-11.4
-14.5
-18.5
-25.7
-30.3
-39.0
-50.2
-64.6
-84.3
-112.8
-160.4
-261.6
-564.0
Size Bands (upper limits in microns)

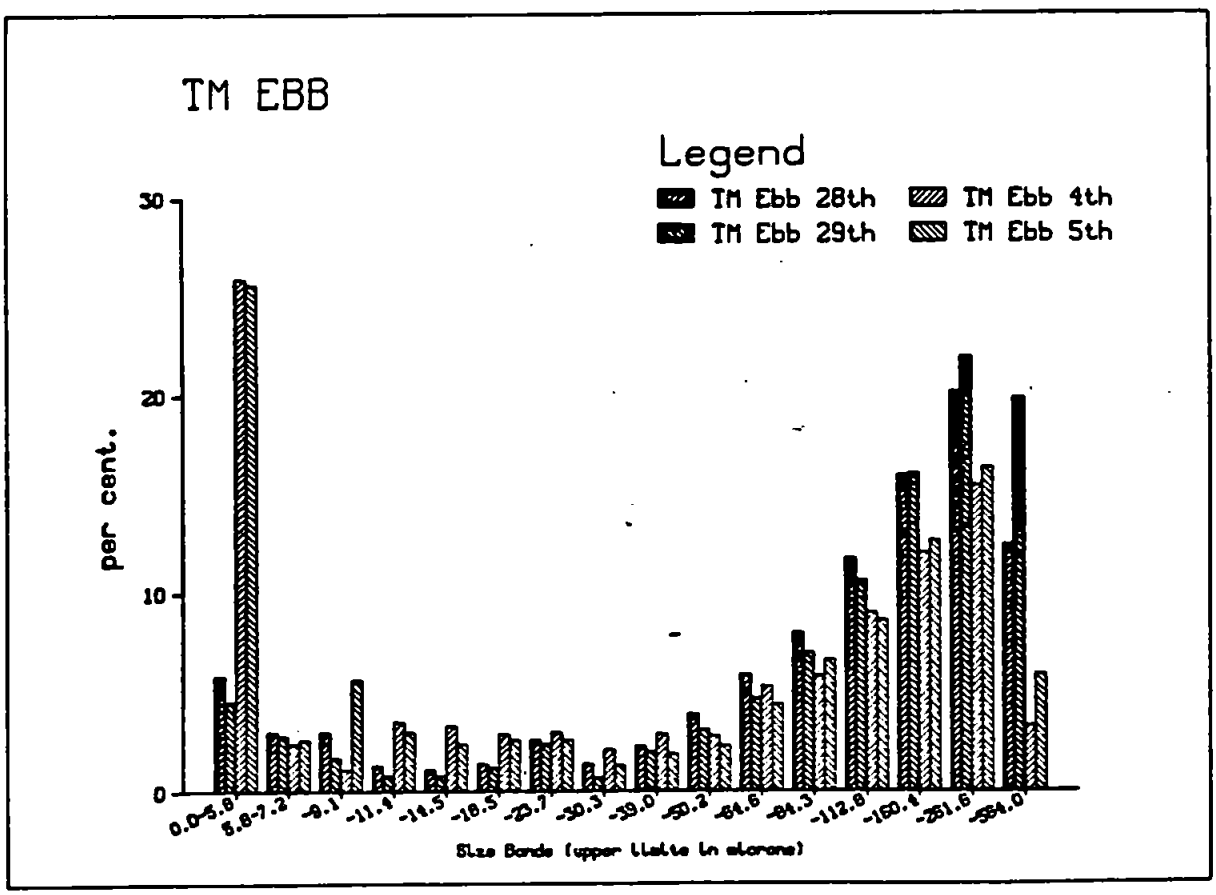
TM EBB
Legend
TM Ebb 28th
TM Ebb 4th
TM Ebb 29th
TM Ebb 5th
30
20
10
0
per cent.
0.0-5.8
5.8-7.2
-8.1
-11.4
-14.5
-18.5
-25.7
-30.3
-39.0
-50.2
-64.6
-84.3
-112.8
-160.4
-261.6
-564.0
Size Bands (upper limits in microns)

X19d

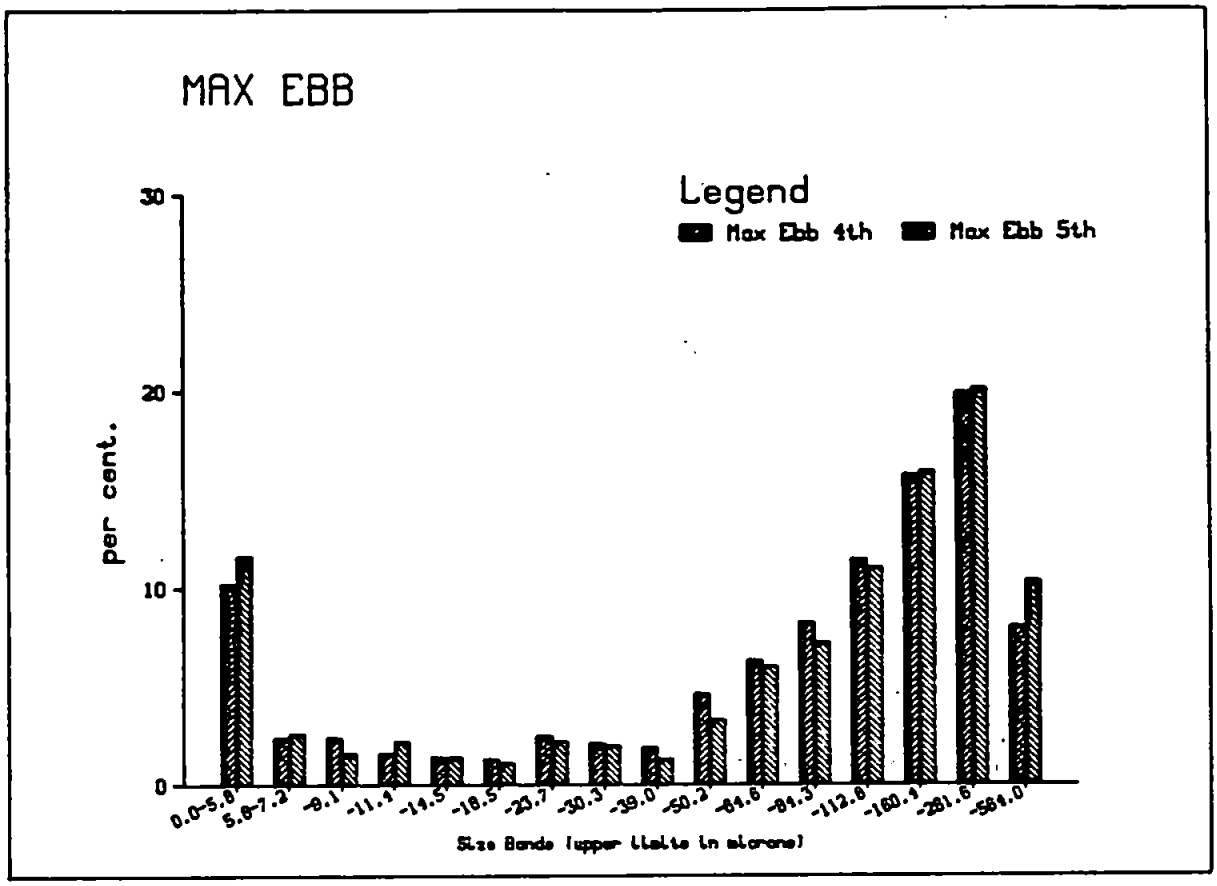
MAX EBB
Legend
Max Ebb 4th
Max Ebb 5th
per cent.
30
20
10
0
0.0-5.8
5.8-7.2
-9.1
-11.1
-14.5
-18.5
-23.7
-30.3
-39.0
-50.2
-64.6
-81.3
-112.8
-160.1
-281.6
-584.0
Size Bands (upper limits in microns)

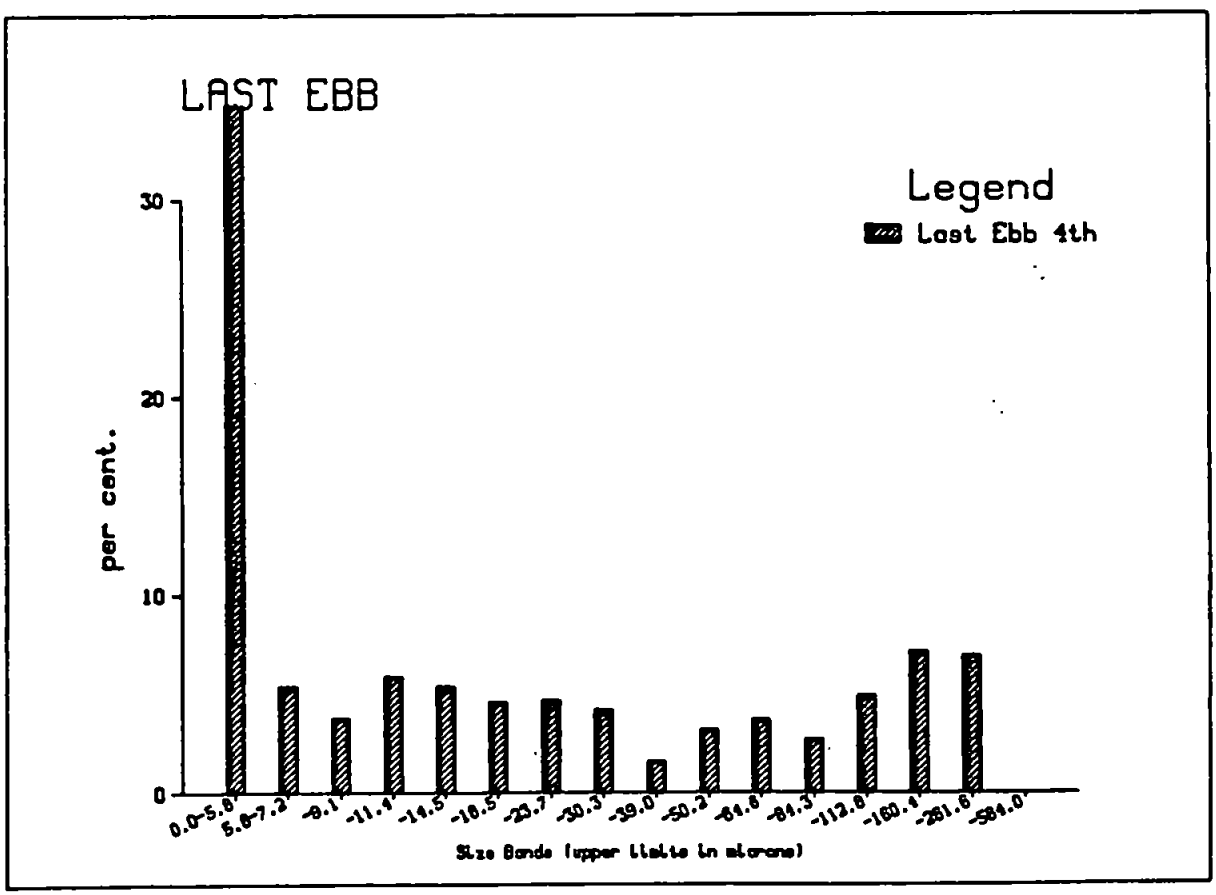
LAST EBB
Legend
Last Ebb 4th
per cent.
30
20
10
0
0.0-5.8
5.8-7.2
-9.1
-11.1
-14.5
-18.5
-23.7
-30.3
-39.0
-50.2
-64.6
-81.3
-112.8
-160.1
-281.6
-584.0
Size Bands (upper limits in microns)

X19e

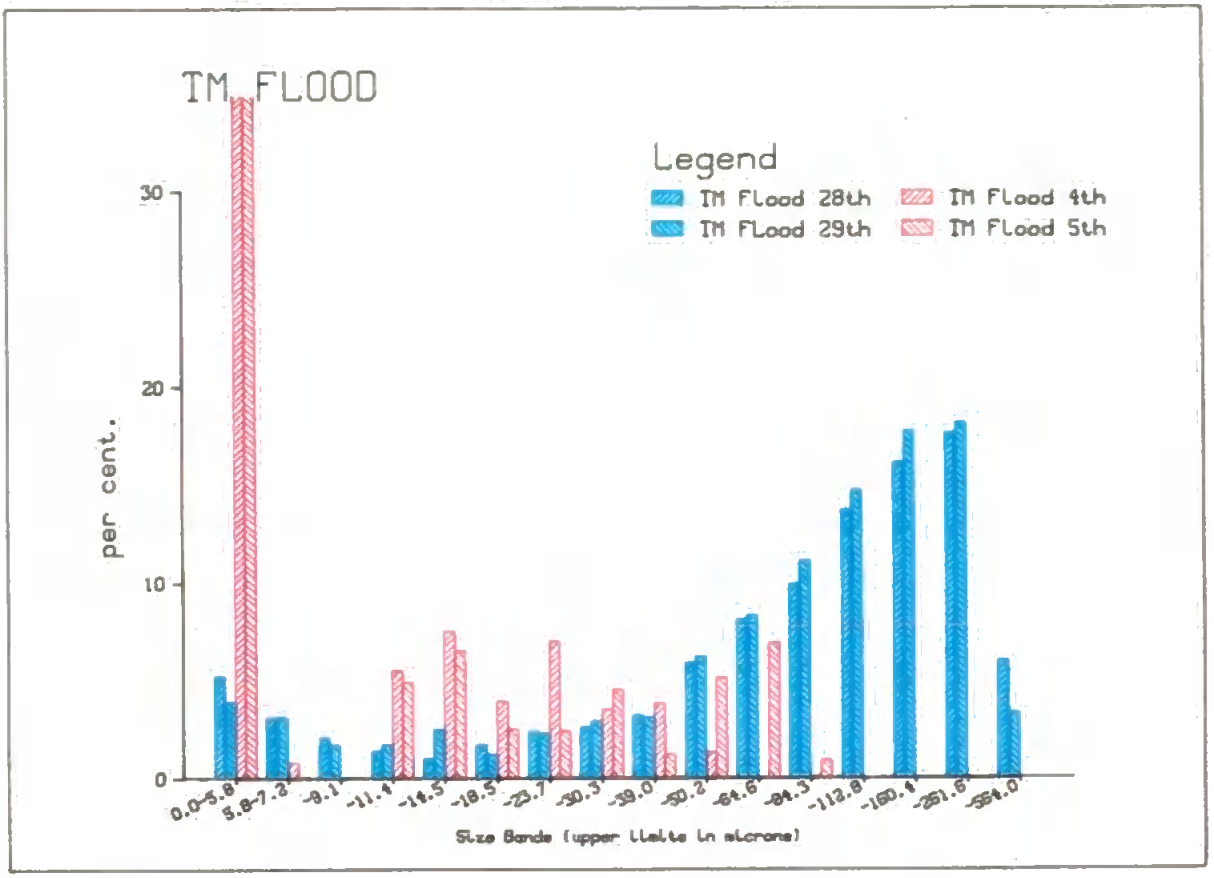
TM FLOOD
Legend
TM Flood 28th
TM Flood 29th
TM Flood 4th
TM Flood 5th
per cent.
30
20
10
0
0.0-5.8
5.8-7.2
-8.1
-11.4
-14.5
-18.5
-23.7
-30.3
-39.0
-50.2
-64.6
-84.3
-112.8
-160.4
-251.6
-564.0
Size Bands (upper limits in microns)

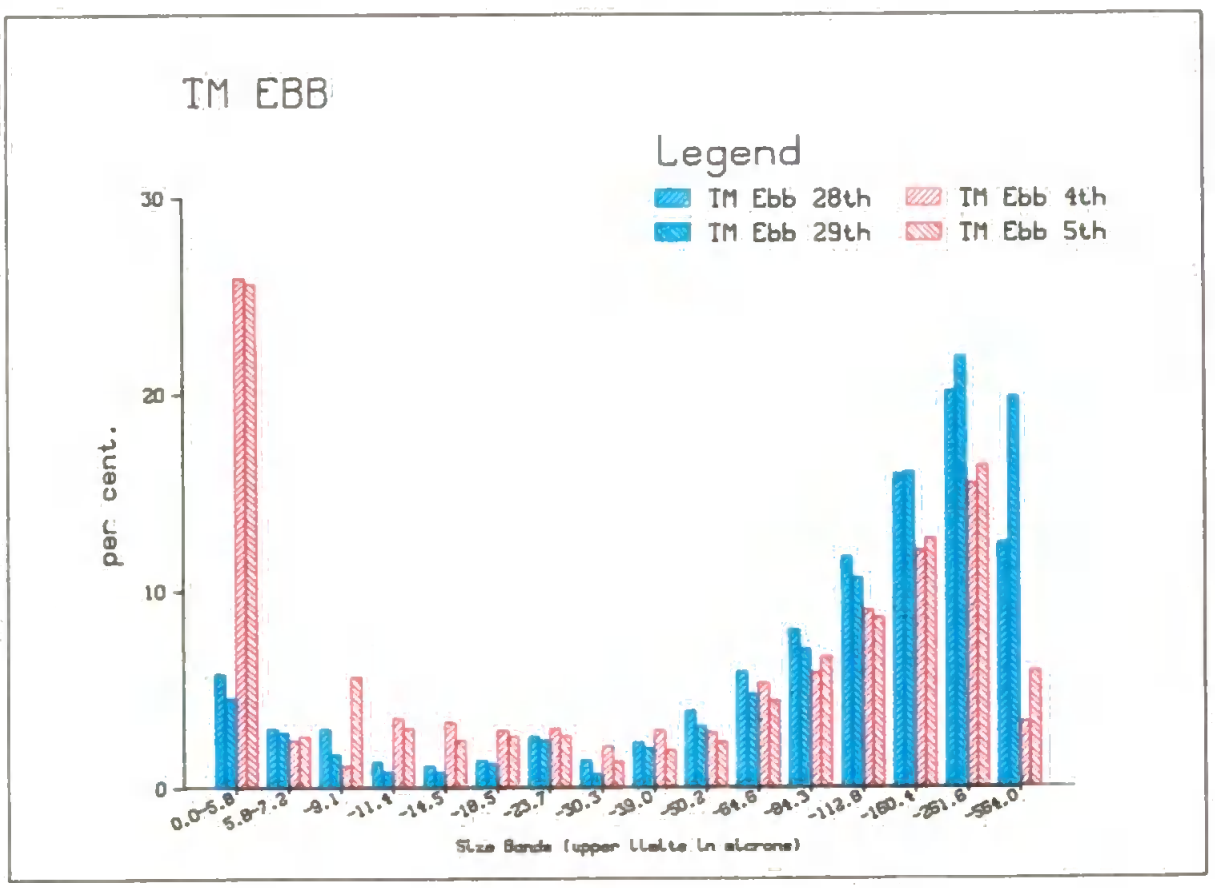
TM EBB
Legend
TM Ebb 28th
TM Ebb 29th
TM Ebb 4th
TM Ebb 5th
per cent.
30
20
10
0
0.0-5.8
5.8-7.2
-8.1
-11.4
-14.5
-18.5
-23.7
-30.3
-39.0
-50.2
-64.6
-84.3
-112.8
-160.4
-251.6
-564.0
Size Bands (upper limits in microns)

X20 Salt Wedge Settling Model.

Output from the computer model described in 4C2.6 is shown. Different sized particles are tracked as they settle through a two layer flow. The vertical grid axis is height above the bed in metres, the horizontal axis is distance upstream of the sampling station that the particles were released. The subsequent motion of the particles is plotted at one tenth of the vertical and horizontal scales respectively (to avoid clutter).

Particles tracked for 3hrs at 3min intervals
Largest particle at right of 'fan'
Tracking stops on reaching bed
or passing downstream

X20
SW settling

Settling velocities for

d= 50, 100, 200, 500, 1000 um

Tracks reduced by factor of 10

Salt tip at 3000.0(m) at t=0

Upper layer speed 40.0 (cm/s)

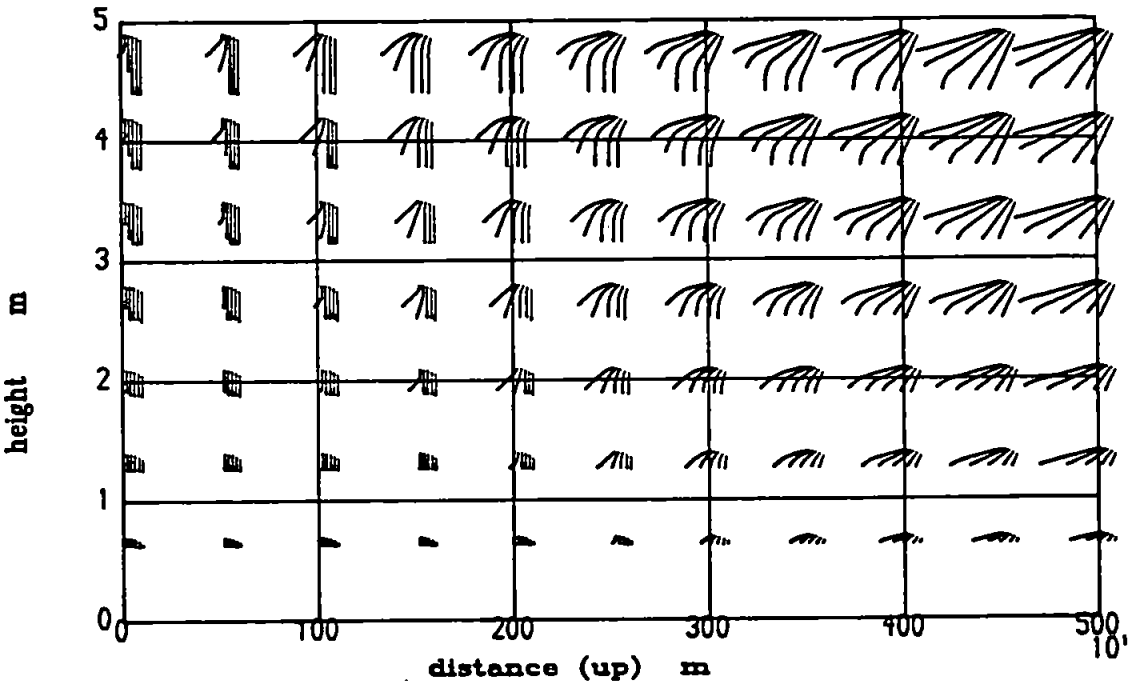

X21 (Fig. 3.9) Examples of Data Time Series.

Output from program *Tamar* is shown. The mean value, over the total record length of just under six minutes, is given beneath each component label. data is plotted as deviations from the mean value. The horizontal scale for velocities, concentrations and temperatures is marked with ticks at 10 cm/s, 10 mg/l, 0.05°C respectively. The time axis (downwards) is marked at one minute intervals. *U-bar* indicates the mean current.

Wavenumber spectra for each of the time series are plotted on logarithmic axes such that a '-5/3' slope is parallel to the diagonal. For each velocity plot the lower left corner is k=0.01 [cm^{-1}], $E(k)$=10^{-4} [cm^2/s^2] and the upper right corner is k=10, E=10.

Run G18 began at 1900 on 29th June during the ebb turbidity maximum. Run D04 began at 1700 on 5th July just before the flood turbidity maximum.

X21a
Fig 3.9

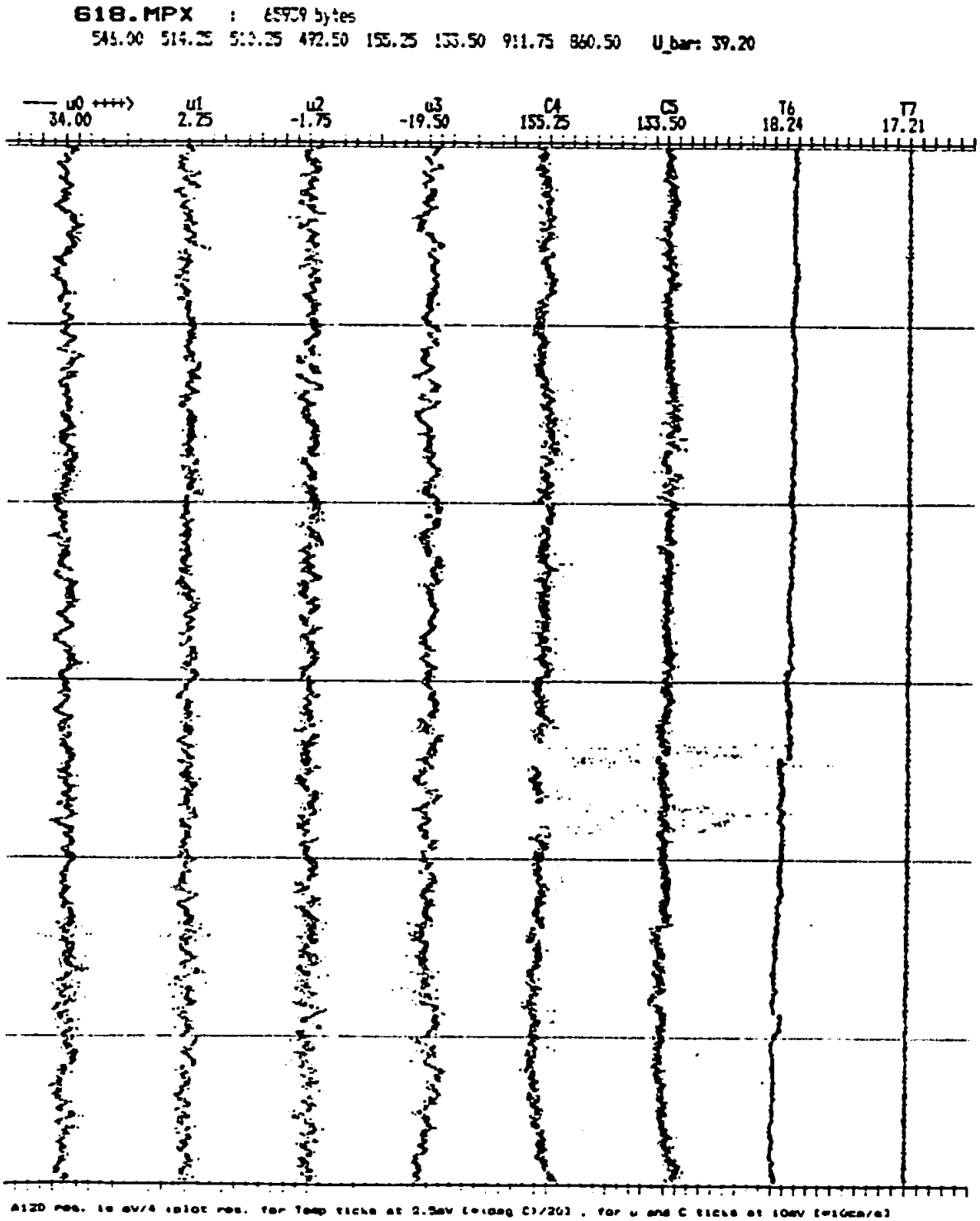
618.MPX : 65939 bytes
545.00 514.25 513.25 492.50 155.25 133.50 911.75 860.50 U_bar: 39.20
u0 <<<<
34.00
u1
2.25
u2
-1.75
u3
-19.50
C4
155.25
C5
133.50
T6
18.24
T7
17.21

X21b

G18.

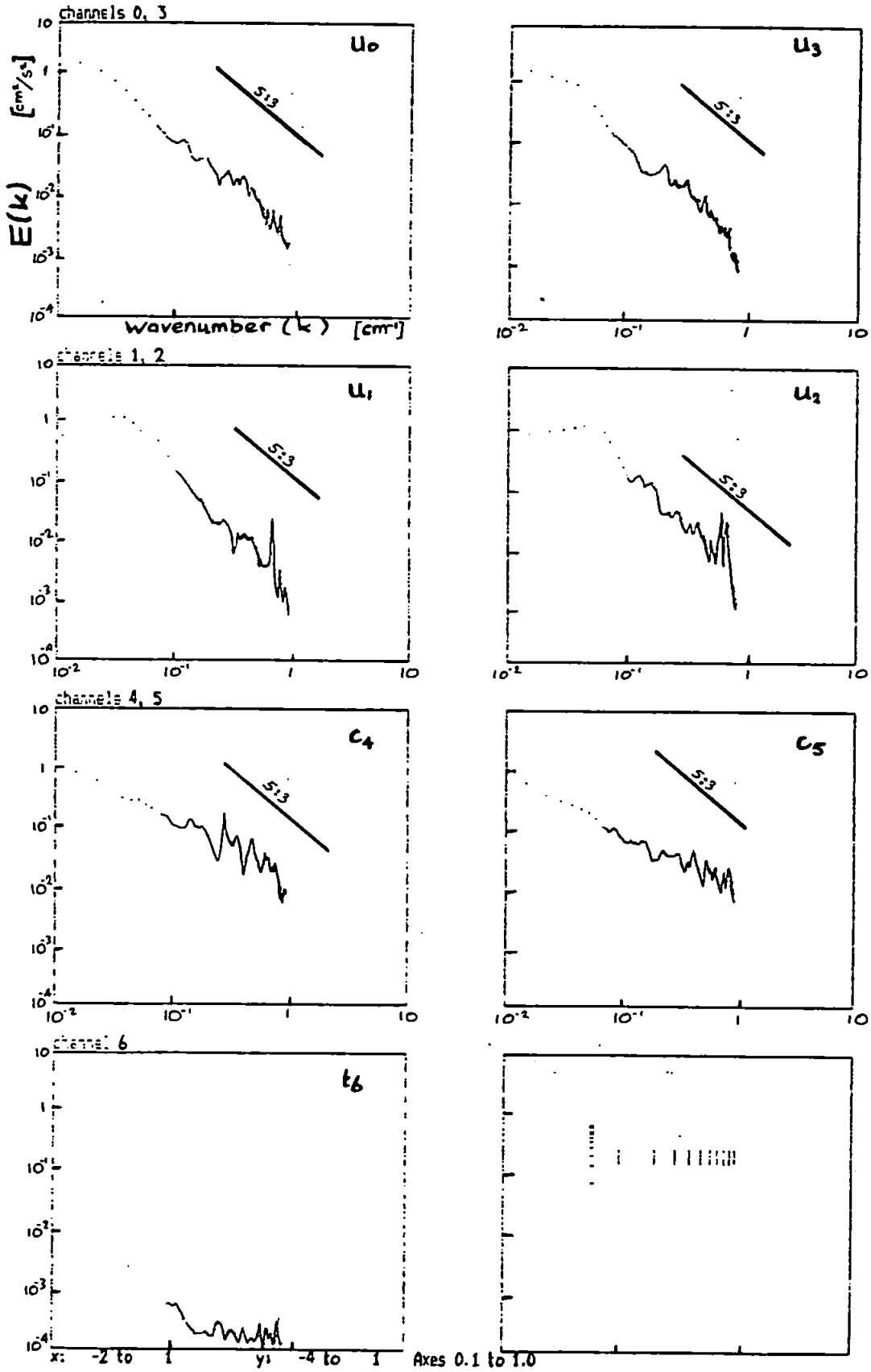
channels 0, 3
u_0
u_3
E(k) [cm²/s²]
Wavenumber (k) [cm⁻¹]
5/3
channels 1, 2
u_1
u_2
channels 4, 5
c_4
c_5
channel 6
t_6
x: -2 to 1
y: -4 to 1
Axes 0.1 to 1.0

X21c

1700

DO4.MPX : 65939 bytes

578.75 512.75 507.75 473.25 740.25 706.75 1005.50 860.50 U_bar: 77.18

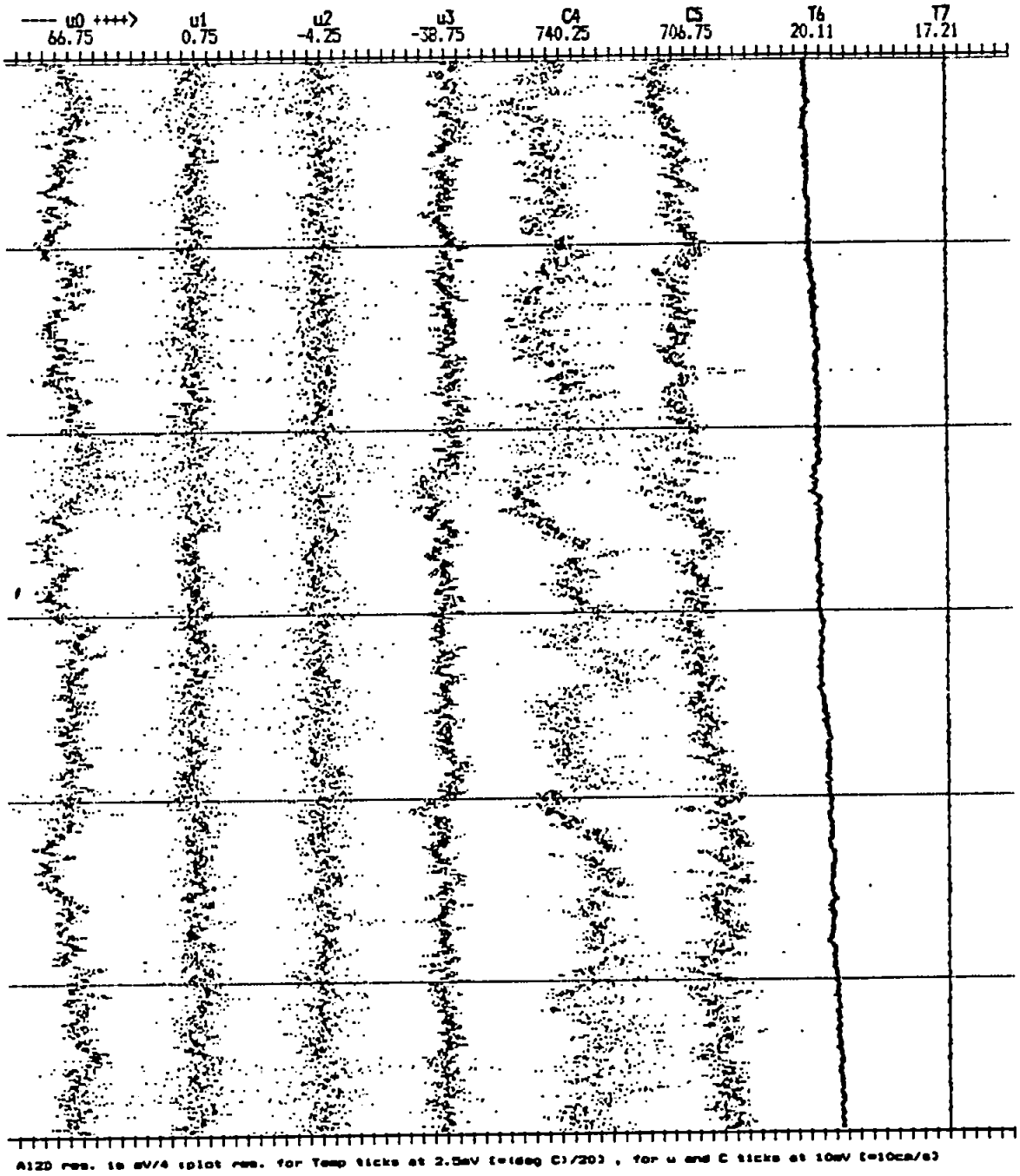

A12D res. is mV/4 splot res. for Temp ticks at 2.5mV (=(deg C)/20) , for u and C ticks at 10mV (=10cm/s)

D04.

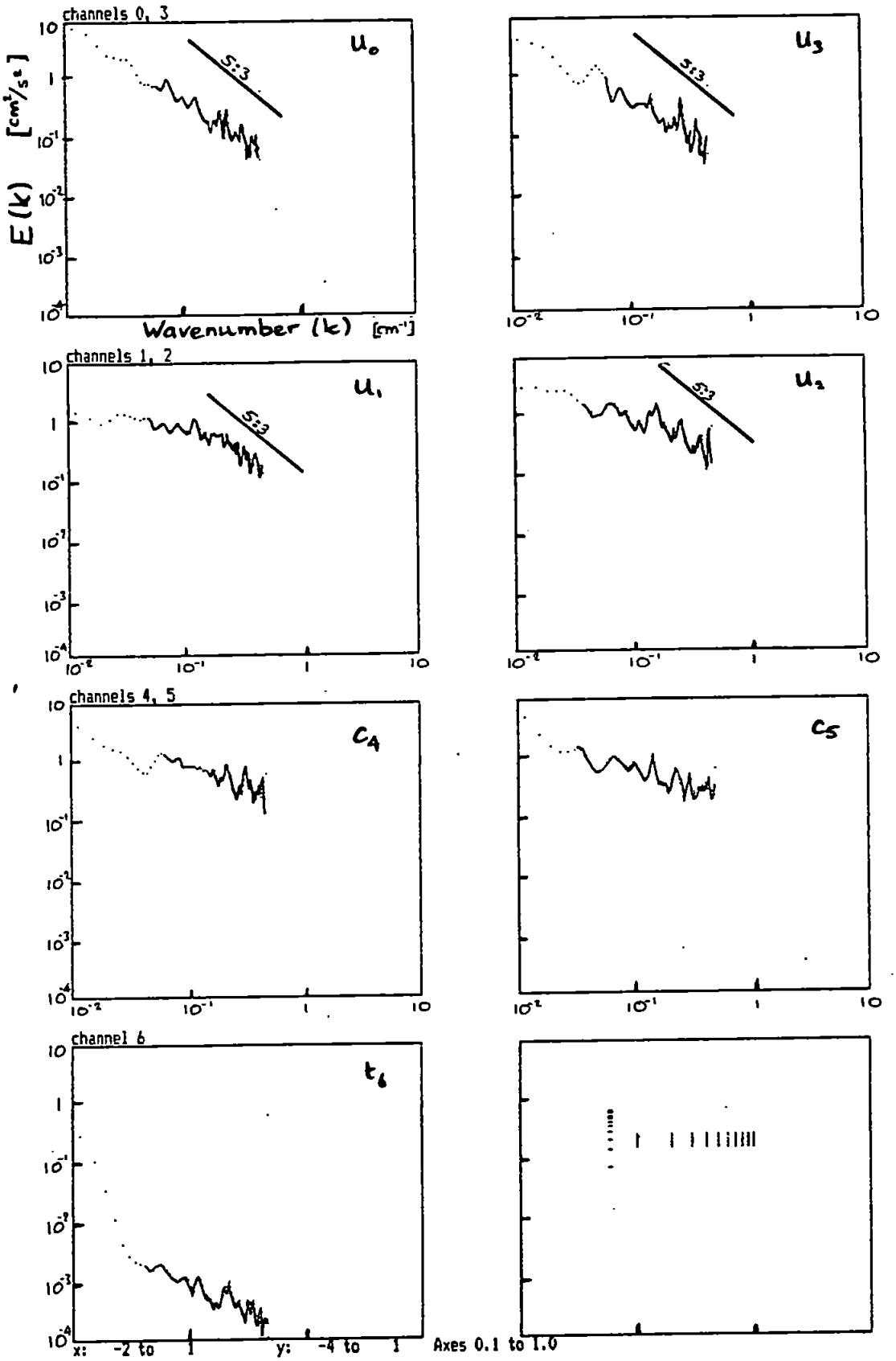
channels 0, 3
u_0
u_3
S:3
E(k) [cm²/s²]
Wavenumber (k) [cm⁻¹]
channels 1, 2
u_1
u_2
channels 4, 5
c_4
c_5
channel 6
t_6
x: -2 to 1
y: -4 to 1
Axes 0.1 to 1.0

June28 <corrected 24/6/91, 18/7/91>

time	run	U	a	e0	e3	m1	m2	e1	e2	c4	c5	f4	f5	temp
1035	W06	46.7	48	-9.0	-9.0	1.8	-5.3	-9.0	-9.0	-10	-10	-9.0	-9.0	17.92
1041	W07	47.3	48	-9.0	-9.0	-6.0	-5.5	-9.0	-9.0	-10	-10	-9.0	-9.0	18.00
1050	W08	46.6	48	-9.0	-9.0	-1.0	-1.3	-9.0	-9.0	-10	-10	-9.0	-9.0	18.11
1100	W09	42.4	49	-9.0	-9.0	2.8	-2.3	-9.0	-9.0	-10	-10	-9.0	-9.0	18.25
1110	W10	41.2	48	-9.0	-9.0	0.3	-1.3	-9.0	-9.0	-10	-10	-9.0	-9.0	18.44
1120	W11	40.1	51	-9.0	-9.0	6.0	-3.0	-9.0	-9.0	-10	-10	-9.0	-9.0	18.50
1140	W12	30.8	45	-9.0	-9.0	4.5	-1.5	-9.0	-9.0	-10	-10	-9.0	-9.0	18.68
1200	W13	24.5	40	-9.0	-9.0	-0.3	-2.5	-9.0	-9.0	-10	-10	-9.0	-9.0	18.89
1223	W14	14.5	44	-9.0	-9.0	2.0	-1.8	-9.0	-9.0	-10	-10	-9.0	-9.0	18.89
1240	W15	8.8	-9	-9.0	-9.0	-9.0	-9.0	-9.0	-9.0	-10	-10	-9.0	-9.0	-9.00
1500	V00	-3.8	53	-0.1	-9.0	-0.7	1.0	-9.0	-9.0	60	190	-9.0	-9.0	18.94
1510	V01	-3.0	76	0.1	0.4	-1.7	0.4	-9.0	-9.0	60	190	-9.0	-9.0	18.94
1520	V02	-5.3	85	-0.2	0.0	-1.6	0.8	-9.0	-9.0	60	190	-9.0	-9.0	18.95
1530	V03	-5.4	79	-0.3	0.1	-1.3	1.1	-9.0	-9.0	60	190	-9.0	-9.0	18.93
1540	V04	-6.5	40	-0.2	0.5	-1.1	0.3	-9.0	-9.0	70	200	-9.0	-9.0	18.92
1600	V05	-12.1	57	-0.6	-0.1	-0.9	-0.1	-9.0	-9.0	70	200	1.9	1.8	18.91
1619	V06	-13.9	63	-0.6	0.2	-1.4	-0.2	0.2	1.1	70	200	2.7	2.7	18.83
1627	V07	-15.6	58	-0.6	0.1	-1.9	-0.7	-9.0	-9.0	70	200	-9.0	-9.0	-9.00
1633	V08	-14.8	53	-0.4	0.4	-1.9	-0.6	-9.0	-9.0	70	200	3.1	3.0	18.78
1639	V09	-15.0	54	-0.1	1.1	-1.9	-1.0	-0.2	1.9	70	200	3.1	3.0	18.74
1645	V10	-15.5	52	-0.3	0.8	-2.2	-1.5	-0.3	1.7	70	200	3.1	4.0	18.69
1652	V11	-14.3	51	-0.1	0.8	-2.2	-1.2	-0.3	1.8	70	200	3.0	3.0	18.66
1700	V12	-15.0	58	-0.1	0.7	-1.3	-0.1	-0.1	2.1	80	210	3.2	3.1	18.61
1707	V13	-16.3	56	0.1	1.1	-1.4	-0.5	0.0	2.3	80	210	3.1	3.1	18.55
1714	V14	-21.0	46	1.4	2.4	-1.4	-1.1	1.8	3.2	90	210	3.1	2.9	18.40
1720	V15	-27.8	44	2.4	3.0	-1.3	-1.9	2.6	3.5	110	230	3.3	3.1	18.20
1727	V16	-38.8	53	0.8	1.1	-0.3	-1.0	2.1	3.1	130	240	4.1	3.4	17.91
1735	V17	-35.6	52	0.7	1.1	1.2	-1.3	-9.0	-9.0	130	250	-9.0	-9.0	17.81
1741	V18	-37.2	51	0.8	1.0	-0.4	-1.3	2.3	3.5	130	250	3.4	3.2	17.73
1748	V19	-37.0	50	0.9	1.2	0.4	-0.7	3.0	3.6	140	250	3.5	3.2	17.63
1755	V20	-40.2	51	1.4	1.8	-0.3	-1.3	3.1	3.8	150	260	3.5	3.4	17.55
1801	V21	-39.2	51	1.9	2.4	1.7	-1.7	4.9	4.9	150	260	3.4	3.3	17.48
1815	V22	-40.7	47	2.1	2.6	-0.5	-1.1	3.9	4.7	160	270	3.6	3.6	17.38
1821	V23	-39.4	48	1.8	2.0	-0.9	-1.4	3.3	3.8	170	270	3.5	3.5	17.35
1829	V24	-36.6	48	1.4	2.2	-1.2	-1.1	2.3	3.9	170	270	3.6	3.4	17.31
1840	V25	-37.0	48	1.4	2.1	-1.7	-2.0	1.7	4.0	170	270	3.7	3.5	17.25
1900	V26	-33.4	43	1.3	2.0	-1.7	-1.0	2.0	4.0	170	270	3.8	3.7	17.13

June29 <corrected 24/6/91, 18/7/91>

time	run	U	a	e0	e3	m1	m2	e1	e2	c4	c5	f4	f5	temp
1020	H00	24.5	83	-9.0	-9.0	0.5	1.3	-9.0	-9.0	-10	-10	-9.0	-9.0	16.63
1030	H01	29.4	83	1.4	1.2	0.7	1.2	1.8	2.4	-10	-10	2.5	2.2	16.70
1040	H02	30.6	80	1.3	1.2	1.7	2.1	2.2	2.2	-10	-10	2.6	2.3	16.70
1047	H03	30.6	80	-9.0	-9.0	1.0	-0.6	4.4	7.3	-10	-10	3.3	2.7	16.73
1059	H04	37.9	80	1.6	-9.0	2.3	3.0	2.8	5.6	-10	-10	3.2	2.6	16.82
1107	H05	42.0	77	-9.0	-9.0	2.8	2.8	3.6	6.3	-10	-10	3.5	3.6	16.91
1113	H06	40.1	75	-9.0	-9.0	4.5	1.8	4.0	6.7	-10	-10	4.9	4.0	16.95
1119	H07	45.4	75	-9.0	-9.0	4.8	1.8	3.1	6.1	-10	-10	4.6	3.0	17.02
1140	H08	47.9	59	2.4	2.6	2.4	1.1	3.1	5.6	-10	-10	5.9	4.9	17.25
1148	H09	44.4	58	1.9	1.5	2.7	4.5	3.6	3.7	-10	-10	4.2	4.3	17.40
1200	H10	46.6	58	2.5	2.0	2.1	2.2	-9.0	-9.0	310	270	-9.0	-9.0	17.61
1207	H11	44.9	60	2.0	1.7	2.4	2.0	2.4	4.0	290	240	4.3	4.3	17.75
1213	H12	46.4	59	1.2	1.2	2.3	1.8	3.0	5.4	270	220	4.3	4.4	17.88
1220	H13	43.9	61	-9.0	-9.0	2.2	1.9	2.5	4.9	230	180	-9.0	4.2	18.01
1226	H14	40.9	61	-9.0	-9.0	2.2	2.2	2.2	4.1	220	170	4.2	4.2	18.12
1234	H15	37.7	64	-9.0	-9.0	2.0	1.9	2.2	4.1	200	150	4.8	4.1	18.22
1240	H16	37.8	60	-9.0	-9.0	1.8	0.8	2.3	4.5	190	130	4.5	4.3	18.26
1250	H17	35.1	63	0.4	0.1	1.1	1.0	0.5	0.7	290	110	4.7	4.2	18.34
1256	H18	32.4	64	-9.0	-9.0	0.8	1.2	2.7	5.1	340	120	5.4	4.4	18.37
1313	H20	26.5	65	-9.0	-9.0	-9.0	-9.0	-9.0	-9.0	-10	-10	-9.0	-9.0	-9.00
1327	H21	28.0	67	-9.0	-9.0	0.2	0.6	-9.0	-9.0	330	40	-9.0	-9.0	18.50
1336	H22	24.4	71	-9.0	-9.0	0.5	1.5	2.8	4.9	380	40	-9.0	3.2	18.50
1342	H23	24.4	71	-9.0	-9.0	-0.2	0.5	3.2	3.0	380	40	-9.0	3.0	18.51
1349	H24	21.8	82	1.8	2.1	0.2	1.5	2.5	3.3	410	40	-9.0	3.0	18.51
1355	H25	23.6	84	1.4	1.9	0.4	2.2	1.9	3.6	400	40	-9.0	2.9	18.53
1401	H26	18.5	87	1.4	1.5	-0.1	1.1	2.3	2.5	360	30	5.8	2.8	18.52
1409	H27	17.4	87	1.5	1.7	-0.4	1.0	2.3	2.8	500	30	5.0	3.0	18.53
1430	H29	21.1	84	-0.2	0.6	-0.2	1.2	0.8	0.7	550	120	-9.0	3.7	18.54
1443	H30	17.3	-89	-0.5	-0.5	-0.8	0.9	1.4	0.8	500	110	5.5	4.6	18.56
1450	H31	16.2	-88	-0.5	-0.3	-0.7	1.0	1.6	1.3	550	100	6.0	-9.0	18.57
1500	H32	17.5	89	-9.0	-9.0	-0.6	1.2	-9.0	-9.0	620	110	-9.0	-9.0	18.58
1632	G00	-10.8	85	-9.0	-9.0	-1.7	-0.2	-9.0	-9.0	60	30	-9.0	-9.0	19.03
1640	G01	-11.3	64	-0.5	0.0	-1.5	-0.4	-0.2	-0.1	60	30	1.8	2.0	19.03
1651	G02	-11.6	67	-0.4	0.5	-2.0	-0.8	-0.3	-0.1	60	30	1.8	1.8	18.41
1702	G03	-10.4	66	0.3	0.8	-2.1	-0.4	1.0	0.9	60	30	2.6	2.6	18.84
1714	G04	-11.5	65	-0.1	0.8	-2.2	-0.6	0.1	-0.2	60	30	2.8	2.9	18.84
1720	G05	-10.8	68	-9.0	-9.0	-1.7	-0.7	-9.0	-9.0	60	30	2.9	2.9	18.84
1730	G06	-4.5	63	-9.0	-9.0	-2.1	-0.2	-9.0	-9.0	60	30	2.6	3.1	18.83
1740	G07	-5.9	72	-9.0	-9.0	-1.6	-1.5	-9.0	-9.0	60	30	2.4	3.0	18.82
1747	G08	-8.6	64	-9.0	-9.0	-1.9	-0.5	-9.0	-9.0	60	30	2.1	2.8	18.83
1753	G09	-10.2	63	-9.0	-9.0	-1.9	-2.2	-9.0	-9.0	-10	-10	-9.0	-9.0	-9.00
1800	G10	-11.8	62	-9.0	-9.0	-2.0	-0.8	-9.0	-9.0	-10	-10	-9.0	-9.0	-9.00
1807	G11	-14.6	60	-9.0	-9.0	-2.1	-0.8	-9.0	-9.0	-10	-10	-9.0	-9.0	-9.00
1814	G12	-16.4	60	0.4	0.4	-2.1	-1.0	0.4	0.5	-10	-10	-9.0	-9.0	-9.00
1821	G13	-19.7	53	1.1	0.9	-1.9	-0.8	1.7	1.8	60	30	2.6	2.7	18.77
1827	G14	-25.0	50	2.2	2.3	-2.5	-2.0	3.2	4.0	70	40	2.6	2.7	18.72
1833	G15	-28.6	52	2.6	2.7	-2.5	-2.8	2.8	3.1	90	60	3.3	3.3	18.58
1839	G16	-35.6	52	2.6	2.6	-1.6	-1.8	2.7	2.9	120	70	4.1	4.2	18.45
1852	G17	-38.6	60	0.4	0.5	-1.3	-1.7	0.5	0.9	120	80	3.1	3.2	18.31
1900	G18	-39.1	60	0.5	0.5	-2.2	-1.6	0.6	0.6	130	90	3.6	3.4	18.23
1906	G19	-40.4	60	2.0	1.7	-1.3	-1.8	-9.0	-9.0	120	90	-9.0	-9.0	18.15
1915	G20	-40.8	59	1.4	1.7	-1.6	-1.7	2.5	2.4	140	110	3.6	3.6	18.09
1920	G21	-44.3	60	1.4	1.4	-2.6	-2.1	1.4	1.7	150	120	4.1	3.7	18.15
1928	G22	-41.8	57	1.8	1.9	-1.9	-2.5	1.9	2.3	160	140	3.9	4.0	18.13
1934	G23	-41.0	58	1.3	1.5	-2.6	-2.4	1.3	1.7	160	140	3.8	3.9	18.14
1940	G24	-39.8	56	1.9	2.0	-2.1	-2.2	2.7	2.9	160	130	3.9	3.8	18.08
1948	G25	-38.7	54	1.0	1.3	-1.2	-2.6	-9.0	2.7	160	130	-9.0	-9.0	17.94
1954	G26	-39.6	54	1.5	1.3	-1.8	-0.5	3.2	-9.0	160	130	5.0	4.0	17.83
2001	G27	-36.9	54	-9.0	-9.0	-1.2	-1.9	2.7	-9.0	160	130	3.7	3.9	17.72
2008	G28	-36.1	54	0.8	1.2	-1.6	-1.5	2.9	-9.0	150	130	3.9	3.9	17.67
2015	G29	-34.9	56	1.4	1.2	-9.0	-9.0	-9.0	-9.0	150	120	3.9	3.9	17.65
2022	G30	-35.9	55	1.2	-9.0	-9.0	-9.0	-9.0	-9.0	140	110	3.8	3.8	17.63
2028	G31	-33.6	55	0.5	0.6	-9.0	-9.0	-9.0	-9.0	140	110	3.8	3.8	17.61
2039	G32	-31.5	54	-0.1	0.4	-9.0	-9.0	-9.0	-9.0	140	110	3.8	3.9	17.58

July4 <corrected 24/6/91, 18/7/91>

time	run	U	a	e0	e3	m1	m2	e1	e2	c4	c5	f4	f5	temp
859	S01	-10.4	73	-9.0	-9.0	-9.0	-9.0	-9.0	-9.0	-10	-10	-9.0	-9.0	19.28
911	S02	-7.6	34	-0.5	-0.3	-9.0	-9.0	-9.0	-9.0	-10	-10	-9.0	-9.0	19.27
920	S03	-6.6	37	-0.3	-0.2	-9.0	-9.0	-9.0	-9.0	-10	-10	-9.0	-9.0	19.27
945	S04	-13.2	75	-9.0	-9.0	-9.0	-9.0	-9.0	-9.0	-10	-10	-9.0	-9.0	19.26
953	S05	-13.0	78	0.2	-0.4	-9.0	-9.0	-9.0	-9.0	-10	-10	-9.0	-9.0	19.25
1000	S06	-13.6	83	0.0	-0.1	-9.0	-9.0	-9.0	-9.0	-10	-10	-9.0	-9.0	19.24
1011	S07	-12.5	-90	0.5	0.4	-9.0	-9.0	-9.0	-9.0	-10	-10	-9.0	-9.0	19.21
1019	S08	-17.0	-79	1.6	1.4	-9.0	-9.0	-9.0	-9.0	-10	-10	-9.0	-9.0	19.17
1034	S09	-28.3	-62	1.6	1.7	-9.0	-9.0	-9.0	-9.0	-10	-10	-9.0	-9.0	19.06
1040	S10	-32.8	-62	2.1	2.0	0.9	2.0	-9.0	-9.0	310	280	-9.0	-9.0	19.06
1051	S11	-45.1	-65	0.4	0.3	-0.6	-2.9	1.8	1.8	300	280	-9.0	-9.0	19.04
1059	S12	-48.5	-65	0.3	0.3	-9.0	-9.0	-9.0	-9.0	310	290	-9.0	-9.0	19.02
1110	S13	-49.4	-65	0.5	0.7	-1.7	-1.5	3.5	3.2	330	310	-9.0	-9.0	18.97
1121	S14	-48.2	65	1.1	1.1	-1.0	-0.6	2.1	1.8	360	500	-9.0	-9.0	18.92
1130	S15	-47.6	65	1.2	1.3	-1.7	-0.9	2.0	1.8	370	740	-9.0	-9.0	18.90
1140	S16	-47.0	63	1.0	1.0	-1.6	-1.0	2.4	1.9	390	630	-9.0	-9.0	18.92
1156	S17	-45.5	62	1.0	0.7	-9.0	-9.0	-9.0	-9.0	400	570	-9.0	-9.0	-9.00
1201	S18	-43.2	64	1.6	1.2	-1.5	-0.9	2.9	2.7	410	580	-9.0	-9.0	18.99
1211	S19	-44.5	62	1.7	1.4	-2.7	-1.9	2.8	2.7	420	570	-9.0	-9.0	18.99
1220	S20	-39.4	64	0.2	0.2	-1.6	-1.1	-9.0	-9.0	430	600	-9.0	-9.0	18.98
1230	S21	-36.5	65	0.8	1.0	-9.0	-9.0	1.3	1.3	-10	-10	-9.0	-9.0	-9.00
1240	S22	-36.3	64	1.5	1.2	-9.0	-9.0	2.6	2.2	-10	-10	-9.0	-9.0	-9.00
1250	S23	-33.2	66	0.5	0.3	-9.0	-9.0	-9.0	-9.0	-10	-10	-9.0	-9.0	-9.00
1300	S24	-31.5	62	1.3	1.2	-2.1	-1.1	2.1	2.4	420	640	-9.0	-9.0	18.75
1307	S25	-29.5	66	0.7	0.9	-2.1	-0.5	2.2	1.9	400	630	-9.0	-9.0	18.72
1314	S26	-27.2	66	0.4	0.6	-2.4	-0.8	-9.0	-9.0	390	620	-9.0	-9.0	18.68
1320	S27	-27.1	64	-9.0	-9.0	-2.9	-0.6	2.1	1.9	400	640	-9.0	-9.0	18.63
1330	S28	-26.9	65	-9.0	-9.0	-2.5	-0.9	2.4	2.7	390	650	-9.0	-9.0	18.65
1340	S29	-25.4	65	0.6	0.8	-2.7	-0.7	2.2	1.9	380	650	-9.0	-9.0	-9.00
1350	S30	-23.3	67	0.5	-9.0	-9.0	-9.0	-9.0	4.1	-10	-10	-9.0	-9.0	18.72
1400	S31	-21.9	70	0.3	0.3	-2.6	-0.7	-9.0	-9.0	360	670	-9.0	-9.0	18.79
1413	S32	-18.8	74	-9.0	-9.0	-2.5	-0.9	2.0	3.4	350	670	-9.0	-9.0	18.75
1420	S33	-18.8	78	-9.0	-9.0	-2.5	-0.1	3.5	2.6	350	670	-9.0	-9.0	20.01
1541	R00	27.2	68	-9.0	-9.0	-1.8	-0.3	2.5	3.0	380	360	4.2	3.4	19.98
1550	R01	28.4	61	-9.0	-9.0	-1.5	-0.7	2.9	3.0	380	370	3.5	3.5	20.35
1600	R02	44.5	58	1.4	1.0	-1.1	-1.3	2.4	2.8	430	400	5.0	3.7	20.37
1606	R03	56.7	55	1.1	1.1	-0.9	-2.4	2.2	2.7	470	480	3.9	4.1	20.27
1613	R04	66.8	54	1.6	1.9	-1.9	-2.3	2.3	2.1	550	560	4.7	3.9	20.41
1620	R05	67.3	53	1.8	1.4	-0.8	-3.4	2.4	2.2	600	630	4.9	4.6	20.60
1628	R06	72.0	49	1.2	1.1	-1.2	-3.2	4.9	-9.0	780	940	5.1	4.5	-9.00
1638	R07	65.2	50	2.9	1.1	-2.5	-2.2	-9.0	-9.0	-10	-10	-9.0	-9.0	20.95
1646	R08	62.7	50	2.9	1.6	-0.3	-2.0	3.6	3.9	910	1540	-9.0	-9.0	21.05
1653	R09	57.8	51	2.1	1.6	1.0	-1.8	3.4	2.7	1000	1440	-9.0	-9.0	21.20
1700	R10	57.1	53	2.1	0.8	0.6	-3.2	-9.0	2.2	1170	1440	-9.0	-9.0	21.30
1707	R11	57.6	53	2.1	1.4	-0.9	-3.5	1.5	1.8	920	1550	2.9	3.3	21.35
1714	R12	51.5	54	1.7	0.8	-0.6	-2.1	1.3	1.7	770	1530	2.7	4.2	21.35
1721	R13	51.1	52	0.7	3.6	0.4	-1.0	1.6	-9.0	700	1450	2.6	4.4	21.35
1728	R14	45.5	57	0.4	2.8	0.3	-1.0	1.4	1.4	730	1330	2.9	3.5	21.30
1736	R15	39.3	57	0.7	1.6	-0.6	-0.6	1.6	1.8	840	1310	2.8	4.1	21.20
1742	R16	34.7	57	-9.0	-9.0	-0.5	-0.1	2.5	2.6	-10	-10	-9.0	-9.0	-9.00
1751	R17	28.7	59	0.4	1.8	-1.1	0.7	-9.0	-9.0	-10	-10	-9.0	-9.0	21.15
1800	R18	26.6	59	1.4	2.8	-1.3	0.6	2.3	2.1	990	940	2.6	-9.0	21.10
1816	R19	15.9	69	-0.2	2.9	-1.8	0.9	1.0	1.0	860	820	2.3	-9.0	21.05
1822	R20	15.0	69	-0.3	-0.2	-2.1	1.1	1.3	1.6	880	740	2.1	-9.0	21.05
1830	R21	12.5	76	-0.3	-0.2	-2.0	1.2	0.8	1.3	920	800	2.2	-9.0	21.05
1835	R22	12.8	76	-0.4	0.4	-2.2	0.9	0.7	1.2	830	740	2.0	2.4	21.00
1841	R23	11.4	76	-0.3	-0.3	-2.2	0.9	0.8	-9.0	820	730	1.6	-9.0	21.00
1848	R24	9.7	82	-0.3	-0.3	-2.1	0.9	-9.0	-9.0	790	730	4.5	4.8	20.95
1859	R25	9.4	88	-0.3	-0.1	-2.1	1.0	-9.0	-9.0	820	860	4.2	3.6	20.95
1905	R26	8.5	-68	-0.3	-0.2	-2.1	1.1	-9.0	-9.0	920	940	3.7	-9.0	20.95
1913	R27	8.5	-62	-9.0	-9.0	-2.4	0.9	-9.0	-9.0	930	940	-9.0	-9.0	20.95
1921	R28	7.8	-61	-0.3	-0.1	-2.4	0.9	-9.0	-9.0	1360	1440	1.3	0.0	20.95
1933	R29	8.2	-67	-0.4	0.0	-2.3	1.0	-9.0	-9.0	1390	1400	0.6	-0.2	20.95
1940	R30	8.8	-71	-1.0	-0.2	-2.4	0.8	-9.0	-9.0	1280	1390	1.7	-0.2	20.95
1948	R31	8.5	-72	-0.3	0.0	-2.4	0.9	-9.0	-9.0	1150	1390	2.0	0.0	20.90
1959	R32	8.3	-69	-0.3	-0.1	-2.4	0.8	-9.0	-9.0	1250	1390	2.3	-0.2	20.90
2011	R33	7.9	-54	-0.2	0.0	-2.5	0.8	-9.0	-9.0	1010	1390	3.0	0.0	20.90
2020	R34	7.5	-43	1.5	1.2	-2.4	0.9	-9.0	-9.0	360	1590	-0.2	-0.1	20.90

July5 <corrected 24/6/91, 18/7/91>

time	run	U	a	e0	e3	m1	m2	e1	e2	c4	c5	f4	f5	temp
947	N00	-9.5	70	0.0	0.0	-1.6	0.2	1.4	1.5	270	240	3.4	3.5	20.32
1000	N01	-15.9	-85	0.1	-0.2	-1.5	0.5	2.8	2.7	270	240	-0.4	-0.2	20.40
1010	N02	-16.6	-89	0.2	-0.3	-1.8	0.5	-9.0	-9.0	270	240	3.4	3.4	20.40
1019	N03	-16.4	-89	-0.1	-0.6	-1.7	0.4	0.0	-0.2	270	250	3.4	3.4	20.40
1026	N04	-18.0	87	0.1	-0.5	-1.9	-0.4	0.1	-0.1	270	240	3.0	3.1	20.40
1034	N05	-19.4	85	0.3	-0.2	-2.3	-0.1	0.4	0.0	270	240	2.9	3.0	20.40
1040	N06	-19.1	85	0.6	-0.2	-2.1	0.2	0.4	0.1	270	240	2.9	2.9	20.40
1046	N07	-20.3	83	1.4	0.4	-2.1	-0.4	0.7	0.5	270	250	2.8	2.9	20.40
1053	N08	-20.0	83	1.3	0.3	-2.1	0.2	1.0	0.3	270	250	3.0	3.0	20.40
1100	N09	-22.5	83	2.0	1.1	-1.6	0.4	-9.0	1.5	280	250	3.1	3.1	20.40
1106	N10	-26.5	79	1.8	1.1	-1.6	0.2	1.5	1.4	280	260	3.0	3.0	20.40
1113	N11	-30.8	76	1.3	0.8	-0.6	1.4	1.6	1.6	300	270	3.2	2.2	20.40
1119	N12	-33.8	77	2.0	1.3	0.2	1.6	-9.0	-9.0	300	280	-9.0	-9.0	20.45
1130	N13	-49.5	78	0.3	0.0	1.2	1.1	0.4	0.1	310	290	2.7	2.7	20.40
1150	N15	-49.6	78	0.7	0.4	1.5	1.4	0.7	0.2	320	300	2.9	2.8	20.40
1200	N16	-52.7	77	1.2	0.8	0.6	1.1	1.1	1.0	340	330	2.8	3.0	20.40
1210	N17	-51.8	77	1.5	1.2	1.0	1.8	3.6	3.5	360	360	3.1	3.3	20.35
1217	N18	-50.5	77	1.8	1.4	0.1	2.0	3.5	3.5	370	360	3.1	3.3	20.35
1223	N19	-52.6	76	1.4	-9.0	-0.4	1.4	4.4	4.0	380	370	3.3	3.5	30.35
1230	N20	-51.4	76	1.3	0.7	0.2	0.3	3.6	3.7	390	390	3.5	3.8	20.35
1236	N21	-49.1	75	1.7	1.0	0.4	1.6	2.6	2.6	390	390	3.5	3.7	20.35
1300	N22	-44.0	76	1.2	0.8	-0.2	0.4	1.3	1.2	440	400	4.1	3.7	20.25
1306	N23	-40.2	77	1.2	0.6	0.0	1.5	-9.0	-9.0	460	410	-9.0	-9.0	20.18
1320	N24	-39.8	77	1.0	0.4	0.5	0.8	3.2	2.8	450	400	4.1	3.8	19.99
1340	N25	-36.1	73	1.2	0.7	0.0	0.6	1.2	1.0	500	390	4.4	3.9	19.91
1350	N26	-31.9	75	1.5	1.5	-0.7	0.2	2.5	2.5	540	400	4.4	4.3	19.89
1359	N27	-30.3	76	1.7	1.4	-0.5	0.8	2.2	1.9	570	410	4.4	4.3	19.82
1410	N28	-29.6	78	2.0	1.7	-0.3	0.2	2.4	2.0	580	400	4.4	4.2	19.67
1430	N30	-26.1	77	-9.0	-9.0	-1.0	0.5	-9.0	-9.0	580	380	4.5	3.9	19.53
1432	N31	-24.2	80	0.5	0.3	-0.9	0.3	1.7	0.9	590	370	4.8	3.8	19.46
1450	N32	-24.1	79	2.8	-9.0	-1.3	0.9	2.4	1.5	600	410	4.4	3.7	19.41
1501	N33	-19.1	72	3.3	-9.0	-2.3	0.1	2.4	2.6	600	360	4.5	3.8	19.37
1632	D00	29.0	64	-9.0	-9.0	-0.7	-0.3	-9.0	-9.0	410	410	-9.0	-9.0	19.63
1640	D01	41.9	60	1.9	2.0	0.5	-1.4	2.7	2.8	430	440	3.7	3.8	19.78
1647	D02	56.3	61	2.4	2.3	-0.2	-2.4	2.7	2.8	490	510	4.2	-9.0	19.92
1654	D03	68.7	60	1.7	1.8	-1.2	-3.2	2.6	2.8	580	590	3.9	4.2	20.00
1700	D04	77.1	60	2.4	1.4	-0.8	-4.1	2.6	2.8	670	640	5.0	4.6	20.11
1706	D05	76.6	58	2.8	1.7	-0.9	-3.4	2.1	2.2	770	710	5.2	4.4	20.24
1712	D06	76.0	57	1.1	1.4	-0.9	-2.1	2.0	2.0	840	750	5.1	4.9	20.39
1719	D07	74.1	58	1.1	-9.0	-1.7	-2.8	2.3	2.1	870	860	5.2	5.4	20.47
1725	D08	72.3	57	1.7	1.0	-2.3	-3.6	-9.0	2.1	930	900	-9.0	5.2	-9.00
1731	D09	70.5	58	2.8	1.2	-5.7	-4.0	2.6	2.4	930	940	453.3	-9.0	-9.00
1740	D10	65.1	58	-9.0	-9.0	-3.5	-4.3	-9.0	-9.0	1020	910	-9.0	-9.0	20.55
1748	D11	60.7	60	2.9	2.4	-2.7	-5.1	1.9	2.4	1180	990	3.7	2.4	20.60
1755	D12	55.6	59	0.9	2.2	-3.3	-4.8	1.8	1.9	1300	890	3.8	2.8	20.60
1801	D13	56.4	60	1.7	1.2	-4.2	-3.2	2.4	2.6	1260	910	2.6	2.4	20.65
1808	D14	50.4	59	2.0	2.6	-3.7	-2.3	2.8	2.7	1250	1120	2.8	2.2	20.65
1815	D15	42.8	59	1.5	-9.0	-4.1	-2.4	2.0	1.4	1230	1310	2.6	1.8	20.65
1821	D16	41.5	56	0.8	0.6	-4.2	-2.8	1.4	1.4	1250	1360	2.2	1.3	20.60
1830	D17	36.8	56	0.4	0.3	-3.8	-2.4	1.7	1.9	1220	1300	2.7	0.8	20.60
1838	D18	31.8	57	0.5	0.0	-4.3	-1.5	-9.0	1.6	1150	1240	3.3	1.4	20.60
1850	D19	25.1	57	0.2	-0.5	-4.2	-0.7	0.3	1.7	1200	1130	4.5	1.7	20.55
1858	D20	20.4	60	-0.1	1.5	-9.0	-9.0	-9.0	-9.0	1250	1030	-9.0	-9.0	20.50
1906	D21	-9.0	-9	-9.0	-9.0	-9.0	-9.0	-9.0	-9.0	1200	890	-9.0	-9.0	20.50
1914	D22	-9.0	-9	-9.0	-9.0	-9.0	-9.0	-9.0	-9.0	1220	760	-9.0	-9.0	20.50
1920	D23	-9.0	-9	-9.0	-9.0	-9.0	-9.0	-9.0	-9.0	1190	740	-9.0	-9.0	20.50
1947	D24	15.6	-82	-0.4	2.3	-1.2	0.6	0.0	-0.3	270	250	0.6	0.4	20.50
1959	D26	9.8	-77	-0.6	2.2	-1.3	0.9	0.0	-0.1	270	240	0.5	0.6	20.50

June 28 Sizer data (%wt in bands 16..1, salinity)

906	2.5	12.7	8.8	7.7	4.7	4.8	5.6	3.2	3.5	6.2	4.1	4.7	3.1	5.1	2.8	20.5	0.1
922	5.8	17.0	9.8	7.0	4.5	2.8	4.7	3.8	2.2	4.5	3.7	4.5	3.4	3.2	2.8	20.5	0.2
924	4.9	16.3	10.7	7.4	4.5	3.1	4.6	3.1	2.9	4.5	3.7	3.7	4.9	2.3	2.8	20.5	0.2
940	3.0	18.9	16.9	11.4	7.5	5.9	5.1	1.6	3.3	2.5	2.3	3.3	1.4	2.1	2.6	12.1	0.2
941	3.0	16.9	16.4	11.6	8.0	6.7	5.9	1.1	4.1	2.6	1.8	3.2	2.3	2.6	2.5	11.3	0.2
1001	8.4	17.4	15.1	12.7	9.1	7.5	5.4	2.7	2.8	2.5	2.2	0.6	1.9	2.2	3.6	6.0	0.3
1002	8.3	18.0	16.7	11.4	9.2	7.5	4.8	3.2	1.7	3.0	2.2	1.5	0.0	2.2	4.7	5.5	0.3
1020	7.1	16.8	15.6	12.6	9.1	8.0	4.9	4.3	2.8	2.5	1.7	1.0	1.9	2.1	3.0	6.4	0.4
1021	6.9	16.8	14.6	13.3	8.8	8.7	5.1	4.0	2.4	3.1	1.8	1.1	1.4	2.2	4.2	5.5	0.4
1041	3.7	15.5	15.1	14.4	10.7	8.5	7.7	2.2	4.2	2.1	1.8	1.6	1.4	1.6	3.8	5.7	0.8
1042	3.5	17.6	14.4	14.7	10.0	8.8	6.4	3.6	3.0	2.6	1.7	1.5	0.7	2.1	3.7	5.6	0.8
1059	2.9	17.9	16.9	14.9	9.7	9.6	7.0	2.1	2.8	2.9	1.4	1.2	0.9	1.4	2.9	5.4	2.3
1100	4.5	17.4	16.5	14.5	11.0	8.2	6.8	3.2	2.1	2.8	1.9	0.5	1.5	1.3	2.7	5.2	2.3
1121	8.2	19.0	18.6	12.4	12.1	6.1	5.8	3.3	2.1	1.4	0.9	0.7	2.1	2.8	0.9	3.6	4.7
1122	6.5	20.0	18.0	15.7	9.8	7.6	4.8	3.3	2.2	1.3	1.7	0.0	2.0	2.7	1.8	2.6	4.7
1140	21.8	22.6	16.5	10.9	6.9	5.8	3.4	2.1	0.3	3.2	0.0	0.0	1.7	1.5	2.3	1.2	6.6
1141	23.9	22.3	16.4	8.7	7.5	4.6	4.0	1.9	0.2	2.3	1.2	0.0	0.7	1.6	1.5	3.2	6.6
1201	28.8	27.7	14.8	8.0	5.2	3.3	3.1	0.8	0.0	2.2	0.0	0.9	0.5	1.5	1.5	2.2	7.9
1202	29.1	25.2	17.5	5.9	5.8	3.0	2.8	0.9	0.0	2.0	0.8	0.9	0.0	1.4	1.4	3.1	7.9
1445	17.9	17.6	11.1	5.7	4.5	3.4	4.4	2.4	2.0	3.5	3.5	2.8	3.8	2.2	1.8	13.4	13.5
1446	16.9	17.5	9.9	5.7	5.2	3.6	4.5	2.6	2.2	3.6	3.6	3.4	3.3	2.7	1.8	13.5	13.5
1501	13.5	14.3	10.4	7.5	4.2	5.7	4.2	2.9	3.7	4.1	3.4	3.7	3.3	2.9	2.0	14.3	13.7
1502	11.1	14.3	10.2	6.5	5.6	5.0	4.9	3.4	2.9	4.4	3.6	4.5	2.5	3.1	2.2	15.8	13.7
1521	15.5	17.7	9.6	7.1	3.3	5.8	4.3	2.7	3.8	3.9	3.8	2.8	2.5	3.1	1.7	12.4	13.8
1522	17.9	15.5	10.0	5.7	4.2	4.9	4.8	2.5	3.8	4.1	3.3	3.5	2.6	2.6	1.8	12.9	13.8
1542	33.6	14.4	5.8	4.9	4.4	3.5	3.0	2.8	3.5	3.0	2.8	2.4	2.0	1.7	1.5	10.8	13.8
1543	16.7	15.0	9.4	5.0	3.6	5.3	4.6	3.3	4.3	4.4	3.6	3.3	3.2	2.2	1.9	14.0	13.8
1600	21.4	15.7	8.3	4.2	3.1	2.9	3.5	3.1	3.4	4.2	3.4	3.2	2.8	2.4	2.2	16.2	13.1
1601	20.4	15.8	8.1	4.9	2.6	3.4	2.6	3.3	3.0	4.4	4.2	3.4	2.4	2.2	2.3	17.2	13.1
1620	36.9	13.8	9.8	2.7	4.5	2.3	1.7	2.8	2.5	2.4	2.3	2.1	1.9	1.7	1.5	11.2	11.9
1621	34.3	15.2	8.0	5.2	3.5	2.5	1.8	2.9	2.6	2.5	2.4	2.2	1.9	1.7	1.6	11.5	11.9
1640	59.0	13.7	10.1	0.0	0.0	3.3	2.3	0.0	1.0	0.9	0.0	0.0	5.2	0.0	0.0	4.5	10.2
1641	55.0	17.9	5.1	3.6	0.0	3.0	2.1	0.0	1.1	1.0	1.0	0.0	4.8	0.0	0.7	4.9	10.2
1701	45.4	20.4	3.6	7.4	1.1	0.0	2.1	1.8	1.6	1.5	1.5	1.5	1.3	1.2	1.2	8.5	8.2
1702	46.3	15.9	8.0	3.8	3.2	0.0	2.2	1.8	1.6	1.5	1.5	1.5	1.3	1.3	1.2	8.8	8.2
1721	49.9	20.7	10.7	4.8	4.1	0.0	1.6	0.0	2.0	0.3	0.2	0.3	0.1	1.5	1.5	2.2	5.4
1722	53.5	18.4	11.1	4.1	2.2	2.3	1.3	0.7	0.3	0.1	0.0	1.6	0.0	1.3	1.2	1.9	5.4
1742	13.9	19.6	15.4	12.6	8.0	5.8	3.6	2.6	1.7	2.0	1.3	0.7	1.6	3.0	2.9	5.3	1.1
1743	14.1	20.2	14.3	12.8	7.2	5.7	4.6	2.0	1.1	2.5	1.4	0.7	1.6	3.0	3.4	5.2	1.1
1802	11.4	19.1	15.4	12.0	8.7	7.2	3.3	3.9	0.2	3.3	1.5	1.4	0.7	3.1	3.5	5.3	0.4
1803	11.5	18.2	15.3	11.5	8.9	6.8	4.6	1.9	2.6	2.4	1.7	1.5	0.8	3.2	3.1	6.0	0.4
1821	14.0	19.7	14.2	12.0	8.8	5.1	5.2	1.0	2.3	2.6	1.4	1.3	1.1	2.9	3.4	5.1	0.3
1822	11.7	18.5	15.0	11.7	8.5	7.4	3.0	3.6	1.0	2.9	2.2	1.0	0.8	3.3	3.2	6.1	0.3
1842	14.3	20.6	16.4	10.9	8.2	5.0	3.9	1.9	1.7	2.4	1.3	1.2	1.0	2.9	2.8	5.6	0.2
1843	7.4	19.8	16.6	12.6	8.8	6.7	4.5	2.9	1.4	2.8	1.6	0.9	1.7	3.2	3.6	5.5	0.2
1901	10.3	20.2	18.6	11.2	7.7	6.9	2.3	3.6	1.2	2.6	1.3	0.7	1.5	3.0	4.0	4.8	0.2
1902	10.7	21.5	18.0	10.7	8.4	5.1	4.6	1.8	1.0	2.6	1.8	0.6	1.5	2.4	3.4	5.8	0.2
1922	12.3	22.3	16.0	12.2	8.1	4.1	4.1	2.0	1.1	2.6	1.3	0.7	1.6	3.1	3.0	5.5	0.2
1923	17.7	22.8	16.0	10.2	4.6	5.1	2.6	0.8	1.7	2.6	0.0	3.0	1.3	2.7	0.0	8.9	0.2

June 29 Sizer data (%wt in bands 16..1, salinity)

1020	2.1	16.8	15.3	8.9	7.4	5.5	4.7	3.2	3.6	3.8	3.7	2.4	2.7	3.9	2.6	13.5	0.2
1022	2.8	17.7	15.9	9.5	7.2	5.2	5.2	2.2	4.7	2.4	2.9	2.9	3.8	2.8	1.8	13.2	0.2
1040	7.6	22.8	17.3	12.4	6.4	4.5	5.0	0.0	2.3	3.7	0.8	2.3	2.9	1.3	2.6	8.2	0.2
1041	5.3	22.6	18.1	12.3	6.5	6.2	3.0	1.8	1.8	4.1	0.8	2.2	2.2	2.6	2.4	8.0	0.2
1101	9.6	21.4	19.1	12.5	7.5	6.9	4.1	2.5	0.3	3.0	1.6	0.9	0.8	1.6	3.2	5.0	0.2
1102	7.6	21.7	19.5	11.9	8.2	7.0	4.3	2.6	0.5	3.1	1.7	1.0	0.9	1.7	3.3	5.1	0.2
1120	6.0	18.5	17.3	13.6	9.6	8.2	5.3	2.5	2.6	2.8	1.4	1.2	1.0	1.8	3.4	4.7	0.3
1121	5.0	20.2	16.5	14.2	10.1	6.4	6.4	2.4	2.7	2.7	1.4	1.2	1.0	1.8	3.4	4.7	0.3
1141	0.3	16.0	17.4	14.4	11.0	8.6	7.9	3.1	3.1	3.2	1.7	0.9	1.2	2.1	3.7	5.2	0.5
1142	2.1	17.9	16.2	15.3	9.7	9.5	5.9	4.1	2.3	2.5	2.1	0.7	1.1	2.0	3.0	5.5	0.5
1203	2.7	16.0	18.1	14.6	11.7	9.8	6.4	3.1	3.7	2.1	0.8	1.1	1.8	2.2	2.9	3.1	1.7
1204	2.0	15.9	17.2	15.7	11.5	10.1	6.6	3.2	3.1	2.8	0.8	0.5	1.8	2.3	3.0	3.2	1.7
1219	4.7	20.4	19.5	14.6	12.5	6.3	5.7	3.3	2.8	1.1	0.6	0.0	2.8	0.8	2.5	2.4	3.4
1220	3.7	19.7	19.7	14.8	12.9	7.3	5.1	3.5	2.8	1.2	0.7	0.0	2.8	0.8	2.6	2.5	3.4
1240	9.4	22.1	21.2	14.1	10.1	7.3	3.0	2.3	0.0	3.5	0.0	0.0	1.7	0.4	1.5	3.3	5.8
1303	17.4	27.8	18.7	12.7	6.4	5.4	1.3	2.2	1.4	1.0	0.0	0.0	1.4	1.3	1.2	1.9	7.4
1304	14.1	27.7	21.4	10.0	8.1	5.8	2.6	1.4	0.4	2.2	0.0	0.0	1.5	1.4	1.3	2.0	7.4
1322	18.9	27.3	17.9	10.4	4.1	4.9	2.4	1.0	0.7	1.6	1.3	1.0	1.1	1.9	1.9	3.8	8.7
1323	24.9	25.6	17.5	8.7	5.1	3.4	3.0	0.0	1.4	1.3	1.2	0.0	0.9	2.8	1.7	2.5	8.7
1340	33.2	24.9	7.7	9.4	2.9	0.0	2.2	1.8	1.5	1.3	1.3	1.4	3.5	1.1	0.9	6.8	10.4
1341	27.9	25.3	11.7	6.8	3.6	3.0	0.0	2.6	2.0	1.4	1.4	2.1	1.2	3.0	1.0	7.0	10.4
1407	24.1	18.8	11.4	5.7	5.6	2.4	3.1	1.0	1.5	3.3	2.3	3.4	2.2	2.1	1.6	11.7	11.8
1408	23.4	18.5	10.6	7.4	4.9	2.5	3.9	1.1	0.8	3.3	2.3	3.4	2.2	2.1	1.6	11.9	11.8
1419	20.3	17.7	11.5	6.6	4.9	3.8	3.2	1.5	1.2	4.0	2.5	3.4	2.3	2.7	1.7	12.6	12.2
1420	21.4	17.7	10.9	6.6	5.0	3.0	4.2	0.7	1.1	4.2	2.5	3.5	2.3	2.1	1.8	13.0	12.2
1500	16.6	17.1	11.6	8.4	5.3	4.4	4.4	0.6	2.7	3.5	2.6	3.5	3.0	2.6	1.6	12.0	12.7
1501	16.5	17.1	11.1	9.3	4.6	4.4	4.9	0.0	2.7	3.4	3.3	2.8	3.6	2.6	1.6	12.0	12.7
1631	21.9	15.1	9.6	5.7	5.1	3.6	3.0	3.0	2.0	4.5	3.8	2.9	3.1	2.6	1.7	12.5	14.2
1632	19.1	15.7	9.5	6.5	5.3	3.2	3.7	2.0	2.8	4.5	3.8	3.0	4.3	2.1	1.7	12.7	14.2
1640	22.8	16.5	10.1	7.4	3.7	3.6	3.3	1.8	2.2	4.3	2.8	3.4	2.9	2.6	1.5	11.3	13.9
1641	24.8	16.7	10.1	7.2	3.4	3.6	2.7	1.5	2.2	3.9	2.9	4.3	0.8	2.8	1.6	11.5	13.9
1702	37.4	13.4	9.2	5.3	3.4	2.2	1.5	2.9	2.7	2.6	2.4	2.2	1.8	1.5	1.4	10.0	13.2
1703	36.2	17.0	7.9	5.3	3.3	2.1	1.4	2.9	2.6	2.6	2.4	2.1	1.8	1.5	1.3	9.6	13.2
1722	43.3	11.8	8.3	5.8	1.1	1.4	2.7	2.6	2.5	2.4	2.2	2.0	1.7	1.5	1.3	9.6	12.4
1723	44.9	14.6	6.7	3.9	2.1	1.0	2.6	2.5	2.3	2.2	2.1	1.9	1.6	1.4	1.2	9.0	12.4
1739	51.4	10.1	8.6	2.6	0.0	2.5	2.0	2.1	2.0	2.0	1.9	1.8	1.5	1.4	1.2	9.0	11.6
1740	43.5	11.5	8.6	2.2	5.2	0.0	2.3	2.3	2.3	2.3	2.2	2.1	1.8	1.6	1.5	10.7	11.6
1801	45.1	14.1	4.9	6.0	0.0	2.4	2.0	2.0	2.0	2.0	2.0	3.5	0.0	3.1	1.3	9.6	10.4
1802	47.9	13.4	5.0	4.6	0.0	4.3	2.1	0.0	2.0	2.0	2.0	2.0	3.6	0.0	1.3	9.8	10.4
1820	72.1	14.5	0.0	0.0	5.0	0.0	0.5	0.5	0.4	0.4	0.0	0.8	0.0	5.7	0.0	0.0	4.4
1821	68.9	12.7	3.4	0.0	3.6	0.0	0.0	0.0	4.0	0.0	0.4	0.7	0.0	4.2	0.0	2.2	4.4
1839	29.0	27.2	15.0	8.7	6.9	2.1	2.9	0.5	0.0	2.0	0.0	0.4	0.3	1.4	1.4	2.1	3.5
1840	21.1	25.4	18.9	9.2	6.4	5.2	2.4	1.4	0.5	2.2	0.0	0.0	1.8	0.5	2.6	2.4	3.5
1900	19.8	21.4	15.0	11.7	7.8	4.7	2.5	3.4	0.0	2.1	1.4	0.7	0.6	1.5	3.1	4.3	1.8
1901	18.1	22.9	17.0	10.7	7.5	4.4	3.6	1.9	0.0	2.7	1.2	1.2	0.0	1.3	2.9	4.7	1.8
1920	19.1	20.0	16.8	10.2	7.8	4.8	4.6	1.2	1.3	2.3	1.5	0.8	0.7	1.5	2.6	4.9	0.6
1921	17.8	19.3	15.3	11.7	7.6	6.0	3.9	2.4	0.4	2.9	1.6	0.9	0.8	1.6	3.1	4.8	0.6
1941	19.0	19.3	16.8	10.9	7.4	5.2	3.2	2.8	0.9	2.2	1.5	0.8	0.7	1.5	3.0	4.7	0.3
2022	17.6	20.4	13.7	12.0	6.3	6.0	2.7	2.0	1.7	2.6	1.4	1.3	1.0	3.0	2.9	5.7	0.2
2023	17.6	21.0	16.1	10.5	7.0	5.1	3.6	1.0	1.4	2.9	1.1	1.0	0.9	2.7	3.1	4.9	0.2
2039	21.2	22.0	15.5	10.7	5.1	3.9	2.7	2.2	0.6	2.4	1.1	1.0	1.9	1.6	2.7	5.6	0.2
2040	18.6	22.6	16.1	10.1	7.1	3.9	2.1	2.8	0.8	2.3	1.6	1.0	0.2	2.7	3.2	5.0	0.2

July 4 Sizer data (%wt in bands 16..1, salinity)

853	43.2	22.8	3.7	0.0	0.0	0.0	0.0	0.0	0.0	2.5	4.0	2.2	4.3	2.2	1.8	13.4	13.4
854	54.1	19.0	2.1	0.0	0.0	0.0	0.0	0.0	0.0	1.2	4.4	2.2	2.2	0.0	1.8	13.0	13.4
904	68.5	14.3	0.0	0.0	0.0	0.0	0.0	0.0	0.0	4.1	3.7	0.0	0.0	0.8	0.0	8.7	12.7
905	64.1	18.2	0.0	0.0	0.0	0.0	0.0	0.0	3.8	0.0	4.1	0.0	0.0	4.8	0.0	5.0	12.7
920	70.9	4.5	0.0	0.0	0.0	0.0	0.0	0.0	0.0	8.8	0.0	0.0	0.0	0.0	0.0	15.7	12.4
921	65.0	4.4	0.0	0.0	0.0	0.0	0.0	0.0	6.7	6.3	0.0	0.0	0.0	0.0	0.0	17.6	12.4
946	31.4	14.2	6.6	3.3	2.6	2.9	2.9	3.0	3.9	4.5	3.3	2.9	3.2	1.9	1.6	12.0	10.7
947	32.9	14.0	6.6	3.7	3.5	2.9	2.0	3.0	4.0	3.7	3.3	3.9	1.4	1.9	1.6	11.6	10.7
1001	35.7	13.9	5.5	4.6	3.4	2.7	1.6	3.9	3.8	3.4	3.0	2.5	2.1	1.7	1.5	10.7	9.8
1002	40.7	11.8	6.2	3.8	2.8	2.2	2.2	3.6	3.4	3.1	2.7	2.3	1.9	1.6	1.4	10.2	9.8
1021	77.3	9.2	3.2	0.0	0.0	2.7	0.0	0.2	0.1	0.0	2.5	0.0	0.0	0.0	1.9	2.9	7.8
1022	73.0	14.2	5.5	0.0	0.9	0.3	0.0	0.0	0.0	1.8	0.0	0.0	1.8	0.0	1.0	1.6	7.8
1041	29.9	25.9	15.5	8.5	4.8	2.9	2.7	0.0	2.1	0.9	0.0	0.0	1.6	1.5	1.5	2.2	4.5
1042	31.9	24.7	15.1	8.2	3.6	4.0	2.7	0.7	1.1	0.9	0.0	0.0	1.7	1.6	1.5	2.3	4.5
1101	13.1	19.9	17.0	9.9	9.2	6.5	3.1	3.1	1.6	2.0	1.3	0.6	1.0	3.0	4.0	4.8	2.7
1102	12.9	21.1	16.0	11.0	8.3	6.1	4.9	0.9	2.8	1.4	1.2	1.1	1.0	2.4	3.0	6.0	2.7
1122	12.1	20.7	16.6	11.5	8.1	4.3	6.7	0.0	2.0	2.6	0.0	1.4	2.8	2.7	1.1	7.5	1.2
1123	10.0	20.1	16.1	11.5	8.3	7.3	4.5	1.1	3.5	1.6	1.4	0.8	1.6	2.6	3.6	6.0	1.2
1143	7.6	20.7	15.9	11.5	7.8	6.1	4.6	2.1	1.5	2.9	1.9	1.0	1.8	1.8	1.8	11.1	0.7
1144	6.8	21.2	14.9	12.2	7.2	6.9	4.0	2.9	1.5	2.7	1.9	1.1	1.8	1.7	1.7	11.6	0.7
1202	7.3	19.4	14.5	9.9	9.8	5.1	5.4	1.9	2.3	3.5	0.6	1.8	2.1	2.6	2.6	11.3	0.5
1203	4.4	19.9	15.8	12.3	8.1	6.9	4.0	2.9	1.4	3.1	1.8	1.7	1.1	1.6	1.6	13.4	0.5
1220	2.2	17.9	15.7	12.6	8.3	6.1	5.2	1.9	2.3	2.8	1.5	2.0	2.0	2.3	2.8	14.3	0.4
1221	3.5	18.2	14.7	11.8	6.7	7.4	3.9	2.1	2.5	2.7	1.7	2.3	1.1	3.5	2.2	15.6	0.4
1244	1.2	15.8	12.5	9.0	7.9	5.3	3.8	2.9	2.5	3.1	2.3	3.3	3.2	1.5	2.3	23.5	0.3
1245	3.1	14.2	11.9	10.1	7.5	5.8	4.7	2.3	2.4	3.0	3.1	2.2	3.1	2.1	2.2	22.3	0.3
1302	3.5	15.7	12.4	11.3	5.5	5.4	3.1	1.6	2.9	2.9	2.1	3.2	3.2	1.5	2.3	23.4	0.3
1303	2.9	16.0	12.9	10.8	5.8	5.5	3.2	2.4	2.2	2.9	2.1	3.1	3.2	1.4	2.3	23.1	0.3
1321	5.9	16.3	11.6	5.6	3.5	4.3	0.7	3.0	0.6	3.2	3.7	4.0	4.1	0.0	2.1	31.4	0.3
1322	3.0	14.2	10.4	7.4	4.8	5.3	1.3	1.9	1.9	3.4	3.8	4.1	4.0	0.0	3.1	31.4	0.3
1343	0.0	3.7	6.8	5.6	2.9	4.2	2.9	3.2	3.6	4.1	4.7	5.2	5.4	3.8	5.3	38.5	0.2
1344	0.0	9.7	8.4	5.8	1.8	4.1	1.6	3.0	3.4	3.8	4.4	4.9	6.2	0.1	6.1	36.6	0.2
1401	0.0	9.6	3.8	6.0	1.2	2.6	3.8	0.7	3.5	5.5	4.7	5.2	5.4	5.7	4.1	38.2	0.2
1402	0.0	8.7	6.2	2.5	2.2	2.6	4.9	0.0	3.5	5.5	4.8	5.3	6.6	2.2	6.7	38.5	0.2
1422	0.0	4.4	5.4	3.3	0.9	4.8	2.7	0.0	6.3	4.3	5.0	6.9	6.8	4.4	6.6	38.3	0.2
1423	0.0	3.9	5.4	2.9	1.8	2.2	2.5	1.7	6.3	4.3	5.0	6.9	5.6	6.7	6.6	38.2	0.2
1540	0.0	9.5	9.7	6.6	5.2	3.7	3.5	2.3	3.6	4.9	4.2	4.4	5.5	4.2	3.9	28.7	0.2
1541	0.0	6.0	11.0	6.4	5.9	5.1	3.9	1.8	3.8	5.1	4.3	4.5	5.4	3.4	4.0	29.3	0.2
1601	0.0	4.6	11.1	9.8	8.6	6.7	5.4	3.7	3.6	4.2	4.1	4.1	3.0	1.1	3.6	26.4	0.3
1602	0.0	2.6	13.9	9.2	10.6	4.9	6.2	3.4	3.6	4.0	4.0	3.0	4.6	1.9	2.5	25.6	0.3
1621	0.0	0.0	7.4	11.3	9.5	7.4	7.3	5.9	4.7	4.9	3.2	4.1	2.7	1.3	2.5	27.8	0.3
1622	0.0	0.0	7.9	8.4	10.4	7.5	8.6	4.9	4.8	5.0	3.3	4.2	1.7	2.6	2.6	27.8	0.3
1642	0.0	0.0	0.0	0.0	0.0	0.0	0.2	3.9	4.9	5.9	4.1	7.7	5.8	0.0	0.0	67.5	0.5
1643	0.0	0.0	0.0	0.0	0.0	0.0	2.4	3.7	2.0	8.1	3.7	7.2	5.2	0.0	1.6	66.1	0.5
1700	0.0	0.0	0.0	0.0	0.0	13.4	0.0	8.5	6.6	6.5	6.3	4.4	4.4	1.0	4.3	44.6	1.1
1701	0.0	0.0	0.0	0.0	4.6	4.2	9.3	6.8	7.9	7.5	4.2	5.5	1.0	7.8	3.6	37.7	1.1
1723	0.0	0.0	6.2	10.2	11.5	12.0	10.7	8.1	7.4	7.1	3.9	1.6	3.0	4.6	6.0	7.6	5.5
1724	0.0	0.0	7.0	11.4	11.7	11.7	10.8	8.0	7.9	6.1	3.3	2.3	2.9	4.0	5.3	7.5	5.5
1741	3.5	16.0	14.1	13.8	11.9	10.4	8.0	4.8	3.7	3.7	1.1	0.6	1.4	2.7	1.7	2.6	8.4
1742	4.0	14.4	15.6	13.7	13.9	8.7	8.4	3.0	6.4	1.6	0.8	1.2	2.2	1.9	1.7	2.6	8.4
1802	6.0	21.0	19.0	13.5	13.2	8.1	5.1	3.3	1.8	2.8	0.4	0.0	1.5	1.3	1.2	1.8	10.8
1803	9.7	21.1	17.8	14.6	9.8	9.4	4.6	3.1	1.6	2.6	0.3	0.0	1.4	1.2	1.1	1.7	10.8
1823	21.9	27.5	18.4	11.0	8.3	3.7	3.1	0.0	2.1	0.5	0.0	0.0	0.9	0.8	0.7	1.1	12.8
1824	22.7	25.8	20.7	8.5	9.4	2.7	4.1	0.0	2.2	0.5	0.0	0.0	0.9	0.8	0.7	1.1	12.8
1841	27.7	29.1	16.4	8.2	7.1	1.3	2.7	0.0	2.2	0.7	0.0	1.4	0.0	1.0	0.9	1.3	14.3
1842	28.1	28.6	16.9	9.8	4.6	2.7	1.3	1.5	0.0	1.9	0.0	1.5	0.0	1.0	0.9	1.4	14.3
1900	30.4	24.1	13.5	3.7	4.3	2.2	2.7	1.0	1.0	4.5	2.6	1.3	1.7	2.2	1.9	2.9	15.2
1901	30.8	24.4	12.1	5.0	3.9	2.9	1.3	2.1	0.7	4.4	2.4	1.2	2.5	2.0	1.7	2.6	15.2
1921	27.6	21.9	9.3	5.7	1.8	4.0	2.2	1.1	1.8	6.1	4.1	3.4	0.0	3.6	3.3	4.1	15.8
1922	24.0	21.5	9.2	6.4	3.4	1.9	3.8	1.4	1.5	7.4	4.0	2.8	2.1	3.5	3.2	4.0	15.8
1942	24.7	20.0	11.6	5.9	1.9	4.6	1.7	2.6	1.0	6.7	4.6	3.1	0.6	3.6	3.4	4.1	16.0
1943	21.1	20.9	11.7	5.5	4.0	3.1	3.5	1.3	2.2	6.8	4.5	2.7	1.7	3.6	3.3	4.1	16.0
2001	22.1	20.7	10.5	6.4	2.8	3.4	3.0	1.3	2.3	7.2	5.1	2.2	2.5	3.5	3.2	3.9	16.4
2002	21.8	21.0	10.7	5.6	3.3	3.5	2.4	1.8	1.9	7.9	4.6	2.0	3.0	3.4	3.1	3.9	16.4
2024	18.2	17.6	11.5	6.3	1.9	2.9	3.1	1.6	3.9	7.6	6.5	4.0	3.2	3.4	3.4	4.9	16.8
2025	15.6	15.2	10.7	7.0	1.8	4.0	4.5	1.0	4.4	8.4	7.0	4.1	4.3	4.1	3.4	4.6	16.8

July 5 Sizer data (%wt in bands 16..1, salinity)

950	46.3	19.3	4.7	5.1	0.0	1.9	0.0	1.4	0.0	3.6	1.9	1.8	3.7	1.3	1.1	8.0	13.0
951	49.8	16.1	10.6	0.0	2.4	0.0	1.0	0.0	1.4	0.0	2.0	4.5	1.8	0.0	1.2	9.1	13.0
1002	44.5	19.2	8.1	5.0	0.9	0.0	1.9	1.8	1.7	1.6	1.8	1.6	4.0	0.0	1.0	7.0	12.4
1003	45.2	18.8	9.9	0.6	3.5	0.0	1.9	1.7	1.7	1.6	1.7	1.6	4.0	0.0	0.9	6.9	12.4
1027	44.1	17.7	7.5	5.0	1.4	0.0	3.7	0.0	1.8	1.7	1.9	1.7	3.4	0.0	1.2	8.9	10.6
1028	45.1	20.8	7.2	2.2	3.1	0.4	0.0	1.6	1.7	1.6	1.8	1.6	3.3	0.0	1.2	8.6	10.6
1042	47.4	15.8	8.7	2.5	0.0	2.1	1.7	1.7	1.7	1.7	1.8	1.6	1.5	1.4	1.2	9.2	9.7
1043	44.8	19.0	6.7	2.8	0.0	2.2	1.8	1.8	1.8	1.8	1.9	1.7	1.6	1.4	1.3	9.5	9.7
1103	50.5	21.4	8.9	3.8	0.0	2.5	0.0	0.7	0.6	0.6	0.0	0.0	4.4	0.7	0.7	5.3	7.2
1104	52.9	24.6	5.8	0.0	2.7	2.9	0.0	0.5	0.5	0.0	0.0	0.0	4.6	0.6	0.6	4.3	7.2
1122	22.7	27.4	17.4	9.7	5.9	3.5	1.9	0.0	2.3	0.0	0.0	1.0	0.0	2.0	3.2	3.1	5.0
1123	26.3	25.4	16.9	6.9	7.5	2.4	2.8	0.0	1.3	0.0	1.0	0.0	1.0	2.0	3.2	3.2	5.0
1142	11.3	21.7	17.5	11.5	8.0	5.1	3.1	0.9	1.6	2.4	0.0	1.3	2.8	1.3	2.7	8.7	3.3
1143	9.6	22.5	17.9	10.9	7.6	7.7	2.4	0.0	3.3	1.1	1.6	0.0	2.5	2.1	2.7	8.0	3.3
1203	10.1	21.2	15.8	11.9	7.5	5.6	2.5	3.2	2.1	1.9	0.4	1.8	1.8	1.8	1.8	10.5	1.7
1204	11.6	20.0	15.7	10.7	7.6	5.5	5.2	0.0	3.3	1.7	1.6	0.8	2.2	1.5	2.8	10.0	1.7
1220	10.1	20.0	16.8	10.9	7.0	6.7	4.1	0.0	3.0	2.4	0.0	2.1	2.5	1.5	2.7	10.1	1.0
1221	11.0	21.7	14.6	12.2	6.8	5.4	4.3	0.7	2.0	2.6	0.7	1.1	2.5	1.5	2.7	10.2	1.0
1239	10.8	17.4	15.3	11.2	7.0	6.8	3.5	2.2	1.3	3.2	1.1	1.1	2.8	1.1	2.7	12.6	0.7
1240	8.0	18.9	16.3	11.2	8.2	7.1	2.5	2.0	1.7	3.2	1.0	1.0	2.2	2.3	2.7	11.7	0.7
1302	9.6	19.0	14.0	10.5	6.0	5.0	2.9	2.0	1.5	1.3	2.2	2.3	1.6	1.6	2.5	18.0	0.5
1303	11.6	19.1	15.4	8.8	6.4	5.1	2.8	2.4	0.4	1.9	2.0	2.1	1.3	1.6	2.8	16.2	0.5
1322	7.7	16.3	14.0	9.1	6.1	4.7	3.4	1.9	0.9	2.4	2.7	1.9	2.2	2.1	2.2	22.4	0.4
1323	10.3	17.3	13.4	9.0	5.9	4.8	2.6	1.2	1.5	2.3	2.5	1.8	2.0	2.3	2.1	21.2	0.4
1342	3.7	15.7	11.1	8.6	6.5	3.9	1.0	4.0	0.0	2.8	3.2	2.4	4.0	0.7	3.0	29.6	0.3
1343	2.0	16.1	11.7	7.8	8.0	4.2	2.1	0.6	2.7	2.8	2.0	3.6	3.7	0.6	2.9	29.3	0.3
1403	9.3	18.4	10.6	6.6	5.6	3.1	0.3	2.2	1.2	2.5	3.0	2.2	3.7	0.5	2.8	28.0	0.3
1404	11.6	18.2	10.7	7.5	5.0	2.0	2.4	1.1	1.1	2.4	1.7	3.3	3.4	0.5	1.6	27.4	0.3
1421	6.7	12.3	9.6	5.4	1.7	3.8	2.1	0.0	1.3	3.0	3.8	4.4	3.4	1.8	1.4	39.2	0.3
1422	5.9	18.4	7.0	6.3	4.4	1.0	2.0	1.0	0.9	2.8	3.4	4.0	3.1	1.8	2.4	35.7	0.3
1634	0.0	8.9	10.4	7.3	7.3	7.4	2.8	4.2	2.6	3.6	3.8	4.0	3.0	1.8	4.0	29.1	0.3
1635	0.0	9.4	10.5	7.2	7.3	6.7	3.6	3.4	2.7	3.7	3.8	4.0	3.0	1.0	4.0	29.5	0.3
1643	0.0	8.3	9.4	9.7	8.2	7.1	4.7	3.7	3.1	2.6	3.7	3.8	2.8	1.8	1.7	29.2	0.3
1644	0.0	5.6	11.9	7.5	9.5	7.3	5.1	4.1	3.4	2.7	3.8	3.8	2.6	1.9	2.8	28.1	0.3
1702	0.0	0.0	4.3	5.9	10.3	8.9	5.6	6.2	5.3	3.2	4.3	2.9	3.0	3.0	3.2	33.7	0.4
1703	0.0	0.0	3.2	7.0	10.1	6.8	9.4	3.7	6.5	3.3	2.9	4.4	1.7	4.2	3.3	33.6	0.4
1721	0.0	0.0	0.0	0.0	0.0	10.7	3.8	1.4	4.6	2.5	2.6	6.3	4.7	0.0	0.0	63.4	0.6
1722	0.0	0.0	0.0	0.0	1.9	3.0	6.5	1.0	4.5	2.3	2.4	6.6	5.1	0.0	0.0	66.6	0.6
1743	0.0	0.0	0.0	6.3	7.3	9.3	9.0	6.9	7.0	4.7	5.2	3.4	3.2	3.0	3.0	31.6	1.8
1744	0.0	0.0	0.0	5.3	8.3	9.0	8.9	6.9	7.0	4.7	5.3	3.5	3.4	3.1	3.1	31.6	1.8
1803	0.0	0.0	5.0	8.1	11.8	10.6	9.8	7.6	7.8	6.6	2.8	3.1	5.4	3.0	2.8	15.6	5.0
1804	0.0	0.7	4.0	9.7	11.2	10.0	11.5	6.6	7.3	6.6	2.2	4.2	3.9	3.1	2.9	16.1	5.0
1824	0.0	5.2	11.8	12.5	13.9	10.2	11.1	5.9	7.0	3.2	2.7	1.7	1.4	3.3	3.6	6.3	8.1
1825	0.0	6.0	11.5	12.3	12.3	12.4	9.6	7.3	6.0	3.7	2.7	1.8	1.9	2.2	4.7	5.6	8.1
1843	0.0	10.6	15.3	15.7	13.9	11.0	9.0	4.5	4.9	2.7	1.2	0.7	1.9	3.2	1.3	4.1	10.5
1844	0.0	11.3	17.1	15.8	14.0	10.7	8.5	4.2	5.0	1.7	1.6	0.3	1.6	3.1	2.0	3.1	10.5
1903	1.0	19.0	19.6	16.7	12.9	8.0	5.7	4.6	2.4	2.1	0.6	0.2	0.9	2.5	1.5	2.3	11.0
1904	3.7	22.1	20.1	16.4	10.5	7.9	4.7	3.0	3.6	0.8	0.0	0.9	1.6	0.4	1.3	3.0	11.0
1943	36.4	51.3	0.0	0.0	0.0	0.0	0.0	0.0	0.0	0.0	0.0	1.0	1.2	4.5	0.0	5.7	16.5
1944	42.1	39.7	9.0	0.0	0.0	0.0	0.0	0.0	0.0	0.0	0.4	1.1	1.0	0.0	2.7	4.1	16.5
1945	43.9	40.4	7.3	0.0	0.0	0.0	0.0	0.0	0.0	0.0	0.0	0.7	2.5	0.0	2.1	3.1	16.5
1946	43.0	47.8	0.0	0.0	0.0	0.0	0.0	0.0	0.0	0.0	0.3	1.1	1.0	0.0	2.7	4.1	16.5
2001	82.4	0.0	0.0	0.0	0.0	0.0	0.0	0.0	0.0	0.0	0.0	1.9	2.0	1.8	0.0	11.9	16.9
2002	81.6	0.0	0.0	0.0	0.0	0.0	0.0	0.0	0.0	0.0	0.0	2.1	2.2	5.7	0.0	8.4	16.9
2003	82.6	0.0	0.0	0.0	0.0	0.0	0.0	0.0	0.0	0.0	0.0	1.6	5.0	0.0	1.3	9.5	16.9

June 28 lowest profile data

time	ht	S	U	dir	C	temp
908	0.5	0.5	0.20	155	120	17.4
923	0.5	0.4	0.33	160	120	17.4
940	0.5	0.5	0.30	160	200	17.4
1000	0.3	0.5	0.45	160	350	17.8
1020	0.3	0.7	0.45	155	520	18.0
1040	0.2	1.3	0.45	155	450	18.2
1100	0.4	3.0	0.50	155	370	18.5
1120	0.2	5.2	0.25	160	160	18.7
1140	0.5	6.9	0.30	160	120	18.8
1200	0.5	8.1	0.28	160	80	18.9
1223	0.6	9.0	0.20	175	40	18.9
1240	0.2	9.5	0.10	210	50	18.9
1320	0.5	11.7	0.30	170	40	19.0
1340	0.5	12.7	0.17	190	35	19.0
1420	0.3	13.5	0.05	175	25	19.1
1445	0.3	13.6	0.10	140	25	19.1
1500	0.6	13.4	0.05	150	20	19.1
1520	0.6	13.7	0.05	130	20	19.1
1540	0.4	13.6	-0.05	15	20	19.1
1600	0.2	13.1	-0.08	10	25	19.1
1619	0.5	11.3	-0.15	330	25	19.1
1639	0.2	9.7	-0.15	330	45	18.9
1700	0.5	6.9	-0.25	340	45	18.7
1720	0.3	4.0	-0.47	335	110	18.5
1741	0.6	1.1	-0.45	350	150	17.9
1801	0.5	0.6	-0.50	350	190	17.7
1821	0.2	0.5	-0.45	335	240	17.5
1840	0.5	0.5	-0.40	345	220	17.4
1900	0.3	0.5	-0.45	340	220	17.3
1920	0.2	0.5	-0.30	350	200	17.3

June 29 lowest profile data

time	ht	S	U	dir	C	temp
1005	0.3	0.5	0.22	170	150	16.5
1020	0.5	0.5	0.30	160	120	16.6
1040	0.3	0.5	0.30	175	150	16.8
1059	0.6	0.5	0.45	150	220	16.8
1119	0.5	0.5	0.45	160	360	17.1
1142	0.4	0.7	0.45	155	520	17.4
1200	0.3	2.0	0.45	150	400	17.8
1220	0.5	4.0	0.40	160	270	18.2
1234	0.3	5.9	0.25	160	180	18.4
1256	0.5	7.5	0.30	160	130	18.6
1320	0.2	9.1	0.25	160	90	18.7
1342	0.3	10.8	0.15	140	80	18.7
1403	0.4	11.8	0.10	170	35	18.8
1420	0.4	12.4	0.14	160	30	18.8
1443	0.4	13.0	0.07	155	35	18.9
1500	0.5	13.4	0.10	165	30	18.9
1521	0.4	13.7	0.05	160	30	18.9
1541	0.4	14.0	0.10	160	10	18.9
1600	0.4	14.1	0.00	120	10	18.9
1620	0.2	14.1	0.00	0	15	18.8
1640	0.6	13.7	-0.10	340	15	18.8
1703	0.3	12.9	-0.04	2	10	18.8
1720	0.2	12.3	-0.02	350	10	18.8
1740	0.5	11.2	-0.02	350	20	18.7
1800	0.3	10.4	-0.03	330	30	18.7
1821	0.5	8.4	-0.22	340	25	18.6
1839	0.3	3.8	-0.35	330	95	18.3
1900	0.6	1.8	-0.40	340	150	18.2
1920	0.3	0.8	-0.35	350	240	18.0
1940	0.6	0.6	-0.33	340	250	17.8
2001	0.4	0.5	-0.37	340	240	17.7
2022	0.3	0.5	-0.28	345	230	17.6
2039	0.6	0.5	-0.35	330	200	17.6

July 4 lowest profile data

time	ht	S	U	dir	C	temp
840	0.3	13.4	-0.10	340	40	19.5
859	0.6	12.3	-0.05	335	50	19.5
920	0.5	11.3	-0.02	345	35	19.5
945	0.2	10.7	-0.02	345	30	19.4
1000	0.5	8.9	-0.10	330	35	19.4
1019	0.4	7.3	-0.11	340	50	19.4
1040	0.5	4.3	-0.35	330	85	19.4
1059	0.3	2.8	-0.40	345	140	19.3
1121	0.5	1.3	-0.45	345	270	19.2
1140	0.2	0.9	-0.40	330	340	19.2
1201	0.5	0.7	-0.35	330	390	19.2
1220	0.3	0.6	-0.40	340	430	19.2
1242	0.6	0.6	-0.33	330	400	19.3
1300	0.3	0.6	-0.30	330	420	19.0
1320	0.2	0.5	-0.28	330	410	19.0
1340	0.2	0.5	-0.17	320	350	19.0
1400	0.5	0.5	-0.20	320	310	19.1
1420	0.4	0.5	-0.12	340	280	19.2
1500	0.4	0.5	-0.05	340	250	19.6
1525	0.3	0.5	0.00	280	270	19.7
1541	0.5	0.5	0.10	180	300	20.0
1600	0.3	0.5	0.40	160	410	20.2
1622	0.4	0.6	0.85	160	1000	20.4
1641	0.5	0.8	0.95	160	1000	20.8
1700	0.5	1.9	0.80	150	1000	21.1
1722	0.4	5.0	0.70	160	840	21.2
1736	0.5	7.7	0.50	155	720	21.0
1800	0.5	10.6	0.30	160	430	21.0
1820	0.3	13.0	0.15	155	360	20.9
1841	0.4	14.6	0.18	155	160	20.9
1900	0.5	15.2	0.07	160	140	20.9
1920	0.5	15.7	0.02	160	140	20.8
1940	0.3	16.0	0.12	165	100	20.8
1959	0.5	16.4	0.07	162	90	20.8
2020	0.4	16.6	0.00	180	120	20.8

July 5 lowest profile data

time	ht	S	U	dir	C	temp
941	0.2	13.7	-0.05	330	20	20.1
1000	0.6	11.8	-0.10	350	50	20.1
1020	0.3	10.6	-0.12	335	25	20.1
1040	0.6	9.1	-0.18	340	30	20.1
1100	0.4	6.8	-0.17	342	55	20.2
1120	0.6	4.7	-0.35	340	70	20.2
1140	0.4	3.1	-0.48	348	130	20.2
1200	0.6	1.7	-0.50	350	230	20.1
1221	0.3	1.1	-0.43	350	310	20.0
1240	0.6	0.9	-0.40	345	410	20.0
1300	0.4	0.7	-0.29	350	410	20.0
1320	0.2	0.6	-0.25	345	430	19.9
1340	0.4	0.5	-0.40	340	390	19.7
1400	0.4	0.6	-0.20	350	450	19.5
1420	0.2	0.5	-0.18	340	380	19.4
1442	0.2	0.5	-0.18	345	370	19.2
1500	0.5	0.5	-0.15	340	340	19.2
1520	0.3	0.5	-0.10	330	310	19.1
1543	0.3	0.5	-0.11	330	310	19.1
1600	0.3	0.5	-0.10	330	290	19.2
1620	0.5	0.5	0.18	160	340	19.4
1640	0.3	0.5	0.50	155	470	19.6
1700	0.5	0.6	0.75	160	950	19.9
1720	0.5	0.9	0.85	160	1000	20.3
1740	0.2	2.2	0.65	155	950	20.4
1803	0.6	5.9	0.70	160	630	20.4
1823	0.4	8.9	0.45	160	600	20.4
1841	0.5	11.4	0.35	155	500	20.4
1900	0.2	14.0	0.13	155	350	20.4
1920	0.5	15.7	0.22	165	50	20.4
1941	0.6	16.5	0.10	165	50	20.4
2000	0.6	16.8	0.05	190	40	20.4

June 28th variances

T	U	u0	u1	u2	u3	c4	c5
1240	8.8	5.6	4.7	8.8	3.9	0.0	-9
1340	16.8	144.3	76.7	44.2	104.2	0.0	0.0
1350	14.4	15.2	12.5	8.9	7.3	0.0	0.0
1500	3.6	3.6	5.6	6.5	2.9	0.4	0.4
1510	3.0	1.7	7.2	6.8	2.2	6.7	0.6
1520	5.5	2.1	5.3	6.2	2.2	3.6	0.8
1530	5.1	2.3	5.2	5.9	2.5	0.4	0.4
1540	6.6	2.3	5.2	5.9	2.5	0.4	0.4
1600	11.9	2.9	6.8	8.0	3.2	4.7	0.4
1619	14.0	3.6	6.9	9.3	5.7	3.4	1.6
1639	15.1	3.6	6.8	27.2	11.0	3.5	1.9
1645	14.8	2.9	6.2	17.9	7.2	3.1	1.6
1652	14.7	3.1	5.7	21.9	8.8	2.9	1.5
1700	15.4	3.3	6.8	28.8	8.9	2.9	1.5
1707	16.4	4.8	7.4	44.1	18.2	5.5	3.1
1714	21.9	21.9	39.7	160.2	84.1	23.5	7.7
1720	28.5	66.4	68.7	356	204	121.0	41.7
1727	38.1	31.2	50.6	173.5	38.3	339	66.0
1735	37.9	21.0	22.8	180.3	35.2	53.2	9.8
1741	37.9	36.0	124.6	309	39.8	33.0	9.9
1748	37.1	29.7	163.5	346	35.6	38.2	11.6
1755	40.2	42.9	305	552	55.7	38.3	17.1
1801	39.8	2900	3400	2600	2100	33.7	13.7
1815	40.0	459	548	1821	449	77.8	33.6
1821	38.6	46.2	100.8	973	82.3	74.2	35.4
1829	37.3	39.3	61.4	912	79.8	70.2	28.2
1840	37.3	34.7	32.4	875	84.0	64.2	25.7
1900	34.1	28.5	37.4	591	60.2	138.5	69.6

June 29th variances

T	U	u0	u1	u2	u3	c4	c5
1020	22.5	25.4	44.7	57.7	10.4	44.9	1.0
1030	28.8	52.8	57.2	63.1	22.3	23.8	1.8
1040	30.6	45.4	50.0	59.2	29.9	22.7	7.0
1047	32.4	1560	497	5e4	7600	23.9	2.8
1059	38.6	272	137.7	1e4	1400	63.6	43.5
1107	42.4	624	319	3e4	3400	91.2	51.3
1113	41.7	957	757	3e4	3400	2200	58.7
1119	45.9	347	246	2e4	1900	184.3	10.3
1140	48.0	251	276	2e4	263.4	5e4	268
1148	45.2	434	178.5	7600	52.4	155.2	214
1200	46.5	186.1	105.0	1900	92.2	221	325
1207	44.6	169.7	72.5	1530	96.3	207.3	300
1213	46.1	812	127.1	8300	489	428	458
1220	43.2	416	71.9	3370	256	293	296
1226	40.5	442	89.2	3060	288	206	183.6
1234	37.8	136.8	40.2	838	89.8	336	173.8
1240	37.3	257	691.0	1650	172.0	786	351
1250	35.0	180.8	45.8	1170	132.0	702	162.1
1256	32.5	465	55.3	3070	318	1790	209
1327	28.1	150.2	41.4	1270	124.2	2850	15.6
1336	24.4	273.4	134.4	1480	171.4	6140	5.5
1342	24.4	206	160.3	891	177.7	3900	3.45
1349	21.7	27.6	58.4	248	38.8	2e4	15.7
1355	23.6	28.5	33.5	342	44.7	6200	252
1401	18.5	16.6	52.1	60.8	15.2	1e4	2.59
1409	17.3	16.6	44.6	82.6	19.5	1e4	1.64
1430	21.1	7.5	28.6	20.9	10.9	1e4	199.8
1443	17.3	6.2	13.7	6.2	3.6	3e4	1760
1450	16.3	3.6	18.0	9.4	2.8	2e4	124.6
1500	17.5	7.6	28.2	82.6	18.1	8500	72.8
1632	10.8	76.0	76.7	11.8	82.8	4.6	4.2
1640	11.4	3.3	5.0	5.3	3.7	0.4	0.6
1651	11.7	2.1	4.3	4.8	2.8	0.4	0.7
1702	10.4	2.8	5.4	5.6	4.1	1.1	1.8
1714	11.6	15.9	24.4	318	28.9	1.9	2.4
1720	10.8	31.9	37.9	680	52.9	2.0	2.5
1730	4.5	52.9	68.0	1270	86.1	1.69	3.8
1740	5.8	38.2	50.2	895	56.5	2.0	4.3
1747	8.6	73.6	101.2	2100	102.6	1.4	2.2
1821	19.8	12.9	51.9	150.1	15.3	1.3	2.2
1827	25.0	66.7	170.2	1200	73.8	13.2	15.2
1833	28.5	79.3	85.9	158.7	86.0	221.7	268.7
1839	35.6	87.5	72.5	130.4	84.9	591	328
1852	38.6	22.8	15.0	22.5	22.8	18.5	16.2
1900	39.2	23.1	20.2	27.9	29.4	781	22.2
1906	40.4	33.2	23.0	38.6	32.6	31.0	23.1
1915	40.8	35.2	28.5	41.5	41.3	114.2	115.5
1920	44.3	34.7	32.9	61.8	41.3	59.2	51.2
1928	41.8	48.4	46.8	72.3	49.6	152.0	168.7
1934	41.0	31.2	24.0	48.6	37.8	78.2	73.5
1940	39.8	49.4	84.9	204	54.5	57.3	56.2
1948	38.7	33.4	168.6	196.5	39.6	103.7	119.2
1954	39.5	255	290	1e4	1350	2630	174.9
2001	36.9	397	289	2e4	2240	60.2	76.2
2008	36.2	113.5	148.5	3400	518	76.8	96.2
2015	35.0	212	236	389	75.6	103.9	95.5
2022	35.9	39.4	98.1	755	117.9	55.1	61.9
2028	33.7	21.3	42.9	96.6	31.1	79.3	82.5
2039	31.5	17.2	14.0	36.5	16.7	61.5	72.9

July 4th variances

T	U	u0	u1	u2	u3	c4	c5
0854	10.1	3.0	28.2	7.8	5.5	3.2	5.4
0859	10.4	2.4	26.0	8.2	2.3	3.3	5.0
0911	7.6	1.0	18.8	1.8	1.0	19.4	14.7
0920	6.6	1.4	7.6	1.7	1.1	1.7	13.1
0945	13.2	39.0	36.3	24.2	31.4	3.9	3.4
0953	13.0	4.8	7.2	9.3	2.0	1.7	1.9
1000	13.6	3.4	9.6	10.1	3.1	1.4	1.5
1011	12.5	5.2	10.4	9.6	5.5	1.6	2.3
1019	17.1	16.6	737	149.9	32.4	2.6	2.9
1034	28.3	37.9	1900	970	70.1	276	103.7
1040	32.8	113.2	2470	2870	189.3	117.8	241
1051	45.2	96.5	1640	2020	181.7	55.5	35.5
1059	48.5	316	6340	1e4	623	37.9	27.8
1110	49.2	307	255	212.2	240.4	54.8	54.8
1121	48.2	436	58.2	46.7	42.5	44.8	9810
1130	47.5	37.4	46.6	47.1	42.9	43.1	1280
1140	47.1	34.4	77.7	43.0	33.6	172.7	619
1201	43.3	44.69	122.9	86.8	29.4	116.6	703.1
1211	44.5	43.5	132.6	101.8	44.7	133.7	453
1220	39.5	30.2	90.3	42.8	25.9	253.4	570
1300	31.5	23.2	79.4	61.2	16.9	158.6	567
1307	29.7	17.0	112.0	49.6	22.4	146.9	592
1314	27.1	14.0	73.0	38.2	13.8	57.8	141.1
1320	27.2	17.3	79.3	69.7	15.5	71.69	188.8
1330	27.0	22.8	93.1	69.3	15.3	66.8	179.0
1340	25.4	13.9	83.8	40.4	13.4	21.4	146.3
1400	21.9	13.0	453	82.6	9.8	14.4	91.2
1413	18.9	251	370	188.2	44.2	9.6	505
1420	18.9	19.4	418	87.4	15.3	10.8	65.0
1541	27.3	444	52.8	196.0	22.8	647	30.6
1550	28.5	231	100.7	117.1	157.2	68.9	60.1
1600	44.6	63.7	53.1	102.6	38.3	5650	326
1606	56.7	88.9	72.5	132.9	71.5	522	582
1613	66.7	125.3	108.3	142.3	131.9	5400	452
1620	67.3	146.9	118.0	134.8	119.4	940	659
1628	72.1	93.7	68.1	93.2	86.5	1e4	0.0
1646	62.8	188.3	646	921	68.7	19.8	95.7
1653	57.9	101.5	994	130.2	60.4	191.4	71.0
1700	57.0	86.0	1170	92.6	140.4	1310	58.4
1707	57.6	95.9	39.8	57.1	53.1	41.1	165.2
1714	51.6	66.5	33.8	45.3	39.8	79.7	204
1721	51.5	54.5	33.2	385	2910	17.9	261
1728	45.5	39.8	30.2	30.8	603	18.9	275
1736	39.3	34.3	31.6	41.1	37.3	26.2	232
1751	28.9	22.4	43.6	590	37.6	18.9	127.3
1800	26.6	23.5	50.0	39.0	83.9	279	152.8
1816	16.0	10.3	8.6	11.6	79.5	17.6	117.2
1822	15.0	7.2	12.3	14.1	6.8	2.1	65.3
1830	12.6	5.8	7.3	10.8	3.8	64.0	80.8
1835	12.9	5.7	8.3	10.3	4.4	3.6	70.2
1841	11.3	5.7	7.1	9.6	4.5	4.4	77.7
1848	9.6	4.9	18.6	9.0	3.6	770	4450
1854	9.5	3.0	5.8	8.2	2.1	341	1040
1905	8.6	3.0	5.3	8.2	2.0	861	0.0
1913	8.5	2.6	4.8	7.8	1.3	20.4	0.0
1926	7.7	2.9	6.5	7.4	1.1	40.9	0.5
1933	8.2	2.6	5.1	7.2	1.2	4.6	0.1
1940	8.8	2.7	5.1	6.9	1.5	53.1	0.3
1948	8.4	2.9	5.7	7.2	1.8	140	0.8
1959	8.3	3.0	4.7	7.6	1.5	108	0.4
2011	7.9	2.8	4.7	7.6	1.7	2530	11.5
2020	7.4	2.7	5.0	7.5	1.3	5.1	2.5

July 5th Variances

T	U	u0	u1	u2	u3	c4	c5
0947	9.6	8.4	8.0	12.2	11.1	4.3	7.7
1000	15.8	5.4	8.2	7.0	4.5	4.4	8.5
1010	16.5	6.0	8.1	7.9	3.4	4.1	5.8
1019	16.5	5.1	7.3	6.2	3.8	4.3	6.8
1026	18.0	4.3	7.2	6.6	2.6	2.3	2.8
1034	19.3	4.2	7.6	6.3	2.5	1.7	3.0
1040	19.1	5.2	7.4	5.9	2.2	1.7	2.5
1046	20.4	11.1	11.4	7.5	4.3	1.8	2.9
1053	20.0	12.4	11.2	8.2	4.4	3.6	5.6
1100	22.5	28.0	346	17.5	10.9	3.6	3.8
1110	26.5	22.7	22.4	18.1	10.2	7.1	9.7
1113	30.7	24.4	23.8	26.5	11.8	38.7	30.4
1119	33.9	43.4	27.3	19.9	19.8	121.1	72.6
1130	49.5	45.6	25.2	22.6	30.3	30.1	23.5
1150	49.6	32.3	27.3	26.1	29.5	52.2	29.1
1200	52.8	42.7	34.1	31.4	32.2	32.4	30.4
1210	51.9	153.4	380.6	392.7	178.8	54.6	74.4
1217	50.5	483	687	740	427	49.2	62.5
1223	52.5	978	1130	922	600	56.5	74.4
1230	51.3	355	458	404	214	118	115
1236	49.1	56.4	95.2	127.3	35.3	86.0	98.4
1300	44.1	38.4	38.2	37.6	35.0	203.6	105
1306	40.1	28.8	30.7	36.2	23.2	296	157.4
1320	39.8	84.9	308	184.0	44.0	180.3	111.2
1340	36.1	28.3	73.7	33.9	19.0	213	58.2
1350	31.9	42.6	114.4	94.9	33.1	236	122.1
1359	30.4	33.0	107.5	43.3	16.3	344	121.7
1410	29.5	37.2	142.4	62.9	19.7	305	90.5
1430	26.1	1220	490	263	540	298	29.5
1442	24.1	20.8	86.3	45.2	4.7	363	19.6
1450	24.2	78.6	108.9	44.3	38.1	280	17.7
1501	19.1	162.2	56.9	72.1	88.1	702	19.2
1632	29.0	118.6	82.5	96.9	127.8	51.1	81.0
1640	41.9	75.2	105.0	161.4	57.4	219.6	308.2
1647	56.3	193.8	203.8	240.8	139.4	427.4	629.5
1654	68.7	97.5	124.1	193.1	90.3	4770	369
1700	77.2	177.8	190.1	233.7	75.6	771	430
1706	76.7	169.3	83.7	115.4	80.2	1520	404
1712	75.9	91.4	96.9	103.3	106.7	3110	634
1719	74.1	82.6	132.1	108.4	162.3	1870	2800
1725	72.3	110.5	248	96.8	70.6	0.0	1790
1731	70.5	184.9	212	139.8	82.2	115.6	7.6
1740	65.1	890	153.9	442.1	170.8	68.7	17.1
1748	60.8	291	116.0	105.6	103.4	108.8	42.7
1755	55.5	63.0	44.7	60.5	103.2	44.0	55.9
1801	56.3	69.1	82.1	114.5	50.4	30.3	83.6
1808	50.4	74.5	109.1	149.1	117.0	23.0	19.0
1815	42.8	47.9	60.0	209	500	20.8	40.1
1821	41.5	37.3	27.8	32.5	285	14.8	2.9
1830	36.8	31.8	28.4	53.7	734	34.7	9.2
1838	31.8	23.9	306	38.9	781	43.0	6.4
1850	25.2	19.7	9.4	63.0	10.2	35.9	6.2
1858	19.6	12.8	38.4	109.8	43.4	32.7	9.1
1906	16.9	6.3	7.0	23.1	46.7	64.0	32.1
1914	16.3	7.0	7.1	27.5	74.1	43.7	3.4
1920	16.5	6.6	6.7	19.0	56.4	58.0	4.7
1947	15.7	4.7	4.7	6.0	42.8	0.1	0.1
1959	9.8	3.6	4.8	5.5	25.6	0.0	0.1

June 28th 1989

time	vol.	mass	temp.	salt	SPM	Ri	U|av	d_S	ht.
908	0.45	0.45	0.66	0.22	50.5	0.00	0.22	0.0	2.0
923	0.67	0.68	0.94	0.27	76.5	0.00	0.34	0.0	2.0
940	1.09	1.09	1.52	0.54	195.2	0.00	0.43	0.0	2.5
1000	1.71	1.71	3.02	0.85	515.0	0.00	0.61	0.0	2.8
1020	2.18	2.19	4.37	1.53	838.4	0.00	0.66	0.0	3.3
1040	2.56	2.56	5.64	3.00	757.2	0.01	0.69	-0.3	3.7
1100	2.55	2.56	6.17	6.85	638.8	0.05	0.66	-0.8	3.9
1120	2.26	2.27	6.00	11.05	329.2	0.07	0.54	-0.8	4.2
1140	1.84	1.85	5.11	12.05	162.5	0.14	0.41	-0.8	4.5
1200	1.41	1.42	4.10	11.14	84.5	0.17	0.31	-0.6	4.5
1223	0.73	0.74	2.12	6.35	30.0	0.69	0.16	-0.6	4.6
1240	0.30	0.30	0.87	2.78	10.6	4.97	0.06	-0.7	4.7
1320	0.73	0.73	2.17	7.79	21.4	3.76	0.15	-2.5	5.0
1340	0.62	0.62	1.83	7.08	15.2	9.15	0.12	-4.4	5.0
1420	-0.24	-0.24	-0.65	-0.95	-11.1	83.42	-0.05	-6.2	4.8
1445	-0.55	-0.55	-1.52	-3.36	-18.6	17.19	-0.11	-7.1	4.8
1500	-0.62	-0.62	-1.73	-4.20	-23.1	13.28	-0.13	-7.9	4.6
1520	-0.93	-0.93	-2.61	-6.54	-34.2	6.63	-0.20	-9.0	4.6
1540	-1.33	-1.34	-3.77	-10.13	-51.5	2.86	-0.30	-9.2	4.4
1600	-1.48	-1.49	-4.11	-9.95	-64.0	2.03	-0.35	-9.3	4.2
1619	-1.62	-1.62	-4.18	-8.95	-72.6	1.30	-0.40	-8.2	4.0
1639	-1.55	-1.55	-3.92	-6.99	-73.2	0.89	-0.42	-6.5	3.7
1700	-1.40	-1.40	-3.45	-5.37	-71.9	0.69	-0.40	-4.9	3.5
1720	-1.66	-1.66	-3.75	-4.46	-134.7	0.14	-0.50	-1.6	3.3
1741	-1.64	-1.64	-3.24	-1.91	-218.5	-0.01	-0.53	0.1	3.1
1801	-1.51	-1.51	-2.49	-0.97	-284.3	-0.01	-0.50	0.1	3.0
1821	-1.47	-1.47	-2.20	-0.73	-288.7	0.00	-0.54	0.0	2.7
1840	-1.09	-1.09	-1.52	-0.54	-211.6	0.00	-0.44	0.0	2.5
1900	-1.12	-1.12	-1.46	-0.56	-200.7	0.00	-0.49	0.0	2.3
1920	-0.96	-0.96	-1.17	-0.48	-160.0	0.00	-0.44	0.0	2.2

June 29th 1989

time	vol.	mass	temp.	salt	SPM	Ri	U|av	d_S	ht.
1005	0.40	0.40	0.20	0.20	56.6	0.00	0.22	0.0	1.8
1020	0.62	0.63	0.37	0.31	78.1	0.00	0.31	0.0	2.0
1040	0.76	0.76	0.61	0.38	118.6	0.00	0.33	0.0	2.3
1059	1.11	1.11	0.89	0.56	241.9	0.00	0.43	0.0	2.6
1119	1.60	1.60	1.76	0.80	473.7	0.00	0.53	0.0	3.0
1142	2.11	2.12	2.96	1.48	797.3	0.00	0.62	0.0	3.4
1200	2.38	2.39	4.24	4.19	738.7	0.03	0.63	-0.5	3.8
1220	2.25	2.26	4.90	8.51	431.0	0.04	0.56	-0.5	4.0
1234	1.86	1.87	4.47	10.42	282.2	0.09	0.43	-0.6	4.3
1256	1.72	1.73	4.48	12.63	179.2	0.12	0.38	-0.6	4.5
1320	1.37	1.38	3.71	12.03	109.0	0.32	0.29	-0.9	4.7
1342	0.69	0.70	1.92	7.11	43.3	2.18	0.14	-1.5	4.8
1403	0.35	0.35	0.98	4.06	12.8	12.65	0.07	-2.1	4.9
1420	0.32	0.32	0.88	3.83	9.3	19.89	0.06	-2.7	4.9
1443	0.16	0.16	0.45	1.99	4.8	117.93	0.03	-4.0	4.9
1500	0.17	0.17	0.49	2.27	4.9	110.53	0.03	-4.2	5.0
1521	-0.08	-0.08	-0.25	-0.21	-4.5	766.59	-0.02	-5.7	4.9
1541	-0.14	-0.14	-0.46	-0.35	-3.7	309.22	-0.03	-6.9	4.9
1600	-0.40	-0.40	-1.23	-2.94	-9.8	36.44	-0.08	-7.5	4.9
1620	-0.73	-0.73	-2.23	-6.31	-17.8	10.38	-0.15	-8.1	4.7
1640	-1.40	-1.41	-4.06	-11.60	-35.5	2.79	-0.30	-8.7	4.6
1703	-1.34	-1.35	-3.88	-9.49	-33.7	2.41	-0.31	-8.4	4.3
1720	-1.28	-1.29	-3.65	-8.20	-48.8	2.30	-0.31	-7.9	4.2
1740	-1.19	-1.19	-3.27	-6.91	-51.6	2.25	-0.30	-7.6	4.0
1800	-1.08	-1.08	-2.80	-5.58	-49.8	2.00	-0.28	-6.5	3.8
1821	-1.31	-1.31	-3.24	-5.83	-53.7	0.82	-0.37	-5.0	3.5
1839	-1.67	-1.68	-3.85	-5.60	-110.7	0.07	-0.51	-0.8	3.3
1900	-1.44	-1.44	-3.12	-2.58	-196.3	0.00	-0.46	0.0	3.1
1920	-1.33	-1.33	-2.67	-1.07	-290.7	0.00	-0.48	0.0	2.8
1940	-1.11	-1.11	-1.99	-0.66	-211.9	0.00	-0.43	0.0	2.6
2001	-1.02	-1.02	-1.73	-0.51	-208.2	0.00	-0.42	0.0	2.4
2022	-0.80	-0.80	-1.29	-0.40	-104.8	0.00	-0.35	0.0	2.3
2039	-0.70	-0.70	-1.12	-0.35	-126.0	0.00	-0.33	0.0	2.1

July 4th 1989

time	vol.	mass	temp.	salt	SPM	Ri	U|av	d_S	ht.
840	-1.43	-1.43	-4.88	-13.74	-57.0	1.98	-0.30	-5.6	4.8
859	-1.33	-1.33	-4.52	-11.37	-58.9	1.72	-0.29	-4.8	4.6
920	-1.10	-1.10	-3.75	-8.35	-48.7	2.36	-0.24	-4.8	4.5
945	-1.18	-1.19	-4.03	-7.59	-56.6	1.72	-0.28	-5.0	4.2
1000	-1.28	-1.28	-4.33	-7.46	-61.6	1.17	-0.32	-4.6	4.0
1019	-1.38	-1.39	-4.71	-6.87	-79.3	0.58	-0.35	-2.9	3.9
1040	-1.39	-1.39	-4.74	-5.50	-105.9	0.07	-0.40	-0.5	3.5
1059	-1.66	-1.66	-5.52	-4.50	-224.1	0.01	-0.50	-0.1	3.3
1121	-1.59	-1.59	-5.08	-2.07	-409.6	0.01	-0.53	-0.1	3.0
1140	-1.36	-1.36	-4.34	-1.22	-436.8	0.00	-0.50	0.0	2.7
1201	-1.18	-1.18	-3.86	-0.83	-435.5	0.01	-0.47	-0.1	2.5
1220	-1.07	-1.07	-3.42	-0.64	-433.9	0.00	-0.47	0.0	2.3
1242	-0.78	-0.78	-2.57	-0.47	-316.6	0.00	-0.37	0.0	2.1
1300	-0.70	-0.70	-2.17	-0.39	-267.4	0.01	-0.39	-0.1	1.8
1320	-0.50	-0.50	-1.50	-0.25	-196.0	0.00	-0.29	0.0	1.7
1340	-0.40	-0.40	-1.20	-0.20	-132.8	0.00	-0.24	0.0	1.7
1400	-0.38	-0.38	-1.20	-0.19	-118.6	0.00	-0.26	0.0	1.5
1420	-0.22	-0.22	-0.71	-0.11	-62.7	0.00	-0.15	0.0	1.5
1500	-0.11	-0.11	-0.40	-0.05	-26.9	0.00	-0.08	0.0	1.4
1525	0.00	0.00	0.00	0.00	0.0	0.00	0.00	0.0	1.3
1541	0.20	0.20	0.80	0.10	58.5	0.00	0.13	0.0	1.5
1600	0.71	0.71	2.97	0.35	273.6	0.00	0.39	0.0	1.8
1622	2.30	2.30	9.96	1.38	2250.0	0.00	0.96	0.0	2.4
1641	2.45	2.45	11.76	1.96	2450.0	0.00	0.98	0.0	2.5
1700	3.82	3.83	19.42	6.57	3060.7	0.01	0.96	-0.4	4.0
1722	3.49	3.50	18.16	16.06	2175.6	0.03	0.90	-0.8	3.9
1736	3.64	3.66	18.37	26.85	1884.5	0.07	0.73	-1.1	5.0
1800	3.02	3.04	15.11	30.45	940.8	0.11	0.60	-1.2	5.0
1820	2.10	2.12	10.34	26.59	449.7	0.22	0.40	-1.0	5.3
1841	1.34	1.35	6.54	19.03	180.7	0.62	0.25	-1.1	5.4
1900	0.33	0.33	1.62	4.89	46.6	9.53	0.06	-1.0	5.5
1920	-0.01	-0.01	-0.04	0.08	-0.9	563157.48	-0.00	-2.1	5.5
1940	0.08	0.08	0.38	1.69	6.5	566.45	0.01	-3.2	5.8
1959	0.04	0.04	0.17	1.34	3.5	2331.63	0.01	-4.5	5.5
2020	-0.51	-0.51	-2.51	-6.11	-52.2	21.93	-0.09	-5.5	5.4

July 5th 1989

time	vol.	mass	temp.	salt	SPM	Ri	U|av	d_S	ht.
941	-1.68	-1.69	-6.96	-16.22	-61.7	1.28	-0.36	-5.4	4.7
1000	-1.54	-1.55	-6.41	-12.80	-93.9	1.22	-0.33	-4.6	4.6
1020	-1.31	-1.31	-5.46	-9.86	-56.2	1.18	-0.30	-3.9	4.3
1040	-1.24	-1.25	-5.20	-8.11	-56.3	1.08	-0.30	-3.7	4.1
1100	-1.37	-1.38	-5.77	-7.55	-82.0	0.35	-0.35	-1.7	3.9
1120	-1.44	-1.44	-6.04	-6.57	-96.8	0.09	-0.40	-0.6	3.6
1140	-1.83	-1.84	-7.70	-5.78	-212.3	-0.01	-0.54	0.1	3.4
1200	-1.66	-1.66	-6.79	-2.82	-340.3	0.00	-0.53	0.0	3.1
1221	-1.58	-1.58	-6.33	-1.74	-464.4	0.00	-0.56	0.0	2.8
1240	-1.29	-1.29	-5.14	-1.16	-477.4	0.00	-0.49	0.0	2.6
1300	-1.06	-1.06	-4.23	-0.74	-410.3	0.00	-0.44	0.0	2.4
1320	-0.94	-0.94	-3.66	-0.56	-373.5	0.00	-0.43	0.0	2.2
1340	-0.74	-0.74	-2.74	-0.37	-274.2	0.00	-0.39	0.0	1.9
1400	-0.56	-0.56	-2.01	-0.33	-215.4	0.00	-0.29	0.0	1.9
1420	-0.43	-0.43	-1.45	-0.21	-159.0	0.00	-0.25	0.0	1.7
1442	-0.35	-0.35	-1.11	-0.17	-120.4	0.00	-0.20	0.0	1.7
1500	-0.28	-0.28	-0.89	-0.14	-92.3	0.00	-0.19	0.0	1.5
1520	-0.19	-0.19	-0.60	-0.10	-57.6	0.00	-0.15	0.0	1.3
1543	-0.11	-0.11	-0.36	-0.06	-35.0	0.00	-0.09	0.0	1.3
1600	-0.17	-0.17	-0.54	-0.08	-48.6	0.00	-0.13	0.0	1.3
1620	0.28	0.28	0.94	0.14	98.1	0.00	0.19	0.0	1.5
1640	0.86	0.87	3.11	0.43	385.7	0.00	0.48	0.0	1.8
1700	2.16	2.16	8.45	1.30	1931.9	0.00	0.86	0.0	2.5
1720	3.50	3.50	15.06	3.15	3370.9	0.00	1.00	0.0	3.5
1740	4.18	4.18	17.60	8.37	2806.6	0.01	0.99	-0.5	4.2
1803	4.09	4.11	18.01	21.73	1481.6	0.06	0.89	-1.5	4.6
1823	3.96	3.98	17.43	33.56	1063.3	0.06	0.81	-1.2	4.9
1841	3.05	3.07	13.42	33.58	620.0	0.10	0.61	-1.2	5.0
1900	2.11	2.13	9.30	28.96	209.0	0.20	0.41	-1.0	5.2
1920	1.41	1.42	6.20	21.57	56.0	0.59	0.26	-1.1	5.5
1941	0.31	0.32	1.38	5.09	13.0	14.50	0.06	-1.3	5.6
2000	0.02	0.02	0.08	0.41	1.2	4880.34	0.00	-2.3	5.6
2000	0.02	0.02	0.08	0.41	1.2	4880.34	0.00	-2.3	5.6

Axial profile 6th July 1989

Station	km	C	S	T
Barge	7.6	35	9.3	19.9
ST2	6.8	50	7.6	20.0
Rock	6.3	50	6.4	20.0
ST3	5.7	65	5.0	19.9
ST4	4.9	90	3.3	19.7
ST5	4.1	150	1.6	19.7
Morwellham	3.6	190	1.0	19.6
Island	3.0	280	0.7	19.3
bend_above	*	335	0.4	19.4
Slimeford	1.9	410	0.3	19.1
MorwellRks	1.2	500	0.2	18.7
WeirHead	0.2	10	0.2	18.6
Weir	0.0	1	0.2	18.5

Axial profile 5th July 1988

Station	km	time	S	C	Z1	Z16
Narrows	31.0	0846	34.3	5	*	*
DkYdCorner	29.2	0858	34.1	5	*	*
Torpoint	28.2	0905	34.1	5	*	*
OilJetty	27.2	0910	33.5	5	*	*
LkGlassPt	26.4	0913	33.0	5	*	*
BullPt	24.8	0918	33.3	9	*	*
Bridge	23.9	0924	32.6	11	10.2	0.0
Time	*	0933	33.0	15	*	*
NealPt	21.5	0938	31.1	20	*	*
WeirPt	20.6	0944	32.0	25	10.1	15.4
Cargreen	19.9	0950	32.0	25	*	*
Time	*	0954	31.1	25	*	*
Pylons	18.1	0959	29.9	30	2.7	66.7
HolesHole	17.2	1006	29.9	35	*	*
SHooe	16.2	1012	29.5	40	18.7	0.5
SHooe	16.2	1013	29.5	40	13.9	33.3
Clifton	15.6	1016	28.8	45	*	*
PentQuay	14.2	1025	25.6	50	4.9	72.5
HaltonQy	13.3	1033	19.8	65	2.5	76.7
STR	11.6	1044	15.9	80	*	*
DeadTree	10.5	1051	13.3	90	23.4	45.4
Cotehele	9.9	1100	11.0	95	40.9	9.0
WhiteHorse	8.9	1107	4.5	145	44.2	14.3
Bridge1	8.5	1114	3.2	170	*	*
ST1	7.6	1117	2.0	185	58.5	5.9
ST2	6.8	1127	1.1	205	*	*
Rock	6.3	1134	0.6	230	33.7	13.5
ST3	5.7	1141	0.4	255	32.0	10.9
ST4	4.9	1148	0.3	275	32.5	9.5
ST5	4.1	1156	0.2	285	48.3	0.0
Morwellham	3.6	1202	0.2	285	47.9	0.0
Island	3.0	1207	0.1	250	43.4	0.8
Slimeford	1.9	1216	0.1	40	28.6	10.1
MorwellRks	1.2	1223	0.1	35	24.7	6.9

Axial profile 6th July 1988

Station	km	time	S	C	Z1	Z16
Narrows	31.0	1037	34.5	10	*	*
DkYdCorner	29.2	1045	*	*	*	*
Torpoint	28.2	1050	34.2	15	7.3	24.6
OilJetty	27.2	1055	33.1	15	*	*
LkGlassPt	26.4	1058	*	*	*	*
BullPt	24.8	1103	33.1	15	*	*
Bridge	23.9	1110	32.8	25	13.8	23.0
NealPt	21.5	1126	32.5	30	*	*
WeirPt	20.6	1132	31.5	30	2.2	84.3
Cargreen	19.9	1140	31.4	12	*	*
Pylons	18.1	1150	30.1	22	12.5	22.1
HolesHole	17.2	1200	27.3	35	*	*
SHooe	16.2	1206	27.6	40	17.7	10.9
Clifton	15.6	1210	24.6	45	*	*
PentQuay	14.2	1219	20.6	55	25.8	4.1
HaltonQy	13.3	1227	18.4	60	31.5	0.0
STR	11.6	1242	11.0	110	36.5	7.0
DeadTree	10.5	1301	3.1	190	8.8	69.5
Cotehele	9.9	1313	1.6	220	42.7	7.7
WhiteHorse	8.9	1321	0.6	250	49.5	1.5
Bridge1	8.5	1326	0.3	270	*	*
ST1	7.6	1330	0.3	250	26.0	7.0
ST2	6.8	1336	0.2	380	38.5	0.5
Rock	6.3	1345	0.2	500	27.1	6.9